QA: QA

ANL-EBS-MD-000030 REV 04

October 2004

Ventilation Model and Analysis Report

Prepared for:
U.S. Department of Energy
Office of Civilian Radioactive Waste Management
Office of Repository Development
1551 Hillshire Drive
Las Vegas, Nevada 89134-6321

Prepared by:
Bechtel SAIC Company, LLC
1180 Town Center Drive
Las Vegas, Nevada 89144

Under Contract Number
DE-AC28-01RW12101

DISCLAIMER

This report was prepared as an account of work sponsored by an agency of the United States Government. Neither the United States Government nor any agency thereof, nor any of their employees, nor any of their contractors, subcontractors or their employees, makes any warranty, express or implied, or assumes any legal liability or responsibility for the accuracy, completeness, or any third party's use or the results of such use of any information, apparatus, product, or process disclosed, or represents that its use would not infringe privately owned rights. Reference herein to any specific commercial product, process, or service by trade name, trademark, manufacturer, or otherwise, does not necessarily constitute or imply its endorsement, recommendation, or favoring by the United States Government or any agency thereof or its contractors or subcontractors. The views and opinions of authors expressed herein do not necessarily state or reflect those of the United States Government or any agency thereof.

QA: QA

Ventilation Model and Analysis Report

ANL-EBS-MD-000030 REV 04

October 2004

OCRWM	MODEL SIGNATURE PAGE/CHANGE HISTORY	Page iii
		1. Total Pages: 332

2. Type of Mathematical Model

☒ Process Model ☐ Abstraction Model ☐ System Model

Describe Intended Use of Model

This model and analysis report predicts the efficiency of preclosure ventilation of a waste emplacement drift. Limitations of this model are that the heat generation/length be nearly uniform, heat transfer by conduction to the invert or drift wall be small compared to radiant heat transfer, thermal loadings yield below boiling wall temperatures, single drift analyses where the repository edge does not significantly affect results, and simultaneous emplacement of waste.

3. Title

Ventilation Model and Analysis Report

4. DI (including Rev. No., if applicable):

ANL-EBS-MD-000030 REV 04

5. Total Appendices	6. No. of Pages in Each Appendix
Nineteen (19)	I-6, II-8, III-8, IV-4, V-4, VI-6, VII-8, VIII-6, IX-78, X-4, XI-4, XII-4, XIII-10, XIV-4, XV-4, XVI-4, XVII-4, XVIII-8, XIX-4

	Printed Name	Signature	Date
7. Originator	R. Walsh	SIGNATURE ON FILE	10-22-04
8. Independent Technical Reviewer	D. Dobson	SIGNATURE ON FILE	10-22-04
9. Checker	Z. Walton/B. Kirstein	SIGNATURE ON FILE	10-22-04
10. QER	J. Heaney	SIGNATURE ON FILE	10-22-04
11. Responsible Manager/Lead	C. Howard	SIGNATURE ON FILE	10-22-04
12. Responsible Manager	E. Hardin	SIGNATURE ON FILE	10/22/04

13. Remarks

Other Originators: Veraun D. Chipman, John Del Mar, Yiming Sun, John Case (Appendices I, II, III, XIII).

Lead Checker: Zane Walton/Bruce Kirstein.

John Case checked Sections 6.4.2-6.4.2.3, DIRS, and Appendices XVIII and XIX.

Jim Kam checked Appendix XIII.

Brian Mitcheltree checked Sections 4-5 and 9.

Bruce Kirstein checked Front through Section 5, Sections 7-8 and Appendices I through XII, and XIV though XVII.

Zane Walton checked Section 6 and other Items/Sections associated with RIT Action Items.

This revision incorporates Errata 1 and 2 to Rev 03 ICN 03.

Change History

14. Revision No.	15. Description of Change
00	Initial issue
01	Complete Revision

01 ICN 01	Issued for checking...for clarification purposes ICN 01 adds definitions for the ventilation heat removal efficiency (Section 6.1.3) and energy balance checks on the downstream use of the heat removal efficiencies to deliver the right amount of energy to the host rock (Section 6.6.2.1 through 6.6.2.3)
02	The use of MULTIFLUX v.2.2 (STN 10485-2.2-10/29/02) software in ANL-EBS-MD-000030 REV 01 ICN 01, correctly characterized as an unqualified code was issued after the exemption for the interim use of unqualified software (Section 5.10) had expired in August, 2002. Work with the MULTIFLUX v2.2 software had actually been performed in March 2002 when the exemption was in effect and full qualification/baselining of the code was in progress. However, a Project-level business decision was made to discontinue efforts to qualify the code. The significance of this decision with regard to the inclusion of the MULTIFLUX work in the Report was not fully appreciated until the ANL-EBS-MD-000030 REV 01 ICN 01 was approved and issued on 10/29/02. A noncompliance was identified as Quality Observation BSC(B)-03-0-029 for the following reasons: 1) The noncompliance is not a significant condition adverse to quality. MULTIFLUX v2.2 was used in the corroboration of the ventilation model; 2) The noncompliance appears to be isolated and attributable to the unusual situation in which a business, not technical, decision resulted in abandoning software qualification activities; 3) The noncompliance requires only remedial action applicable to the ANL-EBS-MD-000030 REV 01 ICN 01; 4) The noncompliance has no impact or residual impact upon completion of the remedial action. Since Multiflux v2.2 was used for corroboration, software output will not be used as input/feeds to downstream analyses; 5) The noncompliance does not require a cause determination; the cause is known, and the uniqueness of the circumstances which led to the noncompliance suggest that specific actions to preclude are not needed. Revised to remove the discussion of the corroborative model using MULTIFLUX v2.2, and other approaches that were used to corroborate the ventilation model and assess the impacts of moisture on the ventilation efficiency.
03	Complete revision in which ventilation model inputs were updated to reflect the current design for License Application. DRIFTFLOW v.1.0 ventilation calculations were replaced with an analytical model for ventilation which is implemented using the standard (built-in) functions of Microsoft Excel. A mixed convection heat transfer correlation is also developed and implemented in the ventilation models.
03 ICN 01	Editorial changes to Section 9, which include updating the revision and ACC numbers for BSC 2003a, and changing the STN for the ANSYS computer software from the HP platform to the Sun/Solaris platform in accordance with Table 3-1.
03 ICN 02	Minor ICN for editorial changes in Attachment IX.
03 ICN 03	Minor ICN for editorial changes.
03 ICN 03 ERRATA 1	Minor Errata for closure of CR 1132.
03 ICN 03 ERRATA 2	Minor Errata for closure of CR 2238

04	This revision addresses CR 2940 in Sections 4.1.11, 6.11, and Appendix XIX, improves the documentation of the adequacy of the model for its intended use, replaces superseded data as appropriate, and makes other changes required by the latest revision of AP-SIII.10Q, *Models*. Because the changes to the procedure required extensive reorganization of the document, the entire document was revised.

INTENTIONALLY LEFT BLANK

CONTENTS

Page

CONTENTS (Continued)

Page

CONTENTS (Continued)

Page

CONTENTS (Continued)

Page

CONTENTS (Continued)

Page

INTENTIONALLY LEFT BLANK

FIGURES

Page

FIGURES (Continued)

Page

TABLES

Page

TABLES (Continued)

Page

ACRONYMS AND ABBREVIATIONS

DTN	data tracking number
ECRB	Enhanced Characterization of the Repository Block
EBS	engineered barrier system
FEPs	features, events, and processes
IED	information exchange drawing
NC1	Natural Convection Test 1
NC2	Natural Convection Test 2
UZ	unsaturated zone
YMP	Yucca Mountain Project

SYMBOLS

a	radius of the drift wall
A_s	area of the waste package surface
A_{us}	waste package area per unit length of drift
A_{uw}	drift wall area per unit length of drift
A_w	drift wall surface area
B_s	coefficient
B_w	coefficient
c_i	coefficient in the Kuehn and Goldstein correlations for natural convection
c_o	coefficient in the Kuehn and Goldstein correlations for natural convection
$\overline{C_i}$	coefficient in the Kuehn and Goldstein correlations for natural convection
$\overline{C_o}$	coefficient in the Kuehn and Goldstein correlations for natural convection
C_p	heat capacity of air at constant pressure
D	determinant of a 2×2 matrix
d_h	hydraulic diameter
d_s	waste package diameter
d_w	drift diameter
e_s	surface emissivity of waste package
e_w	surface emissivity of drift wall
f	arbitrary energy flux
$f(\tau)$	arbitrary function for the flux rate
F_0	step heat flux applied at x = 0
h_{rad}	radiation heat transfer coefficient
h_s	waste package surface convection heat transfer coefficient
h_w	drift wall convection heat transfer coefficient
k	thermal conductivity
L	drift segment length

m	coefficient in the Kuehn and Goldstein correlations for natural convection
$\dot{m}$	ventilation mass flow rate
Nu	Nusselt number
P_b	scale factor depending on system of units
p_s	waste package power
Pr	Prandtl number
Q_{air}	heat convected to the air from the waste package and drift wall surfaces
Q_s	heat generated by the waste package
Q_w	heat conducted into the rock
$Q_{conv\text{-}s}$	heat convected from the waste package to the air
$Q_{conv\text{-}w}$	heat convected from the drift wall to the air
Q_{rad}	heat radiated from the waste package to the drift wall
r	radius
Re	Reynolds number
S	generalized temperature response
T	air temperature
t	time
$T_{air\text{-}bulk}$	average air temperature
T_{in}	ventilation air temperature at the drift segment inlet
T_{out}	ventilation air temperature at the drift segment outlet
T_s or T_{wp}	waste package surface temperature
T_w or T_{dw}	drift wall temperature
u	integration variable
$w_\tau(x,\tau)$	time derivative of the constant heat flux function for a unit loading
x	distance from the drift entrance

GREEK SYMBOLS

κ	thermal diffusivity
$\nu(t)$	temperature change
ρ	density
σ	Stefan-Boltzmann constant
$\eta(t,x)$	instantaneous ventilation efficiency
$\eta_{integrated}$	integrated ventilation efficiency
μ	viscosity
θ	dimensionless temperature
τ	dimensionless time

CONVERSIONS

Heat transfer rate	1 W	= 3.4123 Btu/h
Heat flux	1 W/m^2	= 0.3171 $Btu/h \cdot ft^2$
Heat transfer coefficient	1 $W/m^2 \cdot K$	= 0.17612 $Btu/h \cdot ft^2 \cdot °F$
Temperature difference	1 K	= (9/5)°R = (9/5)°F
Mass flow rate	1 kg/s	= 7936.6 lb_m/h
Specific heat	1 $kJ/kg \cdot K$	= 0.2389 $Btu/lb_m \cdot °F$
Mass	1 kg	= 2.2046 lb_m
Mass	1 grain	= 6.479891×10^{-5} kg
Pressure	1 atmosphere	= 101,330 N/m^2
Pressure	1 Pa	= 1 $Newton/m^2$

NOTE: Conversions for heat transfer, heat flux, heat transfer coefficient, mass, mass flow rate, temperature and specific heat are taken from Incropera and DeWitt 1996 [DIRS 108184], Back Cover; and Perry et al. 1984 [DIRS 125806], Table 1-5. Conversions for pressure are taken from from Rohsenow et al. 1998 [DIRS 169241], Table 1.15 and Table 2.4).

INTENTIONALLY LEFT BLANK

1. PURPOSE

1.1 BACKGROUND

Yucca Mountain, approximately 100 miles northwest of Las Vegas, Nevada, has been selected as the site for the nation's geologic repository for high-level nuclear waste. The Yucca Mountain Project (YMP) is currently developing the design for the underground facilities. The design includes a network of parallel drifts that will hold the waste (emplacement drifts), branching from a main drift. There are two distinct phases considered in the repository operation. The first phase, or preclosure phase, which includes emplacement of the waste, is a period when heat generated from the decay of radionuclides contained in waste packages is actively removed from the repository by ventilating the emplacement drifts. In the second phase, or postclosure phase, forced ventilation of the drifts is stopped and the repository is closed.

A prerequisite for designing the YMP repository is the ability to both understand and control the heat generated from the decay of the radionuclides. The decay heat affects the performance of both the waste packages and the emplacement drift. During the preclosure period, heat transfer from the waste packages occurs through mixed convection (a combination of forced and natural convection), conduction through the waste package supports, and thermal radiation to the invert and drift walls. In the postclosure phase, heat is transferred from the waste package by natural convection (as opposed to mixed convection before closure), conduction, and thermal radiation.

The purpose of the ventilation model, described in this report, is to simulate the heat transfer processes in and around a waste emplacement drift and predict the heat removal by ventilation during the preclosure period. The heat removal by ventilation is temporally and spatially dependent, and is expressed as the fraction or percentage of the heat produced by radionuclide decay that is carried away by the ventilation air. The heat removal by ventilation is also referred to as the ventilation efficiency.

1.2 SCOPE

This document describes the ventilation model. *Technical Work Plan for: Near-Field Environment and Transport In-Drift Heat and Mass Transfer Model and Analysis Reports Integration* (BSC 2004 [DIRS 170950]) describes work performed for this revision. Sections 4.2 and 8.3 of this report discuss acceptance criteria that were not assigned by the technical work plan (TWP). Otherwise, the work presented in this report is consistent with, and contains no deviations from, the governing TWP.

The objectives of this model report are to:

1. Develop and validate a conceptual model for preclosure ventilation of an emplacement drift (Sections 6.3 and 7).

2. Implement the ventilation conceptual model using numerical and analytical methods, and use the License Application design basis inputs and parameters to predict the preclosure ventilation efficiency (Section 6.4).

3. Verify the results of the numerical and analytical implementations of the ventilation conceptual model through comparative analyses (Section 6.6).

4. Develop an alternative conceptual model for preclosure ventilation which includes the impacts of water and water vapor mass transfer on the heat transfer (Section 6.7).

5. Implement the alternative conceptual model using analytical calculations to assess the impacts of moisture on the ventilation efficiency (Sections 6.8 and 6.9).

6. Demonstrate the applicability of the use of the ventilation efficiency as an abstraction method for downstream postclosure models to account for the preclosure heat removal (Section 6.10).

7. Demonstrate the sensitivity of the ventilation efficiency to discretization and uncertainties in key input parameters associated with the host rock and engineered components including thermal conductivity, matrix and lithophysal porosity, specific heat, emissivity, and convection heat transfer coefficient (Sections 6.6.1 and 6.11).

This report conforms to the prescribed outline of AP-SIII.10Q, *Models*, as described in Table 1-1.

Table 1-1. Outline of the Ventilation Model Documentation

Section	Content
1. PURPOSE	Purpose and introduction to the model report.
2. QUALITY ASSURANCE	Identifies the applicability of the YMP Quality Assurance program.
3. USE OF SOFTWARE	Lists controlled and exempt software used in the development, implementation, and validation of the model.
4. INPUTS	Lists data, parameters, and other inputs used in the development, implementation, and validation of the model. Also lists the appropriate criteria, codes, and standards.
5. ASSUMPTIONS	Lists assumptions and the rationale for their use in the development, implementation, and validation of the model.
6. MODEL DISCUSSION	Describes the conceptual model, the mathematical implementations of the conceptual model and the results, the alternative conceptual model, the mathematical implementation of the alternative conceptual model and the results, the appropriate use of the model output (i.e., ventilation efficiency), and the sensitivity of the ventilation efficiency to uncertainties in key model inputs and parameters.
7. VALIDATION	Presents the analyses that validate the conceptual model, which includes corroboration of the engineered barrier system (EBS) Ventilation Test Phase I results with modeling results.
8. CONCLUSIONS	Summarizes the modeling activities and describes the appropriate use of the model output (i.e., ventilation efficiency) in downstream models.
9. INPUTS AND REFERENCES	Lists input and output data tracking numbers (DTNs) and cited references.
APPENDICES	Document supporting analyses.

1.3 LIMITATIONS

Applicability of the ventilation model documented in this report is limited to:

- Ventilation air flow rates between 10 and 30 m^3/s.
- Configurations in which the waste packages are spaced in the drift such that, during the preclosure period, the average heat generation per unit length in each small group of waste packages is approximately the same as the average over the entire drift.
- Conditions in which conduction heat transfer from the waste package to the invert or drift wall is small compared to the heat transfer to the invert and drift wall via thermal radiation.
- Repository average waste package heat loads (or waste streams) that produce sub-boiling temperature conditions in the host rock during the ventilation period.
- Single drift analyses where the repository edges do not significantly affect the near field host rock thermal conduction.
- Simultaneous emplacement of the waste packages at the start of the preclosure period which is conservative with respect to the total heat load applied to the system.

1.4 DOWNSTREAM USE OF THE RESULTS

The main output of the ventilation model is the ventilation efficiency. Downstream models that do not explicitly model the preclosure period rely on the ventilation efficiency as a means of initializing their postclosure analyses. Such models include those presented in *Multiscale Thermohydrologic Model*, *Drift Degradation Analysis*, and *Drift-Scale Coupled Processes (DST and THC Seepage) Models*.

INTENTIONALLY LEFT BLANK

2. QUALITY ASSURANCE

This document was prepared in accordance with *Technical Work Plan for: Near-Field Environment and Transport In-Drift Heat and Mass Transfer Model and Analysis Reports Integration* (BSC 2004 [DIRS 170950]), which directs the work identified in work package ARTM02. As described in the technical work plan (TWP), the Quality Assurance program applies to the development of this document (BSC 2004 [DIRS 170950], Section 8).

The methods used to control the electronic management of data as required by AP-SV.1Q, *Control of the Electronic Management of Information*, were accomplished in accordance with the TWP (BSC 2004 [DIRS 170950], Section 8). There was no variance from the methods for controlling the electronic management of data.

As directed in the TWP, this document was prepared in accordance with AP-SIII.10Q, *Models*, LP-SI.11Q-BSC, *Software Management*, AP-3.15Q, *Managing Technical Product Inputs*, and reviewed in accordance with AP-2.14Q, *Document Review*.

This report supports the investigation of the performance of the engineered barrier system. In accordance with the *Q-list* (BSC 2004 [DIRS 168361], Table A-2, p. A-5), the engineered barrier system is designated as "important to waste isolation," and the Safety Category (SC) is "SC."

INTENTIONALLY LEFT BLANK

3. USE OF SOFTWARE

Table 3-1 lists the software used to perform the analyses as well as the software tracking numbers (where appropriate), CPU(s), operating systems, and physical location where the software was installed. All software listed in Table 3-1 was obtained from Software Configuration Management, was appropriate for the applications used, and was used within the range of validation in accordance with LP-SI.11Q-BSC, *Software Management*. Use of software has been documented in accordance with LP-SI.11Q-BSC.

Table 3-1. Software

Code	Software Tracking Number	CPU	Physical Location	Operating System
ANSYS v5.6.2	10145-5.6.2-00 10145-5.6.2-01	SGI Octane Sun Microsystems UltraSPARC	Las Vegas, NV	IRIX 6.5 Solaris 2.6 and Solaris 2.7
rme6 v1.2	10617-1.2-00	Sun Microsystems Blade 100	Livermore, CA	Solaris 8
YMESH v1.54	10172-1.54-00	Sun Microsystems Blade 100	Livermore, CA	Solaris 8
Mathcad 2001i Professional	Exempt	Dell Pentium Workstation	Las Vegas, NV	Windows 2000
Microsoft Excel 97	Exempt	Various YMP M&O Computers	Las Vegas, NV	Windows 95, Windows 2000

3.1 ANSYS v5.6.2

ANSYS v5.6.2 (BSC 2001 [DIRS 164464]) is a commercially available computer program and is classified as qualified software (per LP-SI.11Q-BSC). ANSYS v5.6.2 is used to implement the ventilation conceptual model. ANSYS v5.6.2 is a general purpose finite element analysis code, and is used in many disciplines of engineering that deal with topics including structural, geotechnical, mechanical, thermal, and fluids. ANSYS was selected for its capability of modeling heat transfer processes and predicting the ventilation efficiency in the thermal model for the License Application design. The use of this software was consistent with the intended use and was within the validation range defined by the test cases for this model (Test 01, Test 02, Test 05, Test 06 and Test 11) identified in the *Software Validation Test Report ANSYS Version 5.6.2 Software* (CRWMS M&O 2001 [DIRS 155138], pp. 8, 9, 11, 12, 16, 17) and *Validation Test Report for ANSYS Version 5.6.2 Software* (Doraswamy 2001 [DIRS 171331], pp. 4, 5, 7, 8, 13). There are no known limitations on outputs.

3.2 rme6 v1.2

rme6 v1.2 (LLNL 2003 [DIRS 163892]) is a developed computer program and is classified as qualified software (per LP-SI.11Q-BSC). rme6 v1.2 was selected for its unique capability of converting the numerical grid from the three-dimensional site scale unsaturated zone (UZ) flow and transport model to a format that is readable by YMESH v1.54. The use of this software was consistent with the intended use and was within the validation range defined by the test cases 1,

2, 3, and 4 identified in *Software Management Report: rme6 Version 1.2* (DOE 2003 [DIRS 171333], pp. 28, 33, 39, 45). Limitations on the software are also specified in *Software Management Report: rme6 Version 1.2* (DOE 2003 [DIRS 171333], Section 2.6). There are no known limitations on outputs. Work performed with the rme6 v1.2 software prior to qualification was reperformed with baselined software; the outputs were identical (see Section 6.5.1).

3.3 YMESH v1.54

YMESH v1.54 (LLNL 2003 [DIRS 163894]) is a developed computer program and is classified as qualified software (per LP-SI.11Q-BSC). YMESH v1.54 was selected for its unique capability of generating the thickness of the geologic layers for a stratigraphic column given by some easting and northing coordinates. The use of this software was consistent with the intended use and was within the validation range defined by the test cases 1 through 7 identified in the *Software Management Report: ymesh Version 1.54* (DOE 2003 [DIRS 171332], pp. 14 to 29). Limitations on the software are also specified in *Software Management Report: ymesh Version 1.54* (DOE 2003 [DIRS 171332], Section 2.6). There are no known limitations on outputs. Work performed with the YMESH v1.54 software prior to qualification was reperformed with baselined software; the outputs were identical (see Section 6.5.1).

3.4 MATHCAD 2001i PROFESSIONAL

Mathcad 2001i Professional is a commercially available software package. The Mathcad software provides a technical computing environment using standard mathematical notation for equations and operations. The use of the Mathcad software in this report is exempt from LP-SI.11Q-BSC per AP-SIII.10Q. The formulas, inputs and outputs of those formulas, and additional information required for an independent technically qualified person to verify the results of these Mathcad analyses are provided in Section 6 and Appendices III and XIII.

3.5 MICROSOFT EXCEL 97

Microsoft Excel 97 is a commercially available spreadsheet software package. Excel 97 is used in conjunction with the ANSYS v5.6.2 software to predict the ventilation efficiency, and as a stand alone implementation of the ventilation conceptual model to predict ventilation efficiency. Each of these applications uses only standard or built in functions. It is also used to make plots of data and perform other computations using standard functions. The use of Excel 97 in this report is exempt from LP-SI.11Q-BSC, per AP-SIII.10Q. The formulas, inputs and outputs of those formulas, and additional information required for an independent technically qualified person to verify the results of these Excel analyses are provided in Section 6, Appendices I, II, IV, V, VI, VII, VIII, X, XI, XII, XIV, XV, and the DTNs listed in Table 8-1. The user must select ‘Analysis ToolPak’ from the Tools/Add-Ins menu and must disable macros if prompted.

4. INPUTS

4.1 DIRECT INPUT

The following data were used as direct inputs to develop the models and analyses described in Section 6. Qualification and justification for use of the direct inputs which are obtained from outside sources, as listed in Tables 4-8, 4-14, and 4-17 through 4-21, are provided in Appendix XVIII.

4.1.1 Thermophysical Properties of the Invert

Tables 4-1 and 4-2 list measured thermophysical properties of 4-10 crushed tuff. The 4-10 crushed tuff is crushed welded tuff that passes through a size 4 sieve (4.75 mm mesh) and is retained on a size 10 sieve (2.00 mm mesh). The justification for the use of the material properties of 4-10 crushed tuff for the invert ballast material is described in Section 5.5. That is, though the 4-10 crushed tuff properties are not exact, they are adequate for use in the ventilation calculations. Tables 4-1 and 4-2 are for the 4-10 crushed tuff, and are used as inputs to the models and analyses described in Section 6 (see Section 5.5).

Table 4-1. Specific Heat, Thermal Conductivity, and Thermal Diffusivity of 4-10 Crushed Tuff

Sample Type	Sample Number	Specific Heat ($J/cm^3 \cdot °C$)	Thermal Conductivity ($W/m \cdot °C$)	Thermal Diffusivity (mm^2/s)	Temperature (°C)
4-10 crushed tuff	TK-CT-01	0.82	0.17	0.21	16.2
4-10 crushed tuff	TK-CT-02	0.84	0.14	0.16	15.8
4-10 crushed tuff	TK-CT-03	0.98	0.17	0.17	16.1
4-10 crushed tuff	TK-CT-04	0.98	0.17	0.17	16.4
4-10 crushed tuff	TK-CT-05	0.99	0.17	0.17	17.1
4-10 crushed tuff	TK-CT-06	0.92	0.16	0.18	17.5
4-10 crushed tuff	TK-CT-07	0.96	0.17	0.17	17.6
4-10 crushed tuff	TK-CT-07a	0.86	0.15	0.18	18.9
4-10 crushed tuff	TK-CT-08	0.88	0.16	0.18	18
4-10 crushed tuff	TK-CT-09	1.06	0.17	0.16	18.1
4-10 crushed tuff	TK-CT-10	0.94	0.17	0.18	18.5

DTN: GS000483351030.003 [DIRS 152932].

Table 4-2. Bulk Density of 4-10 Crushed Tuff

Sample Type	Sample Number	Bulk Density (g/cm^3)	Sample Type	Sample Number	Bulk Density (g/cm^3)
4-10 Crushed Tuff	UNCBD41A	1.3	4-10 Crushed Tuff	UNCBD53B	1.3
4-10 Crushed Tuff	UNCBD41B	1.2	4-10 Crushed Tuff	UNCBD54A	1.3
4-10 Crushed Tuff	UNCBD42A	1.3	4-10 Crushed Tuff	UNCBD54B	1.3
4-10 Crushed Tuff	UNCBD42B	1.3	4-10 Crushed Tuff	UNCBD55A	1.3
4-10 Crushed Tuff	UNCBD43A	1.3	4-10 Crushed Tuff	UNCBD55B	1.2
4-10 Crushed Tuff	UNCBD43B	1.2	4-10 Crushed Tuff	UNCBD56A	1.3
4-10 Crushed Tuff	UNCBD44A	1.3	4-10 Crushed Tuff	UNCBD56B	1.3
4-10 Crushed Tuff	UNCBD44B	1.2	4-10 Crushed Tuff	UNCBD57A	1.3
4-10 Crushed Tuff	UNCBD45A	1.3	4-10 Crushed Tuff	UNCBD57B	1.2
4-10 Crushed Tuff	UNCBD45B	1.2	4-10 Crushed Tuff	UNCBD58A	1.3
4-10 Crushed Tuff	UNCBD46A	1.2	4-10 Crushed Tuff	UNCBD58B	1.3
4-10 Crushed Tuff	UNCBD46B	1.2	4-10 Crushed Tuff	UNCBD59A	1.2
4-10 Crushed Tuff	UNCBD47A	1.3	4-10 Crushed Tuff	UNCBD59B	1.2
4-10 Crushed Tuff	UNCBD47B	1.3	4-10 Crushed Tuff	UNCBD60A	1.2
4-10 Crushed Tuff	UNCBD48A	1.3	4-10 Crushed Tuff	UNCBD60B	1.3
4-10 Crushed Tuff	UNCBD48B	1.3	4-10 Crushed Tuff	UNCBD61A	1.3
4-10 Crushed Tuff	UNCBD49A	1.3	4-10 Crushed Tuff	UNCBD61B	1.3
4-10 Crushed Tuff	UNCBD49B	1.2	4-10 Crushed Tuff	UNCBD62A	1.3
4-10 Crushed Tuff	UNCBD50A	1.2	4-10 Crushed Tuff	UNCBD62B	1.2
4-10 Crushed Tuff	UNCBD50B	1.2	4-10 Crushed Tuff	UNCBD63A	1.2
4-10 Crushed Tuff	UNCBD51A	1.3	4-10 Crushed Tuff	UNCBD63B	1.2
4-10 Crushed Tuff	UNCBD51B	1.3	4-10 Crushed Tuff	UNCBD64A	1.3
4-10 Crushed Tuff	UNCBD52A	1.3	4-10 Crushed Tuff	UNCBD64B	1.3
4-10 Crushed Tuff	UNCBD52B	1.3	4-10 Crushed Tuff	UNCBD65A	1.3
4-10 Crushed Tuff	UNCBD53A	1.3	4-10 Crushed Tuff	UNCBD65B	1.3

DTN: GS020183351030.001 [DIRS 163107], ROWS 321-370.

4.1.2 Relative Humidity

Relative humidity in the ventilated Enhanced Characterization of the Repository Block (ECRB) Cross-Drift was measured during November 1998. The relative humidity ranged from 10 to 41 percent. Appendix XIII requires a single relative humidity to represent average conditions in an open drift. That appendix uses 30% RH, a central value of the measurements taken in the ventilated ECRB, rounded off to one significant digit.

Table 4-3. Measured Relative Humidity in the Ventilated Zone of the ECRB Cross-Drift

Location	Range of Relative Humidity Measurements
Ventilated ECRB	Fluctuated between 10% and 41%

DTN: LB990901233124.006 [DIRS 135137].

4.1.3 Laboratory Measured Saturation for Tptpll from Borehole Cores

Table 4-4 lists laboratory-measured values of saturation from borehole core data. Column headings designate area boreholes that pass through the Tptpll (lower lithophysal unit). These data are used in Appendix XIII, and the average of these measurements is referred to in Section 6.9.1.

Table 4-4. Laboratory Measured Saturation for Tptpll from Borehole Cores

USW SD-7 [a]		USW SD-9 [b]		USW NRG-6 [c]		USW NRG-7/7A [d]		USW UZ-7A [e]	
Depth (ft)	Sat.	Depth (ft)	Sat.	Depth (ft)	Sat.	Depth (m)	Sat.	Depth (m)	Sat.
809.2	0.862	847.2	0.852	816.6	0.24	269.1	0.8	184.2	0.606
819	0.904	849.6	0.775	817.9	0.71	271.9	0.84	185.3	0.702
824.7	0.911	853.4	0.843	820.8	0.8	272.8	0.71	186.3	0.669
835.4	0.874	859	0.974	823	0.87	274.1	0.61	188.6	0.636
836.8	0.698	865.3	0.907	826.1	0.63	276.7	0.67	189	0.715
842.5	0.891	879.6	1.02	829.2	0.78	280	0.57	190.7	0.733
847.6	0.862	888.8	0.774	831.7	0.98	285.7	0.71	191	0.635
848.4	0.775	897	0.898	835.4	0.54	287.5	0.64	197.1	0.73
856.9	0.794	899.5	0.854	838.6	0.71	288.3	0.61	198.3	0.76
857.7	0.845	905.8	0.886	841.7	0.39	290.2	0.62	198.9	0.84
862.3	0.863	921.9	0.794	844.8	0.89	291.1	0.63	203.6	0.705
864.9	0.778	924.2	0.717	851.9	0.75	292.1	0.56	205.1	0.818
867.4	0.942	936.1	0.728	854.9	0.83	293.9	0.66	205.4	0.839
872	0.72	938.9	0.812	857.8	0.12	295.7	0.6	206.6	0.779
874.4	0.772	944.6	0.787	861	0.08	296.4	0.57	207	0.803
875.5	0.835	948	0.796	862.7	0.28	297.2	0.56	208.1	0.85
878.8	0.844	954	0.865	865.8	0.64	298.2	0.7	210	0.846
884.2	0.821	958.1	0.776	867.7	0.7	300.3	0.69	210.7	0.844
885	0.879	962.6	0.791	871.5	0.83	301.1	0.78	211.7	0.876
887.6	0.888	968.7	0.837	873.8	0.64	304.8	0.6	212.8	0.749
891	0.843	971.9	0.716	877.6	0.58	306.7	0.97	213.2	0.776
894	0.864	975.5	0.91	879.7	0.77	313	0.46	213.7	0.744
897.3	0.904	981	0.793	886	0.86	314.1	0.55	214.8	0.784
899.5	0.924	984.7	0.742	890.7	0.66	314.9	0.5	215.7	0.678

Table 4-4. Laboratory Measured Saturation for Tptpll from Borehole Cores (Continued)

USW SD-7 [a]		USW SD-9 [b]		USW NRG-6 [c]		USW NRG-7/7A [d]		USW UZ-7A [e]	
Depth (ft)	Sat.	Depth (ft)	Sat.	Depth (ft)	Sat.	Depth (m)	Sat.	Depth (m)	Sat.
904.9	0.793	986.6	0.744	892.8	0.31	316.9	0.4	216.7	0.751
910.7	0.855	995.7	0.809	898.6	0.72	317.4	0.65	217.5	0.852
914.7	0.854	1003	0.672	901.6	0.75	318.5	0.56	218.2	0.719
916.2	0.902	1007.3	0.781	904.8	0.85	319.4	0.34	219.2	0.706
919.1	0.818	1012.3	0.731	910.7	0.69	322.1	0.72	220.2	0.756
920.4	0.831	1017.2	0.886	912.8	0.8	323.1	0.74	220.9	0.678
924.1	0.847	1023.8	0.89	917.1	0.78	324.9	0.57	221.7	0.814
928.4	0.903	1028.9	0.81	920.4	0.71	326.7	0.72	222.9	0.723
929.7	0.871	1033.1	0.903	928.8	0.8	328.5	0.66	224.4	0.779
932.8	0.798	1035.1	0.922	932	0.72	331.3	0.69	225.4	0.499
936.7	0.781	1038.8	0.95	936	0.67	332.2	0.73	227.7	0.664
940.7	0.903	1041	0.895	942.7	0.81	334.2	0.58	228.7	0.769
941.5	0.879	1044.2	0.874	949.3	0.49	334.9	0.53	230.1	0.762
946.4	0.825	1047.2	0.932	952.5	0.65	336.9	0.63	231.2	0.784
951.2	0.906	1050.2	0.871	955.4	0.75	337.8	0.68	234.2	0.579
954.5	0.847	1053.6	0.985	959	0.71	338.4	0.51	—	—
957	0.778	1055.8	0.909	962	0.77	340	0.52	—	—
961.4	0.762	1064.8	0.958	968.2	0.69	342.4	0.38	—	—
962.5	0.956	1068.1	0.798	970.8	0.65	344	0.79	—	—
966.9	0.839	1070.4	0.821	975.1	0.64	346	0.59	—	—
968.9	0.881	1076.7	0.92	977	0.82	348	0.53	—	—
971.4	0.905	1080.1	0.837	978.9	0.72	348.8	0.57	—	—
974.5	0.85	1086.4	0.918	985.1	0.77	353.2	0.48	—	—
978.1	0.918	1091.1	0.863	989	0.73	354.3	0.39	—	—
981	0.846	1095.4	0.84	991.6	0.75	355	0.52	—	—
983.8	0.831	1098.4	0.712	995.6	0.41	357	0.39	—	—
986.2	0.965	1101.3	0.757	1004.1	0.71	357.9	0.5	—	—
990.2	0.918	1104.1	0.596	1010.2	0.62	358.9	0.38	—	—
993.1	0.995	1106.4	0.761	1015.7	0.84	359.6	0.66	—	—
994.3	0.985	1110.3	0.729	1018.5	0.88	360.5	0.42	—	—
999	0.878	1113.5	0.706	1024.1	0.5	361.5	0.53	—	—
1005	0.901	1116	0.749	1033.8	0.41	362.6	0.53	—	—
1008.2	0.909	1119.2	0.755	1036	0.62	363.2	0.35	—	—
1013.3	0.955	1125.1	0.806	1040.1	0.84	366	0.76	—	—
1017.6	0.952	1128.6	0.877	1042.7	0.87	366.9	0.56	—	—
—	—	1133.6	0.799	1049	0.66	367.8	0.7	—	—
—	—	1139.6	0.84	1054.8	0.37	368.9	0.75	—	—
—	—	1142	0.903	1058.3	0.87	370.6	0.68	—	—
—	—	1146.1	0.863	1060.9	0.83	373.2	0.56	—	—
—	—	1149	0.865	1063.5	0.81	—	—	—	—
—	—	1152.7	0.855	1067	0.52	—	—	—	—

Table 4-4. Laboratory Measured Saturation for Tptpll from Borehole Cores (Continued)

USW SD-7 [a]		USW SD-9 [b]		USW NRG-6 [c]		USW NRG-7/7A [d]		USW UZ-7A [e]	
Depth (ft)	Sat.	Depth (ft)	Sat.	Depth (ft)	Sat.	Depth (m)	Sat.	Depth (m)	Sat.
—	—	1158.5	0.69	1069.8	0.82	—	—	—	—
—	—	1161.1	0.864	1076.1	0.68	—	—	—	—
—	—	1163.8	0.828	1079.1	0.72	—	—	—	—
—	—	1166.6	0.862	1081.9	0.75	—	—	—	—
—	—	1170.5	0.813	1084.2	0.77	—	—	—	—
—	—	1172.8	0.88	1087.1	0.8	—	—	—	—
—	—	1179	0.868	1090.3	0.86	—	—	—	—
—	—	—	—	1096.6	0.8	—	—	—	—

[a] DTN: GS951108312231.009 [DIRS 108984], S96037_007.
[b] DTN: GS950408312231.004 [DIRS 108986], S96021_007.
[c] DTN: GS000508312231.006 [DIRS 153237].
[d] DTN: GS951108312231.010 [DIRS 108983].
[e] DTN: GS951108312231.011 [DIRS 108992].

4.1.4 Water Potential Measurements Taken at the ECRB Station 15+00

Table 4-5 lists measurements of water potential taken at the ECRB Station 15+00 on 7/29/00. This data set was chosen because it was the first set of measurements that appear to be typical of later measurements. These data are used in Appendix XIII to demonstrate that the latent heat of vaporization can be neglected in the calculation of ventilation efficiency.

Table 4-5. Water Potential Measurements Taken at the ECRB Station 15+00

Station	Distance from Borehole (m)	Water Potential (m)
ST-1500-0.62	0.62	−259
ST-1500-1.12	1.12	−91
ST-1500-1.69	1.69	−10
ST-1500-2.12	2.12	−24
ST-1500-2.62	2.62	−37
ST-1500-3.12	3.12	−5
ST-1500-3.62	3.62	4
ST-1500-4.12	4.12	−12
ST-1500-4.62	4.62	−14
ST-1500-5.12	5.12	−8
ST-1500-5.62	5.62	−10

DTN: LB0110ECRBH2OP.001 [DIRS 156883], C7-1500.xls, worksheet “wp-2000-plot”, row 4.

NOTE: Water potential in the source DTN and in this table follows the convention that a positive pressure results in a positive water potential while a negative capillary pressure results in a negative water potential. Except as presented in this table, this report uses the opposite convention: positive water potential corresponds to negative capillary pressure.

4.1.5 Thermophysical Properties of the Stratigraphic Layers

Tables 4-6 through 4-11 list the thermophysical properties of the repository and non-repository stratigraphic units. Except for emissivity, these properties are obtained from qualified data found in the Technical Data Management System. The emissivity values for rocks (see Table 4-8) are from *Fundamentals of Heat and Mass Transfer* (Incropera and DeWitt 1996 [DIRS 108184], Table A.11 for rocks). Their range of 0.88 to 0.95 is adapted from sources for hemispherical emissivity of rock at 300K. The range is corroborated by handbook values (Knudsen et al. 1984 [DIRS 170057], Table 10-17, pp. 10-51 to 10-52) for normal emissivity of rough silica and rough fused quartz, ranging from 0.8 to 0.93. Therefore, the data are qualified for use as emissivity of the repository stratigraphaphic units and the invert material (see Section 4.1.15) in the calculation of ventilation efficiency.

Parameter distributions are only included for the repository stratigraphic units. These parameters are used as inputs to the models and analyses described in Section 6.

Table 4-6. Thermophysical Properties of the Repository Stratigraphic Units

Unit (UZ Model Layer)	Dry Bulk Thermal Conductivity (W/m·K)		Wet Bulk Thermal Conductivity (W/m·K)		Dry Bulk Density (g/cc)		Matrix Porosity		Lithophysal Porosity	
	Mean	Std. Dev.	Mean	Std. Dev.	Mean	Std. Dev.	Mean	Std. Dev.	Mean	Std. Dev.
Tptpul (tsw33)	1.1829	0.2440	1.7749	0.2474	1.8344	0.1496	0.1667	0.0412	0.1228	0.0613
Tptpmn (tsw34)	1.4189	0.2654	2.0741	0.2517	2.1483	0.0932	0.1287	0.0323	0.0254	0.0225
Tptpll (tsw35)	1.2784	0.2511	1.8895	0.2484	1.9793	0.1381	0.1486	0.0340	0.0883	0.0540
Tptpln (tsw36)	1.4900	0.2844	2.1303	0.2676	2.2114	0.0857	0.1058	0.0264	0.0302	0.0253
	Dry Matrix Thermal Conductivity (W/m·K)		Wet Matrix Thermal Conductivity (W/m·K)		Solid Thermal Conductivity (W/m·K)		Solid Connectivity			
Unit (UZ Model Layer)	Mean	Std. Dev.	Mean	Std. Dev.	Mean	Std. Dev.	Mean	Std. Dev.		
Tptpul (tsw33)	1.3453	0.2639	2.0201	0.2484	2.6011	0.3493	0.8517	0.1158		
Tptpmn (tsw34)	1.4553	0.2690	2.1276	0.2519	2.6033	0.3518	0.8476	0.1094		
Tptpll (tsw35)	1.3998	0.2640	2.0707	0.2455	2.6030	0.3413	0.8531	0.1130		
Tptpln (tsw36)	1.5356	0.2908	2.1958	0.2764	2.6017	0.3505	0.8492	0.1151		

DTN: SN0404T0503102.011 [DIRS 169129], file ReadMe.Doc, Tables 7-10 and 7-11.

NOTE: Nomenclature correlation between stratigraphic units and UZ model layer is based on BSC 2004 [DIRS 169855], Table 6-11.

Table 4-7. Specific Heat of the Repository Stratigraphic Units

Unit	UZ Model Layer	Average Rock Grain Specific Heat (J/g·K)	
		Mean	Std. Dev.
Tptpul	tsw33	0.93	0.12
Tptpmn	tsw34	0.93	0.14
Tptpll	tsw35	0.93	0.13
Tptpln	tsw36	0.93	0.10

DTN: SN0307T0510902.003 [DIRS 164196], file rock_grain_heat_capacity.xls, worksheet “Cp grain 25-325”, rows 8-11, columns y and z.

NOTES: T = 25 to 325°C.

Nomenclature correlation between stratigraphic units and UZ model layer is based on BSC 2004 [DIRS 169855], Table 6-11.

Table 4-8. Emissivity of Rocks Used as Inputs for the Repository Stratigraphic Units

Unit	UZ Model Layer	Emissivity	
		Minimum	Maximum
Tptpul	tsw33	0.88	0.95
Tptpmn	tsw34	0.88	0.95
Tptpll	tsw35	0.88	0.95
Tptpln	tsw36	0.88	0.95

Source: Incropera and DeWitt 1996 [DIRS 108184], Table A.11 for Rocks.

NOTE: Nomenclature correlation between stratigraphic units and UZ model layer is based on BSC 2004 [DIRS 169855], Table 6-11.

Table 4-9. Matrix Permeability and Van Genuchten Parameters of the Repository Stratigraphic Units

Unit	UZ Model Layer	Permeability (m^2)	Residual Saturation	α (1/Pa)	Van Genuchten’s m
Tptpul	tsw33 (tswM3)	6.57e-18	0.12	6.17e-6	0.283
Tptpmn	tsw34 (tswM4)	1.77e-19	0.19	8.45e-6	0.317
Tptpll	tsw35 (tswM5)	4.48e-18	0.12	1.08e-5	0.216
Tptpln	tsw36 (tswM6)	2.00e-19	0.20	8.32e-6	0.442

DTN: LB0208UZDSCPMI.002 [DIRS 161243], drift-scale calibrated properties for mean infiltration2.xls.

NOTE: Nomenclature correlation between stratigraphic units and UZ model layer is based on BSC 2004 [DIRS 169855], Table 6-11. (In the source spreadsheet, one character of the UZ model is changed to “M” for matrix properties or “F” for fracture properties.)

Table 4-10. Thermophysical Properties of the Non-Repository Stratigraphic Units

Unit	UZ Model Layer	Dry Matrix Thermal Conductivity (W/m·K)		Wet Matrix Thermal Conductivity (W/m·K)		Dry Bulk Density (kg/m^3)		Matrix Porosity	
		Mean	Std. Dev.	Mean	Std. Dev.	Mean	Std. Dev.	Mean	Std. Dev.
Tpcr	tcw11	1.30	0.23	1.81	0.20	2190	177	0.12	0.05
Tpcp	tcw12	1.30	0.23	1.81	0.20	2190	177	0.12	0.05
TpcLD		1.30	0.23	1.81	0.20	2190	177	0.12	0.05
Tpcpv3	tcw13	0.69	0.23	0.80	0.25	2310	89	0.04	0.04
Tpcpv2		0.49	0.16	1.06	0.15	1460	337	0.39	0.13
Tpcpv1	ptn21	0.49	0.16	1.06	0.15	1460	337	0.39	0.13
Tpbt4	ptn22	0.49	0.16	1.06	0.15	1460	337	0.39	0.13
Yucca	ptn23	0.49	0.16	1.06	0.15	1460	337	0.39	0.13
	ptn24								
Tpbt3_dc		0.49	0.16	1.06	0.15	1460	337	0.39	0.13
Pah	ptn25	0.49	0.16	1.06	0.15	1460	337	0.39	0.13
Tpbt2	ptn26	0.49	0.16	1.06	0.15	1460	337	0.39	0.13
Tptrv3		0.49	0.16	1.06	0.15	1460	337	0.39	0.13
Tptrv2		0.49	0.16	1.06	0.15	1460	337	0.39	0.13
Tptrv1	tsw31	0.69	0.23	0.80	0.25	2310	89	0.04	0.04
Tptrn	tsw32	1.30	0.23	1.81	0.20	2190	177	0.12	0.05
Tptrl	tsw33	1.30	0.23	1.81	0.20	2190	177	0.12	0.05
Tptf		1.30	0.23	1.81	0.20	2190	177	0.12	0.05
Tptpv3	tsw38	0.69	0.23	0.80	0.25	2310	89	0.04	0.04
Tptpv2	tsw39	0.49	0.16	1.06	0.15	1460	337	0.39	0.13
Tptpv1	ch1	0.49	0.16	1.06	0.15	1460	337	0.39	0.13
Tpbt1		0.49	0.16	1.06	0.15	1460	337	0.39	0.13
Calico	ch2	0.60	0.11	1.26	0.14	1670	157	0.33	0.05
	ch3								
	ch4								
	ch5								
Calicobt	ch6	0.60	0.11	1.26	0.14	1670	157	0.33	0.05
Prowuv	pp4	0.57	0.10	1.13	0.12	1790	117	0.30	0.04
Prowuc	pp3	0.57	0.10	1.13	0.12	1790	117	0.30	0.04
Prowmd	pp2	1.06	0.18	1.63	0.17	2070	139	0.21	0.06
Prowlc		0.57	0.10	1.13	0.12	1790	117	0.30	0.04
Prowlv	pp1	0.57	0.10	1.13	0.12	1790	117	0.30	0.04
Prowbt		0.57	0.10	1.13	0.12	1790	117	0.30	0.04
Bullfroguv		0.66	0.13	1.19	0.14	1880	167	0.23	0.06
Bullfroguc	bf3	0.66	0.13	1.19	0.14	1880	167	0.23	0.06
Bullfrogmd		1.30	0.24	1.81	0.20	2260	138	0.12	0.05
Bullfroglc		0.66	0.13	1.19	0.14	1880	167	0.23	0.06
Bullfroglv	bf2	0.66	0.13	1.19	0.14	1880	167	0.23	0.06
Bullfrogbt		0.66	0.13	1.19	0.14	1880	167	0.23	0.06
Tramuv		0.54	0.11	1.10	0.12	1760	195	0.33	0.06
Tramuc	tr3	0.54	0.11	1.10	0.12	1760	195	0.33	0.06

Table 4-10. Thermophysical Properties of the Non-Repository Stratigraphic Units (Continued)

Unit	UZ Model Layer	Dry Matrix Thermal Conductivity (W/m·K)		Wet Matrix Thermal Conductivity (W/m·K)		Dry Bulk Density (kg/m^3)		Matrix Porosity	
		Mean	Std. Dev.	Mean	Std. Dev.	Mean	Std. Dev.	Mean	Std. Dev.
Trammd	tr3	1.06	0.18	1.63	0.17	2140	78	0.21	0.06
Tramlc		0.54	0.11	1.10	0.12	1760	195	0.33	0.06
Tramlv	tr2	0.54	0.11	1.10	0.12	1760	195	0.33	0.06
Trambt		0.54	0.11	1.10	0.12	1760	195	0.33	0.06

DTN: SN0303T0503102.008 [DIRS 162401].

NOTE: Nomenclature correlation between stratigraphic units and UZ model layer is based on BSC 2004 [DIRS 169855], Table 6-11.

Table 4-11. Specific Heat of the Non-Repository Stratigraphic Units

Unit	UZ Model Layer	Average Rock Grain Specific Heat (J/g·K)	
		Mean	Std. Dev.
Tpc	tcw11, tcw12	0.93	0.11
Tpcpv23	tcw13	0.95	0.11
pTn	ptn21 to ptn26	0.96	0.23
Tptrv1	tsw31	0.95	0.10
Tptrnf	tsw32	0.93	0.13
Tptpv3	tsw38	0.98	0.24
Tptpv2	tsw39	0.98	0.19
Tptpv1-Tpbt1	ch1	1.08	0.42
Tac4	ch2	1.07	0.42
Tac3	ch3	1.07	0.38
Tac2	ch4	1.07	0.36
Tac1	ch5	1.07	0.35
Tacbt	ch6	1.02	0.24
Tcpuv	pp4	1.04	0.28
Tcpuc-Tcplc	pp3, pp2	0.93	0.13
Tcplv-Tcbuv	pp1	1.10	0.19
Tcbuc-Tcblc	bf3	0.93	0.12
Tcblv-Tctuv	Bf2	1.05	0.22
Tctuc-Tctlc	tr3	0.94	0.12
Tctlv-Tctbt	tr2	0.94	0.12

DTN: SN0307T0510902.003 [DIRS 164196].

NOTES: T = 25 to 325°C.

Nomenclature correlation between stratigraphic units and UZ model layer is based on BSC 2004 [DIRS 169855], Table 6-11.

4.1.6 Ground Surface and Water Table Elevations and Temperatures

UZ Flow Models and Submodels (BSC 2004 [DIRS 169861], pp. 6-36 to 6-37) develops a linear correlation of measured mean surface temperature with elevation. The reference surface temperature is 18.23°C at an elevation of 1,231.0 m, averaged using measured data from borehole NRG-6. Based on measurements at NRG-7a, the calculated mean lapse rate is 0.009°C/m.

The water table elevation and temperature are contained in Table 4-12. The location identified as R5C10 (Northing 170730, Easting 234913) (see Section 5.1), used in this report, is nearest to the grid column BTb76 (Northing 170840, Easting 234950) in DTN: LB0303THERMSIM.001 [DIRS 165167].

Table 4-12. Information Used to Calculate the Ground Surface and Water Table Temperatures

Grid/Mesh Column ID	Easting (m)	Northing (m)	Water Table Elevation [a] (m)	Water Table Temperature (°C)
BTb76	170840	234950	730	28.27

DTN: LB0303THERMSIM.001 [DIRS 165167] (file bot_temp_thermal_grid.dat).

[a] DTN: MO0106RIB00038.001, Water Table Altitude, midpoint of small-gradient area.

4.1.7 Waste Package Heat Decay

Table 4-13 shows the repository average lineal heat load as a function of time since waste emplacement. This design information is used as input to the models and analyses described in Section 6.

Table 4-13. Waste Package Heat Decay

Time Since Emplacement (years)	Lineal Heat Load (kW/m)	Time Since Emplacement (years)	Lineal Heat Load (kW/m)
0.000001	1.45E+00	26	8.525E-01
1	1.399E+00	27	8.382E-01
2	1.357E+00	28	8.245E-01
3	1.321E+00	29	8.114E-01
4	1.289E+00	30	7.992E-01
5	1.259E+00	31	7.858E-01
6	1.232E+00	32	7.730E-01
7	1.206E+00	33	7.610E-01
8	1.181E+00	34	7.493E-01
9	1.157E+00	35	7.381E-01
10	1.135E+00	36	7.262E-01
11	1.110E+00	37	7.150E-01
12	1.088E+00	38	7.042E-01
13	1.068E+00	39	6.938E-01
14	1.049E+00	40	6.838E-01
15	1.033E+00	41	6.733E-01
16	1.012E+00	42	6.632E-01
17	9.934E-01	43	6.535E-01

Table 4-13. Waste Package Heat Decay (Continued)

Time Since Emplacement (years)	Lineal Heat Load (kW/m)	Time Since Emplacement (years)	Lineal Heat Load (kW/m)
18	9.759E-01	44	6.441E-01
19	9.595E-01	45	6.351E-01
20	9.443E-01	46	6.258E-01
21	9.267E-01	47	6.169E-01
22	9.103E-01	48	6.083E-01
23	8.950E-01	49	6.000E-01
24	8.805E-01	50	5.920E-01
25	8.666E-01		

Source: BSC 2004 [DIRS 167754], Table 12.

4.1.8 Kuehn and Goldstein Parameters for Natural Convection

Table 4-14 lists constants for large Rayleigh numbers in the Kuehn and Goldstein correlations for natural convection. These constants are used in the mixed convection correlation to calculate convection heat transfer coefficients. This information is used as input to the models and analyses described in Sections 6 and 7.

Table 4-14. Constants for Large Rayleigh Numbers in the Kuehn and Goldstein Correlations for Natural Convection

Term	Value
c_i	0.5
$\overline{C_i}$	0.12
c_o	1
$\overline{C_o}$	0.12
m	15

Source: Kuehn and Goldstein 1978 [DIRS 130084], Eq. 1a and 1b.

4.1.9 Thermophysical Properties of the Waste Package

Section 5.2 provides rationale for using a 21-PWR as a representative waste package. Table 4-15 shows the thermophysical properties and dimensions of a 21-PWR waste package, its inner stainless steel shell, and its outer Alloy 22 shell. This design information was used as input to a multilayer model of the waste package in the ANSYS calculations described in Section 6.

Subsequent to completion of the analyses, the design-basis dimensions for a typical 21-PWR were superseded due to the evolution of waste package design; the design-basis thickness of the inner shell became 50.8 mm instead of 50 mm, and the nominal diameter became 1718.3 mm instead of 1644 mm (BSC 2004 [DIRS 169472], Table 1). The increase of the inner shell thickness is less than 2%, which is expected to have insignificant effect on the results because the magnitude of change is far smaller than the range of variations in different waste package

diameters. The more significant change is in the nominal diameter, an increase of about 5%. This would result in a 5% increase in the surface area available for heat transfer. However, because nominal diameters of waste packages vary from 1375.4 mm to 2126.0 mm (BSC 2004 [DIRS 169472], Table 1), the inputs in Table 4-15 are suitable for intended use because they are within the range of waste package dimensions of interest and, therefore, justified for use as dimensions of a representative waste package.

Table 4-15. Thermophysical Properties of the Waste Package

	Reference Temperature (°C) [a]	Thermal Conductivity (W/m·K) [a]	Specific Heat (J/kg·K) [a]	Density (kg/m^3) [a]	Emissivity [a]	Thickness 21-PWR (mm)	Nominal Diameter 21-PWR (mm)
Waste Package Internal Cylinder (21-PWR)	N/A	1.5	378	3495	N/A	N/A	
Waste Package Inner Shell (316NG)	21.11	13.33	482.93	7980	N/A	50 [b]	1644 [b]
	37.78	13.67	488.19				
	65.56	14.19	499.38				
	93.33	14.54	500.68				
	121.11	15.06	511.31				
	148.89	15.58	521.64				
	176.67	15.92	522.43				
	204.44	16.44	528.75				
Waste Package Outer Shell (Alloy 22)	48, 52	10.1	414	8690	0.87	20 [c]	
	100	11.1	423				
	200	13.4	444				

[a] BSC 2001 [DIRS 156276], pp. 13 and 14.
[b] BSC 2003 [DIRS 165406], Table 1 (superseded data, justified in text).
[c] BSC 2004 [DIRS 169472], Table 1.

4.1.10 In-Drift Geometry and Ventilation Parameters

Table 4-16 lists various in-drift geometric and preclosure ventilation parameters. This design information is used as input to the models and analyses described in Section 6.

The design-bases configurations for the height from the invert top to the center of 21-PWR waste package and the invert height were superseded because of the changes in waste package design and invert structure design. The design-basis height from the invert top to the center of 21-PWR waste package and invert height have been changed to 1051 mm (BSC 2004 [DIRS 168489]) and 864 mm (2’ 10”) (BSC 2004 [DIRS 169503]) from 1018 mm (BSC 2003 [DIRS 164069]) and 806 mm (BSC 2003 [DIRS 164101]), respectively. Since the heights from the invert top to the center of different types of waste packages vary from 887 mm to 1286 mm (BSC 2004 [DIRS 168489]), the inputs in Table 4-16 are within the range of properties of interest.

The use of the invert height of 806 mm is justified through comparison of the analytical model to the ANSYS model (Section 6.6.2). The analytical model does not explicitly account for thermal conduction through the invert, whereas such thermal conduction is included in the ANSYS

model. A comparison shows that the results are not sensitive to the presence of the invert because of the agreement between the ANSYS and analytical models. Therefore, the inputs in Table 4-16 are justified for their intended use in this report.

Table 4-16. Emplacement Drift Geometries, Ventilation Flow Rate, Ventilation Duration

Parameter	Value	Source
Emplacement Drift Diameter (m)	5.5	BSC 2004 [DIRS 168489]
Emplacement Drift Spacing (m)	81	BSC 2004 [DIRS 168489]
Nominal Ventilation Airflow Rate Preclosure (m^3/s)	15	BSC 2004 [DIRS 168489]
Ventilation Duration After Final Emplacement (years)	50	BSC 2004 [DIRS 168489]
Height from Invert Top to Center of 21-PWR (mm)	1018	BSC 2003 [DIRS 164069][a]
Invert Height (mm)	806	BSC 2003 [DIRS 164101][a]

[a] Superseded data, justified in text.

4.1.11 Thermophysical Properties of Air

Table 4-17 lists the thermophysical properties of air at one atmosphere, which corresponds to pressure at sea level. This information is used as input to the models and analyses described in Section 6.

However, the emplacement drifts will be located above sea level, where the pressure is about 0.88 atmosphere (Appendix XIX). The major effect of this 0.12 atmosphere difference in pressure is that the air density will be about 12 percent lower than shown in Table 4-17, resulting in a 12 percent reduction in the mass of air flowing through the drift for a given volumetric flow rate, based on the ideal gas law. The effect of this can be calculated with a 12 percent reduction in air density. The effect of reducing the total air pressure as indicated results in a reduction of the ventilation efficiencies by approximately 1% as reported in Section 6.11.

Table 4-17. Thermophysical Properties of Air

Reference Temperature (K)	Density (kg/m^3)	Specific Heat (kJ/kg·K)	Viscosity 10^7 (N·s/m^2)	Kinematic Viscosity 10^6 (m^2/s)	Thermal Conductivity 10^3 (W/m·K)	Thermal Diffusivity 10^6 (m^2/s)	Prandtl Number
250	1.3947	1.006	159.6	11.44	22.3	15.9	0.720
300	1.1614	1.007	184.6	15.89	26.3	22.5	0.707
350	0.995	1.009	208.2	20.92	30.0	29.9	0.700
400	0.8711	1.014	230.1	26.41	33.8	38.3	0.690

Source: Incropera and DeWitt 1996 [DIRS 108184], Table A.4.

This change in total pressure from one atmosphere to 0.88 atmosphere does not affect the other pertinent physical properties, which are specific heat, viscosity, and thermal conductivity. The other properties in Table 4-17, the kinematic viscosity, thermal diffusivity, and Prandtl number, are derived quantities and need no further discussion.

Because the specific heat has units of energy per unit mass per degree K, the volumetric heat capacity depends on the gas density, which can be predicted by the ideal gas law. The heat capacity of an ideal gas is not dependent upon pressure (Reid et al. 1977 [DIRS 130310], Section

7-1), and air behaves as an ideal gas around one atmosphere total pressure because its compressibility factor (usually denoted as Z) is close to unity, which defines an ideal gas (Reid et al. 1977 [DIRS 130310], Section 3-2). The compressibility at conditions of interest can be determined from reduced properties. Using a critical pressure of 37.2 atmospheres and a critical temperature of –140.7°C for air (Perry et al. 1984 [DIRS 125806], p. 3-111, Table 3-161), the reduced pressure at one atmosphere is $P/P_c = 1/37.2 \approx 0.027$, and the reduced temperature at 100°C is $T/T_c = 373/132.4 \approx 2.8$. According to a generalized compressibility chart for these reduced properties (Reid et al. 1977 [DIRS 130310], Figure 3-1), $Z \approx 1$ for pressures and temperatures relevant to the ventilation caclulations, and thus air behaves as an ideal gas.

The other two properties are not significantly affected by a small pressure change. The viscosity of air is essentially constant with pressure changes around one atmosphere (Reid et al. 1977 [DIRS 130310], Figure 9-8). The thermal conductivity of gases at low pressure (up to 10 atmospheres) increases about 1 percent per atmosphere (Reid et al. 1977 [DIRS 130310], Section 10-5) so that a change of 0.12 atmosphere results in a thermal conductivity relative change of about 0.12 percent, which is small enough to be ignored.

Therefore, the gas-phase density is the only physical property in Table 4-17 that changes significantly as the pressure changes from one atmosphere to 0.88 atmosphere, and the gas-phase density can be calculated from the ideal gas law.

4.1.12 Thermophysical Properties of Water

Table 4-18 lists the thermophysical properties of pure water. This information is used in Section 6.9 and Appendix XIII to demonstrate that the contribution of latent heat of vaporization may be neglected in calculating the ventilation efficiency. The composition of the water is not relevant.

Table 4-18. Thermophysical Properties of Water

Reference Temperature (K)	Specific Volume 10^3 (m^3/kg)	Heat of Vaporization (kJ/kg)	Specific Heat (kJ/kg·K)	Viscosity 10^6 (N·s/m^2)	Thermal Conductivity 10^3 (W/m·K)
273.15	1.000	2502	4.217	1750	569
300	1.003	2438	4.179	855	613
350	1.027	2317	4.195	365	668

Source: Incropera and DeWitt 1996 [DIRS 108184], Table A.6.

4.1.13 Kays and Leung Parameters for Forced Convection

Table 4-19 lists Kays and Leung parameters used in the mixed convection correlation to calculate forced convection heat transfer coefficients. This information is used as input to the models and analyses described in Sections 6 and 7.

Table 4-19. Kays and Leung Parameters for Forced Convection

	Annulus Radius Ratio (r^*)	Reynolds Number (Re)	Nusselt Number – Inner Surface Condition, Inner Surface Heated Alone (Nu_{ii})	Non-Dimensional Temperature – Inner Surface (θ_i)	Nusselt Number - Outer Surface Condition, Outer Surface Heated Alone (Nu_{oo})	Non-Dimensional Temperature – Outer Surface (θ_o)
Fluid with Prandtl Number = 0.700	0.2	1.00E+04	38.6	0.412	29.4	0.063
		3.00E+04	79.8	0.338	64.3	0.055
		1.00E+05	196	0.286	165	0.049
		3.00E+05	473	0.26	397	0.044
		1.00E+06	1270	0.235	1070	0.04
	0.5	1.00E+04	30.9	0.3	28.3	0.137
		3.00E+04	66	0.258	62	0.119
		1.00E+05	166	0.225	158	0.107
		3.00E+05	400	0.206	380	0.097
		1.00E+06	1080	0.185	1040	0.09

Source: Kays and Leung 1963 [DIRS 160763], Table 1.

4.1.14 Physical Constants

Table 4-20 lists physical constants used as inputs to the model and analyses of Sections 6 and 7.

Table 4-20. Physical Constants

Property	Value	Source
Stefan-Boltzmann ($W/m^2 \cdot K^4$)	5.670×10^{-8}	Incropera and DeWitt 1996 [DIRS 108184], Back cover
Gravity (m/s^2)	9.8	Incropera and DeWitt 1996 [DIRS 108184], Back cover
Ideal Gas Law Constant (kJ/kmol·K)	8.315	Incropera and DeWitt 1996 [DIRS 108184], Back cover
Prandtl Number Exponent (Dittus-Boelter Correlation)	0.4	Incropera and DeWitt 1996 [DIRS 108184], Section 8.5
Molecular Weight of Water (g/mol)	18	Weast 1977 [DIRS 106266], p. B117
Molecular Weight of Dry Air (g/mol)	29	Weast 1977 [DIRS 106266], p. F13 – F15

4.1.15 Emissivity of the Invert Material

Table 4-21 lists the emissivity of rocks used for the invert material. Justification for use of the data for the invert material is provided in Section 4.1.5. This information is used as input to the models and analyses described in Section 6 and the validation exercises described in Section 7.

Table 4-21. Emissivity of Rocks Used for the Invert

Minimum	Maximum
0.88	0.95

Source: Incropera and DeWitt 1996 [DIRS 108184], Table A.11 for Rocks at 300K.

4.1.16 Direct Inputs from Outside Sources

Table 4-22 lists the direct inputs that are obtained from outside sources. Appendix XVIII contains the demonstrations for each of these sources that it is suitable for its use in this report.

Table 4-22. Direct Inputs Obtained from Outside Sources

Information Used	Reference Identification
Equations for annular radiant heat transfer	Bird et al., 1960 [DIRS 103524]
Linearization of radiant heat transfer, conduction equations in cylindrical and slab systems	Carslaw and Jaeger 1959 [DIRS 100968]
Van Genuchten and retention relations, steady-state unsaturated flow equation	Fetter 1993 [DIRS 102009]
Emissitivity of rock and concrete, thermophysical properties of air and water, Dittus-Boelter heat transfer correlation, definitions, radiation equation for annulus, treatment of air as non-radiant absorber, conditions for boundary layer, constants	Incropera and DeWitt 1996 [DIRS 108184]
Nusselt number definition for forced convection	Kays and Leung 1963 [DIRS 160763]
Natural convection heat transfer in annulus, correlation from experiment	Kuehn and Goldstein 1978 [DIRS 130084]
Effective Reynolds number in mixed flow	Morgan 1975 [DIRS 160791]
Superposition principle	Nagle and Saff 1994 [DIRS 100922]
Physical properties of air	Reid et al. 1977 [DIRS 130310]
Standard atmosphere	White 1986 [DIRS 111015]

4.2 CRITERIA

This section addresses the applicable acceptance criteria from *Yucca Mountain Review Plan, Final Report* (NRC 2003 [DIRS 163274]), the required documentation of level of accuracy (BSC 2004 [DIRS 170950], Section 3.3), and the completion criteria (BSC 2004 [DIRS 170950], Section 3.4). Each of these criteria is detailed below, in separate sections.

4.2.1 Yucca Mountain Review Plan Criteria

The TWP does not state specific acceptance criteria for this report. However, this report provides results that feed indirectly into the model abstraction for quantity and chemistry of water contacting engineered barriers and waste forms. *Yucca Mountain Review Plan, Final Report* (NRC 2003 [DIRS 163274]) lists the following acceptance criteria for that model abstraction (NRC 2003 [DIRS 163274], Section 2.2.1.3.3.3) that are applicable to this report:

- **Acceptance Criterion 1** – System Description and Model Integration Are Adequate.

  (1) Total system performance assessment adequately incorporates important design features, physical phenomena, and couplings, and uses consistent and appropriate assumptions throughout the quantity and chemistry of water contacting engineered barriers and waste forms abstraction process;

  (3) Important design features, such as waste package design and material selection, backfill, drip shield, ground support, thermal loading strategy, and degradation processes, are adequate to determine the initial and boundary conditions for calculations of the quantity and chemistry of water contacting engineered barriers and waste forms;

  (6) The expected ranges of environmental conditions within the waste package emplacement drifts, inside of breached waste packages, and contacting the waste forms and their evolution with time are identified. These ranges may be developed to include:

    (i) the effects of the drip shield and backfill on the quantity and chemistry of water (e.g., the potential for condensate formation and dripping from the underside of the shield);

    (ii) conditions that promote corrosion of engineered barriers and degradation of waste forms;

    (iii) irregular wet and dry cycles;

    (iv) gamma-radiolysis; and

    (v) size and distribution of penetrations of engineered barriers;

- **Acceptance Criterion 2** – Data Are Sufficient for Model Justification.

  (2) Sufficient data were collected on the characteristics of the natural system and engineered materials to establish initial and boundary conditions for conceptual models of thermal-hydrologic-mechanical-chemical coupled processes, that affect seepage and flow and the engineered barrier chemical environment.

- **Acceptance Criterion 3** – Data Uncertainty Is Characterized and Propagated Through the Model Abstraction.

  (1) Models use parameter values, assumed ranges, probability distributions, and bounding assumptions that are technically defensible, reasonably account for uncertainties and variabilities, and do not result in an under-representation of the risk estimate;

  (2) Parameter values, assumed ranges, probability distributions, and bounding assumptions used in the total system performance assessment calculations of

quantity and chemistry of water contacting engineered barriers and waste forms are technically defensible and reasonable, based on data from the Yucca Mountain region (e.g., results from large block and drift-scale heater and niche tests), and a combination of techniques that may include laboratory experiments, field measurements, natural analog research, and process-level modeling studies;

(3) Input values used in the total system performance assessment calculations of quantity and chemistry of water contacting engineered barriers (e.g., drip shield and waste package) are consistent with the initial and boundary conditions and the assumptions of the conceptual models and design concepts for the Yucca Mountain site. Correlations between input values are appropriately established in the U.S. Department of Energy total system performance assessment. Parameters used to define initial conditions, boundary conditions, and computational domain in sensitivity analyses involving coupled thermal-hydrologic-mechanical-chemical effects on seepage and flow, the waste package chemical environment, and the chemical environment for radionuclide release, are consistent with available data. Reasonable or conservative ranges of parameters or functional relations are established;

4.2.2 Required Documentation of Level of Accuracy

The TWP requires this report to state the level of accuracy, precision, and representativeness for the results of the analyses, and how these were determined (BSC 2004 [DIRS 170950], Section 3.3).

4.2.3 Completion Criteria

The TWP (BSC 2004 [DIRS 170950], Section 3.4) requires that the work that is done be consistent with the activities performed as part of *Technical Work Plan: Regulatory Integration Evaluation of Analysis and Model Reports Supporting the TSPA-LA* (BSC 2004 [DIRS 169653]) and that it fulfill a portion of the Phase 2 work identified in that plan. That is, the work should address the prioritized list of actions selected in Phase 1 for disposition in Phase 2 (BSC 2004 [DIRS 169653], Section 1.3).

Another completion criterion in the TWP (BSC 2004 [DIRS 170950], Section 3.4) is that the work satisfy the requirements of AP-16.1, *Condition Reporting and Resolution*, to enable closure of Condition Reports (CRs) CR-2049 and CR-1841D. CR-2049 pertains to providing discussion of criteria to establish that the adequacy of the scientific basis for the model is consistent with the intended use of the model. CR-1841D (Level D) pertains to transparency in the documentation of the conceptual model processes, the validation method, and the criteria used to determine validation.

4.3 CODES, STANDARDS AND REGULATIONS

4.3.1 Codes

This report was prepared to comply with 10 CFR Part 63, the U.S. Nuclear Regulatory Commission rule on high-level radioactive waste. Subparts of this rule that are applicable to data

include Subpart E, Section 114 (Requirements for Performance Assessment). The subpart applicable to models is also outlined in Subpart E, Section 114. The subparts applicable to features, events, and processes (FEPs) are 10 CFR 63.114(d), (e), and (f). Other codes and standards used in this report are ANSI/NCSL Z540-2-1997 [DIRS 157394], *American National Standard for Calibration — U.S. Guide to the Expression of Uncertainty in Measurement*, and ASME PTC 19.1-1998 [DIRS 153195], *Test Uncertainty, Instruments and Apparatus*.

INTENTIONALLY LEFT BLANK

5. ASSUMPTIONS

5.1 REPRESENTATIVE LOCATION WITHIN THE REPOSITORY FOOTPRINT

Northing 234913 and Easting 170730 was chosen as the location within the repository footprint to perform the ventilation analyses because it is representative of rock properties, in situ temperature, and stratigraphy information. This assumption does not require confirmation. The rationale for choosing this location is that the repository lies within the tsw35 geologic unit in this area. In addition, this location is representative because it does not lie on an edge or corner of the repository footprint, and it experiences average infiltration rates. This is used in Section 6.5.1.

5.2 THERMAL PROPERTIES OF A 21-PWR WASTE PACKAGE AS REPRESENTATIVE

The thermal properties of a 21-PWR waste package were used as representative properties for all waste packages emplaced in the repository. This assumption does not require confirmation. The rationale for using these thermal properties is that the 21-PWR accounts for the majority of the repository inventory. This is used throughout Section 6.

5.3 INITIAL WATER SATURATION OF EACH OF THE STRATIGRAPHIC LAYERS

The initial water saturation of the stratigraphic layers is assumed to be approximately 90.5% (a value of 90.54% is used in Appendix II). This assumption does not require confirmation. The rationale for this assumption is that measurements and hydrologic models demonstrate the range of saturation to be between 35 and 99.5%. Sections 6.9.1 and 6.9.2 investigate the effect of a range of matrix saturations on ventilation and Section 6.11 shows that the ventilation efficiency is not sensitive to the choice of saturation. This is used in Section 6.5.2 and Appendix II to account for saturation in obtaining effective thermophysical properties of the stratigraphic units. The sensitivity of the ventilation efficiency with respect to saturation is documented in Section 6.11.

5.4 LITHOPHYSAL PORES ARE AIR-FILLED

The lithophysal pores are assumed to be 100% air-filled. This assumption does not require confirmation. The rationale for this assumption is that, based on water retention theory, large voids do not retain liquid water. This is used in Section 6.5.2 and Appendix II to account for air-filled lithophysal porosity in obtaining effective thermophysical properties of the stratigraphic units.

5.5 INVERT BALLAST MATERIAL

Repository Design Project, Repository/PA IED Emplacement Drift Committed Materials (2) (BSC 2003 [DIRS 164101]) describes the invert ballast material as crushed tuff. The nominal particle diameter of the crushed tuff is not specified. Therefore, the thermophysical properties of a 4-10 crushed tuff (for which these properties have been measured) are used. This assumption

does not require confirmation as the model is not sensitive to this parameter (Section 6.6.2). The rationale for this assumption is that difference in particle sizes has little effect on the bulk thermophysical properties of the material. This is used in Section 6.5.3.

5.6 MIXED CONVECTION CORRELATION

The mixed convection correlation incorporates forced and natural convection correlations from experimental data. The correlations are for idealized configurations that are not the same as the EBS configuration. With one exception, the development of the correlation (documented in Appendix IX) recognizes these idealizations and considers their effects in an uncertainty analysis. The one exception applies to natural convection when the outer convective surface is hotter than the air. During the preclosure period the ventilating air removes heat. Because the drift wall is heated by thermal radiation from the waste package, the drift wall (outer convective surface) will be hotter than the air. The development of the mixed convection correlation assumes that the Kuehn-Goldstein correlation remains valid when the drift wall is hotter than the ventilation air. This assumption does not require confirmation. This is used in Appendix IX. The mixed convection correlation is used throughout Sections 6 and 7 to calculate convection heat transfer coefficients.

5.7 TEMPERATURE OF THE VENTILATION AIR AT THE INLET

The average temperature of the ventilation air at the inlet to the drift is assumed to be equal to the ambient temperature of the host rock. The reason for choosing equality of the inlet air temperature and initial rock temperature is to avoid removing or putting energy into the rock due to a difference in these temperatures. The concept behind this choice is illustrated by considering an inlet air temperature hotter than the rock which will result (initially anyway) in sensible heat from the air being transferred to the rock. This will increase the efficiency because the efficiency is calculated as a temperature difference at the inlet and outlet multiplied by the volumetric heat capacity of the air. Thus, if energy from the hot air is transferred (initially) to the rock from the air, this does not have relevance to the energy removed from the waste package power sources. This difference of the inlet air and initial rock temperatures complicates the calculation of the efficiency because of the transfer of sensible heat from the air to the rock when the objective is to determine how much energy from the waste package power sources is transferred to the air, and to the rock. Thus, the choice of equal inlet air and initial rock temperatures is justified when the ventilation efficiency for the heat removal from waste packages is the calculation objective.

For the Northing and Easting coordinates chosen for analysis, the average temperatures in the ambient state vary from 17°C at the surface to 28°C at the water table (Section 6.5.5). The calculated ambient temperature of the host rock is 22.8°C (Section 6.5.6), which this assumption assigns to the average temperature of the air entering the drift. The study of sensitivity to uncertainty (Section 6.11) assigns 5°C as the standard deviation in inlet air temperature. Because this assignment captures uncertainty introduced by the assumption, the assumption does not require confirmation.

5.8 EMPLACEMENT SCHEDULE

Heat transfer to the rock during emplacement is assumed to be negligible. This assumption does not require confirmation. The rationale for neglecting this transient is that the time scale for placing waste in a drift is small compared to the preclosure period and that the drift will be ventilated during emplacement.

INTENTIONALLY LEFT BLANK

6. MODEL DISCUSSION

Section 6 provides a description of the conceptual models and the scientific, engineering, and mathematical concepts/principles on which the mathematical models are based. Section 6.1 establishes the appropriateness of the model for the purpose of predicting ventilation efficiency, within the limitations stated in Section 1. Direct inputs are listed in Section 4.1. No other corroborating/supporting data, models, or product output were used to develop the model.

A conceptual model and an alternative conceptual model for the preclosure heat transfer in and around a waste emplacement drift are developed, implemented, and documented in this section. Table 6-1 outlines the organization of this section. The primary output of the ventilation model is the ventilation efficiency, defined as the fraction of source heat removed by the ventilating air. The ventilation efficiency is expressed as both an instantaneous efficiency (time and distance from the drift inlet dependent), and an integrated efficiency (instantaneous efficiencies integrated over time and drift length).

Table 6-1. Outline of the Ventilation Model Documentation

Section	Content
6.1	Modeling and analysis objectives.
6.2	Lists and describes FEPs assigned to the ventilation model and a summary of their disposition.
6.3	Develops the conceptual model for preclosure heat transfer in and around a ventilated emplacement drift including the basic mathematical equations. The conceptual model includes thermal radiation, convection, and conduction heat transfer.
6.4	Describes the numerical implementations of the conceptual model using the ANSYS/Excel methodology and an analytical approach.
6.5	Lists additional inputs developed from the inputs of Section 4.
6.6	Presents and discusses the results of the numerical and analytical implementations of the conceptual model described in Section 6.4.
6.7	Develops the alternative conceptual model for preclosure heat transfer in and around a ventilated emplacement drift which includes the effects of moisture in the host rock.
6.8	Describes the implementations of the alternative conceptual model using analytical approaches.
6.9	Presents and discusses the results of the analytical approaches which implement the alternative conceptual model.
6.10	Discusses the applicability of the downstream use of the output of the ventilation model (i.e., ventilation efficiency) as a means of representing the preclosure heat transfer to initialize postclosure analyses.
6.11	Discusses the uncertainties associated with the ventilation modeling approaches and the design inputs and parameters, and quantifies the sensitivity of the model output (i.e., ventilation efficiency).

6.1 MODELING OBJECTIVES

The thermal energy removed by ventilation is determined by analyzing thermal radiation, thermal convection, and thermal conduction which occur simultaneously in the drift and the surrounding rock mass. The ventilation efficiency, expressed as the percentage of the total thermal energy removed by convection, is the primary output of the ventilation modeling. The ventilation efficiency is used as input in downstream models that do not explicitly simulate the preclosure period. Examples of these models include the multiscale thermohydrologic, UZ coupled process, and drift degradation models. The ventilation modeling and analysis objectives are to:

1. Develop a conceptual model for preclosure ventilation of an emplacement drift (Section 6.3).

2. Implement the ventilation conceptual model using developed software and methods, and the License Application design basis inputs and parameters to predict the preclosure ventilation efficiency (Section 6.4).

3. Verify the results of the numerical application of the ventilation conceptual model through comparative analyses (Section 6.6).

4. Develop an alternative conceptual model for preclosure ventilation which includes the impacts of water and water vapor mass transfer on the heat transfer (Section 6.7).

5. Implement the alternative conceptual model using analytical calculations to assess the impacts of moisture on the ventilation efficiency (Sections 6.8 and 6.9).

6. Demonstrate the applicability of the use of the ventilation efficiency as an abstraction method for downstream postclosure models to account for the preclosure heat removal (Section 6.10).

7. Demonstrate the sensitivity of the ventilation efficiency to discretization and uncertainties in key input parameters associated with the host rock and engineered components including thermal conductivity, matrix and lithophysal porosity, specific heat, emissivity, and convection heat transfer coefficient (Sections 6.6.1 and 6.11).

6.2 FEATURES, EVENTS, AND PROCESSES

Table 6-2 provides a listing of FEPs addressed in this document, in accordance with the TWP (BSC 2004 [DIRS 170950]) and DTN: MO0407SEPFEPLA.000 [DIRS 170760]. The table provides specific references to sections within this document.

Table 6-2. Included FEPs Addressed in This Document

FEP Number	FEP Name	Section Where Addressed
1.1.02.02.0A	Preclosure ventilation	Section 6.6
2.1.08.03.0A	Repository dryout due to waste heat	Sections 6.6 and 6.7

6.3 CONCEPTUAL MODEL FOR IN-DRIFT VENTILATION

Thermal energy released from the waste packages is transferred to the in-drift and host rock surroundings. During the preclosure period, some heat will be removed from the waste packages and emplacement drift by the ventilation system. The heat transfer processes are time and axial position (i.e., the distance down the length of the drift from the airflow entrance point) dependent. A description of the conceptual model follows. No corroborating/supporting data, models, or product output was used to develop the model.

6.3.1 Heat Transfer Processes

The heat transfer processes for ventilation of an emplacement drift are shown in Figure 6-1. Figure 6-1 also includes other heat and mass transfer processes that will be outlined later in Section 6.7 where the alternative conceptual model for ventilation is presented.

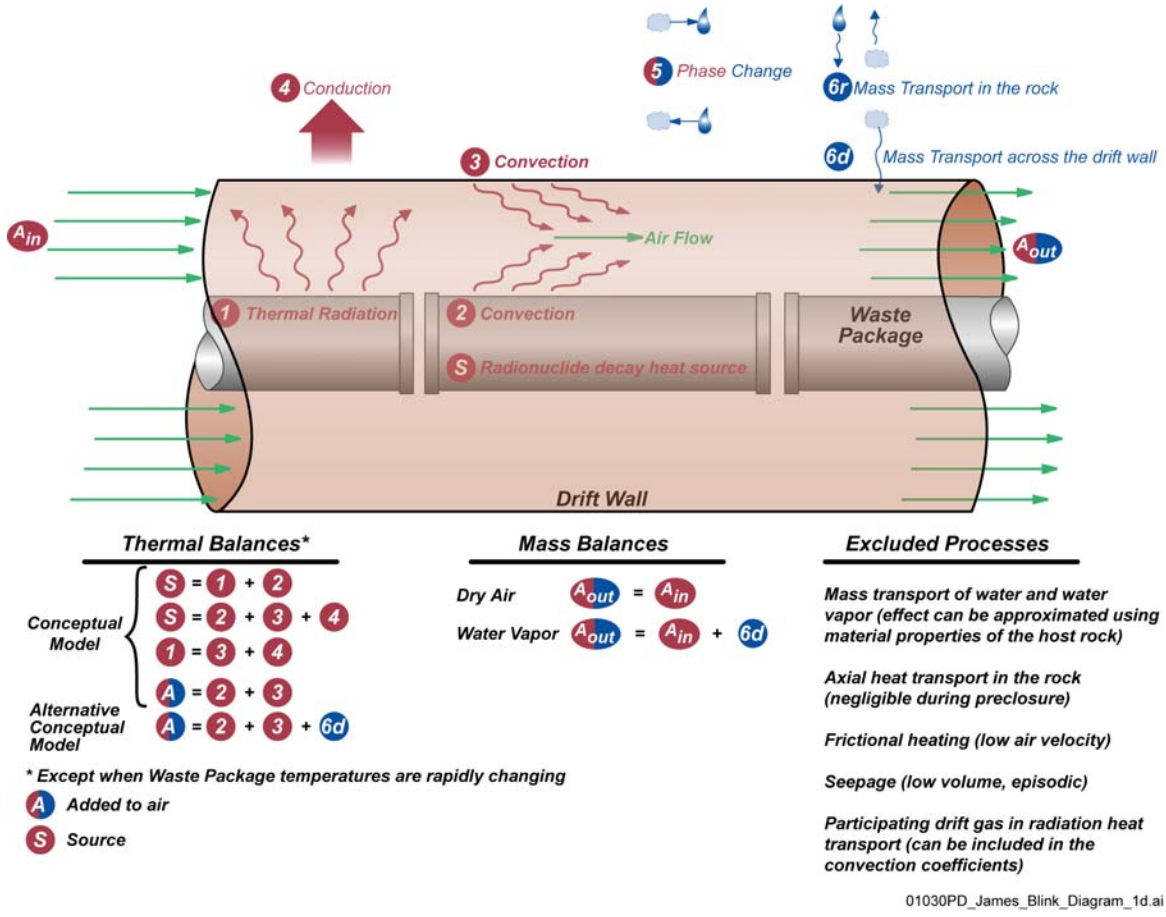

Figure 6-1. Conceptual Model for Heat and Mass Transfer Within and Around an Emplacement Drift

The heat transfer processes depicted in Figure 6-1 include:

Process 1.

Thermal radiation heat transfer from the surface of the waste package to the drift wall. The rate at which the heat is transferred is calculated using the Stefan-Boltzmann Law for gray surface radiation exchange, at any time during the preclosure period, using the waste package surface and drift wall temperatures. This calculation also requires knowledge of the geometry and emissivities of the waste package and drift wall surfaces.

Process 2.

Convective heat transfer from the surface of the waste package to the airflow due to the temperature differences between the surface and the moving air. The heat flow rate can be calculated using Newton's Law of Cooling at any time during the preclosure period, using the bulk temperature of the airflow and the temperature of the waste package surface. This calculation also requires knowledge of the convective heat transfer coefficients that implicitly describe the effects of the airflow, the drift geometry, the thermal conductivity of air, and the surface properties on the heat transfer rates. The correlations used (Apendix IX) have simple thermal conduction as a limiting case.

Process 3.

Convective heat transfer from the drift wall surface directly to the airflow due to the temperature differences between the wall surface and the moving air, similar to process 2. The sum of the two convective heat transfer rates determines the rate of energy addition to the moving air, and can be used to calculate the axial rate of air temperature increase. This calculation also requires knowledge of the convective heat transfer coefficients that implicitly describe the effects of the airflow, the drift geometry, and surface properties on the heat transfer rates. Axially along the drift, the convective heat transfer (processes 2 and 3) is combined with the air mass flow rate and its specific heat to calculate the axial change of air temperature.

Process 4.

Conductive heat transfer within the rock mass due to changes in drift wall temperature. The heat flow rate into the rock can be determined using Fourier’s Law of Conduction, at any time during the preclosure period, using the temperature gradient in the rock mass. This calculation requires knowledge of the thermal conductivity, saturation, density, and heat capacity of the rock (which vary spatially).

The heat transfer for the processes described above can be related by considering the overall conservation of thermal energy except during the early transient response when the waste package temperature is rapidly changing. The following summarizes the coupled components of

the thermal energy conservation during quasi-steady-state conditions when energy storage is relatively constant:

- The sum of the radiative heat transfer rate from the waste package to the drift wall (process 1 from above), and the convective heat transfer rate from the waste package into the airflow (process 2), must equal the total rate of heat released from the waste package.

- The sum of the convective heat transfer rates from the waste package and drift wall into the airflow (processes 2 and 3), and the conductive heat transfer rate into the rock (process 4), must equal the total rate of heat released from the waste package.

- The sum of the convective heat transfer rates from the drift wall into the airflow (process 3), and the conductive heat transfer rate into the rock (process 4), must equal the rate of radiant heat released from the waste.

Five additional processes have not been explicitly included in the conceptual model. The first includes the mass transport of water and water vapor and the coupled latent and sensible heat transfer associated with the phase change and movement of water. However, these latent heat effects and near-field host rock mass transport processes can be approximated using boiling point temperature dependent values for the thermal conductivity and specific heat of the rock. This can account for vaporization of pore water and dryout in an approximate sense, but cannot accurately track changes of saturation and evolution of properties. In most cases, the temperatures needed to change these properties are not reached during the preclosure period. These processes are presented in greater detail in Section 6.7.

The second process excluded from the conceptual model is the axial transport of heat and mass within the rock domain. This process has negligible influence on the ventilation efficiency during the 50-year preclosure period due to the small thermal diffusivity of rock ($\sim 1 \times 10^{-7}$ m^2/s) and the large (hundreds of meters) scale of the repository footprint. The axial heat transport process, especially about the end of the drift, is captured in the multiscale thermohydrologic model.

The third process not included in the ventilation conceptual model is the frictional heating of the air and engineered components due to the moving air. This process is negligible when compared to the waste package heat source due to the low air flow velocities.

The fourth process not included in the ventilation conceptual model is episodic flow of liquid water into the drift air (due to heterogeneities in the host rock and episodic infiltration). The total heat added to the airflow by vaporizing such seeps is small compared to the heat from radionuclide decay. It should be noted here that the alternative conceptual model does account for vaporization of liquid water within the host rock and movement of the vapor into the drift, but that process adds only the sensible heat due to the temperature difference between the entering water vapor and the airflow.

Finally, the fifth process not included in the ventilation conceptual model is the participation of the drift gas in the radiation process. Water vapor is an effective absorber of infrared radiation;

however, the effect of its absorption and re-radiation of thermal energy is negligible due to low in-drift relative humidity (absolute humidity much less than one atmosphere) during the ventilation period.

6.3.2 Heat Transfer Equations for the Ventilation Model

The following three equations represent energy balances for processes 1, 2, and 3 as outlined above in Section 6.3.1 and Figure 6-1:

$$Q_s = \pi L \cdot \left[d_s h_{rad} \left(T_s^4 - T_w^4 \right) + d_s h_s \left(T_s - T_{air-bulk} \right) \right] \quad \text{(Eq. 6-1)}$$

$$Q_w = \pi L \cdot \left[d_s h_{rad} \left(T_s^4 - T_w^4 \right) - d_w h_w \left(T_w - T_{air-bulk} \right) \right] \quad \text{(Eq. 6-2)}$$

$$\left(\dot{m} C_p \right)_{air} \left(T_{out} - T_{in} \right) = \pi L \cdot \left[d_s h_s \left(T_s - T_{air-bulk} \right) + d_w h_w \left(T_w - T_{air-bulk} \right) \right] \quad \text{(Eq. 6-3)}$$

where

Q_s = heat generated by the waste package (W)
Q_w = heat transferred into the rock by convection and radiation (W)
T_s = waste package surface temperature (K)
T_w = drift wall temperature (K)
$T_{air\text{-}bulk} = (T_{air\text{-}in} + T_{air\text{-}out})/2$ (K)
T_{in} = ventilation air temperature at the drift segment inlet (K)
T_{out} = ventilation air temperature at the drift segment outlet (K)
h_s = waste package surface convection heat transfer coefficient ($W/m^2 \cdot K$)
h_w = drift wall convection heat transfer coefficient ($W/m^2 \cdot K$)
h_{rad} = radiation heat transfer coefficient ($W/m^2 \cdot K^4$)
L = drift segment length (m)
d_s = waste package diameter (m)
d_w = drift diameter (m)
$\dot{m}$ = ventilation mass flow rate (kg/s)
C_p = specific heat of air (J/kg·K)

In the above definitions, temperatures are averages over applicable surfaces. The heat transfer coefficients are effective coefficients for circumferentially integrated heat transfer using averaged temperatures.

6.3.3 Mixed Convection Heat Transfer Coefficient Correlation

Energy from the waste package is transferred to the ventilating air by a combination of forced and natural convection, or mixed convection. Morgan developed a general approach for calculating the average heat transferred from horizontal cylinders in mixed convection for various flow regimes and various flow directions (Gebhart et al. 1988 [DIRS 152234], Section 10.4.1). While this approach can be used for the YMP geometry, the specific correlations cannot (they are for external flow). The approach is simplistic:

- Calculate an effective Reynolds number for mixed convection.
- Use the mixed convection Reynolds number to calculate a mixed convection Nusselt number.
- Use the mixed convection Nusselt number to calculate a mixed convection heat transfer coefficient. The drift wall and waste package surfaces are considered independently, thus coefficients for each wall are derived.

Calculating the Reynolds number for forced convection is completed using the definition for Reynolds number for flow in a circular tube (Incropera and DeWitt 1996 [DIRS 108184], p. 421, Equation 8.1).

Calculating the Reynolds number for natural convection is not as straightforward. It involves first using literature-provided correlations to calculate a Nusselt number for pure natural convection, and then using this value with the chosen forced convection correlation to determine a Reynolds number that would result in the same heat transfer. The Kuehn-Goldstein (1978 [DIRS 130084]) correlation is generally accepted as the best available model for natural convection, and was chosen for the mixed convection model. The correlation defines Nusselt numbers for the inner and outer cylinders as a function of the Rayleigh number and constants derived from experimental data. The Kays-Leung (1963) model for forced convection in a circular annulus was chosen as the forced convection correlation. In this model the Nusselt number is defined as a function of the heat fluxes and temperatures of the surfaces, and influence coefficients. The influence coefficients are semi-empirical in nature and were determined in conjunction with experimental data. The radii of the cylinders, Reynolds number, and the fluid's Prandtl number influence the values.

The two Reynolds numbers are then combined to give a "mixed" Reynolds number (using Morgan's approach) as the square root of the sum of the squares of the Reynolds number for forced convection and an equivalent Reynolds number for natural convection. Once a "mixed" Reynolds number is calculated, it can be used in conjunction with the chosen forced convection model (Kays and Leung 1963 [DIRS 160763]) to determine the heat transfer coefficients from the inner (waste package) and outer (drift wall) surfaces.

Appendix IX of this report provides a detailed review of the mixed convection correlation, including the development of the method, a review of the sensitivity of the method to each of its parameters, the estimated uncertainty in the heat transfer coefficients predicted by the method, and a comparison of the method results to experimental data from the ventilation tests. Based on these analyses, the mixed convection correlation is valid for the flow conditions attributed to the design parameters presented in Section 4, including a ventilation air flow rate between 10 and 30 m^3/s.

6.3.4 Radiation Heat Transfer Coefficient

The radiation heat transfer coefficient is calculated from an analytical solution for concentric cylinders (Incropera and DeWitt 1996 [DIRS 108184], p. 739, Table 13-3):

$$h_{rad} \equiv \frac{\sigma A_s}{\frac{1}{e_s} + \left(\frac{1-e_w}{e_w}\right) \cdot \frac{d_s}{d_w}} \quad \text{(Eq. 6-4)}$$

where

σ = Stefan-Boltzmann constant ($W/m^2 \cdot K^4$)
e_s= surface emissivity of source
e_w= surface emissivity of drift wall

Because the geometry is eccentric rather than concentric, the local radiation heat transfer coefficients are not constant, being larger at the bottom of the con figuration and smaller at the top. However, the value calculated from Equation 6-4 is a reasonable approximation to the effective coefficient for circumferentially integrated energy transfer using averaged temperatures.

6.3.5 Ventilation Efficiency

The instantaneous ventilation efficiency is both a function of time and distance from the entrance and is defined by:

$$\eta(t,x) \equiv \frac{Q_{air}(t,x)}{Q_s(t)} \quad \text{(Eq. 6-5)}$$

where

$\eta(t,x)$ = instantaneous ventilation efficiency (dimensionless)
Q_{air} = heat convected to the air from the waste package and drift wall surfaces (W/m)
Q_s = heat generated by the waste package (W/m)
t = time since ventilation began
x = distance from the drift entrance (m)

The integrated ventilation efficiency is defined by:

$$\eta_{\text{integrated}} \equiv \frac{\int_0^b \left[\int_0^a Q_{air}(t,x) \cdot dx \right] dt}{x \cdot \int_0^b Q_s(t) \cdot dt} \quad \text{(Eq. 6-6)}$$

where

$\eta_{integrated}$ = integrated ventilation efficiency (dimensionless)
a = limit of integration in terms of the total drift length
b = limit of integration in terms of the total ventilation duration

6.4 NUMERICAL APPLICATION OF THE CONCEPTUAL MODEL

Two numerical applications and one analytical application of the conceptual model for in-drift ventilation heat transfer are performed. The two numerical applications use the ANSYS software code, and the analytical uses a spreadsheet. The results of each application are compared later in Section 6.6. The first ANSYS based application, named ANSYS-LA-Coarse, divides the drift into segments of 1, 10, 100, 200, 300, 400, 500, 600, 700, and 800 meters. The second ANSYS based application, named ANSYS-LA-Fine, divides the drift into 24 equal segments of 25 meters, for a total of 600 meters. The spreadsheet application, named Analytical-LA-Coarse, is similar to the ANSYS-Coarse model, and was developed to benchmark the analytical approach against ANSYS.

6.4.1 ANSYS Methodology

The ANSYS methodology implemented to calculate the various dependent variables in the ventilation model is based on the following energy balances shown in Equations 6-1 through 6-3:

- The waste package is the power source in the drift and transfers heat (actually power, i.e., energy per unit time) to the flowing air by forced convection and to the drift wall by radiant heat transfer. The energy balance based on these two heat transfer mechanisms is written in Equation 6-1. In the methodology, the energy is removed uniformly from the surface of the waste package.

- The drift wall, as a cylindrical surface, receives energy by radiant heat transfer from the waste package, transfers energy to the flowing air by forced convection, and transfers energy into the rock by conduction. The energy balance based on these three heat transfer mechanisms is written in Equation 6-2. In the methodology, the energy from radiation and convection is transferred uniformly into the drift wall.

- The flowing air stream receives energy from the two convection surfaces (i.e., the waste package surface and the drift wall, and the resulting temperature change is written in the energy balance in Equation 6-3).

The energy balance that describes the temperature of the drift wall, and in the rock, is written as a two-dimensional transient heat conduction equation for a cylinder in a medium bounded vertically by the location of the mountain surface, the water table, and two vertical insulated boundaries located (usually) equidistant horizontally (to the left and right). There is no heat transfer in the rock along the axis of the drift. Thus, at this point in this methodology description there are three explicit energy balance equations and one implicit (the transient energy balance).

Implementation of the ANSYS methodology proceeds by dividing the total drift length into a number of equal lengths, or segments. Within each segment the energy balances for the waste-package surface, drift wall surface, and rock mass, are solved with the restriction that the inlet air temperature is held (fixed) constant at its inlet value for the duration of a time step (a form of explicit time-stepping). For the first segment that receives (fresh) air this temperature is usually fixed for the entire ventilation duration. Information supplied to ANSYS includes the heat transfer coefficients for the waste package and drift wall surfaces, the dimensions of the waste

package and drift wall, the waste package power as a function of time, and the inlet air temperatures in the form of a lookup table, and the thermophysical properties of the surrounding rock layers. The transient solution is then calculated for each time step up to some specified ventilation duration. Then, in order to calculate the exiting air temperature from the segment, the energy that was transferred to the fixed air temperature for each time step is used to calculate this exiting air temperature based on the total flow (in the time step) and heat capacity of air. This exiting air temperature for this segment for this time step then becomes the inlet air temperature to the next segment. This air exit-temperature calculation is performed external to ANSYS in a spreadsheet.

The waste-package power is specified as the average linear power density, for example, kilowatts per meter. This specified linear power density is applied to the entire segment as if the waste package were continuous over the entire segment. This representation is appropriate for the close end-to-end spacing of the waste packages (i.e., 0.1 meter).

By fixing the air temperature at the inlet value for the duration of the time step, an assertion is made that the (air) temperature within a segment is everywhere the same (i.e., the air is well-mixed). The concept of a well mixed segment, sometimes referred to as a volume element, is invoked in the engineering design of plug-flow, or "pipe" reactors, and thus this concept has been extensively used in other applications. It can be shown that a series of well-mixed volume elements approximates a plug flow reactor with the restriction that the total volume of the well-mixed volume elements equals that of the plug flow reactor (Levenspiel 1972 [DIRS 156839], p. 137). This concept of a well-mixed volume element means that the air temperature is not a function of location in a segment, even though it is intuitive that the air temperature increases as a function of increasing position within the segment. However, when invoking the concept of a well-mixed volume element, there is no difference in the temperature at the beginning of the segment relative to that at the end of the segment. The question that then arises is: How many segments must be specified in order to obtain results that are considered to be descriptive of the tubular flow situation? The number of series segments is determined by comparing results when the number of segments is increased (through a range) and it is observed that the results do not change; this is sometimes called a "discretization" study.

6.4.1.1 Radiation Heat Transfer Model

Use of the Stefan-Boltzmann Law to calculate the radiative heat transfer between the surface of an eccentrically located waste package and the drift wall requires the following:

1. An assumption that the in-drift air does not participate in the radiation heat transfer by absorbing significant amounts of energy that would have been otherwise transferred to the drift wall.

2. Appropriate values for the emissivities of the waste package and drift wall surfaces.

3. An assumption that the use of equation 6-4 is appropriate for the YMP geometry.

Emissivity values and their corresponding sources are presented in Section 4 of this report. Emmisivity values were taken from standard engineering sources that are generally accepted in the engineering community. Further confidence is established in the emissivity values through

the fact that the standard deviations of the emissivities of the waste package and drift walls have a negligible effect on the ventilation efficiency based on the sensitivity study presented in Section 6.11 (Table 6-10).

The use of the Stephan-Boltzmann law for thermal radiation heat transfer between the surfaces of the waste package and the drift wall, and also the use in this report of a radiation heat transfer coefficient, are corroborated extensively in the engineering literature. The manner in which radiation heat transfer is described in Section 6.4.2.1 (Eq. 6-11) and described in detail in Section 6.4.2.3, is corroborated by the following engineering references. Kern (1950 [DIRS 130111], p.77) describes a fictitious film coefficient to represent the rate at which radiation transfers heat from one surface to another. This film coefficient is of the form of a heat transfer rate that is proportional to a temperature difference, not a difference of the fourth power of the temperatures. Perry et al. (1984 [DIRS 125806], p. 10-13) also describe this technical approach for radiant heat transfer in the form of a "radiation film coefficient." This description clearly shows that the radiation heat transfer coefficient is a slowly varying function of the temperature difference of the two surfaces, and thus allows the linearization and use as illustrated in Section 6.4.2.1. Also, McAdams (1954 [DIRS 161435], p.78) describes yet another form of this technical approach for the expression of radiation in the form of a first power difference relation for use in combining radiation heat transfer with convection. Thus, the method of determining radiation heat transfer as described in Section 6.4.2.1, and specifically derived in Section 6.4.2.3 is validated through the substantive corroboration with open engineering literature. Additional confidence is achieved by demonstrating that the use of this equation conforms to generally accepted physical principals (i.e. conservation of energy) through its use in the energy balances described in Section 6.3.2 for the ventilation heat transfer model, and the subsequent validation of that model.

For enclosures such as an emplacement drift, a medium such as air that separates the radiating surfaces is said to be nonparticipating if it neither absorbs nor scatters the thermal radiation, and it emits no radiation itself. Incropera and DeWitt (1996 [DIRS 108184], Section 13.5) state that:

> The foregoing conditions and the related equations [summarized in Section 6.3.4 of this report] may often be used to obtain reliable first estimates and, in most cases, highly accurate results for radiation heat transfer in an enclosure…. For *nonpolar* gases, such as O_2 or N_2, such neglect [of participating gaseous radiation] is justified, since the gases do not emit radiation and are essentially transparent to the incident thermal radiation. However, the same may not be said for polar molecules, such as CO_2, H_2O (vapor), NH_3, and hydrocarbon gases, which emit and absorb over a wide temperature range.

The design of the preclosure ventilation system draws air from the outside environment to the intake shafts and then to the emplacement drifts. The initial composition of the ventilation airstream will resemble that of the outside air, or approximately 78% N_2 and 22% O_2 with some small fraction of water vapor. The composition of the ventilation airstream may change as it proceeds through the emplacement drift and acquires additional water vapor and CO_2 from the host rock. The analysis in Section 6.9.1, *Moisture Effects on the In-Drift Ventilation Air Stream*, shows that the ventilating air would have a relative humidity of 7.3% and a temperature of 42°C at the end of 50 years. Under these conditions, the amount of water vapor in the air would be less than 1% by mass. The range of relative humidities observed in the Exploratory Studies

Facility was 10 to 40% with occasional increases over 60% (Section 4.1.2). The maximum temperatures recorded in this zone of the ECRB were near 30°C. Because warmer air can hold more water vapor than cooler air, a conservative estimate of the effects of water vapor on the radiation calculations would be to assume 60% relative humidity and 30°C. These conditions represent a conservative estimate because the water vapor content in the air would be a theoretical maximum under the measured conditions. Air at 30°C and 60% relative humidity has a water vapor content of less than 2% by mass, which supports the assumption that the effects of water vapor on radiation can be neglected.

6.4.1.2 Convection Heat Transfer Model

The use of convective heat transfer coefficients as used in this report to describe the transfer of energy between a flowing fluid and a surface is seen extensively in the engineering literature. The manner in which convective heat transfer is described and used in section 6.4.2.1 (Equations 6-8, 6-9, and 6-11) is corroborated by the following engineering references. Kern (1950 [DIRS 130111], p.3) presents a mathematical form of convective heat transfer which imitates the form of the conduction equation; that is the energy that is transferred is proportional to the product of the area through which the heat is transferring and the temperature difference between the participating media. The proportionality constant is called the heat transfer coefficient and is usually denoted by the letter "h." When the fluid is flowing, as is the case during ventilation, the heat transfer process is called "forced convection." McAdams (1954 [DIRS 161435], p. 187) also discusses the concept of convective heat transfer coefficients, and further distinguishes local and overall heat transfer coefficients. These coefficients pertain to one surface (local) or many surfaces such as the inside and outside of a pipe (overall). The heat transfer coefficients as used for the waste package surface and drift wall surface in section 6.4.2.1 are local heat transfer coefficients.

6.4.1.3 Host Rock Conduction Heat Transfer Model

Conduction heat transfer dominates other heat transfer mechanisms (i.e., convection in fractures and lithophysae, and latent heat) in the host rock (Sass et al. 1988 [DIRS 100644], p. 35). This is supported by conclusions of data and modeling of the Drift Scale Test (Birkholzer and Tsang 2000 [DIRS 154608], p. 1439). For the level of confidence required for the ventilation model, the assertion that conduction dominates the heat transfer in the host rock is consistent with the validity of the conceptual model.

6.4.2 Analytical Approach

The ventilation calculation technique described in this section is based on the same heat-transfer physics used in the previous ANSYS methodology description in Section 6.4.1. The only change relative to the ANSYS methodology here is in the calculation techniques used to solve the heat transfer equations. This technique is based on two technical approaches to problem solving: the use of a steady-state approximation, and the principle of superposition to calculate the temperature response of the drift wall due to an arbitrary heat flux. By implementing these two techniques, it is not necessary to perform a stand-alone spreadsheet calculation for the air temperature from segment to segment, and there is no requirement to solve the energy equation for the drift wall (rock mass) for every segment.

The use of the steady-state approximation, sometimes referred to as a quasi-steady-state approximation, allows the energy balance equations to be written with no time derivatives, only algebraic equations which can then be solved by any number of methods. The solution method used here is to algebraically solve the resulting equations, where there are four equations and four unknowns. The energy balance equations derived as a result of using the steady-state approximation apply for the duration of a time step. The progress of the calculation through time is exactly like that of integrating a function using Euler's method for numerical integration, summing a "stair-step" approximation. Each step represents a steady state for a particular time interval.

Application of the superposition technique is based on the repeated use of a single temperature response of the drift wall due to a short-duration constant flux. This short-duration constant flux is referred to as a "pulse." By repeatedly applying a series of short-duration scaled constant fluxes to the drift wall, the resulting temperature due to an arbitrary flux can be calculated. Thus the arbitrary flux is approximated like "stair steps." Part of the ventilation calculation then involves calculating the temperature response of the drift wall due to a single short-duration constant flux, and demonstrating that the short duration, which is the time step, is sufficient to allow the drift-wall temperature to be calculated by superposition for the time-varying fluxes of interest. This temperature response must be calculated independently of the ventilation calculation itself, but is calculated only once for a given set of thermophysical rock properties. The use of a time-series of a constant flux (pulses) to calculate the temperature of the drift wall as a function of time is presented in Section 6.4.2.2.

6.4.2.1 Derivation of the Energy Balance Equations that Describe an Algebraic Solution for Ventilation Calculations

This section describes the derivation of the energy balance equations of the analytical ventilation heat-transfer process. This derivation uses a common engineering concept described earlier, well-mixed volume elements. In a well mixed volume element the variables of interest, such as temperature, are everywhere the same. The concept of a well-mixed volume element appears under different names in the engineering literature such as backmix reactor, or continuous-stirred-tank-reactor (Levenspiel 1972 [DIRS 156839], p. 139). Using this concept, the drift is divided into a number of well-mixed volume elements that are in series, and the output of air from one is the input to the next (as is done in the ANSYS methodology).

The energy balance equations for the algebraic ventilation calculation derivation that follows uses a linearized radiant heat transfer coefficient, as discussed previously (Perry et al. 1984 [DIRS 125806], p. 10-13). The use of a linearized radiant heat transfer coefficient introduces a trial-and-error calculation itself, but has been found to converge very quickly using a successive approximation solution. This linearization does away with the nonlinear nature of radiant heat transfer. The details on the use of the linearized radiant heat transfer coefficient are presented in Section 6.4.2.3.

The objective of this derivation is to obtain algebraic expressions for the four dependent variables of interest, these are the air temperature, T (no subscript), drift-wall temperature, T_w, the power-source (waste-package) surface temperature, T_s, and the total energy per unit time conducted into the drift wall (into the rock), Q_{wall} (which when divided by the drift-wall area yields an energy flux).

Consider a well-mixed volume element of a tunnel, or tube, with a heated source inside, air moving through this tunnel, at steady state. A volume element is defined by the "air" volume in a specified length of tunnel. The net energy per time transported by air advection through the element is written as:

$$(T - T_{in})\dot{m}C_p = Q_{air} \quad \text{(Eq. 6-7)}$$

where $\dot{m}$ ("m dot") is the air mass flow rate (kg/s), C_p is the heat capacity of air at constant pressure, T_{in} is the inlet air temperature (K), and Q_{air} is the net energy/time transported by the air. The air in the volume element is considered well mixed (i.e., a continuous stirred tank reactor or backmix reactor) thus T is the same everywhere in the volume element.

The energy per time transferred from the heated source or waste package to the air by convection is written as:

$$q_{sa} = h_s A_s (T_s - T) \quad \text{(Eq. 6-8)}$$

where h_s is the appropriate heat transfer coefficient ($W/m^2 \cdot K$), A_s is the area of the source in the well-mixed volume element (m^2), and T_s is the temperature of the source (surface). The energy per time transferred from the tunnel wall to the air by convection (q_{wa}) is written as:

$$q_{wa} = h_w A_w (T_w - T) \quad \text{(Eq. 6-9)}$$

where h_w is the appropriate heat transfer coefficient ($W/m^2 \cdot K$), A_w is the tunnel-wall area in the well-mixed volume element (m^2), and T_w is the tunnel-wall temperature (K). Note that the sign convention is positive toward the air and negative away from the air.

Energy per time transferred to the air occurs only from the wall and source, so replacing Q_{air} in Equation 6-7 with q_{sa} and q_{wa} from Equations 6-8 and 6-9:

$$(T - T_{in})\dot{m}C_p = Q_{air} = h_s A_s (T_s - T) + h_w A_w (T_w - T) \quad \text{(Eq. 6-10)}$$

Now consider the heated source. All of the energy per time is lost instantaneously; the change, if any, in the heat content of the source is negligible compared to the heat lost. The energy per time balance for the source is written as:

$$h_s A_s (T_s - T) + h_{rs} A_s (T_s - T_w) - p_s = 0 \quad \text{(Eq. 6-11)}$$

where p_s is the source power in the well-mixed volume element (W), the second term on the right is the energy per time transferred to the wall by radiant heat transfer, and h_{rs} is a linearized radiant heat transfer coefficient discussed in Section 6.4.2.3.

The energy per time balance at the wall is written on a coordinate frame where energy per time transferred to the wall (surface) is positive, thus:

$$h_{rs} A_s (T_s - T_w) - h_w A_w (T_w - T) - Q_{wall} = 0 \qquad \text{(Eq. 6-12)}$$

where the first term is the radiant energy per time transferred to the wall for $T_s > T_w$, and is thus positive; the second term is the convective energy per time transferred from the wall to the air for $T_w > T$, and is thus negative; and Q_{wall} is the energy per time transferred by conduction into (from) the wall (medium) in the well-mixed volume element, and is thus negative. Q_{wall} itself can be either negative or positive.

Consider now the approximations that can be made for short time intervals in the well-mixed volume element. Fix the wall flux, Q_{wall}/A_w, and the source energy per time, p_s, for a yet to be determined time interval (time step). In order to progress with respect to time, approximate the power source and wall flux as a series of constant fluxes (not the same). Section 6.4.2.2 describes the details of how a series of constant fluxes (also known as finite-width pulses) can be used to predict the drift-wall temperature. With Q_{wall} and p_s fixed for a short time interval, Equations 6-11 and 6-12 can be used to eliminate T_s and T_w from Equation 6-10.

Rearrange Equation 6-11 as:

$$A_s (h_s + h_{rs}) T_s - A_s h_{rs} T_w = p_s + A_s h_s T \qquad \text{(Eq. 6-13)}$$

And rearrange Equation 6-12 as:

$$A_s h_{rs} T_s - (A_s h_{rs} + A_w h_w) T_w = Q_{wall} - A_w h_w T \qquad \text{(Eq. 6-14)}$$

Rewrite Equations 6-13 and 6-14 in matrix notation as:

$$\begin{bmatrix} A_s (h_s + h_{rs}) & -A_s h_{rs} \\ A_s h_{rs} & -(A_s h_{rs} + A_w h_w) \end{bmatrix} \begin{bmatrix} T_s \\ T_w \end{bmatrix} = \begin{bmatrix} p_s + A_s h_s T \\ Q_{wall} - A_w h_w T \end{bmatrix} \qquad \text{(Eq. 6-15)}$$

Write the determinant of the 2×2 matrix as:

$$D \equiv -A_s (h_s + h_{rs})(A_s h_{rs} + A_w h_w) + A_s^2 h_{rs}^2 \qquad \text{(Eq. 6-16)}$$

Expand D to obtain:

$$D = -A_s^2 h_s h_{rs} - A_s A_w h_s h_w - A_s^2 h_{rs}^2 - A_s A_w h_{rs} h_w + A_s^2 h_{rs}^2 \qquad \text{(Eq. 6-17)}$$

Cancel the squared terms to obtain:

$$D = -(A_s^2 h_s h_{rs} + A_s A_w h_s h_w + A_s A_w h_{rs} h_w) \qquad \text{(Eq. 6-18)}$$

And finally obtain by factoring out $A_s A_w h_w$ from the second and third terms:

$$D = -\left[A_s^2 h_s h_{rs} + A_s A_w h_w (h_s + h_{rs})\right] \quad \text{(Eq. 6-19)}$$

Now solve for T_s using Cramer's rule. Do this by replacing column 1 in the 2×2 matrix with the right side of matrix Equation 6-15, the forcing vector, and obtain (multiply by D to obtain DT_s):

$$DT_s = \begin{bmatrix} p_s + A_s h_s T & -A_s h_{rs} \\ Q_{wall} - A_w h_w T & -(A_s h_{rs} + A_w h_w) \end{bmatrix} \quad \text{(Eq. 6-20)}$$

Expand the 2×2 determinant to obtain:

$$DT_s = -(p_s + A_s h_s T)(A_s h_{rs} + A_w h_w) + A_s h_{rs}(Q_{wall} - A_w h_w T) \quad \text{(Eq. 6-21)}$$

Collect the coefficient of T, and a constant:

$$DT_s = (-A_s h_s (A_s h_{rs} + A_w h_w) - A_s h_{rs} A_w h_w)T + A_s h_{rs} Q_{wall} - p_s (A_s h_{rs} + A_w h_w)$$

(Eq. 6-22)

Rearrange the coefficient of T to obtain:

$$DT_s = -(A_s^2 h_s h_{rs} + A_s A_w h_w (h_s + h_{rs}))T + A_s h_{rs} Q_{wall} - p_s (A_s h_{rs} + A_w h_w)$$

(Eq. 6-23)

Note that the coefficient of T above is D as given by Equation 6-19, so dividing by D to obtain T_s yields:

$$T_s = T + \frac{-Q_{wall} A_s h_{rs} + p_s (A_s h_{rs} + A_w h_w)}{A_s^2 h_s h_{rs} + A_s A_w h_w (h_s + h_{rs})} \quad \text{(Eq. 6-24)}$$

Solve for T_w in the same manner from Equation 6-15 by replacing column 2 with the forcing vector to obtain:

$$DT_w = \begin{bmatrix} A_s (h_s + h_{rs}) & p_s + A_s h_s T \\ A_s h_{rs} & Q_{wall} - A_w h_w T \end{bmatrix} \quad \text{(Eq. 6-25)}$$

Expand the determinant to obtain:

$$DT_w = A_s (h_s + h_{rs})(Q_{wall} - A_w h_w T) - (p_s + A_s h_s T) A_s h_{rs} \quad \text{(Eq. 6-26)}$$

Collect coefficient of T, and a constant:

$$DT_w = -(A_s^2 h_s h_{rs} + A_s A_w h_w (h_s + h_{rs}))T + Q_{wall} A_s (h_s + h_{rs}) - A_s h_{rs} p_s$$

(Eq. 6-27)

So that the result for T_w after dividing by D, Equation 6-19, becomes:

$$T_w = T + \frac{-Q_{wall} A_s (h_s + h_{rs}) + A_s h_{rs} p_s}{A_s^2 h_s h_{rs} + A_s A_w h_w (h_s + h_{rs})} \quad \text{(Eq. 6-28)}$$

Write T_s from Equation 6-24, and T_w from Equation 6-28, as:

$$T_s = T + B_s \quad \text{(Eq. 6-29)}$$

$$T_w = T + B_w \quad \text{(Eq. 6-30)}$$

And the coefficients B_w and B_s are defined (use the ≡ sign) from Equations 6-24 and 6-28 as:

$$B_w \equiv \frac{-Q_{wall} A_s (h_s + h_{rs}) + A_s h_{rs} p_s}{A_s^2 h_s h_{rs} + A_s A_w h_w (h_s + h_{rs})} \quad \text{(Eq. 6-31)}$$

$$B_s \equiv \frac{-Q_{wall} A_s h_{rs} + p_s (A_s h_{rs} + A_w h_w)}{A_s^2 h_s h_{rs} + A_s A_w h_w (h_s + h_{rs})} \quad \text{(Eq. 6-32)}$$

Use Equation 6-29 for T_s and Equation 6-30 for T_w to rewrite the air energy balance as Equation 6-10 for T as:

$$(T - T_{in})\dot{m} C_p = h_s A_s (T + B_s - T) + h_w A_w (T + B_w - T) \quad \text{(Eq. 6-33)}$$

The expression for T becomes:

$$T = T_{in} + \frac{h_s A_s B_s + h_w A_w B_w}{\dot{m} C_p} \quad \text{(Eq. 6-34)}$$

Consider a simplification of Equation 6-34, by rewriting this equation as:

$$(T - T_{in})\dot{m} C_p = h_s A_s B_s + h_w A_w B_w \quad \text{(Eq. 6-35)}$$

and substitute B_w and B_s from Equation 6-31 and Equation 6-32 to obtain:

$$(T - T_{in})\dot{m}C_p = \frac{h_s A_s(-Q_{wall} A_s h_{rs} + p_s(A_s h_{rs} + A_w h_w))}{A_s^2 h_s h_{rs} + A_s A_w h_w (h_s + h_{rs})} + \frac{h_w A_w(-Q_{wall} A_s (h_s + h_{rs}) + A_s h_{rs} p_s)}{A_s^2 h_s h_{rs} + A_s A_w h_w (h_s + h_{rs})}$$

(Eq. 6-36)

Regroup Q_{wall} and p_s and work on the numerator(s) above to obtain:

$$-Q_{wall} A_s^2 h_s h_{rs} + p_s h_s A_s (A_s h_{rs} + A_w h_w) - Q_{wall} A_s A_w h_w (h_s + h_{rs}) + p_s A_s A_w h_w h_{rs} =$$

$$-Q_{wall}(A_s^2 h_s h_{rs} + A_s A_w h_w (h_s + h_{rs})) + p_s (A_s^2 h_s h_{rs} + A_s A_w h_s h_w + A_s A_w h_w h_{rs}) =$$

$$-Q_{wall}(A_s^2 h_s h_{rs} + A_s A_w h_w (h_s + h_{rs})) + p_s (A_s^2 h_s h_{rs} + A_s A_w h_w (h_s + h_{rs})) \quad \text{(Eq. 6-37)}$$

The coefficients of Q_{wall} and p_s cancel with the denominator(s) in Equation 6-36, so the net result is:

$$(T - T_{in})\dot{m}C_p = -Q_{wall} + p_s \quad \text{(Eq. 6-38)}$$

This result can be obtained by writing an energy balance on just the air in the well-mixed volume element. To see this, consider the control envelope to be the air in the volume element, so $T - T_{in} = \Delta T$, and multiplication by $\dot{m}\,C_p$ yields the net rate of energy transported through the volume element carried by the air. Since p_s is the energy per time added by the source, and $+Q_{wall}$ is the energy per time transferred by conduction into the wall (see the text following Equation 6-12 for the sign convection), $-Q_{wall} + p_s$ is the net energy per time removed from the volume element by the air (moving through). This rather simple energy balance is recovered from the preceding equations.

At this point an equation is required that relates T_w and Q_{wall}, and this is obtained from use of the superposition principle as described in Section 6.4.2.2. This equation is (and is also Equation 6-48):

$$\sum_{2 \to N} + \frac{Pt_1 Q_{wall}}{A_w P_b} = T_w \quad \text{(Eq. 6-39)}$$

The summation symbol denotes the pulse contributions to the temperature T_w from all previous wall fluxes, N denotes the number of time steps, and for the situation where the time step is one year, N denotes the total time. The summation runs from 2 to N, not 1 to N, because the current wall flux is not (yet) known (it is Q_{wall}/A_w). The current wall flux is multiplied by Pt_1 which is the pulse temperature response at an age of 1 year due to the application of a constant flux of a known strength (for example, 1.0 W/m^2). In other words, in the stand-alone term above, the contribution to the wall temperature is being calculated at the end of 1 year due to the flux Q_{wall}/A_w being applied for 1 year. But all the other wall fluxes are known and do not change, they are "history," and their contribution to T_w diminishes with respect to time because with each time step they get "older." The contribution of all of the older fluxes to the temperature T_w are taken into account in the summation. The factor P_b is a conversion factor that takes into account any units conversion necessary between the wall flux, Q_{wall}/A_w, and the pulse flux basis. For example, suppose that the

applied constant flux is 1.0 W/m^2 and the units of Q_{wall}/A_w are W/m^2, then the conversion factor is unity. However, if English units for Q_{wall}/A_w are used, such as Btu/(hr·ft^2), then P_b would be 0.3171 (see List of Conversions), which is the conversion of 1.0 W/m^2 to Btu/(hr ft^2).

Now write Equation 6-38 as:

$$T = \frac{-Q_{wall} + p_s}{\dot{m} C_p} + T_{in} \qquad \text{(Eq. 6-40)}$$

And substitute this expression for T in Equation 6-30 to obtain:

$$T_w = \frac{-Q_{wall} + p_s}{\dot{m} C_p} + T_{in} + B_w \qquad \text{(Eq. 6-41)}$$

There are now two equations for T_w, Equations 6-39 and 6-41. Equate T_w from each of these equations to obtain one equation with one unknown, and that unknown is Q_{wall}. Proceeding:

$$\sum_{2 \to N} + \frac{Pt_1 Q_{wall}}{A_w P_b} = \frac{-Q_{wall} + p_s}{\dot{m} C_p} + T_{in} + \frac{-Q_{wall} A_s (h_s + h_{rs}) + A_s h_{rs} p_s}{A_s^2 h_s h_{rs} + A_s A_w h_w (h_s + h_{rs})} \qquad \text{(Eq. 6-42)}$$

The denominator on the right is –D in Equation 6-19, so condense notation one more time keeping –D:

$$\sum_{2 \to N} + \frac{Pt_1 Q_{wall}}{A_w P_b} = \frac{-Q_{wall} + p_s}{\dot{m} C_p} + T_{in} + \frac{-Q_{wall} A_s (h_s + h_{rs}) + A_s h_{rs} p_s}{(-D)} \qquad \text{(Eq. 6-43)}$$

Now solve for Q_{wall}.

$$Q_{wall} \left[\frac{Pt_1}{A_w P_b} + \frac{1}{\dot{m} C_p} + \frac{A_s (h_s + h_{rs})}{(-D)} \right] = -\sum_{2 \to N} + \frac{p_s}{\dot{m} C_p} + T_{in} + \frac{A_s h_{rs} p_s}{(-D)} \qquad \text{(Eq. 6-44)}$$

Or:

$$Q_{wall} = \frac{-\sum_{2 \to N} + \frac{p_s}{\dot{m} C_p} + T_{in} + \frac{A_s h_{rs} p_s}{(-D)}}{\frac{Pt_1}{A_w P_b} + \frac{1}{\dot{m} C_p} + \frac{A_s (h_s + h_{rs})}{(-D)}} \qquad \text{(Eq. 6-45)}$$

The net result is an equation for Q_{wall} in terms of the knowns of the calculation.

The implementation of the calculation proceeds from Q_{wall} above. The calculated value of Q_{wall} is then used to calculate B_w from Equation 6-31, and B_s from Equation 6-32. Then T_s follows immediately from Equation 6-29, and T_w follows from Equation 6-30. T, which is the temperature of the air, follows immediately from Equation 6-38. Thus, the four variables of interest, T, T_w, T_s, and Q_{wall}, are determined.

The use of a linearized radiant heat transfer coefficient introduces a trial-and-error calculation which is implemented as follows. An initial guess of the radiant heat transfer coefficient, h_{rs}, is used to start the calculation. A reasonable value can be obtained by examining the information given in the engineering literature (Perry et al. 1984 [DIRS 125806], p. 10-13). Using the initial guess, the calculation proceeds as described above and values for T_s and T_w are obtained. These just-calculated values are now used to calculate h_{rs}, as described in Section 6.4.2.3, and the entire calculation repeated. This "successive approximation" is repeated until the temperatures T_s and T_w change very little from one trial to the next, say 0.1 degrees. The radiant heat transfer coefficient does not vary excessively for the parameters of the problem, again seen by examining the engineering literature. In other words, h_{rs} varies by about a factor of 2 over the range of parameters of interest, and as a result the convergence is easily obtained.

The calculation progresses with respect to time by solving for the variables of interest at a time step using the equations noted above, and then stepping to the next time interval. The summation in Equation 6-39 then increases by 1 (which is N), and the calculation repeated out to the specified ventilation duration.

6.4.2.2 Description of the Use of a Constant-Flux Temperature Response to Calculate the Temperature Due to an Arbitrary Flux

Consider an arbitrary energy flux applied to a solid. The temperature response of this solid can be calculated by summing the temperature responses from individual constant fluxes applied over short time intervals in such a manner that the constant fluxes approximate the arbitrary flux. The temperature response being referred to here is the temperature at the surface of the drift wall. The temperature response can be calculated in this way due to the use of the superposition principle for the heat conduction equation (Nagle and Saff 1994 [DIRS 100922], p. 166). In order to illustrate this calculation technique and establish an indexing system, the following description is presented.

Suppose that the temperature response S due to a single unit flux pulse f is tabulated at every $n \cdot \Delta t$ for n = 1,2,3,...., refer to Figure 6-2, specifically to the upper plot of the temperature S versus time. In the first time interval, Δt, the unit flux pulse is "on," and from here on refer to the unit flux pulse as the "pulse." After Δt the pulse is "off," and the boundary condition where the flux was applied is flux = 0. The temperature response S decreases with respect to time because the energy delivered to the solid is being conducted, or diffused, into the solid (rock mass), and as such the temperature decreases.

Now suppose an arbitrary flux is available in functional or tabulated form. Refer to the middle plot in Figure 6-2 of an arbitrary flux f as a function of time.

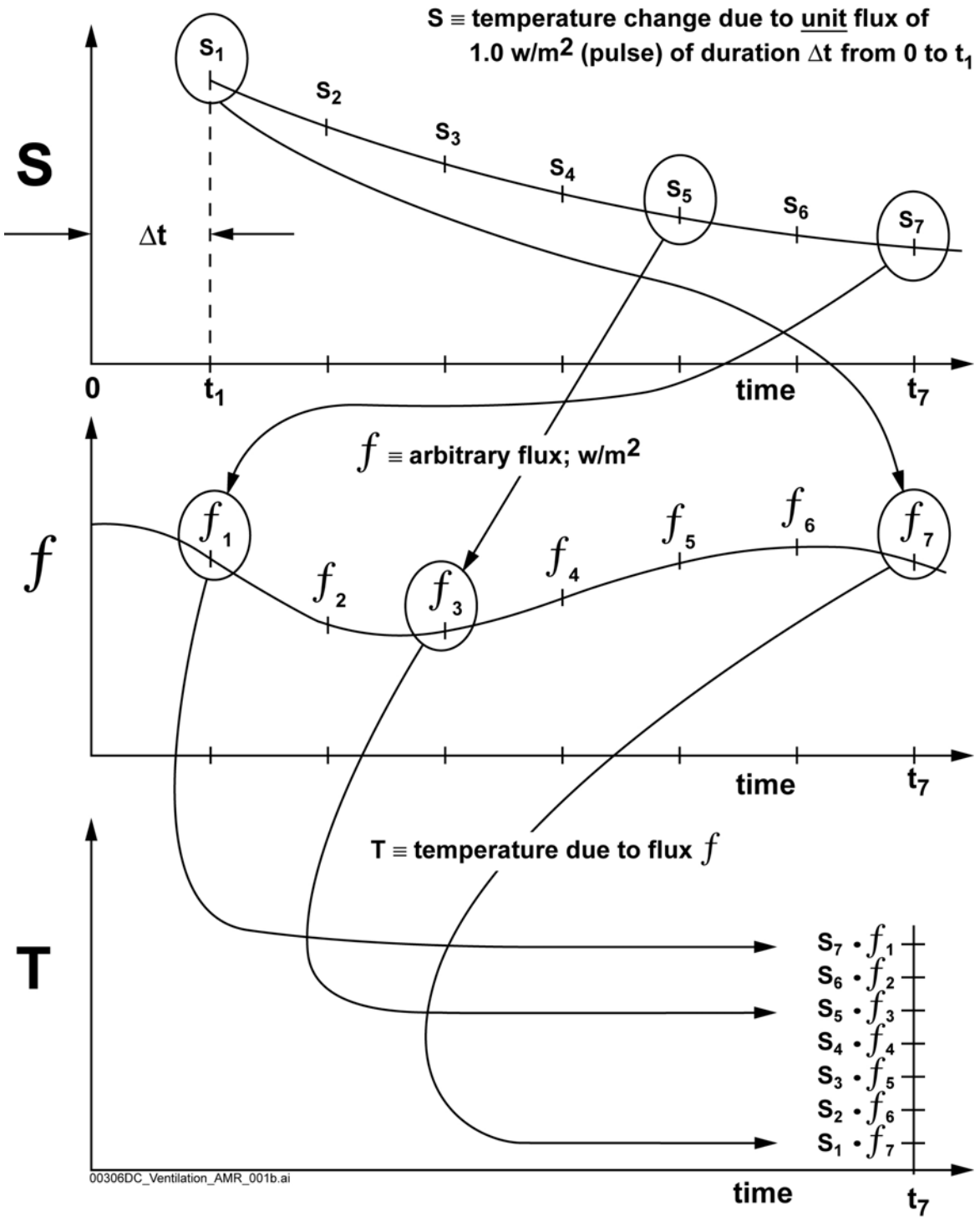

NOTE: Illustration shows how to calculate a temperature t due to an arbitrary flux f using the repeated application of the temperature response s due to a unit flux pulse applied initially between time = 0 and t_1. This calculation methodology is based on the superposition principle and thus adds the temperature contributions from each scaled flux, s·f, to obtain the temperature t at the indicated time.

Figure 6-2. Diagram of the Pulse Response by the Superposition Method

In order to calculate the temperature T illustrated in Figure 6-2 due to the arbitrary flux applied up to time = $7 \cdot \Delta t$ (the 7 is arbitrary, for illustration only), the temperature contribution from each of the applied single pulses within each Δt is scaled by the flux at the time the flux was applied, and the temperature contributions summed. In order to illustrate this, consider the contribution to the temperature T due to the pulse applied in the first Δt between t_0 and t_1. The temperature response will "age," or "decay," to the value indicated at S_7. But the S-versus-time plot is based on a unit flux (or whatever flux one chooses). Therefore S_7 must be scaled by the value of the arbitrary flux applied in the first Δt, so the contribution to the temperature T at t_7 due to this flux is $S_7 \cdot f_1$, and this is illustrated in the plot of T versus time with a "line" connecting S_7 and f_1. This "line" means multiply these two values. Instead of using f_1 as indicated, a midpoint or average value of the flux in this time interval can be used.

Likewise, consider the contribution to the temperature T due to the flux applied between t_6 and t_7. This temperature response is S_1 because it is only one Δt from its origin in time. This value of S_1 is scaled by the flux used between the times indicated. Thus the contribution to the temperature T at t_7 due to this flux is $S_1 \cdot f_7$, and this is added to the sum of contributions, and also illustrated in the plot of T versus time with a "line" connecting S_1 and t_7.

In general, suppose the time index of interest is N, and the time is $t = N \cdot \Delta t$, then T_N is written as:

$$T_N = \sum_{n=1}^{N} S_n f_{N-n+1} \qquad \text{(Eq. 6-46)}$$

To illustrate the indexing in this summation, consider N = 7, let n = 1, then N – n + 1 = 7, and the product is $S_1 \cdot f_7$. Now let n = 7, then N – n + 1 = 1, and the product is $S_7 \cdot f_1$.

A table of how the indices run for N = 7 can be found in Table 6-3.

Table 6-3. Example of the Indexing for the Pulse Response Method

n	N - n +1	$S_n \cdot f_{N-n+1}$
1	7	$S_1 \cdot f_7$
2	6	$S_2 \cdot f_6$
3	5	$S_3 \cdot f_5$
4	4	$S_4 \cdot f_4$
5	3	$S_5 \cdot f_3$
6	2	$S_6 \cdot f_2$
7	1	$S_7 \cdot f_1$

The temperature T_N is then the sum of $S_n f_{N-n+1}$ in the last column. This computation scheme is intended to calculate the temperature on the time "nodes" as indicated.

Now suppose that the flux f in the last time interval, Δt between t_6 and t_7, is an unknown. All the other fluxes are "history" because they have already occurred, and hence are known. Thus the above summation can be written as a sum of what occurred (known), and what is going to occur (unknown) in the current time step as:

$$T_N = \sum_{n=2}^{N} S_n f_{N-n+1} + S_1 f_N \qquad \text{(Eq. 6-47)}$$

In the illustration using N = 7 the indices of the last term above are $S_1 f_7$ which illustrates, referring to Figure 6-2, that the flux in the indicated time interval (the last one) is being scaled by S_1. This form of the summation equation for the temperature is used in Section 6.4.2.1 as Equation 6-39, and rewritten with the following notation:

$$\sum_{2 \to N} + \frac{Pt_1 Q_{wall}}{A_w P_b} = T_w \qquad \text{(Eq. 6-48)}$$

In this form of the summation equation, Pt_1 corresponds to S_1, Q_{wall}/A_w corresponds to f_N, and P_b is a scale factor (inserted for future convenience). Q_{wall} in Section 6.4.2.1 is the total energy per time delivered to the total drift wall in the segment; thus, dividing by the total drift wall area in the segment, A_w, yields the indicated flux Q_{wall}/A_w.

6.4.2.3 Linearized Radiant Heat Transfer Coefficient

The linearization of radiant energy transfer is discussed in numerous texts (Carslaw and Jaeger 1959 [DIRS 100968], p. 21, and Perry et al. 1984 [DIRS 125806], p. 10-13, use the terminology "radiation film coefficient"; Kern 1950 [DIRS 130111], p. 77, describes a fictitious film coefficient to represent the rate at which radiation passes from one surface of a radiator). In order to derive a linearized radiant heat transfer coefficient for a heated tunnel, consider the transport of heat by radiation in an annulus as given by Bird et al. (1960 [DIRS 103524], p. 453, problem 14.G_2):

$$Q_{12} = \frac{\sigma(T_1^4 - T_2^4)}{\left[\frac{1}{A_1 e_1} + \frac{1}{A_2}\left(\frac{1}{e_2} - 1\right)\right]} \; [\equiv] \; \frac{\text{energy}}{\text{time} \cdot \text{length}} \qquad \text{(Eq. 6-49)}$$

Q_{12} (W/m) is the net radiant energy interchange between surface 1 and 2, T_1 (K) and T_2 (K) are the respective surface absolute temperatures, e_1 and e_2 are the respective emissivities, σ is the Stephan Boltzmann constant, and A_1 is the surface area of the inner cylinder per unit length (m^2/m) (see Bird et al. 1960 [DIRS 103524], p. 448, Example 14.5-2, for a similar problem where "unit length" is used), and the [≡] symbol means "has units of." Therefore, change the subscripts from 1 ⇒ s (the source which is the inner cylinder), and from 2 ⇒ w (the wall which is the outer cylinder). So the energy per time (heat) transferred becomes:

$$Q_{sw} = \frac{\sigma(T_s^4 - T_w^4)}{\left[\frac{1}{A_s e_s} + \frac{1}{A_w}\left(\frac{1}{e_w} - 1\right)\right]} \; [\equiv] \; \frac{\text{energy}}{\text{time} \cdot \text{length}} \qquad \text{(Eq. 6-50)}$$

The energy (heat) transferred for a length Δx (i.e., the length of the well-mixed volume element) is:

$$Q_{sw}\,\Delta x = \frac{\sigma(T_s^4 - T_w^4)\,\Delta x}{\left[\dfrac{1}{A_s e_s} + \dfrac{1}{A_w}\left(\dfrac{1}{e_w} - 1\right)\right]}\,[\equiv]\,\frac{energy}{time} \qquad \text{(Eq. 6-51)}$$

At this point it is necessary to recognize that the areas here, A_s and A_w, as written above in Equation 6-51 are not the same areas that appear in Equation 6-10. The areas in Equation 6-51 are more appropriately "specific" areas (i.e., area per unit length). Those areas in Equation 6-10 are areas in the well-mixed volume element. Therefore, change the notation in Equation 6-51 to denote "specific" areas; to do this, define the specific area for A_s as A_{us} where the subscript "us" denotes per unit length. Likewise for A_w use A_{uw}. Equation 6-51 now appears as:

$$Q_{sw}\,\Delta x = \frac{\sigma(T_s^4 - T_w^4)\,\Delta x}{\left[\dfrac{1}{A_{us} e_s} + \dfrac{1}{A_{uw}}\left(\dfrac{1}{e_w} - 1\right)\right]}\,[\equiv]\,\frac{energy}{time} \qquad \text{(Eq. 6-52)}$$

Note that $Q_{sw}\Delta x$ is the total energy per time transferred from the source in the well-mixed volume element. Now define (use the ≡ symbol for "define") a linearized radiant transfer coefficient based on the power source area A_s in the well-mixed volume element (see Equation 6-11) as:

$$h_{rs}\,A_s(T_s - T_w) = h_{rs}(\pi D_s \Delta x)(T_s - T_w) \equiv Q_{sw}\,\Delta x \qquad \text{(Eq. 6-53)}$$

So using Equation 6-52 for Q_{SW}:

$$h_{rs}\,\pi D_s(T_s - T_w) \equiv \frac{\sigma(T_s^4 - T_w^4)}{\left[\dfrac{1}{A_{us} e_s} + \dfrac{1}{A_{uw}}\left(\dfrac{1}{e_w} - 1\right)\right]} \qquad \text{(Eq. 6-54)}$$

So that by definition:

$$h_{rs} \equiv \frac{\sigma(T_s^4 - T_w^4)/(T_s - T_w)}{\pi D_s\left[\dfrac{1}{A_{us} e_s} + \dfrac{1}{A_{uw}}\left(\dfrac{1}{e_w} - 1\right)\right]}\,[\equiv]\,\frac{energy}{time{\cdot}area{\cdot}temperature} \qquad \text{(Eq. 6-55)}$$

Carrying out the indicated division yields:

$$h_{rs} \equiv \frac{\sigma(T_s^3 + T_s^2 T_w + T_s T_w^2 + T_w^3)}{\pi D_s\left[\dfrac{1}{A_{us} e_s} + \dfrac{1}{A_{uw}}\left(\dfrac{1}{e_w} - 1\right)\right]} \qquad \text{(Eq. 6-56)}$$

And hence when using such a linearization a trial-and-error calculation is introduced because T_s and T_w must be specified.

Therefore, the linearized radiant-heat transfer coefficient defined in Equation 6-55, h_{rs}, is the coefficient that multiplies the source area in the well-mixed volume element, but note that the areas appearing in Equation 6-56 are specific areas.

6.4.2.4 Thermal Pulse Calculation

In order to implement the ventilation calculation using the analytical approach described in Section 6.4.2, it is necessary to have a temperature response of the drift wall due to the application of a pulse of energy put into the drift wall. This temperature pulse response was introduced in Equation 6-39 in the derivation of the analytical equations, and its use further described in Section 6.4.2.2. The sections that follow here describe how to calculate this temperature response analytically using results from the open literature. This analytical temperature pulse response is based on using two analytical temperature solutions; these are the temperature in the infinite region bounded internally by a cylinder for a constant heat flux (Carslaw and Jaeger 1959 [DIRS 100968], p. 338), and the temperature in the semi-infinite solid for a constant heat flux (Carslaw and Jaeger 1959 [DIRS 100968], p. 75). The first analytical solution, that for the region bounded internally by a cylinder, is used to describe the drift-wall temperature for the early times of the pulse response, and the second analytical solution, that for the semi-infinite solid, is used for the drift-wall temperature for the later, or long-term, times of the pulse response. The reason that the temperature response from the semi-infinite solid can be used for later times is that a pulse of energy entering the drift wall spreads out to the adiabatic boundary at midpillar at later times, and then transports vertically within the rock. A pulse response for each of these time frames is obtained from these constant-flux solutions by shifting the analytical result by one year (for a one-year pulse) and subtracting from the unshifted solution. This shift-and-subtract operation to yield the pulse is based on the superposition principle as described by Nagle and Saff (1994 [DIRS 100922], p. 166). The entire temperature pulse response is then generated by taking the maximum of these two pulses out to the maximum time of interest.

The discussions presented in Sections 6.4.2.4.1 and 6.4.2.4.2 below pertain to how to compute the drift wall temperature in an infinite medium. This is then used to calculate the pulse response.

6.4.2.4.1 The Infinite Region Bounded Internally by a Cylinder

The temperature in the infinite region bounded internally by a cylinder is (Carslaw and Jaeger 1959 [DIRS 100968], p. 338, Equation 17):

$$v = -\frac{2Q}{\pi K}\int_0^\infty (1 - e^{-\kappa u^2 t})\frac{J_o(ur)Y_1(ua) - Y_o(ur)J_1(ua)}{u^2[J_1^2(ua) + Y_1^2(ua)]}du \qquad \text{(Eq. 6-57)}$$

where v is the temperature, Q is a constant flux, a is the cylinder radius, J_o, J_1, Y_o, and Y_1 are Bessel functions as used by Carslaw and Jaeger (1959 [DIRS 100968]), and the other symbols are previously described. This equation can be put into a dimensionless form that is convenient because it is then necessary to perform the calculation indicated only once for any value of drift

radius (m), a, thermal conductivity (W/m·K), K, and thermal diffusivity (m^2/s), κ. To put the above equation in dimensionless form, proceed by defining the dimensionless variable ξ as:

$$\xi \equiv ua \qquad \text{(Eq. 6-58)}$$

which differentiating with respect to the integration variable u yields:

$$d\xi = a\, du \qquad \text{(Eq. 6-59)}$$

Substituting the above two results into Equation 6-57 yields:

$$v = -\frac{2Q}{\pi K}\int_0^{\infty}(1 - e^{-\kappa(\xi/a)^2 t})\frac{J_o\left(\xi\frac{r}{a}\right)Y_1(\xi) - Y_o\left(\xi\frac{r}{a}\right)J_1(\xi)}{\frac{\xi^2}{a^2}[J_1^2(\xi) + Y_1^2(\xi)]}\frac{d\xi}{a} \qquad \text{(Eq. 6-60)}$$

Now define a dimensionless time τ as:

$$\tau \equiv \frac{\kappa t}{a^2} \qquad \text{(Eq. 6-61)}$$

And evaluate the temperature at the cylinder surface (i.e., drift wall) by setting r = a and obtain a dimensionless temperature written as:

$$\theta \equiv \frac{K\, v(r=a)}{Q\, a} = -\frac{2}{\pi}\int_0^{\infty}(1 - e^{-\xi^2\tau})\frac{J_o(\xi)Y_1(\xi) - Y_o(\xi)J_1(\xi)}{\xi^2[J_1^2(\xi) + Y_1^2(\xi)]}d\xi \qquad \text{(Eq. 6-62)}$$

This equation is used to generate the temperatures of interest at specific times as follows. Suppose that the dimensionless temperatures have been generated as a function of dimensionless time, τ, for $\Delta\tau$ = 1, 2, … up to some maximum τ_{max}. Now suppose that the temperature is required at times of every year, Δt = 1; use Equation 6-61 to write:

$$\tau_n = \left(\frac{\kappa}{a^2}\right)(n\,\Delta t), \quad for\ n = 1,2,3... \qquad \text{(Eq. 6-63)}$$

To further illustrate, suppose that κ = 26 m^2/year and a = 2.75 meters (for a 5.5-meter diameter drift), so that the above becomes:

$$\tau_n \approx 3.44(n\,\Delta t), \quad for\ n = 1,2,3... \qquad \text{(Eq. 6-64)}$$

To generate the temperature v at the desired times of one-year increments, the *a priori* calculated dimensionless temperature and dimensionless time at discrete values of τ can be interpolated accordingly from those at τ_n in Equation 6-63.

6.4.2.4.2 The Semi-Infinite Slab

The temperature in the semi-infinite slab is (Carslaw and Jaeger 1959 [DIRS 100968], p. 75, Equation 7):

$$v(t) = \frac{2 \cdot F_0}{K} \cdot \left[\left(\frac{\kappa \cdot t}{\pi} \right)^{\frac{1}{2}} \cdot e^{\frac{-x^2}{4 \cdot \kappa \cdot t}} - \frac{x}{2} \cdot erfc\left(\frac{x}{2\sqrt{\kappa \cdot t}} \right) \right] \quad \text{(Eq. 6-65)}$$

where v is the temperature, F_0 is a constant flux (equal to one-half the linear power at the drift wall, applied over the area determined by the drift spacing), erfc(z) is the complementary error function, and the other symbols are as previously described. The temperature at the face, or x = 0, is:

$$v(t) = \frac{2 \cdot F_0}{K} \cdot \sqrt{\frac{\kappa \cdot t}{\pi}} \quad \text{(Eq. 6-66)}$$

To generate the temperature response due to a one-year pulse, again shift the solution by one year and subtract from the unshifted solution:

$$v(t) = 2 \cdot \frac{F_0}{K} \cdot \left(\sqrt{\frac{\kappa \cdot t}{\pi}} - \sqrt{\frac{\kappa \cdot (t-1)}{\pi}} \right) \quad \text{(Eq. 6-67)}$$

for $t \geq 1$.

For geometries modeled here, F_0 is 1 W/m applied at the drift wall.

6.5 DEVELOPED INPUTS, BOUNDARY CONDITIONS, AND MESHES

This section summarizes the inputs developed from Section 4.1.1, which are used in the ANSYS and analytical models.

6.5.1 Thickness of Each of the Stratigraphic Layers

The rme6 v1.2 and YMESH v1.54 software routines (Sections 3.2 and 3.3) were used to generate product output in the form of stratigraphic layer thickness at a specified northing and easting coordinate pair (DTN: MO0306MWDSLTLC.000, P2WR5C10.col). This product output was used in the ANSYS based ventilation models. The stratigraphic layer thicknesses are presented in Table 6-4. The computed surface elevation and water table elevation are 1363.4m and 774.4m, respectively (DTN: MO0306MWDSLTLC.000, P2WR5C10.col). The computed center of the emplacement drift is located at 310.5m from the surface (DTN: MO0306MWDSLTLC.000, P2WR5C10.col).

The data used in ANSYS ventilation models was based on the preliminary product outputs generated by the unqualified rme6 v1.2 and YMESH v1.54 software routines (DTN: MO0303MWDSLTLC.000). Qualified versions of rme6 v1.2 and YMESH v1.54 were

later used to generated the another set of stratigraphic layer thickness at the same northing and easting coordinate (DTN: MO0306MWDSLTLC.000). The two sets of data were compared. There was no difference between the product outputs from the preliminary and the qualified versions of rme6 v1.2 and YMESH v1.54. Therefore, DTN: MO0306MWDSLTLC.000 for the qualified data set is listed as the source in Table 6-4.

Table 6-4. Thickness of the Stratigraphic Layers

	rme6 v.12 and YMESH v1.54
Northing	234912.719
Easting	170730.297
Stratigraphic Unit	**Thickness (m)**
tcw12	20.2
tcw13	4.0
ptn21	7.2
ptn22	5.6
ptn23	2.0
ptn24	12.5
ptn25	36.5
ptn26	11.3
tsw31	2.0
tsw32	45.6
tsw33	85.3
tsw34	33.0
tsw35	104.7
tsw36	25.8
tsw37	12.9
tsw38	21.9
tsw9z	6.6
ch1z	15.0
ch2z	20.3
ch3z	20.3
ch4z	20.3
ch5z	20.3
ch6z	17.6
pp4	19.7
pp3	14.3
pp2	4.1

Output DTN: MO0306MWDSLTLC.000, P2WR5C10.col.

6.5.2 Effective Thermophysical Properties of the Stratigraphic Layers

Table 6-5 lists the effective thermophysical properties of the stratigraphic units which take into account the effects of 90.5% water saturation of the matrix porosity (Section 5.3) and 100% air saturation of the lithophysal porosity (Section 5.4) on the thermal conductivity, density, and

specific heat. These properties were obtained using Table 4-6, Table 4-7, Table 4-10, and Table 4-11. The calculation of these properties is documented in Appendices I and II. These properties were used in the ANSYS-based models.

Table 6-5. Effective Thermophysical Properties of the Stratigraphic Units Used in the ANSYS Models

Unit	Effective Thermal Conductivity (W/m·K)	Effective Specific Heat (J/kg·K)	Effective Density (kg/m^3)
tcw12	1.76	930	2673
tcw13	0.90	950	2721
ptn21	1.01	960	2973
ptn22	1.01	960	2973
ptn23	1.01	960	2973
ptn24	1.01	960	2973
ptn25	1.01	960	2973
ptn26	1.01	960	2973
tsw31	1.27	940	2561
tsw32	1.76	930	2673
tsw33	1.74	930	2578
tsw34	2.01	930	2665
tsw35	1.83	930	2563
tsw36	2.07	930	2635
tsw37	2.07	930	2635
tsw38	0.79	980	2449
tsw9z	1.01	980	2942
ch1z	1.01	1080	2805
ch2z	1.20	1070	2844
ch3z	1.20	1070	2844
ch4z	1.20	1070	2844
ch5z	1.20	1070	2844
ch6z	1.20	1020	2902
pp4	1.08	1040	2878
pp3	1.08	930	3007
pp2	1.33	930	2962

Source: Appendices I and II of this report.

6.5.3 Average Thermophysical Properties of the Invert and Impact Evaluation for Error in Input Heat Capacity

Table 6-6 lists the average thermophysical properties of the invert ballast material taken from Tables 4-1 and 4-2.

A specific heat value of 1177 J/kg·K instead of the value of 735 J/kg·K was used in the ANSYS model for calculating the ventilation efficiency. Because the mass of the invert per unit length is 3,095 kg/m (BSC 2003 [DIRS 164101], Table 3), the error in specific heat of 442 J/kg·K

produced an error in heat capacity per unit length of 1.37×10^6 J/m·K. The average temperature rise in the invert was always less than 50 K, so that the extra heat required to raise the temperature was less than 7×10^7 J/m. At the initial heat decay of 1.4 kJ/m·s, the time required to produce that amount of heat is less than 5×10^4 s, which is less than one day. Therefore, the impact of the discrepancy in specific heat had no significant impact on the ANSYS results.

As will be seen in Section 6.6, this is verified by comparison of the ANSYS results with the results of the analytical model.

Table 6-6. Average Thermophysical Properties of the Invert

Specific Heat		Thermal Conductivity		Thermal Diffusivity (mm^2/s)[e]	Bulk Density	
($J/cm^3 \cdot °C$)[a]	($J/kg \cdot K$)[b]	($W/m \cdot °C$)[c]	($W/m \cdot K$)[d]		(g/cm^3)[f]	(kg/m^3)[g]
0.93	735 (1177)	0.16	0.16	0.18	1.266	1266

[a] Average of Table 4-1 for Specific Heat.
[b] Convert [a] from $J/cm^3 \cdot °C$ to $J/kg \cdot K$ using the Bulk Density [f]; value in parentheses was used in ANSYS model.
[c] Average of Table 4-1 for Thermal Conductivity.
[d] Convert [c] from °C to K.
[e] Average of Table 4-1 for Thermal Diffusivity.
[f] Average of Table 4-2 for Bulk Density.
[g] Convert [f] from g/cm^3 to kg/m^3.

6.5.4 In-Drift Cross-Sectional Area Available for Flow

The in-drift cross-sectional area available for air flow is calculated in Appendix XVI and is 19.5 m^2. This calculation takes into account the cross-sectional area of the drift, minus the cross-sectional area of the waste package and the cross-sectional area of the invert.

6.5.5 Temperature and Flux Boundary Conditions at the Ground Surface, Water Table, and Mid-Pillar

The temperature at the ground surface is calculated from the following equation (BSC 2004 [DIRS 169861], Equation 6.3-1):

$$T_s = T_{s-ref} - \lambda\left(Z_s - Z_{s-ref}\right) \quad \text{(Eq. 6-68)}$$

where

T_s = ground surface temperature (°C)
$T_{s\text{-}ref}$ = surface temperature at the reference elevation Z_{ref} (°C)
λ = mean lapse rate
Z_s = ground surface elevation (m)
$Z_{s\text{-}ref}$ = surface elevation for which the temperature $T_{s\text{-}ref}$ is known (m)

T_s is calculated using the information provided in Section 4.1.6, and Section 6.5.1:

$T_{s\text{-}ref}$ = 18.23°C
λ = 0.009°C/m

$Z_{s\text{-}ref}$ = 1231.0 m
Z_s = 1363.4 m
T_s = 17.04°C = 17.0°C

The water table temperature is calculated by linear interpolation using the following equation:

$$T_w = \frac{(Z_w - Z_{w-ref})(T_s - T_{w-ref})}{Z_s - Z_{w-ref}} + T_{w-ref} \quad \text{(Eq. 6-69)}$$

where

T_w = water table surface temperature (°C)
$T_{w\text{-}ref}$ = water table surface temperature at the reference elevation $Z_{w\text{-}ref}$ (°C)
Z_w = water table surface elevation (m)
$Z_{w\text{-}ref}$ = water table surface elevation for which the temperature $T_{w\text{-}ref}$ is known (m)

T_w is calculated using the information provided in Table 4-12, and Section 6.5.1:

$T_{w\text{-}ref}$ = 28.27°C
$Z_{w\text{-}ref}$ = 730.0 m
Z_w = 774.4 m
T_w = 27.48°C = 27.5°C

The calculations in this report used preliminary boundary values of 17°C at the surface and 28°C at the water table. These are the round-off values of the qualified values. In each case, the difference between the preliminary (round-off) values and the qualified values is not large enough to have a significant effect on the calculated efficiency or on the conclusions of this report.

The flux boundary condition at the mid-pillar is adiabatic.

6.5.6 Temperature of the Ventilation Air at the Drift Inlet

The temperature of the ventilation air at the drift inlet is assumed to be equal to the temperature of the host rock at the repository horizon prior to preclosure (Section 5.7). The temperature of the host rock at the repository horizon prior to preclosure was calculated by ANSYS using the boundary conditions described in Section 6.5.5 and the thermophysical properties of the rock layers described in Section 6.5.2. The temperature was calculated to be 22.8°C (DTN: MO0306MWDASLCV.001, air_temp_co.input).

6.6 RESULTS OF THE NUMERICAL APPLICATION OF THE CONCEPTUAL MODEL

The results for the ANSYS-LA-Coarse, ANSYS-LA-Fine, and Analytical-LA-Coarse models are presented in terms of temporally and spatially varying temperatures. In addition, ventilation efficiencies are presented for the ANSYS-LA-Coarse and Analytical-LA-Coarse models. A comparison between the ANSYS-LA-Coarse and ANSYS-LA-Fine models quantifies the impact

of the axial discretization along the drift length and serves as a model verification exercise. A comparison between the ANSYS-LA-Coarse and Analytical-LA-Coarse models benchmarks the analytical approach in preparation for further use in the implementation of the alternative conceptual model and the uncertainty/sensitivity analysis (Sections 6.9.2 and 6.11).

6.6.1 The Effects of Axial Discretization

The general trends of waste package, drift wall, and drift air temperatures as functions of time and drift length for the ANSYS-based models are shown in Figures 6-3 and 6-4 for a 600 meter drift length case. The waste package and drift wall temperatures are perimeter-averaged results, while the in-drift air temperatures are bulk averaged. The temperatures for the waste package, drift wall, and drift air for the ANSYS-LA-Coarse and ANSYS-LA-Fine models are within 0.4°C for all distances from the drift entrance and times since emplacement. The following general observations with respect to waste package, drift wall, and drift air temperatures for the ANSYS-based models can be made:

- With respect to time, temperatures peak at one year into the ventilation period and afterwards decline in an exponential fashion similar to the waste package heat energy input decay curve.

- With respect to location along the length of the drift, temperatures increase linearly, with the maximum temperatures occurring at the end of the drift.

- The ANSYS methodology is insensitive to the number and length of sub-divisions in the axial direction.

6.6.2 Temperature and Ventilation Efficiency Comparisons for the ANSYS-LA-Coarse and Analytical-LA-Coarse Models

The same general trends of temperature variation with time and distance from the drift entrance, as noted in Section 6.6.1 for the ANSYS numerical models, are observed for the Analytical-LA-Coarse. Figure 6-5 shows the ANSYS-LA-Coarse and Analytical-LA-Coarse temperatures as a function of time for locations 100 m, 600 m, and 800 m from the drift entrance. Figure 6-6 shows temperatures as function of axial distance from the drift entrance for ventilation durations of 5 and 50 years. The temperatures for the waste package, drift wall, and drift air for the two models are within 5°C for all distances from the drift entrance and times since emplacement.

The instantaneous ventilation efficiency is calculated using Equation 6-5. Figure 6-7 shows the ANSYS-LA-Coarse and Analytical-LA-Coarse instantaneous ventilation efficiencies as a function of time for locations 100 m, 600 m, and 800 m from the drift entrance. Figure 6-8 shows ventilation efficiencies as function of axial distance from the drift entrance for ventilation durations of 5 and 50 years. The ventilation efficiencies for the two models are within 4% for all distances from the drift entrance and times since emplacement. The overall or integrated ventilation efficiency is calculated using Equation 6-6. Table 6-7 shows the integrated efficiency over 600 and 800 meters of drift length, and 50 years of ventilation for the two models. Use of the ventilation efficiency is discussed in Section 6.10.

It should be noted that the ANSYS-based model simulates an eccentrically located waste package and an invert, while the analytical model simulates a concentrically located waste package and no invert. Based on the reasonable comparisons of temperature and efficiency, the ventilation model is not sensitive to the eccentricity of the waste package, nor the presence of the invert (including its thermophysical properties).

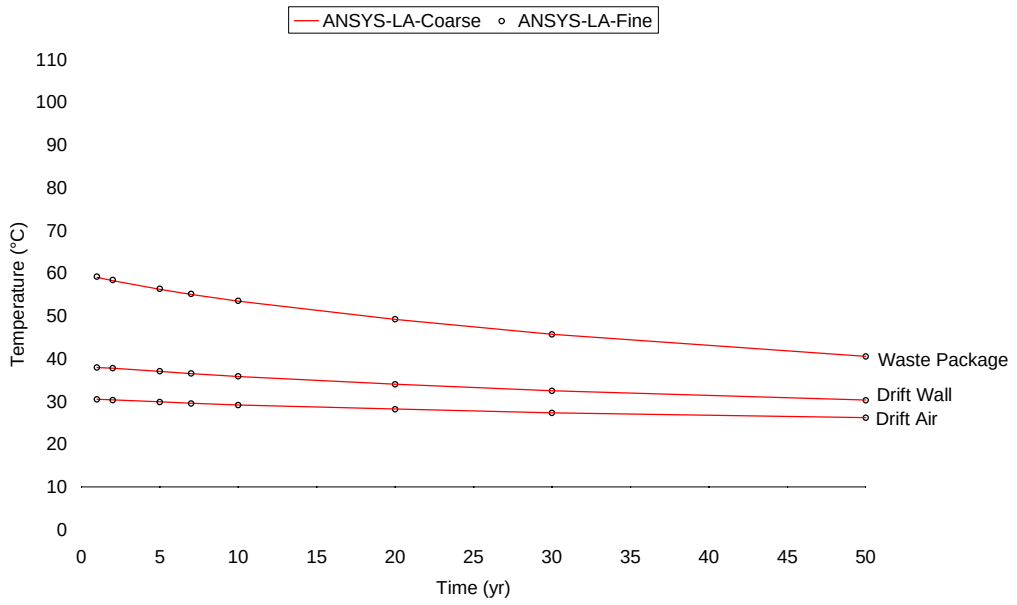

(a) 100 meters

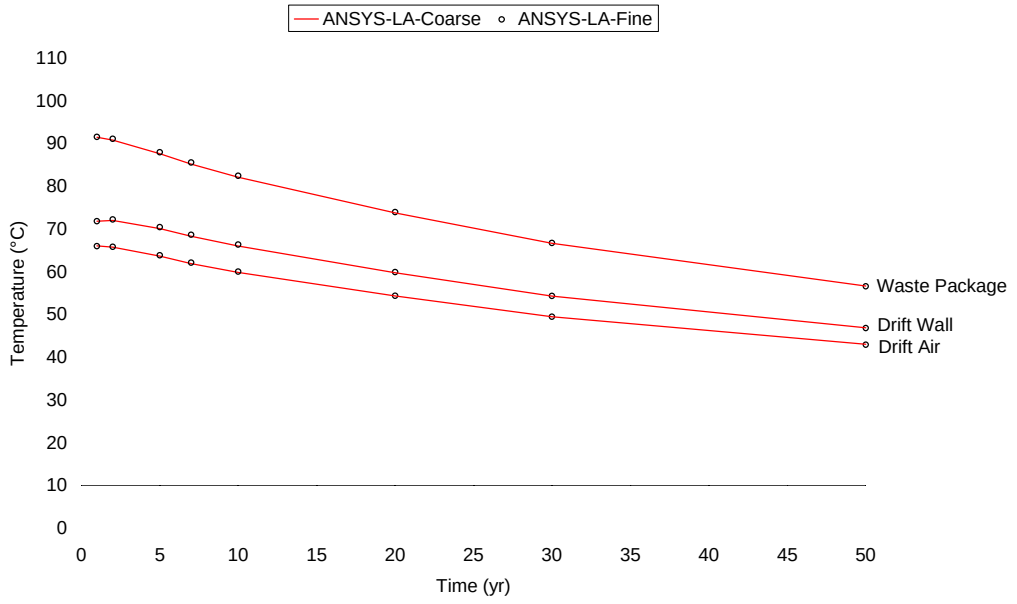

(b) 600 meters

Output DTNs: MO0306MWDASLCV.001; MO0306MWDALAFV.000.

Figure 6-3. Waste Package, Drift Wall, and Drift Air Temperatures as Function of Time for (a) 100 Meters and (b) 600 Meters from the Drift Entrance for the ANSYS-LA-Coarse and ANSYS-LA-Fine Models

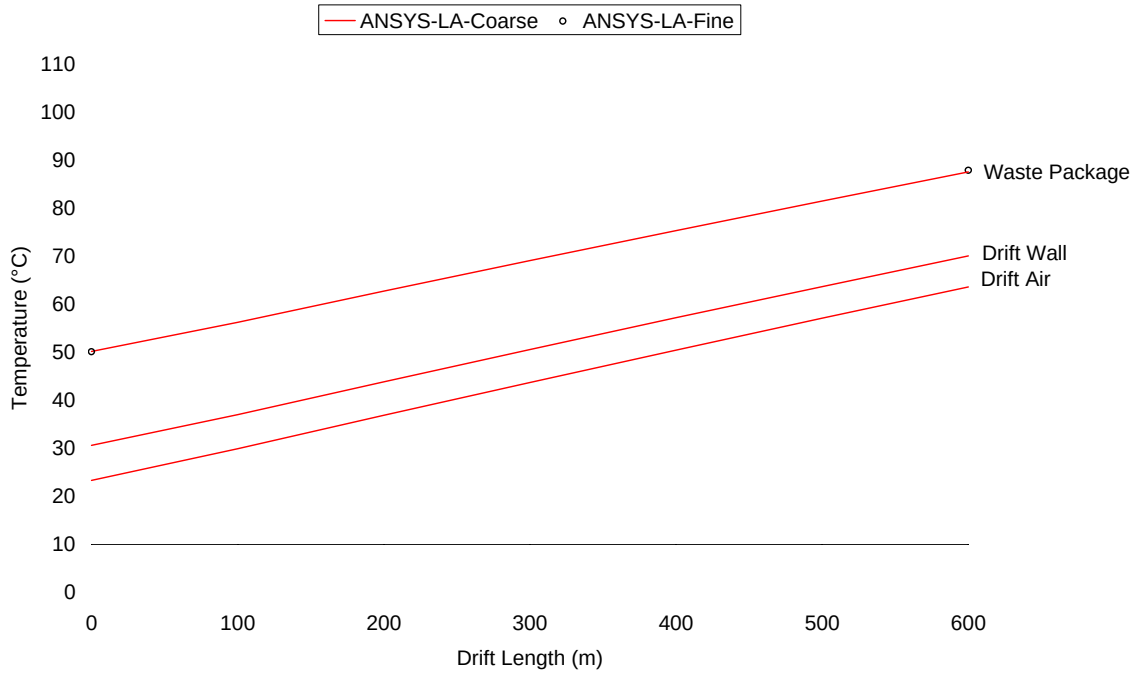

(a) 5 years

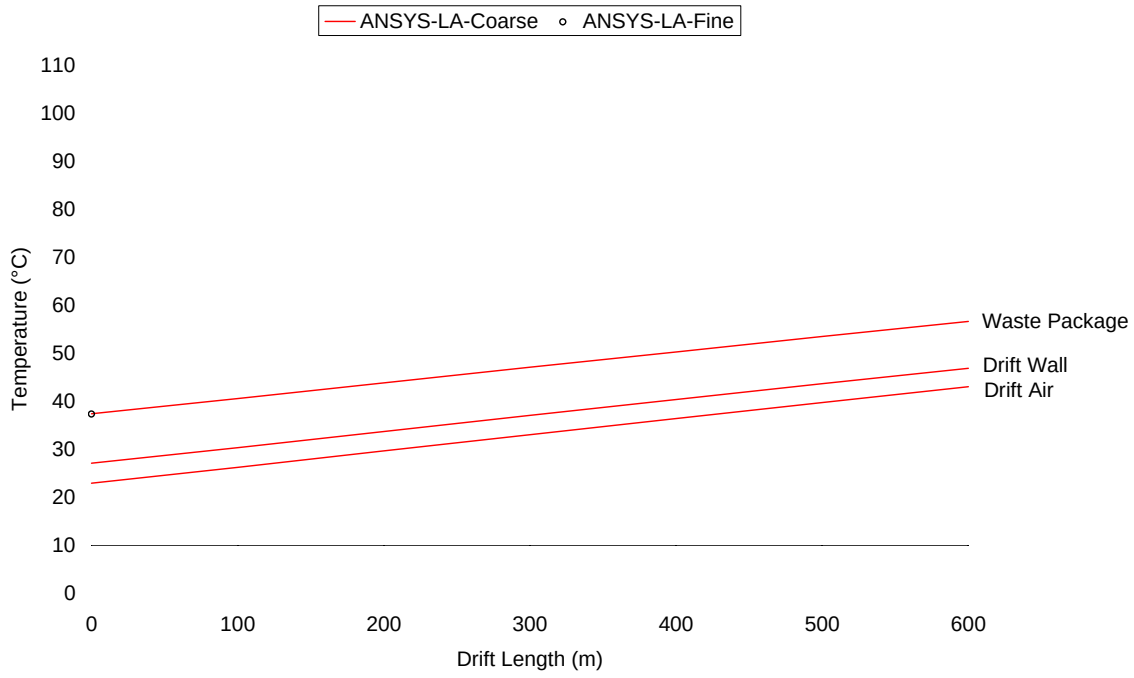

(b) 50 years

Output DTNs: MO0306MWDASLCV.001; MO0306MWDALAFV.000.

Figure 6-4. Waste Package, Drift Wall, and Drift Air Temperatures as Function of Drift Length for (a) 5 Years and (b) 50 Years from the Time of Waste Emplacement for the ANSYS-LA-Coarse and ANSYS-LA-Fine Models

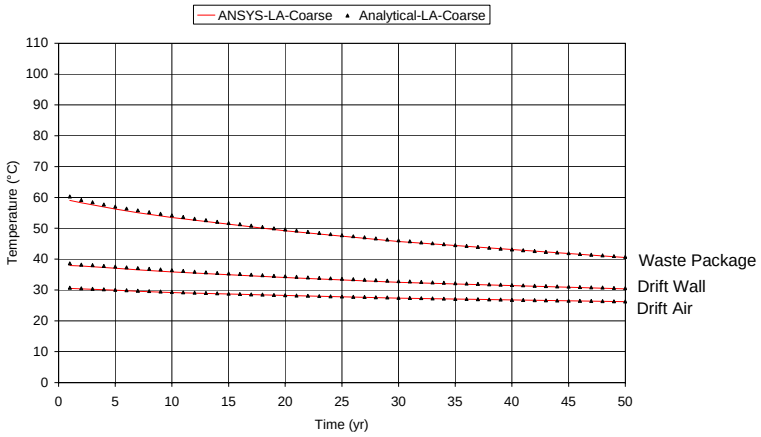

(a) 100 meters

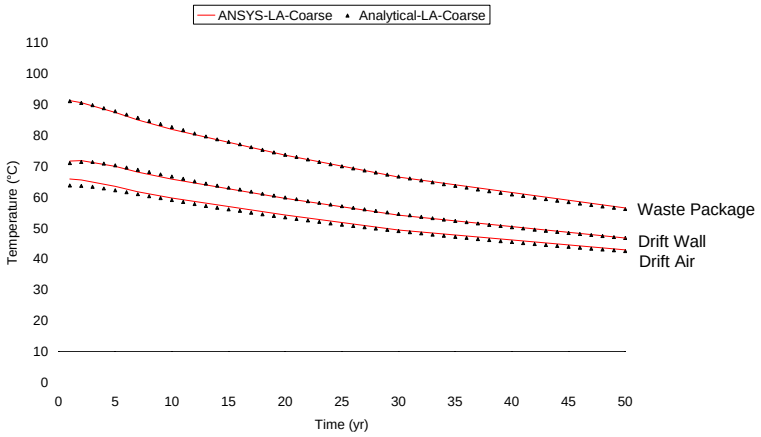

(b) 600 meters

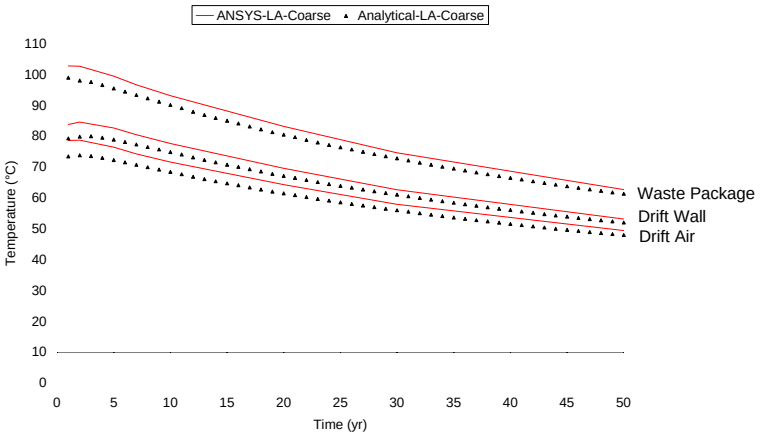

(c) 800 meters

Output DTNs: MO0306MWDASLCV.001, MO0307MWDAC8MV.000.

Figure 6-5. Waste Package, Drift Wall, and Drift Air Temperatures as Function of Time for (a) 100 Meters, (b) 600 Meters, and (c) 800 Meters from the Drift Entrance for the ANSYS-LA-Coarse and Analytical-LA-Coarse Models

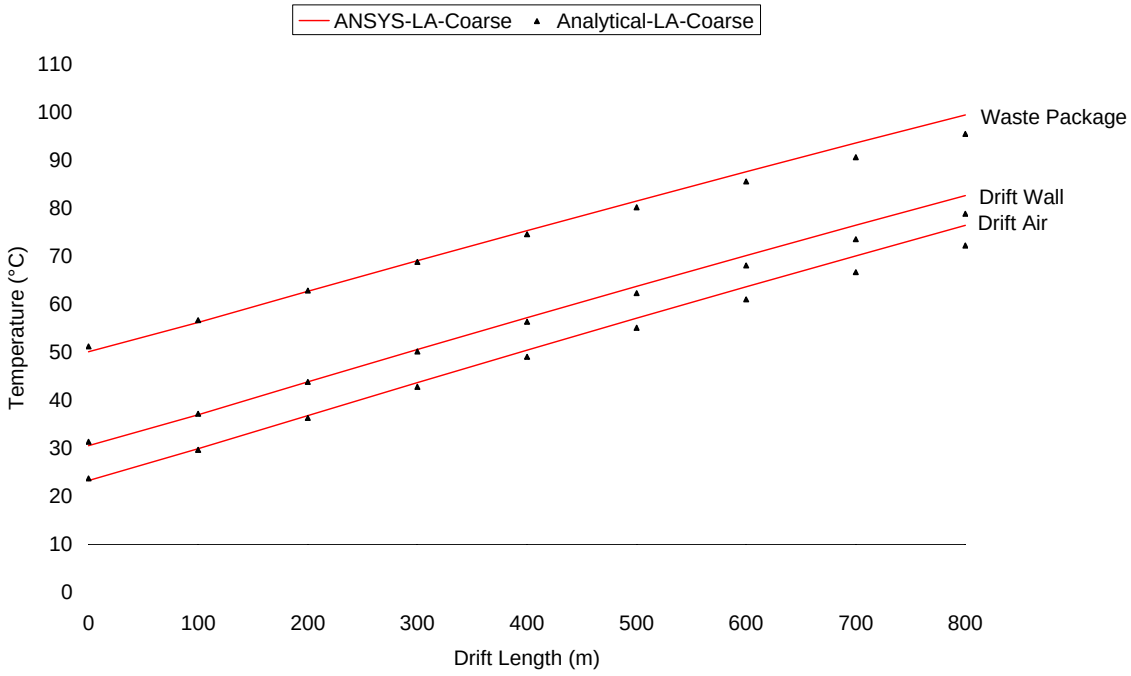

(a) 5 years

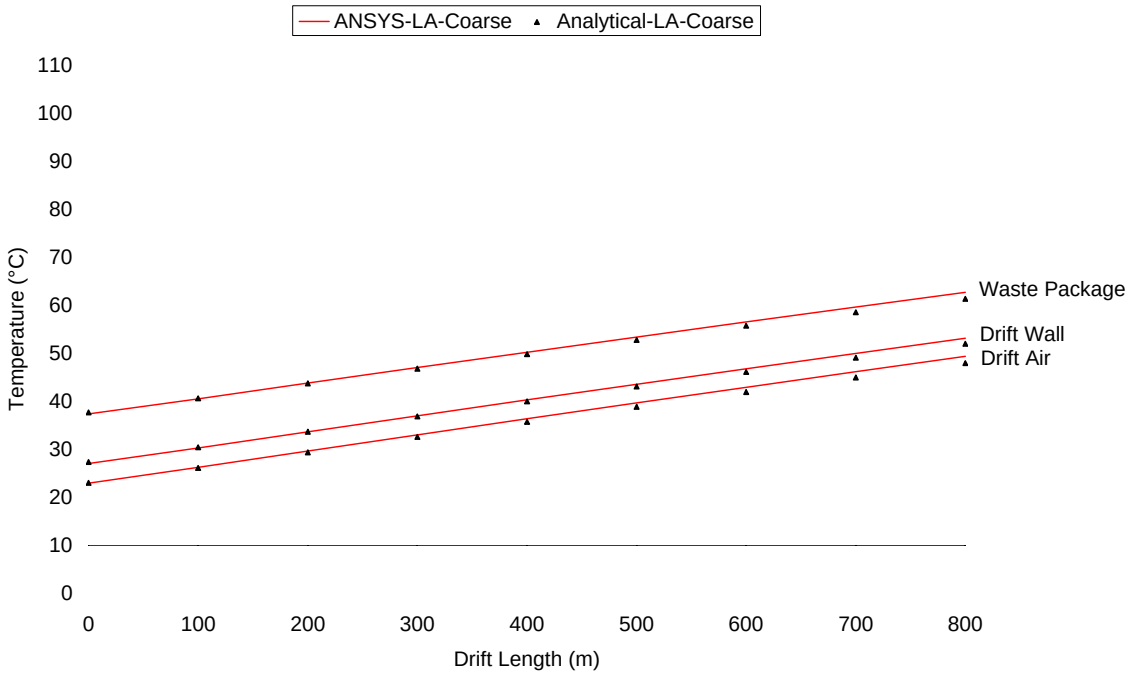

(b) 50 years

Output DTNs: MO0306MWDASLCV.001; MO0307MWDAC8MV.000.

Figure 6-6. Waste Package, Drift Wall, and Drift Air Temperatures as Function of Drift Length for (a) 5 Years and (b) 50 Years from the Time of Waste Emplacement for the ANSYS-LA-Coarse and Analytical-LA-Coarse Models

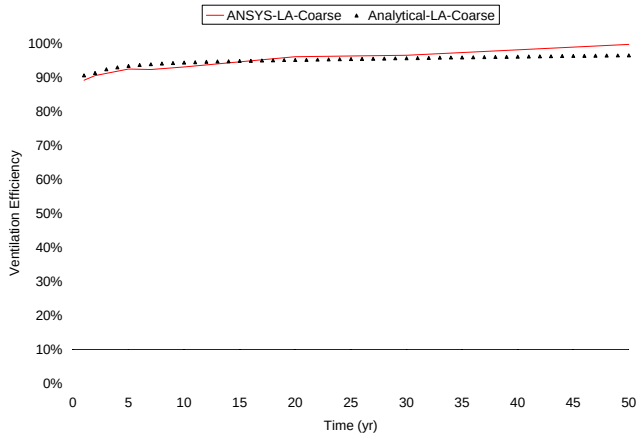

(a) 100 meters

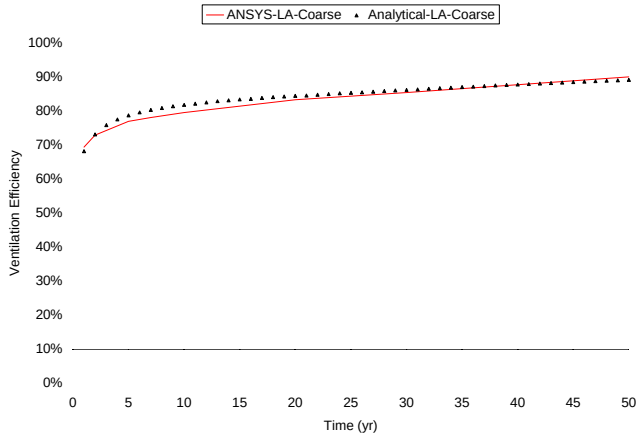

(b) 600 meters

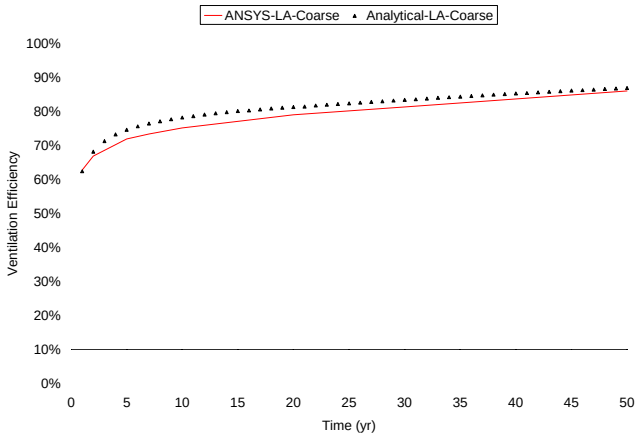

(c) 800 meters

Output DTNs: MO0306MWDASLCV.001; MO0307MWDAC8MV.000.

Figure 6-7. Ventilation Efficiency as Function of Time for (a) 100 Meters, (b) 600 Meters, and (c) 800 Meters from the Drift Entrance for the ANSYS-LA-Coarse and Analytical-LA-Coarse Models

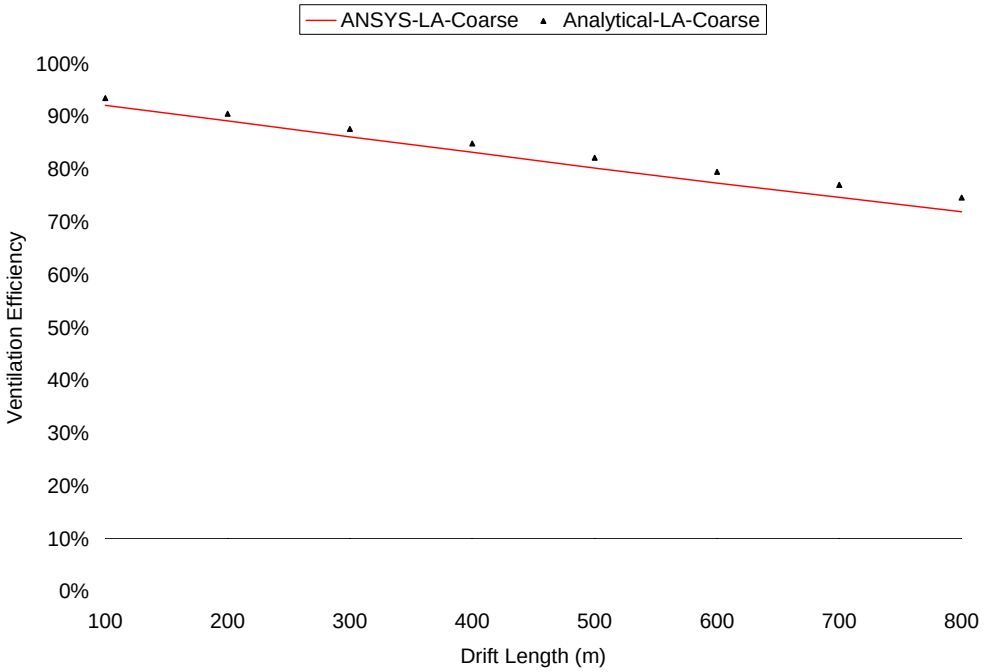

(a) 5 years

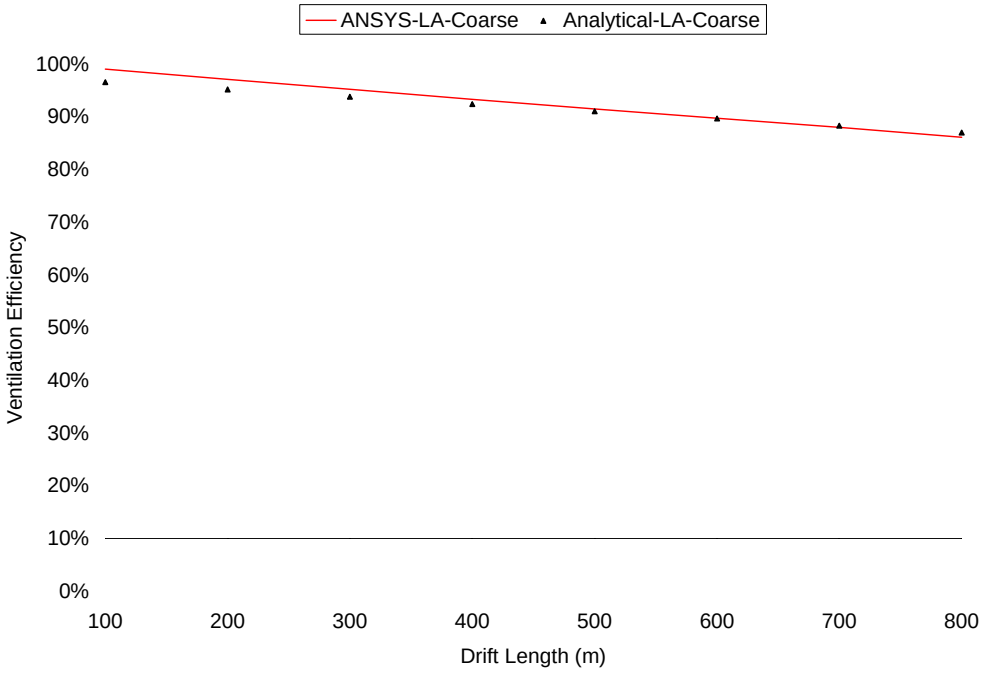

(b) 50 years

Output DTNs: MO0306MWDASLCV.001; MO0307MWDAC8MV.000.

Figure 6-8. Ventilation Efficiency as Function of Drift Length for (a) 5 Years and (b) 50 Years from the Time of Waste Emplacement for the ANSYS-LA-Coarse and Analytical-LA-Coarse Models

Table 6-7. Integrated Ventilation Efficiency for a 600-meter and 800-meter Drift and 50 Years of Ventilation

Model	Integrated Ventilation Efficiency (Eq. 6-6)
600-meter Drift, 50 years of Ventilation	
ANSYS-LA-Coarse [a]	88.3%
Analytical-LA-Coarse [b]	88.0%
800-meter Drift, 50 years of Ventilation	
ANSYS-LA-Coarse [a]	85.8%
Analytical-LA-Coarse [b]	86.0%

[a] DTN: MO0406MWDLACVD.001.
[b] DTN: MO0406MWDAC8VD.001.

6.7 ALTERNATIVE CONCEPTUAL MODEL FOR IN-DRIFT VENTILATION

The alternative conceptual model for in-drift ventilation includes the addition of water and water vapor mass transport in the host rock, across the drift wall, and into the ventilation airstream. Water and water vapor mass transport is directly coupled to the heat transfer processes described in the conceptual model for in-drift ventilation. The impacts of the mass transport, in terms of latent heat transfer, temperature, heat removal rates, and near-field host rock dryout are evaluated using analytical approaches.

6.7.1 Alternative Conceptual Model Heat and Mass Transfer Processes

The coupled heat and mass transfer processes for the alternative conceptual model for in-drift ventilation are the same as those for the conceptual model described in Section 6.3.1 and Figure 6-1 with the addition of two other processes:

Process 5.

Water phase change (evaporation and condensation) occurs within the host rock as the temperature and vapor pressure change which causes the host rock saturation to change, thus altering the thermal conductivity of the rock.

Process 6.

Water (liquid and vapor phases) mass transfer occurs within the host rock and the in-drift air. Water vapor may move within the host rock via diffusion to cooler regions where it condenses. It also may enter the in-drift airflow at the drift wall, causing a change in relative humidity, and can potentially condense in cooler regions of the ventilation system, such as the exhaust main drift and exhaust shafts.

The heat transfer rates for processes 5 and 6 can be related to processes 1 through 4 by again considering the overall conservation of thermal energy except during the early transient response when the waste package temperature is rapidly changing. The following is an addition to the thermal energy conservation described in Section 6.3.1:

- The sum of the convective heat transfer rates from the waste package and the drift wall into the airflow (processes 2 and 3), and the heat of the water vapor transported back across the drift wall (process 6) equal the total heat added to the ventilation air.

Additionally, the mass transfer rates for processes 1 through 6 can be related by considering the overall conservation of mass during the ventilation period. The following summarizes the coupled components of the mass balance:

- The sum of the mass of the ventilation air into the drift and the water vapor that moves across the drift wall from the surrounding host rock equals the mass of the air exiting the drift.

Vapor diffusion or enhanced vapor diffusion has the potential of locally increasing the heat flux rate for saturations that are intermediate to full matrix-fracture saturation, and in the dry condition in which water vapor is absent. Vapor diffusion is defined as the movement of water vapor under Fick's Law. Enhanced vapor diffusion is the movement of water vapor to areas where water vapor is retained, condensed and then evaporated.

6.8 IMPLEMENTATION OF THE ALTERNATIVE CONCEPTUAL MODEL

To assess the impact on the ventilation efficiency of the alternative conceptual model processes, the following analyses were performed:

- An analytical calculation which bounds the latent heat contribution to the in-drift ventilation air stream (Appendix XIII).

- Ventilation analyses using the analytical spreadsheet calculation (named Analytical-LA-Wet-vs-Dry-kth, Appendix VIII) for host rock at different levels of saturation (and therefore different values of thermal conductivity).

- An analysis of experimental data for vapor diffusion and enhanced vapor diffusion.

6.9 RESULTS OF THE APPLICATION OF THE ALTERNATIVE CONCEPTUAL MODEL

The results of the analytical calculation to bound the latent heat contribution to the in-drift ventilation air stream, the Analytical-LA-Wet-vs-Dry-kth model, and the analysis of experimental data to quantify the effects of vapor diffusion and enhanced vapor diffusion follow.

6.9.1 Moisture Effects on the In-Drift Ventilation Air Stream

An analytical calculation was performed which bounds the latent heat contribution to the in-drift ventilation air stream over a 600 m drift length and 50-year ventilation period in terms of the matrix hydrologic properties. Analytical equations for steady-state unsaturated flow in porous media to a specified moisture potential boundary condition at the drift wall were developed with the help of Jury et al. (1991 [DIRS 102010], pp. 51, 60, 113, 151, Section 3.4) and Fetter (1993 [DIRS 102009], pp. 172, 181, 182). Using 30% relative humidity in the drift, the moisture potential at the drift wall was calculated to be 1.985×10^6 cm (see Appendix XIII, p. XIII-5).

The moisture potential in the surrounding host rock at some distance from the drift wall is calculated using two different sets of measured data: the first being the mean of the measurements from borehole core of matrix saturation in the Tptpll (tsw35) geologic unit (Table 4-4) and the second being measurements of water potential taken from the ECRB Cross-Drift in the Tptpll (tsw35) geologic unit (Table 4-5).

The average saturation from the borehole core measurements (Table 4-4) is 74%, which translates to a water potential of 2908 cm (see Appendix XIII, p. XIII-6). Using these potentials, a radius of influence of 6 m, and the hydrologic properties of Tptpll (tsw35) from Table 4-9, the steady-state liquid flux toward the drift (which evaporates) is calculated to be 0.061 mm/year (see Appendix XIII, p. XIII-6).

The measured water potential at 5.62 m from the drift wall is 1000 cm (Table 4-5). Using this value, the potential calculated at the drift wall based on relative humidity conditions, and the hydrologic properties of Tptpll (tsw35) from Table 4-9, the steady-state liquid flux toward the drift (which evaporates) is calculated to be 0.278 mm/year (see Appendix XIII, p. XIII-7).

If all the moisture which fluxes to the drift wall over the entire length of the emplacement drift is evaporated at some constant temperature, the total latent heat contribution to the in-drift air over the 50-year preclosure period can be calculated. The latent heat contribution is then divided by the total heat output by the waste packages over the same 50-year period and 600 meter long drift. The results are presented in Table 6-8.

Table 6-8. Latent Heat Contribution Expressed as a Percentage of the Total Waste Package Heat Over 50 Years and 600 Meters of Drift

Model	Latent Heat Contribution
Analytical model with a moisture flux = 0.061 mm/year[a]	0.01%
Analytical model with a moisture flux = 0.278 mm/year[b]	0.04%

[a] Appendix XIII, p. XIII-6, flux based on the mean saturation from Table 4-4.
[b] Appendix XIII, p. XIII-7, flux based on measured water potential from a borehole in the ECRB Cross-Drift (Table 4-5).

The analytical calculation indicates that:

- The contribution of heat by vaporization of moisture is rate limited by the hydrogeologic properties of the host rock.
- The contribution of heat by vaporization of moisture is a small percentage of the total heat input.

As corroboration, consider a comparative calculation which bounds the latent heat contribution. We take a present day percolation flux and apply it at the drift wall. For northing 234913 and easting 170730, the closest UZ grid mesh column ID is g_9 (see Section 4.1.6). The percolation flux (present day climate, upper case) reported for UZ grid mesh column ID g_9 at the base of the ptn unit is 15.70959 mm/year (DTN: LB0302PTNTSW9I.001 [DIRS 162277], file preq_uz_ptn.q). If this percolation flux is flow focused through matrix and fracture network over the width of two drift diameters, and arrives at the drift wall where it is evaporated, the latent

heat contribution can be calculated. Using the thermophysical properties of water at 350 K (Table 4-18), the total latent heat contribution over the 50-year ventilation period and 600 meters of drift is calculated as follows:

$$\left(\frac{15.70959\text{mm}}{\text{yr}}\right)\cdot\left(\frac{0.001\text{m}}{1\text{mm}}\right)\cdot\left(\frac{2\cdot 5.5\text{m}\cdot 600\text{m}}{1}\right)\cdot\left(\frac{50\text{yr}}{1}\right)\cdot\left(\frac{973.7\text{kg}}{\text{m}^3}\right)\cdot\left(\frac{2317\text{kJ}}{\text{kg}}\right)\cdot\left(\frac{1000\text{J}}{1\text{kJ}}\right)=1.170\cdot 10^{13}\,\text{J}$$

The total waste package heat input over the 50-year ventilation period and 600 meter long drift is $8.605\cdot 10^{14}$ J (DTN: MO0307MWDAC8MV.000, worksheet "Ventilation Efficiency"). The latent heat contribution expressed as a percentage of the total waste package heat input is:

$$\frac{1.170\cdot 10^{13}\,\text{J}}{8.605\cdot 10^{14}\,\text{J}}=1.4\%$$

This calculation supports the conclusion reached earlier, that the contribution of heat by vaporization of moisture is a small percentage of the total heat input. Therefore, neglecting latent heat in the calculation of ventilation efficiencies does not introduce significant error.

The reduction in relative humidity to the in-drift ventilation air for a 600 meter long drift is calculated using the methodology outlined in Attachment XXVII of *ANSYS Calculations in Support of Natural Ventilation Parametric Study for SR* (BSC 2001 [DIRS 155246]) and *Mine Ventilation and Air Conditions* (Hartman 1982 [DIRS 128009], pages 596-597). Using the percolation flux of 15.7 mm/yr, the conversion factor from page xix, and the thermophysical properties of water at 350 K (Table 4-18), the mass flux of water which arrives at the drift wall is:

$$\left(\frac{15.70959mm}{yr}\right)\cdot\left(\frac{0.001m}{1mm}\right)\cdot\left(\frac{1yr}{31556926s}\right)\cdot\left(\frac{2\cdot 5.5m\cdot 600m}{1}\right)\cdot\left(\frac{973.7kg}{m^3}\right)\cdot\left(\frac{1grain}{6.479891\times 10^{-5}kg}\right)=49.371\,\frac{grains_{water}}{s}$$

The mass flux of the ventilation air at 350K (Table 4-17) is:

$$\left(\frac{15m^3}{s}\right)\cdot\left(\frac{0.995kg}{m^3}\right)\cdot\left(\frac{2.2046lb}{1kg}\right)=32.904\,\frac{lb_{air}}{s}$$

The distribution of mass flux of water to the mass flux of ventilation air (percolation component) is:

$$\left(\frac{49.371\,\frac{grains_{water}}{s}}{32.904\,\frac{lb_{air}}{s}}\right)=1.500\,\frac{grains_{water}}{lb_{air}}$$

The relative humidity of the inlet air is taken to be 20.31%, which has a moisture content of 28.210 $\text{grains}_{\text{water}}/\text{lb}_{\text{air}}$ (BSC 2002 [DIRS 161233], Table 5 for P1 Early Emplacement Drift, Intake Main). The new moisture content of the ventilation air is then the sum of the percolation and relative humidity components:

$$28.210\,\frac{grains_{water}}{lb_{air}} + 1.500\,\frac{grains_{water}}{lb_{air}} = 29.710\,\frac{grains_{water}}{lb_{air}}$$

Converting $29.710 grains_{water}/lb_{air}$ to lb_{water}/lb_{air}:

$$\left(\frac{29.710\,grains_{water}}{1\,lb_{air}}\right)\cdot\left(\frac{6.479891\times10^{-5}\,kg}{1\,grain}\right)\cdot\left(\frac{2.2046\,lb}{1\,kg}\right) = 0.00424\,\frac{lb_{water}}{lb_{air}}$$

The average barometric pressure is 26.3322 inHg (BSC 2002 [DIRS 161233], Table 5 for P1 Early Emplacement Drift, Intake Main). The partial pressure can be calculated by (Hartman 1982 [DIRS 128009], Eq. 21-5 rearranging to solve for pv):

$$\frac{0.00424\,\frac{lb_{water}}{lb_{air}}\cdot 26.3322\,inHg}{0.622 + 0.00424\,\frac{lb_{water}}{lb_{air}}} = 0.178\,inHg$$

The air temperature at the outlet of the 600 meter long drift after 50 years of ventilation is approximately 42°C from the results of the Analytical-LA-Coarse ventilation model (Table 8-6). The saturated vapor pressure at 42°C (107.6°F) is (Hartman 1982 [DIRS 128009], Eq. 21-1):

$$0.18079e^{\frac{(17.27\cdot 107.6°F)-552.64}{107.6°F+395.14}} = 2.427\,inHg$$

The relative humidity at the outlet of the 600 meter long drift is (Hartman 1982 [DIRS 128009], Eq. 21-4):

$$\frac{0.178\,inHg}{2.427\,inHg}\cdot 100\% = 7.3\%$$

Neglecting the contribution from percolation, the relative humidity at the outlet is 6.9%. Therefore, while the ventilation air stream picks up moisture through evaporation of the near field host rock pore water at a rate of approximately 15.7 mm/yr, the relative humidity over 600 meters of drift and 50 years of ventilation decreases from approximately 20% to 7%, primarily due to the increase in air temperature.

6.9.2 Ventilation Analysis for Host Rock at Varying Degrees of Saturation

An analytical spreadsheet ventilation analysis (Output DTN: MO0306MWDRTCCV.000, worksheet "Wet vs. Dry" of Analytical-LA-Wet-vs-Dry-kth.xls) assessed the impact of varying degrees of host rock saturation on the waste package, drift wall, and in-drift air temperatures and the ventilation efficiency for a 600 meter long drift. These analyses used the thermophysical properties of the tws35 unit for the repository horizon and matrix water saturation ranging from 0% to 100%. Figure 6-9 shows the impact of a "wet" versus "dry" thermal conductivity on the temperatures of the waste package, drift wall, and in-drift air. The temperatures for the two cases are within 4°C for all distances from the drift entrance and times since emplacement, with the "dry" case being consistently hotter. Figure 6-10 plots the integrated ventilation efficiency as a function of matrix saturation and host rock thermal conductivity. The integrated ventilation

efficiency changes from approximately 87.7% to 90.7% when the matrix saturation goes from wet to dry.

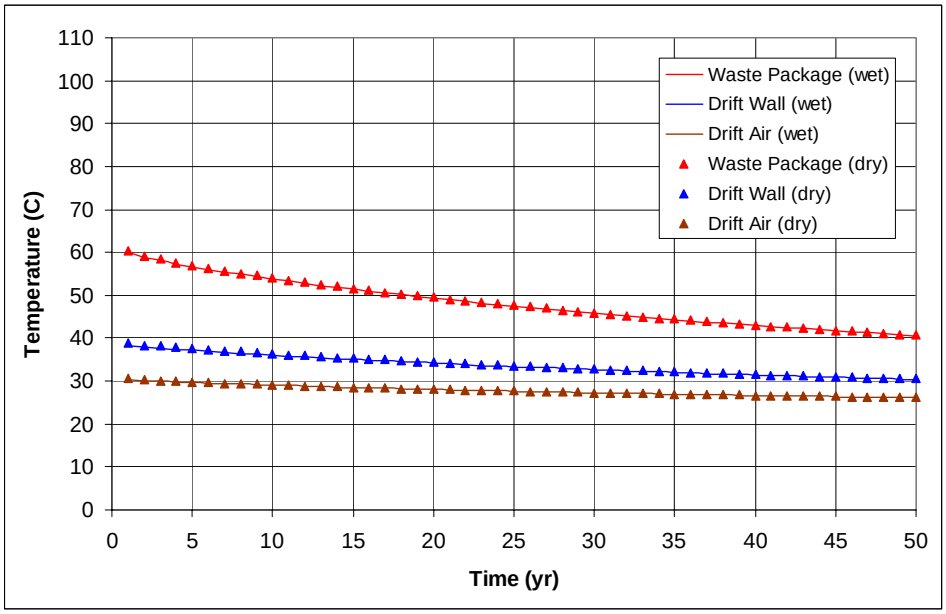

(a) 100 meters

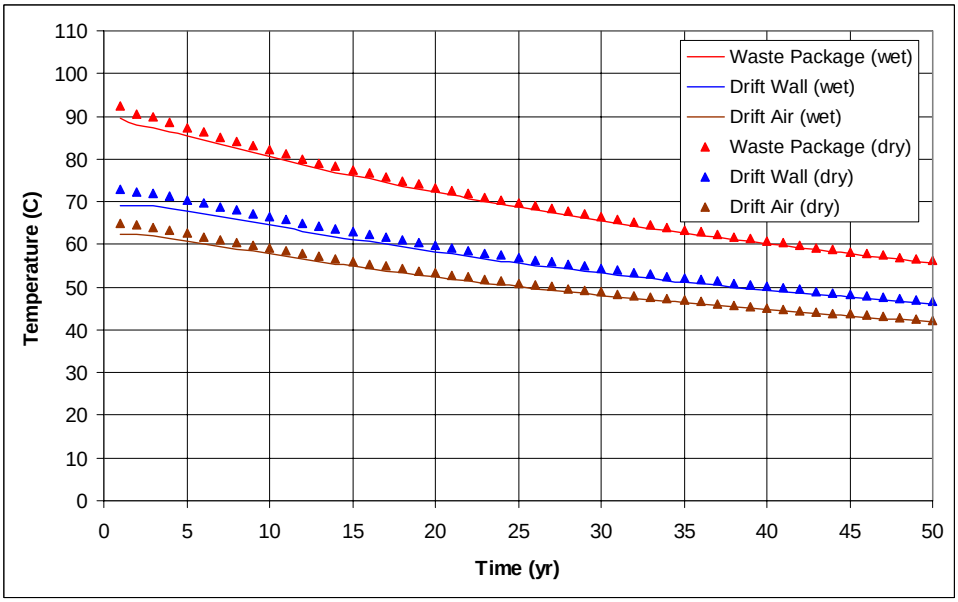

(b) 600 meters

Output DTN: MO0306MWDRTCCV.000, plots generated based on data from worksheet "Wet vs. Dry" of Analytical-LA-Coarse-Wet-vs-Dry-kth.xls.

Figure 6-9. Waste Package, Drift Wall, and Drift Air Temperatures as Function of Time for (a) 100 Meters and (b) 600 Meters from the Drift Entrance for the Analytical-LA-Wet-vs-Dry-kth Ventilation Model (Attachment VIII)

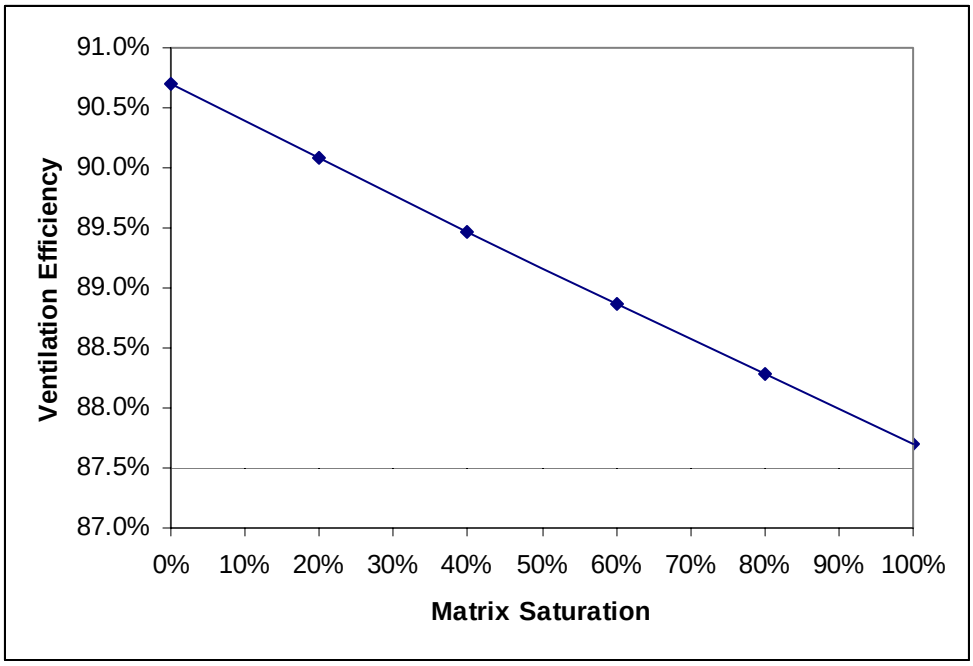

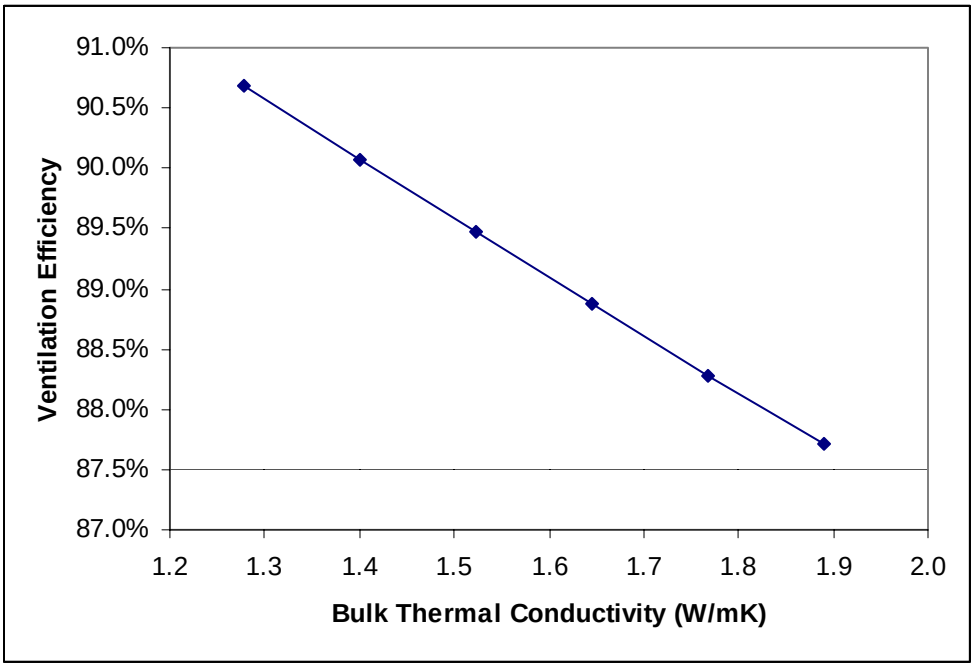

Output DTN: MO0306MWDRTCCV.000, plots generated based on data in worksheet "Wet vs. Dry" of Analytical-LA-Wet-vs-Dry-kth.xls.

Figure 6-10. Ventilation Efficiency as Function of Matrix Saturation and Bulk Thermal Conductivity Calculated Using the Analytical-LA-Wet-vs-Dry-kth Ventilation Model (Attachment VIII)

6.9.3 Evaluation of Vapor Diffusion and Enhanced Vapor Diffusion on the Host Rock Thermal Conductivity and Thus Ventilation Efficiency

The following discussion relates the issue of enhanced vapor diffusion in the surrounding walls of the emplacement drift. Moyne et al. 1990 [DIRS 153164] present information on the effect of enhanced vapor diffusion on increasing the effective thermal conductivity of the rock mass. If enhanced vapor diffusion occurs over intermediate ranges of saturation, the effective thermal conductivity could be two to three times higher than the thermal conductivity under saturated conditions in the matrix (Moyne et al. 1990 [DIRS 153164], Figures 2 through 4). In this case the ventilation efficiency could be lower based upon the higher effective thermal conductivity than would be the case when the saturated thermal conductivity applies.

In addition to the conduction of heat under a temperature gradient, it is possible to have vapor phase diffusion (Jury et al. 1991 [DIRS 102010], p. 211) within the rock mass. In addition, enhanced vapor phase diffusion may occur (Jury et al. 1991 [DIRS 102010], p. 212). These related phenomena are not included in the ventilation analysis presented above nor in the ANSYS calculations. Vapor diffusion and/or enhanced vapor diffusion (due to evaporation and condensation in the pores) tend to increase the aggregate thermal conductivity over that of stagnant fluid components.

The following discussion presents information regarding vapor diffusion and enhanced vapor diffusion by Jury et al. (1991 [DIRS 102010], pp. 211 to 213). Experimental results obtained by Moyne et al. (1990 [DIRS 153164]) are then discussed to illustrate vapor and enhanced vapor diffusion effects. Experimental results obtained from laboratory measurements on core samples and the results from the large scale Drift Scale Test are then presented.

6.9.3.1 Vapor Diffusion by Jury et al.

Jury et al. (1991 [DIRS 102010]) provide a general discussion of vapor diffusion. Laboratory tests have shown that when temperature gradients were placed across soil samples, the measured vapor fluxes were 10 times larger than that predicted by Fick's Law. It was found that two mechanisms could increase the potential for vapor diffusion. The first mechanism is that water vapor that is fluxing towards moisture that is retained in the pore space may condense on one side and evaporate on the other side (Jury et al. 1991 [DIRS 102010], p. 212, Figure 6.7).

The second enhancement mechanism relates to the thermal gradients across the liquid phase contained within the pore space. The thermal conductivity of the solid phase is several times larger than the thermal conductivity of water. Since the thermal gradients within the pore space are more likely to be influenced by liquid water, the effective thermal gradients for a uniform heat flux would be higher. Theoretical considerations suggest that the thermal gradients might be a factor of two to three higher. Moyne et al. 1990 ([DIRS 153164] Figures 2 through 4) show that for materials that have a higher interconnected porosity, that the effective thermal conductivity could be higher and provides a theoretical analysis of the enhanced vapor diffusion.

6.9.3.2 Thermal Conductivity – Saturation Relationship for Welded Tuff

The following presents a discussion of the relationship of apparent thermal conductivity to saturation. The experimental data are for samples from the middle nonlithophysal (Tptmn) unit, whish is adequate to represent response of the host rock units.

Sandia National Laboratories conducted a laboratory investigation of thermal conductivity as a function of saturation state, using welded and nonwelded tuff specimens associated with the Drift Scale Test. Rock core samples were recovered from the repository site to determine the relationship between thermal conductivity and saturation state for both welded and nonwelded tuffs. Welded tuff from the Tptpmn unit was taken from Alcove 5 of the Exploratory Studies Facility. All thermal conductivity tests were conducted at 30°C and at intermediate moisture conditions. The results of the laboratory investigations (DTN: SNL22100196001.006 [DIRS 158213]) below a saturation of 90 percent are presented in Figure 6-11 with a trend line.

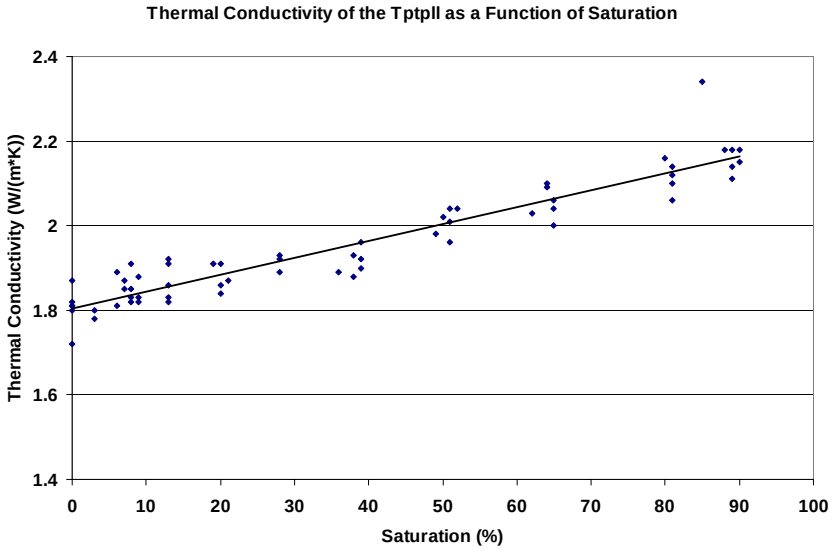

DTN: SNL22100196001.006 [DIRS 158213].

Figure 6-11. Rock Matrix Thermal Conductivity as a Function of Saturation, with Trend Line

The measured results show a similar trend with results for a highly compacted clay from Moyne et al. (1990 [DIRS 153164]), which do not exhibit enhanced vapor diffusion effects. It should be emphasized that at a low temperature of 30°C, the vapor pressure of water is not very high, and the general theory presented by Moyne et al. (1990 [DIRS 153164]) would not predict a very large increase in aggregate thermal conductivity.

Wildenschild and Roberts (1999 [DIRS 131055]) performed an investigation of thermally driven water vapor diffusion, for tuff from the middle nonlithophysal zone of the Topopah Spring Tuff (Tptpmn), associated with the Large Block Test. Thermal conductivity was measured for a single sample of welded tuff indirectly as a function of total pore pressure, temperature and water content. Enhancement of vapor diffusion in welded tuff was not observed at any of the combinations of saturation, temperature and imposed pressures. At a temperature of approximately 50°C, the aggregate rock matrix thermal conductivity increased modestly with the

degree of saturation from about 1.1 W/m·K at a saturation of 0.1 to about 1.3 W/m·K at a saturation of 0.78 (Wildenschild and Roberts 1999 [DIRS 131055], Figure 5). From a saturation of 0.1 to a saturation of 0.35, the thermal conductivity was approximately constant. The results showed a stronger dependence on temperature than on saturation. The guarded heat flow results are corroborative with the experimental results for a single sample of welded tuff presented by Wildenschild and Roberts (1999 [DIRS 131055]). Wildenschild and Roberts (1999 [DIRS 131055]) show that the aggregate thermal conductivity increased by 18 percent as the saturation increased from zero to 78 percent. This increase compares well with increase of about 16 percent in Figure 6-11 over this same saturation range.

In conclusion, experimental studies on welded tuff show that thermal conductivity varies with liquid saturation in a straightforward, monotonic manner. Targeted experiments do not show evidence of enhanced vapor diffusion that increases the aggregate thermal conductivity and affects ventilation efficiency. The results apply over the range of temperature of the host rock during the preclosure period.

6.10 APPLICABILITY OF THE VENTILATION EFFICIENCY AS AN ABSTRACTION METHOD

The ventilation efficiency can be expressed as a single value by integrating over both the duration of the preclosure period and the length of the drift (Equation 6-6). It may also be applied as a function of time and drift length (Equation 6-5). Downstream models that model the ventilation period may implement ventilation efficiency either way.

The first way is to introduce the heat flux adjusted by the ventilation efficiency directly to the drift wall. Typically, a downstream model that uses the ventilation efficiency in this manner does not model the in-drift components. In this case, the only heat transfer mechanism being simulated is the conduction from the drift wall out to the host rock. Because the solution of the heat conduction equation is linear in nature with constant temperature heat sinks at the upper and lower boundaries of the domain, a unique solution for the temperature of the drift wall exists. Therefore, this method will result in both the same heat flux at the drift wall and the same drift wall temperature history as that predicted by the ventilation model from which the ventilation efficiency was derived.

The second way the ventilation efficiency may be used involves downstream models that include the in-drift components in their domains, but cannot model boundary layers and therefore cannot include convective heat transfer. These models typically reduce the waste package heat generation rate by the ventilation efficiency and apply this new heat flux directly to the waste package rather than the drift wall. This type of application relies on both radiation and conduction heat transfer to deliver the right amount of heat to the drift wall, and replicate the drift wall temperature history as predicted by the upstream ventilation model. This approach is less straightforward than the first and requires further discussion as to its feasibility.

6.10.1 Theoretical Use of the Ventilation Efficiency at the Waste Package

Consider the case where the preclosure waste package heat output reduced by the ventilation efficiency (calculated by an upstream ventilation model) is used as a substitute for the preclosure

convection to represent the preclosure heat removal by ventilation. An energy balance for the ventilation model is:

$$Q_s = Q_{conv-s} + Q_{rad} \quad \text{(Eq. 6-70)}$$

where

$$Q_{conv-s} = A \cdot (T_s - T) \quad \text{(Eq. 6-71)}$$

$$Q_{rad} = C \cdot (T_s^4 - T_w^4) \quad \text{(Eq. 6-72)}$$

The fraction of heat removed by the ventilation (i.e., by convection) is:

$$\eta = \frac{Q_{conv-s} + Q_{conv-w}}{Q_s} \quad \text{(Eq. 6-73)}$$

where

$$Q_{conv-w} = B \cdot (T_w - T) \quad \text{(Eq. 6-74)}$$

The constants *A*, *B*, and *C* are defined as:

$$A = d_s \cdot h_s \quad \text{(Eq. 6-75)}$$

$$B = d_w \cdot h_w \quad \text{(Eq. 6-76)}$$

$$C = d_s \cdot h_{rad} \quad \text{(Eq. 6-77)}$$

Substituting Equations 6-71 and 6-72 into Equation 6-70 yields:

$$Q_s = A \cdot (T_s - T) + C(T_s^4 - T_w^4) \quad \text{(Eq. 6-78)}$$

Substituting Equations 6-71, 6-74, and 6-78 into Equation 6-73 yields:

$$\eta = \left[\frac{[A \cdot (T_s - T) + B \cdot (T_w - T)]}{[A \cdot (T_s - T) + C \cdot (T_s^4 - T_w^4)]} \right] \quad \text{(Eq. 6-79)}$$

For the downstream model, the waste package heat output is multiplied by the ventilation efficiency to account for the heat removed during the preclosure ventilation period. Equation 6-80 represents the fraction of heat delivered to the drift wall:

$$Q'_w \equiv Q_s \cdot (1 - \eta) \quad \text{(Eq. 6-80)}$$

Substituting Equations 6-78 and 6-79 into Equation 6-80 yields:

$$Q_w^{'} = \left[A \cdot (T_s - T) + C \cdot \left(T_s^4 - T_w^4\right)\right] \cdot \left[1 - \frac{\left[A \cdot (T_s - T) + B \cdot (T_w - T)\right]}{\left[A \cdot (T_s - T) + C \cdot \left(T_s^4 - T_w^4\right)\right]}\right] \qquad \text{(Eq. 6-81)}$$

An energy balance for the downstream model considered in this case (i.e., where the ventilation efficiency is used as a substitute for the heat transfer via convection) is:

$$Q_w^{'} = Q_{rad}^{'} \qquad \text{(Eq. 6-82)}$$

where

$$Q_{rad}^{'} = C \cdot \left(T_s^{'4} - T_w^{'4}\right) \qquad \text{(Eq. 6-83)}$$

where

$T_s^{'}$ = waste package temperature of the downstream model (K)
$T_w^{'}$ = drift wall temperature of the downstream model (K)

Substituting Equations 6-81 and 6-83 into Equation 6-82 and simplifying yields:

$$\left(T_s^{'4} - T_w^{'4}\right) = \left(T_s^4 - T_w^4\right) - \frac{B}{C} \cdot (T_w - T) \qquad \text{(Eq. 6-84)}$$

If $T_s^{'} = T_s$ and $T_w^{'} = T_w$ are to be true, then the term $\frac{B}{C} \cdot (T_w - T)$ must be zero. For this to be true, either the coefficient B must be zero, and/or the terms T_w and T must be equal. The implication for either of these conditions is that there is no convective heat transfer between the drift wall and the drift air, which of course is not true. Therefore, a downstream application in which the ventilation efficiency is used as a substitute for the convective heat transfer to simulate the preclosure heat removal by ventilation cannot accurately represent both the preclosure waste package and drift wall temperatures as calculated by the ventilation model. Because T_w is controlled by heat flux through the wall and far-field boundary conditions, the preclosure waste package temperatures will bear most of the inaccuracy.

6.10.2 Numerical Example Using the Ventilation Efficiency as an Abstraction Method

Two numerical examples that apply the theoretical use of the ventilation efficiency as described in Section 6.10.1 are presented below in Sections 6.10.2.3 and 6.10.2.4. Beforehand, total energy balances are presented using the results of the ANSYS-LA-Coarse model and Equation 6-5 for calculating the instantaneous heat removal efficiency as a function of time and drift length, and Equation 6-6 for calculating an integrated heat removal efficiency.

6.10.2.1 Using Equation 6-5 to Calculate the Total Energy Delivered to the Host Rock

Using the results of the ANSYS-LA-Coarse model and Equation 6-5 to calculate the heat removal efficiency as a function of both time and drift length, the total energy delivered to the host rock over the 50-year preclosure period and a 600 meter long drift becomes:

$$Energy_{rock-total} = \int_0^{600m} \int_0^{50yr} Q_s(t) \cdot (1 - \eta(t,x)) \cdot dt \cdot dx \qquad \text{(Eq. 6-85)}$$

where

$Energy_{rock\text{-}total}$ = total energy to the host rock (J)
$Q_s(t)$ = waste package lineal heat decay as a function of time (W/m)
$\eta(t,x)$ = instantaneous ventilation heat removal efficiency at some time, t, and some distance from the drift entrance, x, (dimensionless)

Using the heat decay from Table 4-13, and the heat removal efficiencies calculated as a function of time and drift length for the ANSYS-LA-Coarse model (DTN: MO0306MWDASLCV.001), the total energy delivered to the host rock over 50 years and 600 meters is 1.02×10^{14} J (DTN: MO0306MWDASLCV.001, worksheet "Efficiency data" of ANSYS-LA-Coarse.xls, row 49, column O).

6.10.2.2 Using Equation 6-6 to Calculate the Total Energy to the System

Finally, using the results of the ANSYS-LA-Coarse model and Equation 6-6 to calculate an integrated ventilation heat removal efficiency, the total energy to the system over the 50-year preclosure period and 600 meter long drift becomes:

$$Energy_{total} = 600m \cdot \int_0^{50yr} Q_s(t) \cdot (1 - \eta_{integrated}) \cdot dt \qquad \text{(Eq. 6-86)}$$

where

$\eta_{integrated}$ = integrated ventilation heat removal efficiency given by Eq. 6-6 (dimensionless)

Using the heat decay from Table 4-13 and the integrated ventilation efficiency of 88.3% reported in Table 6-7 for the ANSYS-LA-Coarse model, the total energy to the system over 50 years and 600 meters is 1.02×10^{14} J (DTN: MO0306MWDASLCV.001, worksheet "Efficiency data" of ANSYS-LA-Coarse.xls, row 100, column M). This result balances with the energy calculated in Section 6.10.2.1.

6.11 SENSITIVITY OF THE VENTILATION EFFICIENCY TO UNCERTAINTIES IN KEY INPUTS AND DESIGN PARAMETERS

The sensitivity of the ventilation efficiency to uncertainties in key inputs and design parameters was investigated using the Delta Method, also referred to as the "generation of system moments" or "statistical error propagation." The Delta Method involves calculating the mean system

performance, in this case the integrated ventilation efficiency, and its standard deviation using the means and variances of the component variables which make up the system. Equations 6-87 and 6-88 describe the Delta Method mathematically (Hahn and Shapiro 1967 [DIRS 146529], pp. 228 to 231). Equation 6-89 describes the standard deviation based on the variance (Hahn and Shapiro 1967 [DIRS 146529], pp. 228 to 231).

$$E(z) = h[E(x_1), E(x_2), ..., E(x_n)] + \frac{1}{2}\sum_{i=1}^{n} \frac{\partial^2 \bar{h}}{\partial x_i^2} Var(x_i) \quad \text{(Eq. 6-87)}$$

$$Var(z) = \sum_{i=1}^{n} \left(\frac{\partial h}{\partial x_i} \right)^2 Var(x_i) \quad \text{(Eq. 6-88)}$$

$$Var(x_i) = [\sigma(x_i)]^2 \quad \text{(Eq. 6-89)}$$

where

$E(z)$ = mean system performance
$E(x_{1, 2, ..., n})$ = mean of the xth component variable
h = function that describes the system performance based on the components variable (set of equations from Section 6.4.2 describing the ventilation model)
$Var(x_{1, 2, ...n})$ = variance of the xth component variable
$Var(z)$ = variance of the system performance
$\sigma(x_i)$ = standard deviation of the xth component variable

When the system performance is a linear function of the component variables, the second and higher order partial derivatives are zero. In other words, the second term of Equation 6-87 goes to zero and the mean system performance can be calculated using only the means of the component variables.

In terms of the ventilation model, $E(z)$ represents the mean integrated ventilation efficiency where $h[E(x_1), E(x_2),\ldots, E(x_n)]$ represents the equations of Section 6.4.2 used to perform the algebraic ventilation calculation, and $E(x_{1, 2, \ldots, n})$ represents the mean values of the inputs and design parameters. $Var(x_{1, 2, \ldots, n})$ then represents the variances of the inputs and design parameters. $h[E(x_1), E(x_2),\ldots, E(x_n)]$ is evaluated using the analytical method. The variance or standard deviation of the integrated efficiency is calculated using Equation 6-88 which propagates the uncertainties in select inputs and design parameters (expressed by variances or standard deviations).

Table 6-9 shows the key inputs and design parameters selected for the Delta Method, along with their respective standard deviations. Where available, standard deviations were assigned from DTNs. Where unknown, standard deviations using normal distributions were determined based on engineering judgment. The source for each standard deviation is documented in Table 6-9.

Table 6-9. Inputs and Design Parameters, and Their Respective Standard Deviations, Selected for the Delta Method to Assess the Sensitivity of the Integrated Ventilation Efficiency

Input/Design Parameter	Central Value	Source	Standard Deviation	Source for Standard Deviation
Dry Bulk Thermal Conductivity (W/m·K)	1.2784	Table 4-6 for Tptpll (tsw35)	0.2511	Table 4-6 for Tptpll (tsw35)
Wet Bulk Thermal Conductivity (W/m·K)	1.8895	Table 4-6 for Tptpll (tsw35)	0.2484	Table 4-6 for Tptpll (tsw35)
Grain Density (kg/m^3)	2593	Attachment II for tsw35 (column K)	138	Table 4-6 for Tptpll (tsw35) dry bulk density
Solids Specific Heat (J/kg·K)	930	Table 4-7 for Tptpll (tsw35)	130	Table 4-7 for Tptpll (tsw35)
Matrix Porosity	14.86%	Table 4-6 for Tptpll (tsw35)	3.4%	Table 4-6 for Tptpll (tsw35)
Matrix Saturation	90.5%	Section 5.3	9.5%	Saturation cannot exceed 100%
Lithophysal Porosity	8.83%	Table 4-6 for Tptpll (tsw35)	5.4%	Table 4-6 for Tptpll (tsw35)
Drift Diameter (m)	5.5	Table 4-16	0.5	Constrained by construction tolerance
Waste Package Diameter (m)	1.644	Table 4-15	0.5	Cover range of waste packages from 24-BWR to DHLW
Inlet Air Temperature (°C)	22.82	Output DTN: MO0306MWDASLCV.001, air_temp_co.input	5	Constrained by average temperature at the surface and at the water table
Air Flow Rate (m^3/s)	15	Table 4-16	2	Controlled process variable
Drift Wall Emissivity	0.9	Table 4-8 for Tptpll	0.1	Emissivity cannot exceed 1.0
Waste Package Emissivity	0.87	Table 4-15	0.13	Emissivity cannot exceed 1.0
Inner Convection Heat Transfer Coefficient ($W/m^2 \cdot K$)	4.23	Output DTN: MO0307MWDAC8MV.000 (Analytical) (average of hs for all time steps, columns F, H, J, L, N, P, R T, in worksheet "CSTR Analysis" of Analytical-LA-Coarse-800m.xls; converted from 0.74 Btu/h·ft^2·°F)	0.63	15% of the Mean (typical combined random standard uncertainty from Tables IX-24 and IX-25 of Appendix IX)
Outer Convection Heat Transfer Coefficient ($W/m^2 \cdot K$)	3.86	Output DTN: MO0307MWDAC8MV.000 (Analytical) (average of hw for all time steps, columns G, I, K, M, O, Q, S, U, in worksheet "CSTR Analysis" of Analytical-LA-Coarse-800m.xls; converted from 0.68 Btu/h·ft^2·°F)	0.58	15% of the Mean (typical combined random standard uncertainty from Tables IX-24 and IX-25 of Appendix IX)

Using the central values for the inputs and design parameters listed in Table 6-9, the integrated ventilation efficiency is 88% for a 600-meter-long drift, and 86% for an 800-meter-long drift. By employing the Delta Method to propagate the standard deviations of the inputs and design parameters listed in Table 6-9 through the analysis, the standard deviation (normally distributed) of the integrated ventilation efficiency about the central value of 88% is 3% for the 600-meter-long drift, and 3% about the central value of 86% for the 800-meter-long drift. Expressed in terms of the normal distribution, the integrated ventilation efficiency for the 600-meter-long drift will be between approximately 85% and 91%, 68% of the time; between 83% and 93%, 96% of the time; and between 80% and 96%, 99% of the time (Hahn and Shapiro 1967 [DIRS 146529]). The documentation of this analysis is in Appendix VII.

Table 6-10 summarizes the first step of the Delta Method, which is to calculate the system performance (ventilation efficiency) using the central values of the system components (input/design parameters) from Equation 6-87. Then, independently and one at a time, each system component value is replaced by its central value plus/minus a standard deviation, and a new system performance is calculated using Equation 6-87. The standard deviation of the ventilation efficiency is calculated using the 5th and 7th columns of Table 6-10 and Equations 6-88 and 6-89.

In addition to the uncertainty values in Table 6-10, the change in ventilation efficiency due to a reduction in total pressure from 1 atmosphere to 0.88 atmosphere (due to the repository elevation) as discussed in Section 4.1.11 results in the ventilation efficiency for a 600-meter drift changing from 87.98% to 87.00%, or a change from 88% to 87%, a 1% reduction. This calculation is performed using the Excel analytical model presented in DTN: MO0307MWDAC8MV.000. Likewise for an 800-meter drift the ventilation efficiency changes from 85.93% to 84.72%, or a change from 86% to 85%, again a 1% reduction. This 1% change is considered to be insignificant compared to the standard deviation of 3% discussed above. The sensitivity results with respect to the other key input and design variables are not expected to change if the central values are based on a pressure of 0.88 atmosphere.

In addition, the influence of each of the standard deviations of the inputs and design parameters on the integrated ventilation efficiency was determined. Their individual influence on the standard deviation of the integrated efficiency was also determined. These influences are plotted against each other in Figure 6-12. All values of influence for the respective axes of the plot were normalized by dividing by the largest corresponding value. The purpose of Figure 6-12 is to give a qualitative assessment of which inputs and design parameters are most significant (and those that are not significant) in the ventilation model. The significance is determined by the variable's influence, relative to other variables, on both the integrated ventilation efficiency and its standard deviation. Figure 6-12 shows that the most significant variables in the ventilation model are the inlet air temperature, the air flow rate, the host rock wet bulk thermal conductivity (as a function of matrix saturation and specific heat), and the convection heat transfer coefficients.

Table 6-10. Using the Delta Method to Determine the Sensitivity of the Ventilation Efficiency Due to Uncertainties in Key Inputs and Design Parameters for a 600-Meter-Long Drift

Input/Design Parameter	Central Value	Efficiency (Eq. 6-88)	Central Value + Standard Deviation	Efficiency (Eq. 6-88, replacing the mean of the x^{th} component variable with the value in the previous column)	Central Value – Standard Deviation	Efficiency (Eq. 6-88, replacing the x^{th} component variable with the value in the previous column)
Dry Bulk Thermal Conductivity (W/m·K)	1.2784	88.0%	1.5295	87.88%	1.0273	88.06%
Wet Bulk Thermal Conductivity (W/m·K)	1.8895		2.1379	87.12%	1.6411	88.87%
Grain Density (kg/m^3)	2593		2731	87.88%	2455	88.06%
Solids Specific Heat (J/kg·K)	930		1060	87.74%	800	88.22%
Matrix Porosity	14.86%		18.26	87.93%	11.46	88.01%
Matrix Saturation	90.5%		100	87.70%	81.084	88.24%
Lithophysal Porosity	8.83%		14.23	88.10%	3.43	87.85%
Drift Diameter (m)	5.5		6	87.86%	5	88.07%
Waste Package Diameter (m)	1.644		2.144	88.11%	1.144	87.80%
Inlet Air Temperature (°C)	22.82		27.82	85.82%	17.82	90.12%
Air Flow Rate (m^3/s)	15		17	88.81%	13	86.89%
Drift Wall Emissivity	0.9		1	87.94%	0.8	88.00%
Waste Package Emissivity	0.87		1	87.85%	0.74	88.12%
Inner Convection Heat Transfer Coefficient ($W/m^2·K$)	4.23		4.86	88.17%	3.60	87.74%
Outer Convection Heat Transfer Coefficient ($W/m^2·K$)	3.87		4.45	88.24%	3.29	87.63%

DTN: MO0406MWDLACVD.001.

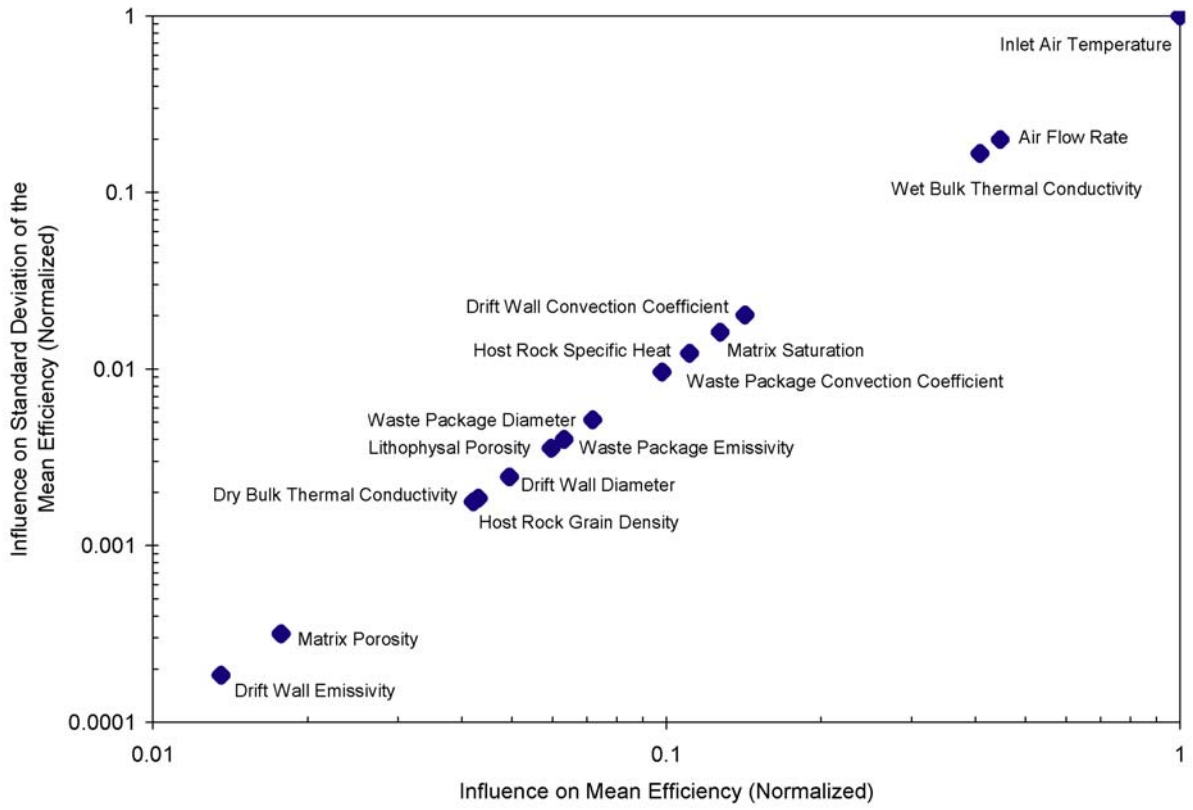

Output DTN: MO0406MWDLACVD.001.

Figure 6-12. Qualitative Plot Showing the Influence of Ventilation Model Inputs and Design Parameters on the Integrated Ventilation Efficiency and Its Standard Deviation

7. VALIDATION

AP-SIII.10Q requires that total system performance assessment model components be validated for their intended purpose and stated limitations, and to the level of confidence required by a component's relative importance to the performance of the repository. Section 1 of this report provides the intended use of the ventilation model and the model limitations.

The governing technical work plan (BSC 2004 [DIRS 170950], Section 2.3.2) identifies Level I as the appropriate level of validation for the ventilation model. The appropriateness of Level I is based on recognition that the model results are not extrapolated over large distances or time frames, and that ventilation efficiency (model output) represents the preclosure response to forced ventilation subject to engineering verification and controls. Variation in the output of the ventilation model is estimated to have only a small effect (less than 0.1 mrem/year) on the estimated mean annual dose for the repository system (BSC 2004 [DIRS 170950], Section 2.3.1).

7.1 CONFIDENCE BUILDING DURING MODEL DEVELOPMENT TO ESTABLISH SCIENTIFIC BASIS AND ACCURACY FOR INTENDED USE

In accordance with AP-2.27Q, *Planning for Science Activities*, Level I validation includes a discussion of model development. In particular, this report documents decisions implemented during model development that build confidence and verify that a reasonable, credible technical approach using scientific and engineering principles was taken. The development of the model is documented in accordance with the requirements of Section 5.3.2(b) of AP-SIII.10Q and Attachment 3 of AP-2.27Q. The development of the ventilation model has been conducted according to these criteria, as follows:

1. *Selection of input parameters and/or input data, and a discussion of how the selection process builds confidence in the model. [AP-SIII.10Q 5.3.2(b) (1) and AP-2.27Q Attachment 3 Level I (a)]*

   The parameters of the mixed convection correlation (Sections 4.1.8 and 4.1.13), standard properties of air and water (Sections 4.1.11 and 4.1.12), and physical constants (Section 4.1.14) are from standard sources that are qualified and justified in Appendix XVIII.

   Inputs relevant to the design of the EBS, including ventilation, are almost entirely from current information exchange drawings (IEDs), except for minor changes to the design subsequent to completion of the calculations reported here (Sections 4.1.7, 4.1.9, and 4.1.10). The input properties of the rock and the EBS materials, as well as the initial conditions in the rock and ventilating air (Sections 4.1.1 through 4.1.6, 4.1.9, and 4.1.15) are from DTNs and controlled engineering calculations that are specific to the site, except for one outside source for emissivity (Tables 4-8 and 4-21) that is qualified and justified in Appendix XVIII.

   The method of selecting input parameters and data builds confidence in the model.

2. *Description of calibration activities, and/or initial boundary condition runs, and/or run convergences, simulation conditions set up to span the range of intended use and avoid*

inconsistent outputs, and a discussion of how the activity or activities build confidence in the model. Inclusion of a discussion of impacts of any non-convergence runs. [AP-SIII.10Q 5.3.2(b)(2) and AP-2.27Q Attachment 3 Level I (e)].

The only calibration activities affecting the model parameters (Tables 4.1.8 and 4.1.13) were performed independently of the model development by Kuehn and Goldstein (1978 [DIRS 130084]) and Kays and Leung (1963 [DIRS 160763]). The reliability of these sources, including their citation in a handbook and textbook, is presented in Appendix XVIII.

Initial and boundary conditions (Tables 4.1.2 and 4.1.6) for the calculations of ventilation efficiency are from DTNs that are specific to the site. All calculations converged.

Simulations were performed for drifts of 600 m and 800 m, spanning the expected lengths of emplacement drifts. Simulations also varied many input parameters over their range of uncertainty (Section 6.11).

The independence of the calibration activities, the specificity of the initial and boundary conditions, the convergence of the calculations, and the range of simulations combine to build additional confidence in the model.

3. *Discussion of the impacts of uncertainties to the model results including how the model results represent the range of possible outcomes consistent with important uncertainties. [AP-SIII.10Q 5.3.2(b)(3) and AP-2.27Q Attachment 3 Level 1 (d) and (f)].*

   Simulations varied many input parameters over their range of uncertainty (Section 6.11). These results are combined, using the Delta Method, to calculate that the uncertainty in the ventilation efficiency is about 3% efficiency. This quantification of the uncertainty provides additional confidence in the results.

4. *Formulation of defensible assumptions and simplifications. [AP-2.27Q Attachment 3 Level I (b)].*

   The limitations stated in Section 1 are equivalent to assumptions and simplifications that are applicable to the current EBS design and are therefore defensible. In particular:

   - The ventilation air flow rate is between 10 and 30 m^3/s.
   - The waste packages are spaced in the drift such that, during the preclosure period, the average heat generation per unit length in each small group of waste packages is approximately the same as the average over the entire drift.
   - Conduction from the waste package is small compared to thermal radiation.
   - Average heat loads produce sub-boiling conditions in the host rock.
   - Repository edges do not significantly affect the near field host rock thermal conduction.

- Simultaneous emplacement of the waste packages, which is conservative with respect to total heat load.

The following further assumptions are presented and defended in Section 5:

- The chosen location for the drift is representative.
- The thermal properties of a 21-PWR waste package are representative.
- An initial water saturation of approximately 90.5% is representative.
- The lithophysal porosity is 100% air-filled.
- The thermophysical properties of 4-10 crushed tuff are representative of the invert.
- The convection correlations for idealized configurations are adequate for the non-ideal configuration of the EBS, and the effects of the differences are captured in the uncertainty analysis.
- The average temperature of the ventilation air at the inlet to the drift is equal to the ambient temperature of the host rock.

The fact that these assumptions and simplification are defensible provides additional confidence in the results of the model calculations.

5. *Consistency with physical principles, such as conservation of mass, energy, and momentum. [AP-2.27Q Attachment 3 Level I (c)]*

   Consistency with physical principles is demonstrated by the conceptual and mathematical formulations for the mass and energy balance equations in Section 6.4 and the selection and use of the ANSYS code based on those physical principles.

7.2 CONFIDENCE BUILDING AFTER MODEL DEVELOPMENT TO SUPPORT THE SCIENTIFIC BASIS OF THE MODEL

Level I validation must include at least one post-development method described in Paragraph 5.3.2 of AP-SIII.10Q. The governing TWP (BSC 2004 [DIRS 170950], Section 2.3.3) specifies one such activity, comparison of relevant model predictions with the results from the one-quarter scale ventilation tests (BSC 2003 [DIRS 160724]). This activity is described in Section 7.2.1.

The validation criteria specified by the TWP are listed in Table 7-1. The following discussion, which describes the importance of the ventilation efficiency as a parameter and the criteria for acceptance of the comparison with test data, was provided by the TWP (BSC 2004 [DIRS 170950], Section 2.3.3). The purpose of the ventilation model is to support the engineering feasibility of the recommended primary value of the ventilation efficiency. It is important not to overestimate the magnitude of the ventilation efficiency, and it is not important if the ventilation efficiency is underestimated, as long as the model meets the requirements for

confidence building during development. Therefore, the validation criterion for comparison with test data is that the model results do not overestimate (i.e., calculated efficiency is less than or equal to) the measured results from testing, expressed in terms of representative or ensemble values and accounting qualitatively for the effects of scale. This section shows not only that this validation criterion is met, but also that a previously proposed criterion is met: matching the model results to the test temperature data within 5°C (BSC 2003 [DIRS 2003 165601], Table 5).

Past modeling of thermal performance of the repository has used values of 70 percent ventilation efficiency without generating concern for the effectiveness of ventilation, signifying that this efficiency is feasible. Therefore, a second validation criterion in the TWP is that the estimate of expected ventilation efficiency for the repository be more than 70 percent (BSC 2004 [DIRS 170950], Section 2.3.4). The second criterion is met by the results of Section 6, which provide average ventilation efficiencies of 86% and 88%, depending on the length of the drift.

Table 7-1. Validation Criteria

Activity	Parameter	Criterion
Simulation of ventilation tests	Ventilation efficiency	Predicted efficiency does not exceed measured efficiency
Simulation of repository ventilation	Ventilation efficiency	Predicted efficiency exceeds 70%

Source: BSC 2004 [DIRS 170950], Section 2.4.3.

The corroborating/supporting data used to complete model validation activities (and as direct input) are contained in Tables 4-1 through 4-5 (also used in Section 6 for the model development and application), 7-3 through 7-6, and IX-6 through IX-10.

7.2.1 One-Quarter Scale Ventilation Tests

Phases 1 and 2 of the one-quarter scale ventilation tests were performed at the North Las Vegas Atlas Facility during 2001 and 2002. A detailed description of the ventilation tests is provided in the Phase 1 report (BSC 2003 [DIRS 160724], Section 2).

The ventilation test train was constructed by connecting segments of concrete pipes. Twenty-five simulated waste packages were fabricated from steel pipe. A steel structure designed to simulate the current waste package support structure and emplacement pallet was used to support the simulated waste packages. Crushed tuff from Yucca Mountain was used as the invert ballast material. Electric heaters within the waste packages simulated the decay heat (BSC 2003 [DIRS 160724], Section 2.2.2). The test configuration is described in the test report (BSC 2003 [DIRS 160724], Sections 2.2.2.1 and 2.2.2.2). The test setup was nominally ¼ scale of a repository drift segment.

The tests were conducted in two phases. The primary difference between Phases 1 and 2 is that the ventilation air in Phase 2 was conditioned to better control its inlet temperature and relative humidity. The Phase 1 test brought in ambient air from outside the test train that exhibited diurnal temperature changes of around 4°C. The same ventilation air flow rates and linear heat loads were used for both phases. Considering these aspects, that the ANSYS methodology for simulating ventilation does not account for the relative humidity of the in-drift air, and that the

results of Section 6.9 show that the moisture has no significant impact on the ventilation, the Phase 1 test data are sufficient to provide the level of validation required for the ANSYS model. Therefore, the use of the ventilation test data for post-test ANSYS modeling and validation for this revision of the ventilation model report is confined to the Phase 1 cases. Table 7-2 lists the Phase 1 ventilation tests and cases for which ANSYS post-test modeling was performed.

Table 7-2. Ventilation Phase 1 Test Matrix

Case No.	Nominal Flow (m^3/s)	Nominal Power (kW/m)
1	1	0.36
2	2	0.36
3	0.5	0.36
4	1	0.18
5	0.5	0.18

Source: BSC 2003 [DIRS 160724], Table 3-1.

7.2.2 Post-Test ANSYS Model

Figure 7-1 shows the saddle-like temperature trends for the waste packages of Case 4 of Ventilation Test Phase 1. The same trend is observed in all the other cases. The temperature peaks that occur around Station 3 are due to heat losses at the inlet and outlet of the test train. However, the ANSYS methodology outlined in Section 6.4.1 is not capable of modeling the profile of axial temperature exhibited by the test data. An underlying assumption of the ANSYS methodology is that temperatures of the in-drift components, drift wall, and ventilation air are always increasing as the calculation proceeds down the length of the drift. This limitation forced the development of a two-dimensional ANSYS-based ventilation model. In other words, only a two-dimensional cross-section at Station 3 was modeled using ANSYS, rather than the ANSYS/Excel methodology described in Section 6.4.1 for a pseudo-three-dimensional analysis from Station 1 to Station 5. One consequence is that there is more model uncertainty in the validation calculations than in the methodology described in Section 6.4.1.

7.2.2.1 Mesh

Figure 7-2 shows a detailed drawing through a cross-section of the test train. It also includes the relative locations of the instrumentation. Figure 7-3 shows the discretization of the test domain or the computational mesh used for the ANSYS post-test modeling. The pallet that supports the simulated waste package is not continuous in the test configuration. Rather, it supports only the ends of the package. The contribution of heat transfer via conduction from the package through the pallet and into the invert is considered to be negligible in comparison to the amount of heat transferred by radiation. For this reason, the pallet was not modeled.

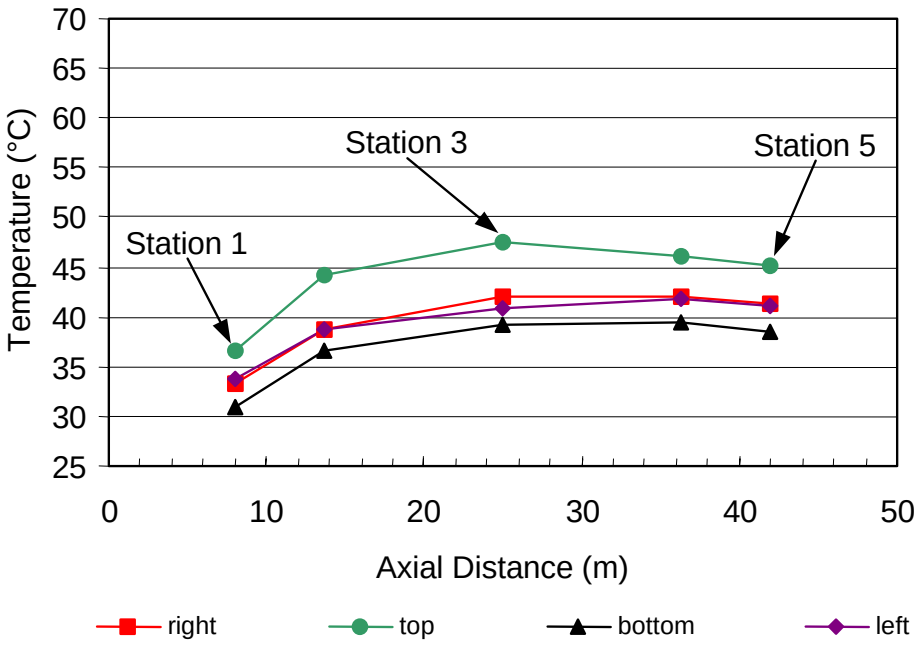

Source: BSC 2003 [DIRS 160724], Figure 5-7.

Figure 7-1. Ventilation Phase 1, Case 4 Waste Package Temperatures versus Axial Distance Down the Test Train for Data Recorded 10/15/00

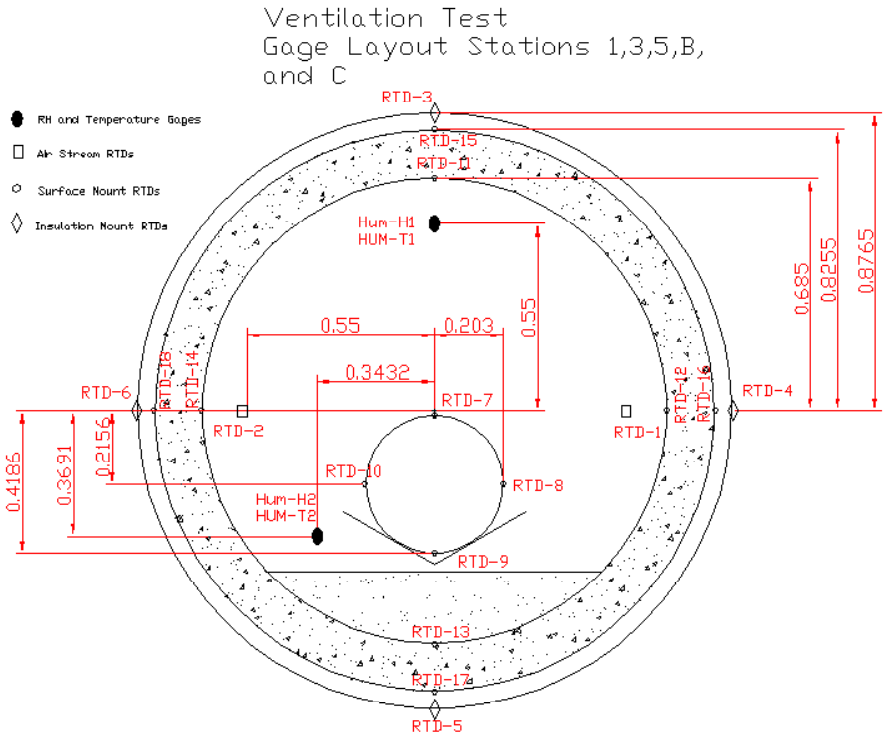

Source: BSC 2003 [DIRS 160724], Figure 2-11.

NOTE: All dimensions are in meters.

Figure 7-2. Cross-Sectional View of the Ventilation Test Train

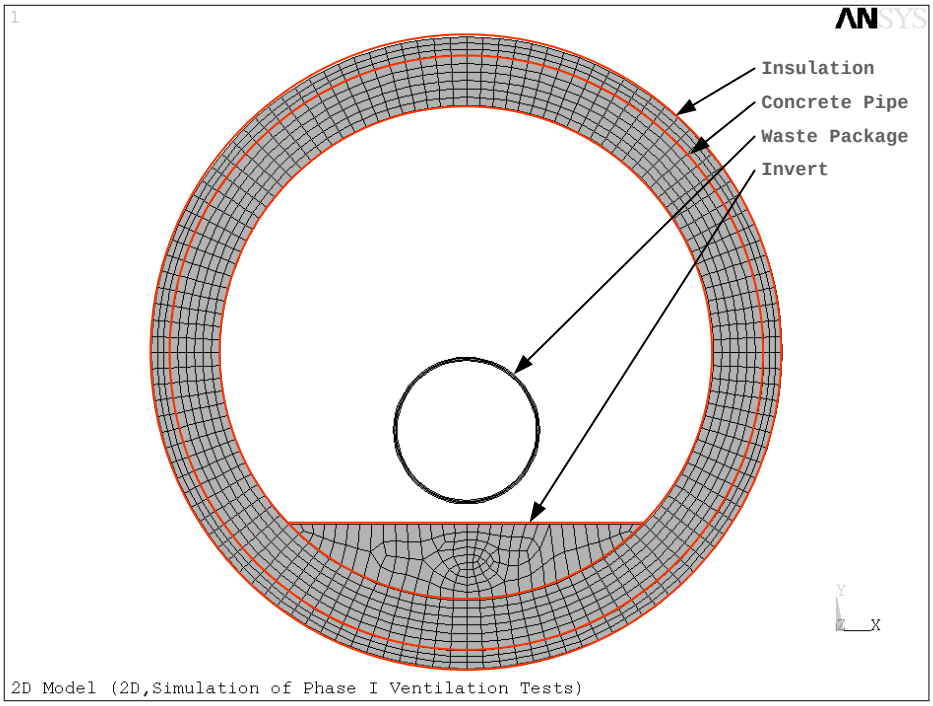

Output DTN: MO0209MWDANS30.017, file vti.db of vti.tar.Z.

NOTE: The plot was generated using the post-processor of ANSYS software and the model database file vti.db.

Figure 7-3. Mesh of ANSYS Model

7.2.2.2 Thermophysical Properties for Model Validation

Thermophysical properties of the invert, simulated waste package, concrete pipe, and insulation are listed in Sections 7.2.2.2.1 through 7.2.2.2.4. These properties are used in the model validation.

7.2.2.2.1 Thermophysical Properties of the Invert

Table 7-3 lists the average thermophysical properties for the fine crushed tuff. The justification for the use of the material properties of fine crushed tuff for the invert ballast material is described in Section 5.5.

Although only the volume specific heat is relevant to the heat transfer calculation, the ANSYS software does not accept that input. Instead, it requires the density and the mass specific heat. The particle density (2530 kg/m^3) was input to the program in lieu of the bulk density. Because the particle density was also used to correct the volume specific heat to a mass specific heat of 363.24 ($J/kg \cdot K$), the effective volume specific heat in the calculation was the same as the value shown in Table 7-3. Therefore, the choice of bulking factor had no effect on the calculation.

Table 7-3. Average Thermophysical Properties of the Invert

Specific Heat[a]	Thermal Conductivity[b]	**Particle Density[c]**
(J/cm^3·°C)	(W/m·°C)	**(g/cm^3)**
0.919	0.14	2.53

[a] DTN: GS000483351030.003 [DIRS 152932], average of specific heat values for fine crushed tuff, samples TK-FT-01 to TK-FT-10, rows 33-43.
[b] DTN: GS000483351030.003 [DIRS 152932], average of thermal conductivity values for fine crushed tuff, samples TK-FT-01 to TK-FT-10, rows 33-43.
[c] DTN: GS000383351030.002 [DIRS 148445], Table S00193_002, particle density for fine (crushed) Topopah Spring tuff, rows 16-21.

7.2.2.2.2 Thermophysical Properties of the Simulated Waste Package

Table 7-4 lists thermophysical properties of the simulated waste package used in the ventilation tests performed at the North Las Vegas Atlas Facility. This information is used as input to the model validation exercises.

Table 7-4. Thermophysical Properties of the Simulated Waste Package

Property	Value	Source
Density (kg/m^3)	7840	Stroe 2001 [DIRS 155633], p. 3 for steel pipe (averaged over 20 to 50°C)
Thermal Conductivity (W/m·K)	38.37	Stroe 2001 [DIRS 155633], p. 3 for steel pipe (averaged over 20 to 50°C)
Specific Heat (J/kg·K)	410.98	Stroe 2001 [DIRS 155633], p. 3 for steel pipe (averaged over 20 to 50°C)
Emissivity	0.8	Holman 1997 [DIRS 101978], Table A-10 for Sheet Steel
Outside Diameter (in.)	16	CRWMS M&O 2000 [DIRS 153503]

7.2.2.2.3 Thermophysical Properties of the Concrete Pipe

Table 7-5 lists thermophysical properties of the concrete pipe used in the ventilation tests performed at the North Las Vegas Atlas Facility. This information is used as input to the model validation exercises.

Table 7-5. Thermophysical Properties of the Concrete Pipe

Property	Value	Source
Density (kg/m^3)	2280	Stroe 2001 [DIRS 155633], p. 3 for Concrete Pipe (averaged over 20 to 50°C)
Thermal Conductivity (W/m·K)	2.75	Stroe 2001 [DIRS 155633], p. 3 for Concrete Pipe (averaged over 20 to 50°C)
Specific Heat (J/kg·K)	1016.16	Stroe 2001 [DIRS 155633], p. 3 for Concrete Pipe (averaged over 20 to 50°C)
Emissivity	0.93	Incropera and DeWitt 1996 [DIRS 108184], Table A.11 for Concrete
Inner Diameter (in.)	54	CRWMS M&O 2000 [DIRS 153503]
Outside Diameter (in.)	65	CRWMS M&O 2000 [DIRS 153503] (Wall Thickness [5.5"] + Inner Diameter)

7.2.2.2.4 Thermophysical Properties of the Insulation

Table 7-6 lists thermophysical properties of the insulation used in the ventilation tests performed at the North Las Vegas Atlas Facility. This information is used as input to the model validation exercises.

Table 7-6. Thermophysical Properties of the Insulation

Property	Value	Source
Density (kg/m^3)	12	CertainTeed 1996 [DIRS 153512] for Type 75 Standard Fiber Glass Duct Wrap
Thermal Conductivity (W/m·K)	0.04	CertainTeed 1996 [DIRS 153512] for Type 75 Standard Fiber Glass Duct Wrap
Specific Heat (J/kg·K)	700	Holman 1997 [DIRS 101978], Table A-3 for Insulation
Thickness (m)	0.0508	CRWMS M&O 2000 [DIRS 153503] (Converted from 2 in.)

7.2.2.3 Boundary Conditions

The recorded temperatures on the outer insulation at Station 3 of the test train were the basis for the outer boundary conditions for each ANSYS post-test model (DTN: SN0208F3409100.007 [DIRS 161729], worksheets "RTDs" of vent_test_C1.xls [case 1], vent_test_C2.xls [case 2], vent_test_C3.xls [case 3], vent_test_C4.xls [case 4], vent_test_C5.xls [case 5]). Each test case had a different set of recorded temperatures over its life span. To aid in the implementation of each outer boundary condition, the several hundred time-stamped results from the test were replaced by a data fit. The data fit consisted of linear interpolations between twenty-four times, chosen to capture the fluctuations in that test's boundary conditions. Figure 7-4 is an example of a working plot that was used to choose the data fit for an outer insulation temperature history. The scatter seen in the temperature data for cases 4 and 5 (Tables 7-7d and 7-7e) was caused by the HVAC system at the test facility, and is representative of test conditions (BSC 2003 [DIRS 160724], Section 3.3.3.6). The measured outer insulation temperature histories contained in the output DTN: MO0410MWDANS30.018 (worksheets "Measured Air and Insu Temp" of vti-aa.xls [case 4], vti-ba.xls [case 5], vti-ca.xls [case 1], vti-da.xls [case 2], vti-ea.xls [case 3]) were imported from DTN: SN0208F3409100.007 ([DIRS 161729], worksheets "RTDs" of vent_test_C1.xls [case 1], vent_test_C2.xls [case 2], vent_test_C3.xls [case 3], vent_test_C4.xls [case 4], vent_test_C5.xls [case 5]) for the data fitting purposes. The "fitted data" were all from the measured values, and selected using visual observation to best represent the bounds and variations of the measured outer insulation temperature histories. These selected (fitted) data from measurements, listed in Tables 7-7a through 7-7e, were then used as inputs for the outer boundary conditions in the ANSYS post-test modeling. The temperatures at the side of outer insulation, as listed in Column E of Tables 7-7a to 7-7e and shown in Figure 7-4, are the average values of those measured on the left and right sides at Station 3.

The ANSYS methodology requires that an inlet ventilation air stream temperature be specified. Therefore, the temperatures of the ventilation air stream recorded at Station 3 were used as input to the ANSYS post-test models (DTN: SN0208F3409100.007 [DIRS 161729], worksheets "RTDs" of vent_test_C1.xls, vent_test_C2.xls, vent_test_C3.xls, vent_test_C4.xls, vent_test_C5.xls). Each test case had a different set of air stream temperature histories. Again, a

data fit for each case was performed on the recorded temperature data to simplify its implementation into the models. Figure 7-5 is an example of a working plot that was used to choose the data fit for a ventilation air stream temperature history. The measured ventilation airstream temperature histories contained in the output DTN: MO0410MWDANS30.018 (worksheets "Measured Air and Insu Temp" of vti-aa.xls [case 4], vti-ba.xls [case 5], vti-ca.xls [case 1], vti-da.xls [case 2], vti-ea.xls [case 3]) were imported from DTN: SN0208F3409100.007 ([DIRS 161729], worksheets "RTDs" of vent_test_C1.xls [case 1], vent_test_C2.xls [case 2], vent_test_C3.xls [case 3], vent_test_C4.xls [case 4], vent_test_C5.xls [case 5]) for the data fitting purposes. Similarly, the fitted data were all from the measured values, and selected based on visual observation to best represent the bounds and variations of the measured air stream temperature histories. These selected (fitted) data from measurements were then used as inputs for ventilation air stream temperatures in the ANSYS post-test modeling. The temperatures shown in Figure 7-5 are the average values of those measured near the left and right sides of concrete pipe (inside) at Station 3.

The simulated waste packages were hollow rolled steel tubes, with heater rods suspended concentrically inside. Due to the nature of the experimental set-up, natural convection cells developed within the placid annulus of the waste packages. This caused a non-uniform heat flux, and hence temperature distribution, around the circumference of the waste package. No temperature measurements were recorded inside the waste package (i.e., the annulus air or the rod-heater). Rather than model the complexity of the natural convection inside of the waste package, the ANSYS model supplied a heat flux at the waste package wall. The heat flux was partitioned around the waste package circumference using the recorded steady-state temperature distributions as a basis. Table 7-8 summarizes the distributions for the test cases listed in Table 7-2. The validity of this partitioning methodology is confirmed by the consistency of the calculated distributions from case to case.

Table 7-7a. Ventilation Test Phase 1, Case 1, Outer Insulation and Air Temperatures Measured at Station 3

Date / Time	Measured Outer Insulation Temperature at Station 3 (°C)					Measured Air Temperature at Station 3 (°C)		
	V3-RTD-03	V3-RTD-04	V3-RTD-05	V3-RTD-06	Average of RTDs –04 and 06	V3-RTD-01	V3-RTD-02	Average of RTDs-01 and 02
	A	B	C	D	E ([B+D]/2)	F	G	H ([F+G]/2)
11/3/2000 14:03	29.14	28.78	28.42	28.08	28.43	27.34	27.36	27.35
11/3/2000 14:18	29.15	28.78	28.79	28.33	28.55	27.68	27.54	27.61
11/3/2000 14:49	29.17	28.32	28.05	27.72	28.02	28.40	28.36	28.38
11/3/2000 15:18	28.11	27.80	27.51	27.44	27.62	29.37	29.03	29.20
11/3/2000 15:48	27.39	27.30	27.03	26.97	27.13	29.46	29.23	29.34
11/3/2000 16:18	27.81	28.41	28.56	27.66	28.03	30.03	29.97	30.00
11/3/2000 16:48	27.75	28.43	28.14	27.75	28.09	30.28	30.14	30.21
11/3/2000 17:18	27.37	28.05	27.78	27.46	27.76	30.42	30.14	30.28
11/3/2000 17:49	27.30	27.75	27.54	27.28	27.52	30.40	30.16	30.28
11/3/2000 18:18	27.08	27.76	27.40	27.19	27.47	30.23	30.19	30.21
11/3/2000 18:49	27.07	27.51	27.24	27.26	27.39	30.50	29.91	30.21
11/3/2000 19:33	26.81	27.39	27.19	26.97	27.18	30.15	29.98	30.07
11/4/2000 7:03	27.16	25.68	24.44	25.23	25.45	29.04	28.77	28.90
11/4/2000 15:48	29.65	29.32	28.21	29.22	29.27	31.76	31.75	31.76
11/5/2000 6:33	28.22	26.60	24.73	25.61	26.11	29.22	29.11	29.16
11/5/2000 11:48	30.99	29.83	29.22	30.04	29.93	32.08	32.10	32.09
11/6/2000 8:03	27.23	26.45	24.80	25.61	26.03	28.93	28.83	28.88
11/6/2000 13:48	31.87	30.04	29.30	29.98	30.01	32.57	32.28	32.43
11/7/2000 6:48	26.41	25.14	23.74	24.27	24.70	27.97	28.03	28.00
11/7/2000 13:33	29.07	28.14	27.60	28.13	28.13	31.18	31.34	31.26
11/8/2000 6:48	27.05	24.84	22.95	23.80	24.32	27.65	27.47	27.56
11/8/2000 13:03	30.93	28.45	28.03	28.39	28.42	31.49	31.18	31.34
11/9/2000 6:18	27.09	25.76	23.95	24.78	25.27	28.08	28.09	28.09
11/9/2000 16:03	29.09	28.32	27.56	28.31	28.31	31.74	31.66	31.70

DTN: SN0208F3409100.007 [DIRS 161729], selected measurements from worksheet “RTDs” of vent_test_C1.xls. Averages from DTN: MO0410MWDANS30.018, vti-ca.xls, worksheet “Measured Air and Insu Temp.”

Table 7-7b. Ventilation Test Phase 1, Case 2, Outer Insulation and Air Temperatures Measured at Station 3

Date / Time	Measured Outer Insulation Temperature at Station 3 (°C)					Measured Air Temperature at Station 3 (°C)		
	V3-RTD-03	V3-RTD-04	V3-RTD-05	V3-RTD-06	Average of RTDs –04 and 06	V3-RTD-01	V3-RTD-02	Average of RTDs –01 and 02
	A	B	C	D	E ([B+D]/2)	F	G	H ([F+G]/2)
11/20/2000 16:03	26.14	24.60	22.42	24.11	24.35	25.91	25.43	25.67
11/20/2000 16:18	26.98	24.40	22.55	24.39	24.40	26.29	25.99	26.14
11/20/2000 16:48	25.01	23.90	22.60	24.06	23.98	25.82	25.49	25.66
11/20/2000 17:19	24.08	23.77	22.58	22.71	23.24	25.08	24.80	24.94
11/20/2000 17:49	25.89	23.51	22.40	23.20	23.35	26.13	25.52	25.83
11/20/2000 18:18	25.97	24.20	22.63	23.36	23.78	25.98	25.70	25.84
11/20/2000 18:49	25.65	23.71	22.43	23.13	23.42	25.98	25.72	25.85
11/20/2000 19:19	25.81	23.31	22.27	23.27	23.29	26.13	25.74	25.93
11/20/2000 19:49	25.27	23.25	22.71	23.03	23.14	25.87	25.52	25.70
11/20/2000 20:19	25.07	23.65	22.52	22.87	23.26	25.76	25.33	25.54
11/21/2000 6:03	24.91	23.59	21.39	22.69	22.98	24.80	24.42	24.61
11/21/2000 14:03	29.57	27.78	24.80	28.23	22.85	29.74	29.30	29.52
11/22/2000 6:33	23.09	22.24	21.21	21.58	24.10	23.55	23.09	23.32
11/22/2000 13:49	29.19	27.41	26.00	27.57	25.58	29.17	29.02	29.10
11/23/2000 5:03	24.77	23.92	23.29	23.68	24.80	25.12	24.78	24.95
11/23/2000 14:48	30.62	29.66	27.00	29.87	27.49	31.38	30.73	31.05
11/24/2000 6:19	25.22	24.12	23.16	23.72	27.10	25.44	24.82	25.13
11/24/2000 14:18	30.47	29.53	27.35	29.69	27.91	30.98	30.58	30.78
11/25/2000 6:48	25.42	24.01	23.51	23.50	25.30	24.85	24.37	24.61
11/25/2000 14:03	30.32	29.22	27.79	29.43	28.15	30.61	30.40	30.51
11/26/2000 6:33	24.33	23.49	22.78	22.66	26.59	24.45	24.09	24.27
11/26/2000 13:33	29.78	28.85	27.48	29.01	28.72	30.67	30.32	30.49
11/27/2000 6:48	24.61	23.95	23.40	23.20	25.64	25.03	24.59	24.81
11/27/2000 11:33	28.96	27.22	26.22	27.17	25.80	28.81	28.19	28.50

DTN: SN0208F3409100.007 [DIRS 161729], selected measurements from worksheet “RTDs” of vent_test_C2.xls. Averages from DTN: MO0410MWDANS30.018, vti-da.xls, worksheet “Measured Air and Insu Temp.”

Table 7-7c. Ventilation Test Phase 1, Case 3, Outer Insulation and Air Temperatures Measured at Station 3

Date / Time	Measured Outer Insulation Temperature at Station 3 (°C)					Measured Air Temperature at Station 3 (°C)		
	V3-RTD-03	V3-RTD-04	V3-RTD-05	V3-RTD-06	Average of RTDs –04 and 06	V3-RTD-01	V3-RTD-02	Average of RTDs –01 and 02
	A	B	C	D	E ([B+D]/2)	F	G	H ([F+G]/2)
12/1/2000 15:03	20.39	20.82	20.61	20.41	20.61	21.10	20.84	20.97
12/1/2000 15:19	20.38	20.22	20.69	20.30	20.26	21.44	21.42	21.43
12/1/2000 15:48	20.00	19.98	20.46	20.31	20.15	22.77	23.04	22.91
12/1/2000 16:18	19.86	20.05	20.06	19.92	19.98	23.98	23.99	23.99
12/1/2000 16:48	19.51	19.10	19.54	19.30	19.20	24.89	24.81	24.85
12/1/2000 17:18	18.76	18.96	19.15	18.98	18.97	25.27	25.11	25.19
12/1/2000 17:49	20.49	21.30	21.45	20.60	20.95	25.46	25.26	25.36
12/1/2000 18:19	18.79	18.90	19.25	18.96	18.93	26.02	25.95	25.99
12/1/2000 18:48	21.13	21.81	22.32	21.38	21.59	26.18	26.07	26.13
12/1/2000 19:19	18.52	18.49	18.58	18.49	18.49	26.29	26.35	26.32
12/2/2000 7:03	22.42	22.90	21.78	22.05	22.47	27.75	27.45	27.60
12/2/2000 15:48	23.60	23.18	22.31	23.27	23.23	30.83	30.61	30.72
12/3/2000 7:18	19.62	18.37	17.99	18.81	18.59	28.36	28.39	28.37
12/3/2000 14:33	25.63	24.85	23.92	24.96	24.90	32.31	31.98	32.14
12/4/2000 7:19	21.23	20.53	20.08	21.08	20.80	28.74	28.78	28.76
12/4/2000 14:49	26.25	25.38	24.53	25.98	25.68	32.54	32.44	32.49
12/5/2000 7:18	22.20	21.96	21.48	22.18	22.07	29.14	29.32	29.23
12/5/2000 15:18	25.17	23.81	23.56	24.31	24.06	32.55	32.42	32.48
12/6/2000 6:34	23.07	22.58	20.64	21.83	22.21	28.97	29.10	29.04
12/6/2000 14:33	25.27	24.12	23.40	24.37	24.25	31.98	32.03	32.01
12/7/2000 7:18	24.60	24.00	23.32	24.28	24.14	29.95	30.04	30.00
12/7/2000 14:33	25.23	24.01	23.47	24.74	24.38	32.65	32.96	32.81
12/8/2000 7:03	22.08	21.63	20.88	21.62	21.62	29.39	29.55	29.47
12/8/2000 11:48	26.08	25.09	24.60	25.56	25.32	32.08	32.08	32.08

DTN: SN0208F3409100.007 [DIRS 161729], selected measurements from worksheet “RTDs” of vent_test_C3.xls. Averages from DTN: MO0410MWDANS30.018, vti-ea.xls, worksheet “Measured Air and Insu Temp.”

Table 7-7d. Ventilation Test Phase 1, Case 4, Outer Insulation and Air Temperatures Measured at Station 3

Date / Time	Measured Outer Insulation Temperature at Station 3 (°C)					Measured Air Temperature at Station 3 (°C)		
	V3-RTD-03	V3-RTD-04	V3-RTD-05	V3-RTD-06	Average of RTDs –04 and 06	V3-RTD-10	V3-RTD-02	Average of RTDs –10 and 02
	A	B	C	D	E ([B+D]/2)	F	G	H ([F+G]/2)
10/9/2000 8:48	35.04	28.39	27.52	29.27	28.83	26.80	26.45	26.62
10/9/2000 9:19	26.45	26.78	26.39	26.33	26.55	27.32	27.08	27.20
10/9/2000 9:49	28.60	27.80	27.30	28.04	27.92	27.66	27.39	27.53
10/9/2000 10:18	27.72	26.88	26.91	27.54	27.21	28.25	27.84	28.04
10/9/2000 10:48	27.40	27.18	26.91	27.35	27.27	28.51	28.28	28.40
10/9/2000 11:19	28.14	27.33	27.28	27.52	27.42	29.12	28.50	28.81
10/9/2000 11:49	28.60	27.79	27.54	27.84	27.81	29.26	28.83	29.05
10/9/2000 12:18	28.34	27.88	27.57	28.33	28.10	29.48	29.54	29.51
10/9/2000 12:48	28.13	27.85	27.42	27.83	27.84	29.66	29.46	29.56
10/9/2000 13:33	28.50	27.85	27.64	28.36	28.11	29.82	29.48	29.65
10/10/2000 5:48	35.53	28.73	25.71	28.18	28.45	26.42	25.97	26.20
10/10/2000 14:19	27.09	26.92	26.69	26.97	26.95	29.04	28.63	28.83
10/11/2000 5:03	37.48	25.34	25.62	28.81	27.07	25.38	25.19	25.28
10/11/2000 12:48	27.93	27.23	26.83	27.40	27.32	28.61	28.36	28.49
10/12/2000 3:48	30.78	26.06	24.92	26.70	26.38	25.70	25.36	25.53
10/12/2000 15:33	34.28	28.56	27.93	29.94	29.25	28.41	28.33	28.37
10/13/2000 5:33	33.54	26.48	24.99	27.95	27.21	25.42	25.01	25.21
10/13/2000 13:33	36.86	28.41	27.91	30.40	29.40	29.13	28.85	28.99
10/14/2000 5:18	25.68	25.42	24.32	24.49	24.96	26.00	25.62	25.81
10/14/2000 14:33	29.05	28.84	27.80	28.86	28.85	29.43	29.13	29.28
10/15/2000 5:33	25.58	25.60	24.57	24.65	25.13	26.07	25.44	25.75
10/15/2000 12:33	28.39	26.87	27.26	27.34	27.10	29.44	29.21	29.33
10/16/2000 5:03	32.50	27.41	26.23	28.70	28.05	26.19	25.60	25.89
10/16/2000 8:03	29.04	27.63	27.26	27.66	27.65	28.26	27.68	27.97

DTN: SN0208F3409100.007 [DIRS 161729], selected measurements from worksheet “RTDs” of vent_test_C4.xls. Averages from DTN: MO0410MWDANS30.018, vti-aa.xls, worksheet “Measured Air and Insu Temp.”

Table 7-7e. Ventilation Test Phase 1, Case 5, Outer Insulation and Air Temperatures Measured at Station 3

Date / Time	Measured Outer Insulation Temperature at Station 3 (°C)					Measured Air Temperature at Station 3 (°C)		
	V3-RTD-03	V3-RTD-04	V3-RTD-05	V3-RTD-06	Average of RTDs –04 and 06	V3-RTD-10	V3-RTD-02	Average of RTDs –10 and 02
	A	B	C	D	E ([B+D]/2)	F	G	H ([F+G]/2)
10/20/2000 8:33	28.89	27.33	27.20	27.44	27.39	26.54	26.25	26.40
10/20/2000 9:03	26.66	25.64	26.08	25.66	25.65	27.10	26.91	27.00
10/20/2000 9:33	28.10	27.41	27.04	27.64	27.52	28.13	27.85	27.99
10/20/2000 10:03	27.63	25.82	26.27	26.05	25.94	28.49	28.39	28.44
10/20/2000 11:03	27.43	26.63	26.50	26.05	26.34	29.28	29.24	29.26
10/20/2000 13:03	28.19	26.94	26.93	27.27	27.10	30.38	29.79	30.08
10/20/2000 20:33	27.77	27.81	27.15	28.25	28.03	30.63	30.64	30.63
10/20/2000 23:18	26.30	26.75	25.92	26.71	26.73	30.30	29.99	30.14
10/21/2000 5:33	26.29	26.58	25.29	26.52	26.55	29.63	29.59	29.61
10/21/2000 10:18	29.61	28.41	27.69	28.80	28.60	31.12	31.17	31.15
10/21/2000 15:48	29.08	28.95	28.12	28.81	28.88	31.49	31.49	31.49
10/22/2000 4:48	28.28	26.95	25.15	26.34	26.65	29.88	29.83	29.85
10/22/2000 12:33	27.61	27.27	26.08	26.85	27.06	30.30	30.01	30.15
10/22/2000 23:18	31.39	27.82	25.40	28.27	28.04	29.17	29.06	29.11
10/23/2000 3:33	32.31	27.53	26.10	28.69	28.11	28.97	29.08	29.03
10/23/2000 15:18	36.94	30.51	26.30	29.27	29.89	29.08	29.24	29.16
10/24/2000 5:18	26.47	25.21	23.93	24.97	25.09	28.59	28.49	28.54
10/24/2000 13:18	35.20	29.25	28.52	30.44	29.85	30.85	30.99	30.92
10/25/2000 6:19	30.79	28.14	25.58	28.70	28.42	28.98	29.04	29.01
10/25/2000 14:18	28.28	27.23	26.99	27.40	27.32	30.98	31.28	31.13
10/26/2000 6:48	35.53	29.25	27.59	30.26	29.76	29.40	29.61	29.51
10/26/2000 12:18	28.52	28.02	27.86	28.09	28.06	30.72	30.85	30.79
10/26/2000 18:48	28.99	28.63	27.97	28.40	28.52	31.44	31.54	31.49
10/27/2000 7:48	29.06	27.91	25.50	26.59	27.25	30.57	30.51	30.54

DTN: SN0208F3409100.007 [DIRS 161729], selected measurements from worksheet “RTDs” of vent_test_C5.xls. Averages from DTN: MO0410MWDANS30.018, vti-ba.xls, worksheet “Measured Air and Insu Temp.”

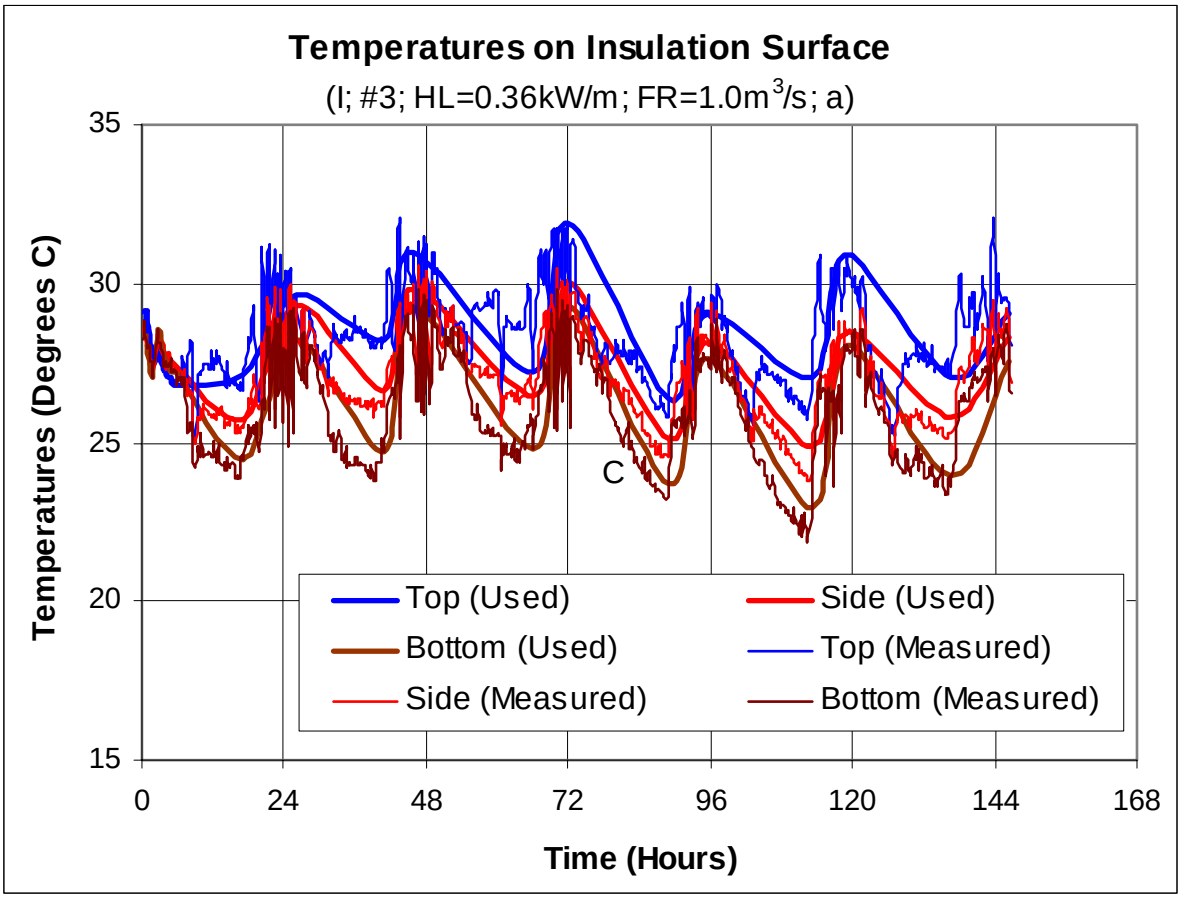

DTN: MO0410MWDANS30.018, worksheet "Measured Air and Insu Temp" of file vti-ca.xls.

NOTE: Data used as input are connected with smooth curves for clarity, but ANSYS uses linear interpolation.

Figure 7-4. Example (Case 1) of Working Plot for Fitting Outer Insulation Boundary Temperatures for the ANSYS Post-Test Ventilation Model

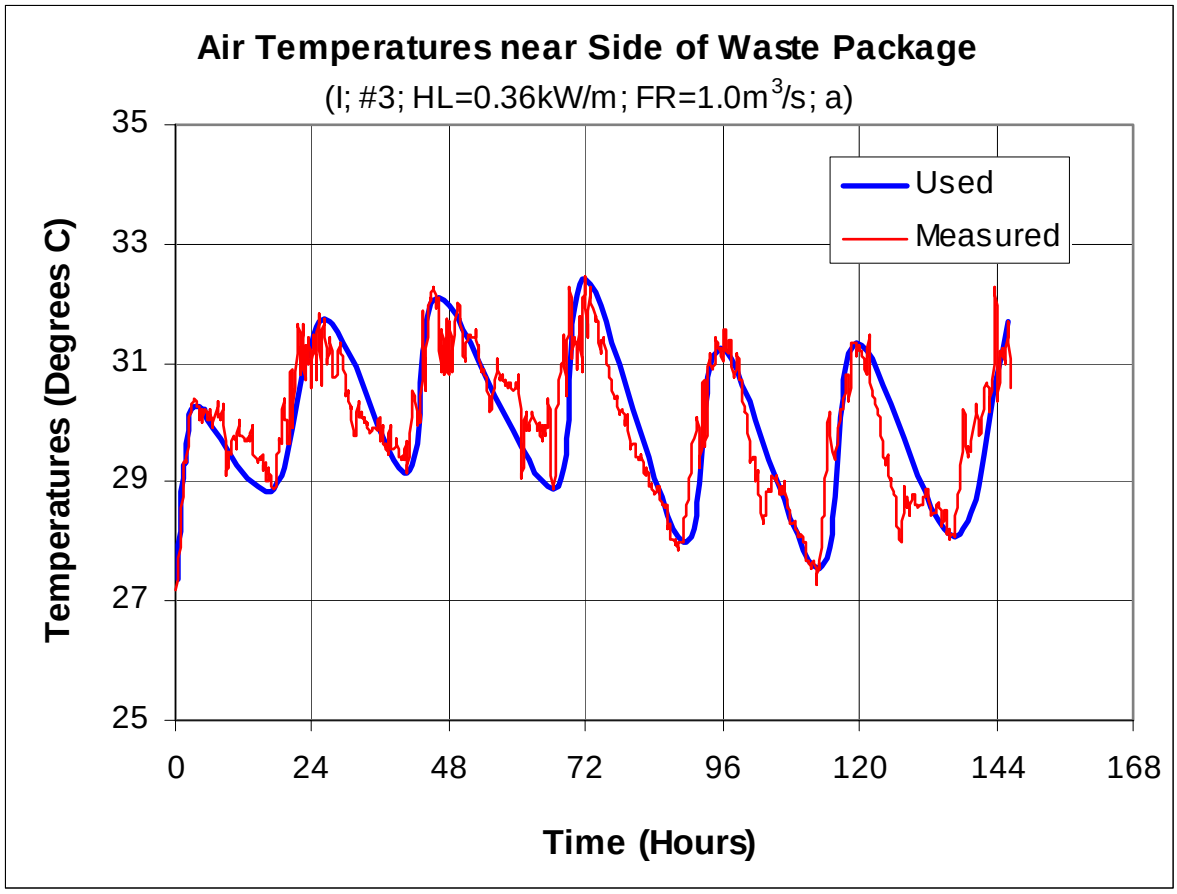

DTN: MO0410MWDANS30.018, worksheet "Measured Air and Insu Temp" of file vti-ca.xls

NOTE: Data used as input are connected with smooth curves for clarity, but ANSYS uses linear interpolation.

Figure 7-5. Example (Case 1) of Working Plot for Fitting Temperatures at Station 3 for Use as Inlet Air for the ANSYS Post-Test Ventilation Model

Table 7-8. Distribution of Total Power to the Top, Sides, and Bottom Quarters of the Waste Package Based on Temperature Measurements

Case No.	WP Top Quarter (%)	WP Side Quarters (%)	WP Bottom Quarter (%)
1	32%	24%	20%
2	32%	24%	20%
3	31%	24%	21%
4	32%	24%	20%
5	32%	24%	20%

DTN: MO0410MWDANS30.018; worksheets “Heat Removal”, rows 10 to 13 of column B of vti-aa.xls (case 4), vti-ba.xls (case 5), vti-ca.xls (case 1), vti-da.xls (case 2), vti-ea.xls (case 3).

7.2.2.4 Correlating the Model Results to the Test Data Using Heat Transfer Coefficients

Having determined appropriate distributions of power around the circumference of the waste package, ANSYS models were run iteratively using different values for the heat transfer coefficients until the model results matched the test data.

7.2.2.5 Results

Table 7-9 shows the heat transfer coefficient values which resulted in close agreement to the measured temperature data. The temperature results from the ANSYS models are compared to the recorded test data in Figures 7-6 through 7-10. Table 7-10 compares the fitted average heat transfer coefficient for each test case from Table 7-9 to heat transfer coefficients calculated using the Mixed Convection Correlation and the Dittus-Boelter correlation for fully developed turbulent flow inside a smooth circular tube (Incropera and DeWitt 1996 [DIRS 108184], Section 8.5). The Dittus-Boelter formula gives the asymptotic Nusselt number for fully developed turbulent flow (Re > 10,000) in circular tubes. This formula was used for the Nusselt number at the outer wall in earlier ventilation model calculations with fully developed turbulent flow. Incropera and DeWitt (1985 [DIRS 114109], p. 400) consider the Dittus-Boelter equation to be a first approximation, in which the inner and outer convection coefficients are assumed to be equal. Appendix XVII presents the calculation of Dittus-Boelter heat transfer coefficients for the ventilation test Phase 1 cases 1 through 5.

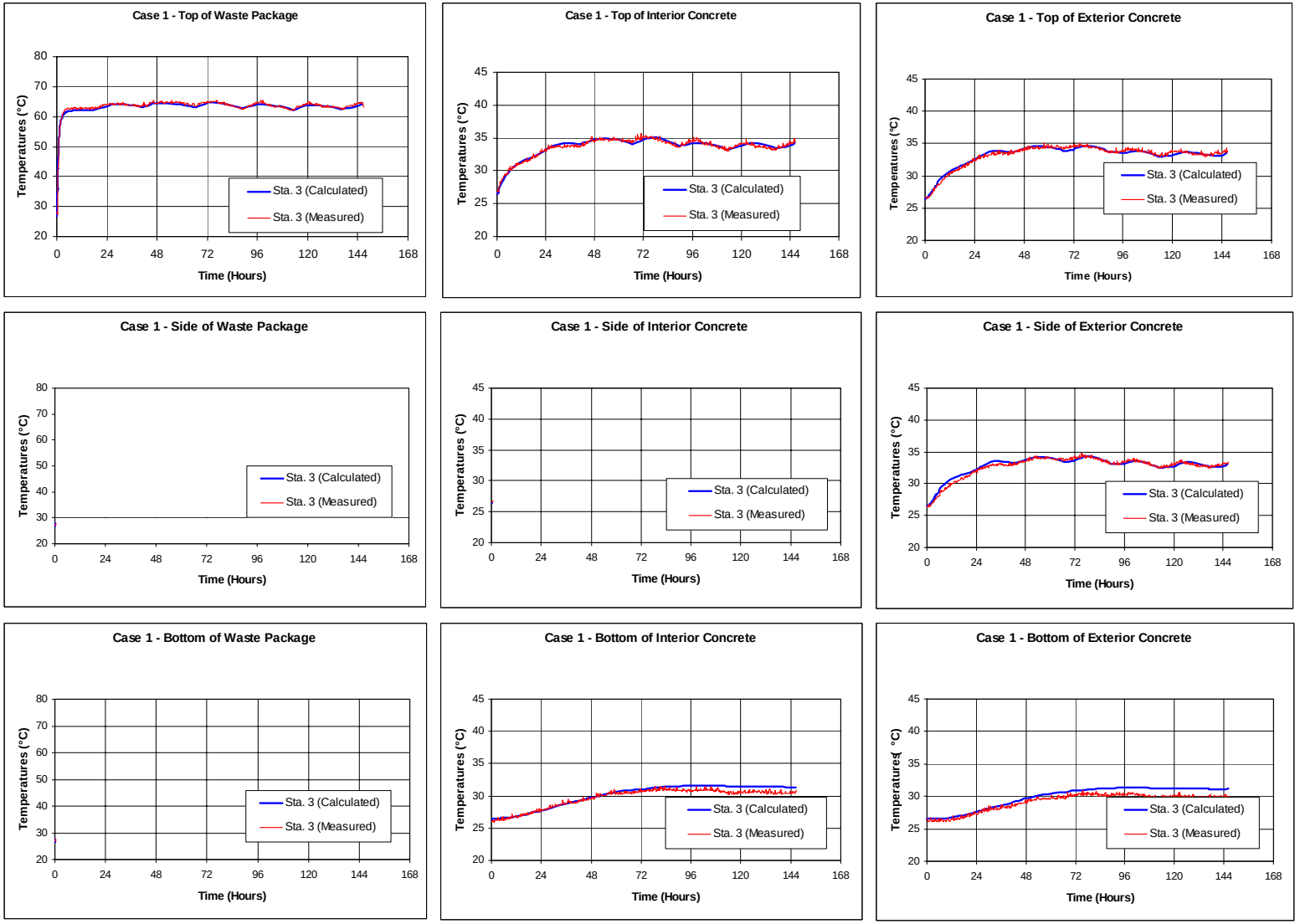

DTN: MO0410MWDANS30.018MO0209MWDANS30.017, data in worksheet “raw data” of vti-c-data.xls and worksheet “ANSYS Results” of vti-ca.xls; plots in worksheet “ANSYS Results” of vti-ca.xls and modified for clarity.

Figure 7-6. ANSYS Post-Test Ventilation Model versus Measured Results for Ventilation Test Phase 1, Case 1

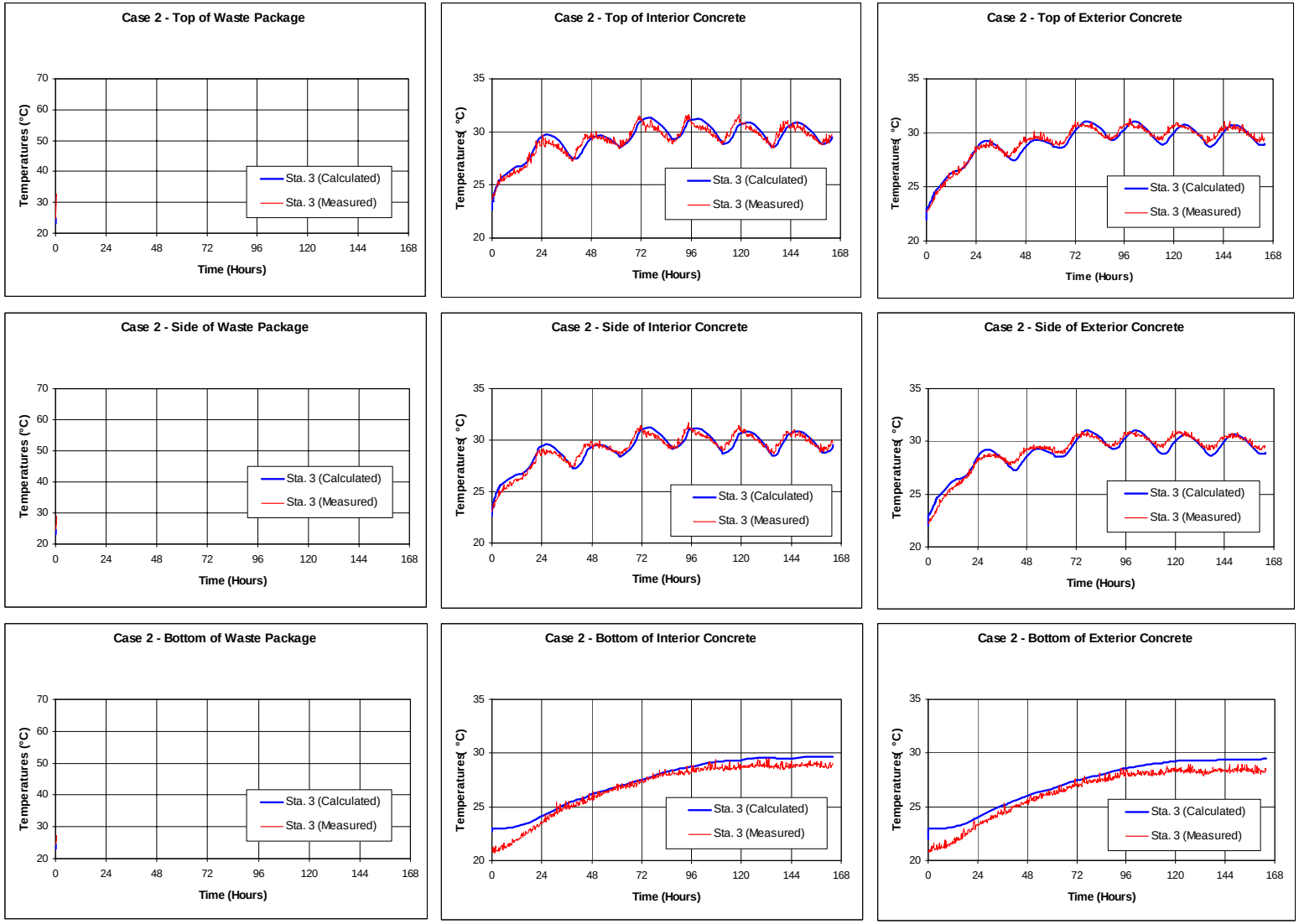

DTN: MO0410MWDANS30.018MO0209MWDANS30.017, data in worksheet “raw data” of vti-d-data.xls and worksheet “ANSYS Results” of vti-da.xls; plots in worksheet “ANSYS Results” of vti-da.xls and modified for clarity.

Figure 7-7. ANSYS Post-Test Ventilation Model versus Measured Results for Ventilation Test Phase 1, Case 2

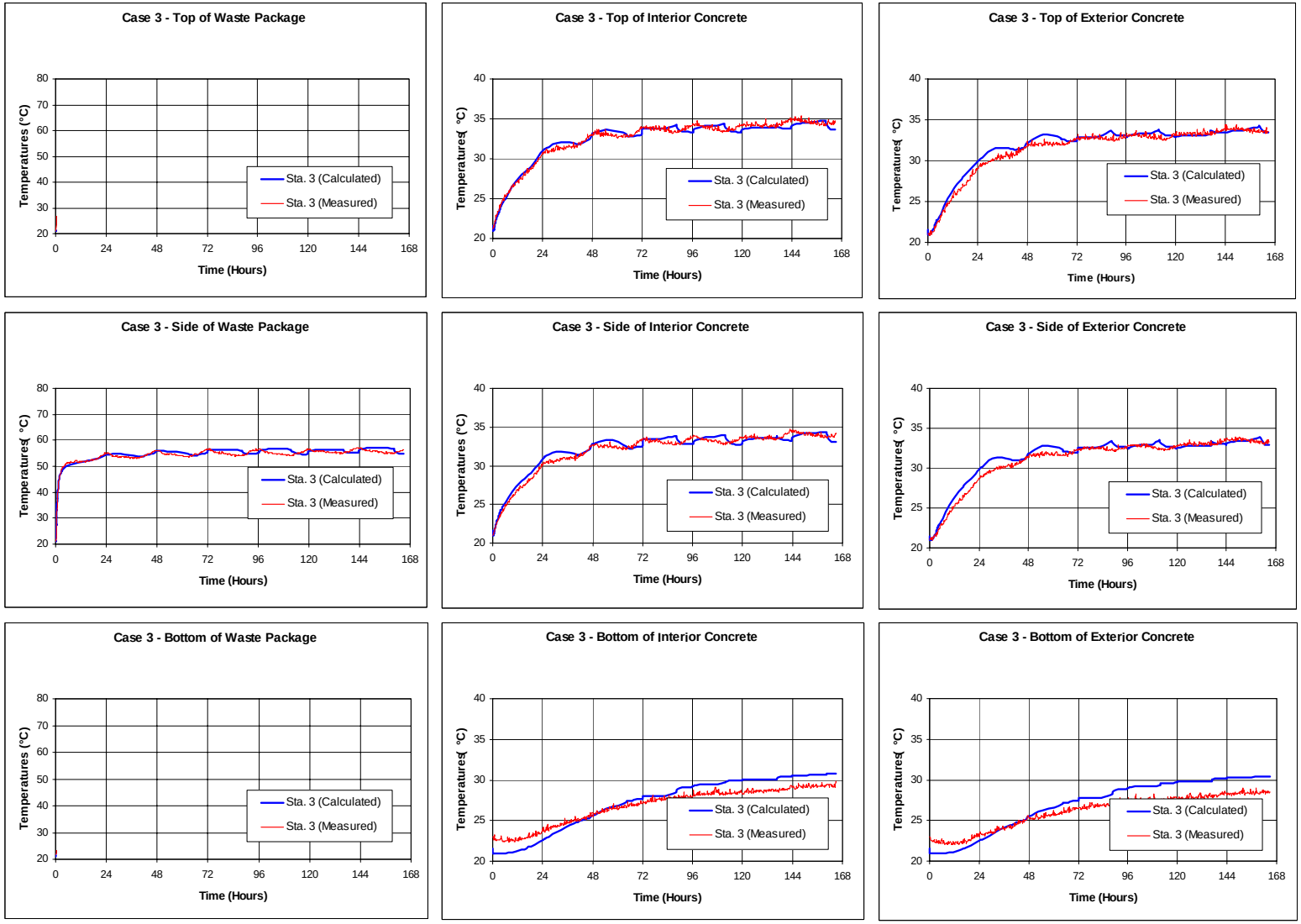

DTN: MO0410MWDANS30.018, data in worksheet “raw data” of vti-e-data.xls and worksheet “ANSYS Results” of vti-ea.xls; plots in worksheet “ANSYS Results” of vti-ea.xls and modified for clarity.

Figure 7-8. ANSYS Post-Test Ventilation Model versus Measured Results for Ventilation Test Phase 1, Case 3

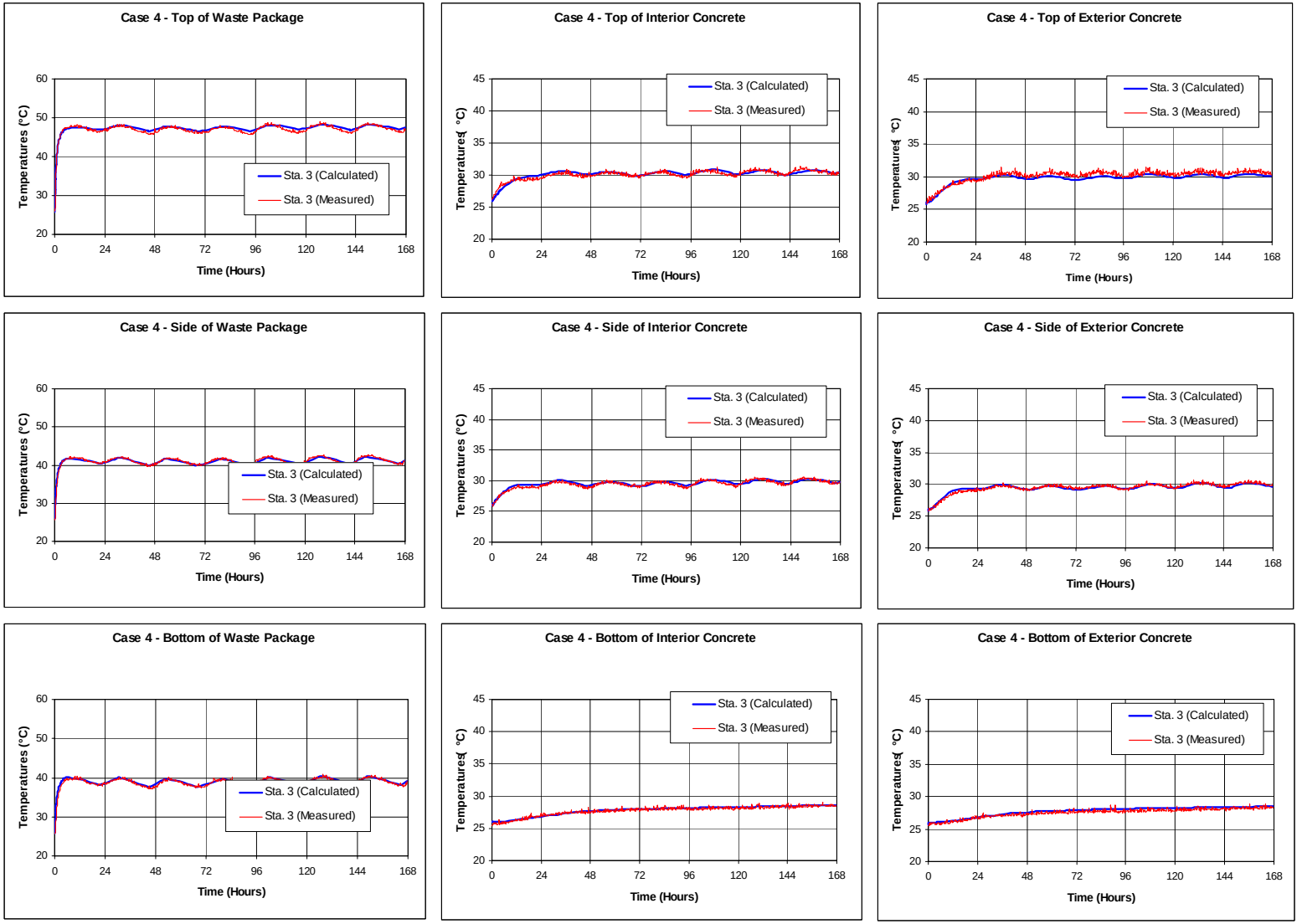

DTN: MO0410MWDANS30.018, data in worksheet “raw data” of vti-a-data.xls and worksheet “ANSYS Results” of vti-aa.xls; plots in the worksheet “ANSYS Results” of vti-aa.xls and modified for clarity.

Figure 7-9. ANSYS Post-Test Ventilation Model versus Measured Results for Ventilation Test Phase 1, Case 4

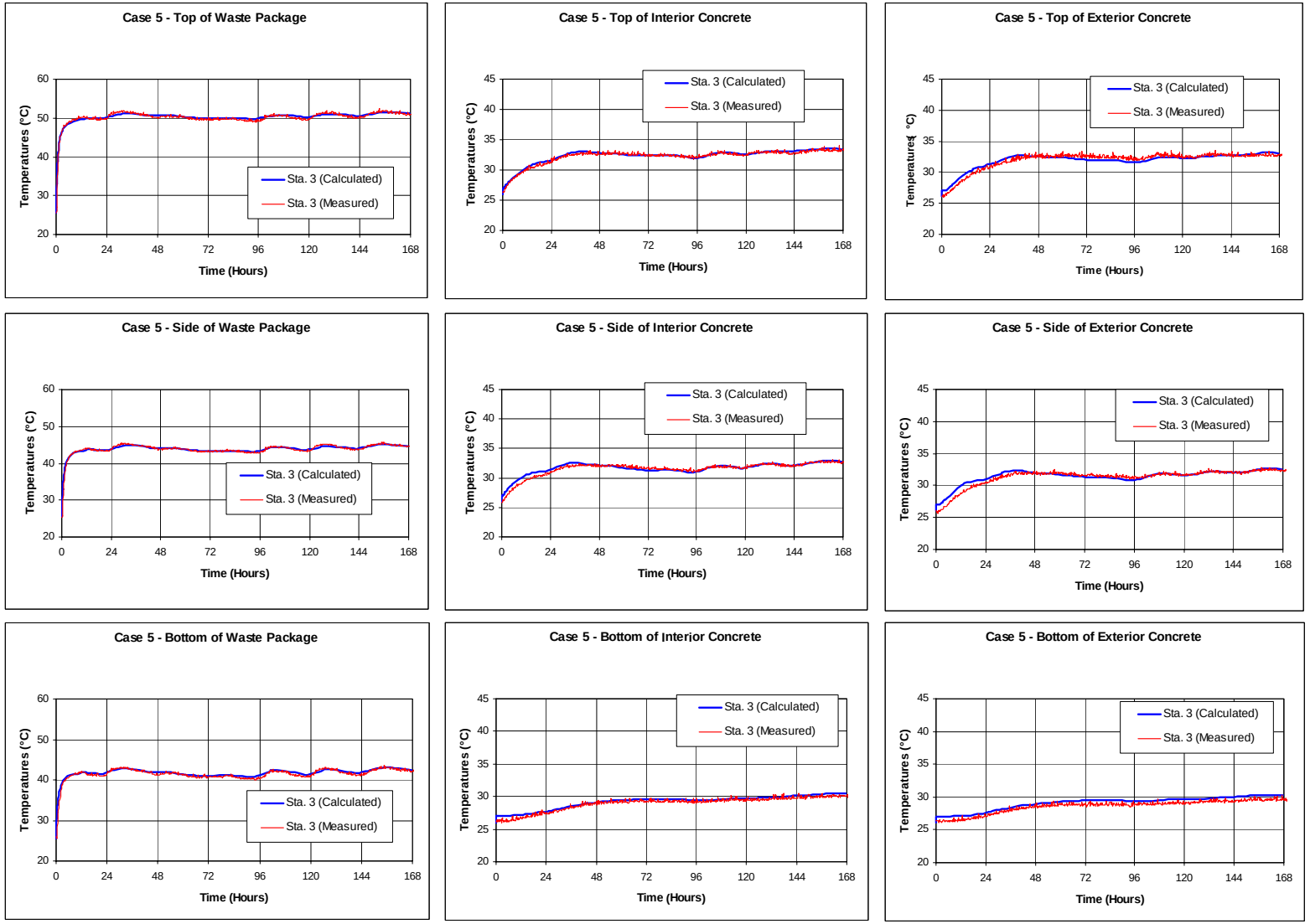

DTN: MO0410MWDANS30.018, data in worksheet “raw data” of vti-b-data.xls and worksheet “ANSYS Results” of vti-ba.xls; plots in the worksheet “ANSYS Results” of vti-ba.xls and modified for clarity.

Figure 7-10. ANSYS Post-Test Ventilation Model versus Measured Results for Ventilation Test Phase 1, Case 5

Table 7-9. Developed Heat Transfer Coefficients from the ANSYS Post-Test Modeling of Phase 1 of the Ventilation Test

	Heat Transfer Coefficient ($W/m^2 \cdot K$)					
Case No.	**WP Top Quarter**	**WP Side Quarters**	**WP Bottom Quarter**	**Upper Concrete**	**Lower Concrete**	**Invert [a]**
1	2.0	8.0	8.0	7.0	11.0	6.0
2	3.5	9.5	10.5	13.0	15.0	2.0
3	1.0	7.5	8.5	9.5	16	5.0
4	0.5	7.5	7.0	5.0	9.0	9.0
5	0.0	7.0	7.0	5.0	15.0	9.0

DTN: MO0410MWDANS30.018, worksheets “Heat Removal” of vti-aa.xls (case 4), vti-ba.xls (case 5), vti-ca.xls (case 1), vti-da.xls (case 2), vti-ea.xls (case 3).

[a] Values from cells (row 12, column F), identified as “dw h coef.”, in worksheets “Heat Removal” of vti-aa.xls (case 4), vti-ba.xls (case 5), vti-ca.xls (case 1), vti-da.xls (case 2), vti-ea.xls (case 3).

Table 7-10. Comparison of Heat Transfer Coefficients Using Data-Fitting to the Mixed Convection and Dittus-Boelter Correlations

		Heat Transfer Coefficient ($W/m^2 \cdot K$)				
Case No.	**Flow Rate (m^3/s)**	**ANSYS WP [a]**	**Mixed Convection Correlation – Inner Surface (i.e., waste package surface)**	**ANSYS Concrete and Invert [a]**	**Mixed Convection Correlation – Outer Surface (i.e., inner concrete surface and invert surface)**	**Dittus-Boelter [b]**
1	1	6.5	5.9 [c]	8.8	6.6 [h]	2.9
2	2	8.3	7.5 [d]	11.3	9.2 [i]	5.0
3	0.5	6.1	5.7 [e]	11.6	7.3 [j]	1.7
4	1	5.6	5.3 [f]	8.0	6.5 [k]	2.9
5	0.5	5.3	4.7 [g]	11.0	7.1 [l]	1.7

[a] Average of values from Table 7-9, with side quarter or lower concrete counted twice.
[b] Value from Table XVII-1.
[c] Value from Table IX-31, Test 3.
[d] Value from Table IX-31, Test 4.
[e] Value from Table IX-31, Test 5.
[f] Value from Table IX-31, Test 1.
[g] Value from Table IX-31, Test 2.
[h] Value from Table IX-34, Test 3.
[i] Value from Table IX-34, Test 4.
[j] Value from Table IX-34, Test 5.
[k] Value from Table IX-34, Test 1.
[l] Value from Table IX-34, Test 2.

Iterating the heat transfer coefficients input to ANSYS until its results matched the test data resulted in heat transfer coefficients very close to those predicted by the mixed-convection correlation. However, the average of the heat transfer coefficients ranges from approximately two to five times larger than heat transfer coefficients calculated using the Dittus-Boelter correlation. Two reasons would tend to account for the differences. First, the Dittus-Boelter equation is a forced convection correlation. Analyses of the ventilation test data indicate a mixed (i.e., natural and forced) convection regime inside the concrete pipe annulus. Second, the Dittus-Boelter correlation for calculating a forced convection heat transfer coefficient was

developed for hollow tube geometries. The correlation can be extended to a cylinder within a tube (i.e., waste package inside a drift) by using the hydraulic diameter instead of the geometric diameter. However, a cylinder within a tube, eccentrically located, is a different geometry which would tend to invalidate the Dittus-Boelter correlation within the range of air flow velocities being considered for preclosure. Add an invert, and the geometry of the problem lies even farther beyond the range of the Dittus-Boelter correlation. The values presented in Table 7-10 for the heat transfer coefficients used in the ANSYS post-test calculations argue that both natural and forced convection are important heat removal mechanisms for the experimental set-up of the Ventilation Test. Although scaling the quarter scale test results to a full scale drift is beyond the scope of this report, it stands to reason that a convection coefficient correlation which considers both natural and forced convection is more appropriate for use than the Dittus-Boelter equation (for the current drift design, heat load range, and ventilation flow rate).

Table 7-11 summarizes the ventilation heat removal ratios for the five cases as modeled by ANSYS. The uncertainty in the predicted efficiency resulting from uncertainties in input data is estimated to be 3 percent on the basis of the analysis in Section 6.11. For four of the five cases (Cases 1, 3, 4, and 5), the predicted efficiency is below the uncertainty bounds, even without considering the additional model uncertainty described in Section 7.2.2. Therefore, the validation criterion is satisfied.

Table 7-11. Heat Removal Ratios for the ANSYS Post-Test Ventilation Models

Case No.	Ventilation Efficiency[a]	Ventilation Efficiency from Measurements[b]
1	78 ± 3%	86.4 ± 0.6%
2	93 ± 3%	79.7 ± 0.2%
3	80 ± 3%	81 ± 2%
4	87 ± 3%	83.8 ± 0.6%
5	83± 3%	79 ± 2%

[a] DTN: MO0410MWDANS30.018, identified as “percent of heat removal” in worksheets “Heat Removal” of vti-aa.xls (case 4), vti-ba.xls (case 5), vti-ca.xls (case 1), vti-da.xls (case 2), vti-ea.xls (case 3).
[b] BSC 2003 [DIRS 160724], Table 5-17.

7.2.2.6 Additional Criterion Met for the Convection Heat Transfer Model

The ANSYS numerical model matched the Phase I Ventilation Test results within the criterion of ±5°C using a reasonable range of heat transfer coefficients (Table 7-10). The range of heat transfer coefficients required to match the test results indicates a mixed convection regime inside the test train. The Dittus-Boelter correlation for calculating forced convection heat transfer coefficients is therefore a conservative approach. The impact of using such a correlation is a lower or more conservative rate of heat removal by ventilation because the Dittus Boelter equation is only valid for forced convection. A lower rate of heat removal translates to a lower efficiency and thus higher temperatures within the drift, which represents a conservative estimate of ventilation efficiency. A more realistic correlation is one that accounts for both natural and forced convection to remove heat from the drift, such as the mixed convection correlation used in these analyses.

7.3 VALIDATION SUMMARY

The ventilation model has been validated by applying acceptance criteria based on an evaluation of the model's relative importance to the performance of the repository system. All validation requirements defined in the applicable TWP (BSC 2004 [DIRS 170950], Section 2.3) have been fulfilled. Requirements for confidence building during model development have also been satisfied. The model development activities and postdevelopment validation activities described herein establish the scientific bases for the ventilation model. Based on this, the model is considered to be sufficiently accurate and adequate for the intended purpose with the stated limitations and to the level of confidence required by the model's relative importance to the performance of the repository system.

8. CONCLUSIONS

This report develops, validates, and implements a conceptual model for heat transfer in and around a ventilated emplacement drift. This conceptual model includes thermal radiation between the waste package and the drift wall, convection from the waste package and drift wall surfaces into the flowing air, and conduction in the surrounding host rock. These heat transfer processes are coupled and vary both temporally and spatially, so numerical and analytical methods are used to implement the mathematical equations which describe the conceptual model. These numerical and analytical methods predict the transient response of the system, at the drift scale, in terms of spatially varying temperatures and ventilation efficiencies. The ventilation efficiency describes the effectiveness of the ventilation process in removing radionuclide decay heat from the drift environment.

An alternative conceptual model is also developed which evaluates the influence of water and water vapor mass transport on the ventilation efficiency. These effects are described using analytical methods which bound the contribution of latent heat to the system, quantify the effects of varying degrees of host rock saturation (and hence host rock thermal conductivity) on the ventilation efficiency, and evaluate the effects of vapor and enhanced vapor diffusion on the host rock thermal conductivity.

8.1 SUMMARY OF RESULTS

As described by the conceptual model and its mathematical implementations, ventilation is found to be an effective way to remove heat produced by the decay of radionuclides in the in-drift environment, and to mitigate the peak waste package and drift wall temperatures that would otherwise occur. Given the License Application design parameters and inputs listed in Section 4 (including a ventilation flow rate of 15 m^3/s, an inlet air temperature of 22.8°C, and a preclosure period of 50 years), the integrated ventilation efficiency is 88% for a 600 meter long drift and 86% for an 800 meter long drift. Temperatures of the waste package, drift wall, and drift air do not exceed 105, 85, or 80°C respectively (Figure 6-5c). The most influential parameters on the effectiveness of the ventilation to remove heat from the drift are the temperature of the inlet ventilation air and the ventilation flow rate (Figure 6-12).

The effects of water and water vapor mass transport under sub-boiling conditions, described by the alternative conceptual model, on the ventilation efficiency and the waste package, drift wall, and drift air temperatures are minor (Section 6.9). The latent heat contribution associated with the evaporation of host rock matrix water near the drift wall is limited by the hydrologic properties of the rock, and is determined to be less than 1% of the total waste package energy provided to the in-drift and host rock environment. The change in temperatures associated with varying the host rock matrix saturation (and hence the bulk thermal conductivity) from completely dry to completely wet is found to be less than 5°C at any given time and distance from the drift entrance. The integrated ventilation efficiency for a 600 meter long drift ranges from about 90% for completely dry conditions, to about 87% for completely wet conditions. Finally, there was no evidence of enhancement to the host rock thermal conductivity due to vapor and enhanced vapor diffusion.

8.2 MODEL OUTPUTS

The DTNs produced by this report are given in Table 8-1.

Table 8-1. DTNs Produced by the Ventilation Model and Analysis Report

DTN	Description
MO0303MWDSLTLC.000	Stratigraphic Layer Thickness (Section 6.5.1)
MO0306MWDASLCV.001	Input/Output and Analysis of the ANSYS-LA-Coarse Ventilation Model (Section 6.6.1 and 6.6.2)
MO0306MWDALAFV.000	Input/Output and Analysis of the ANSYS-LA-Fine Ventilation Model (Section 6.6.2)
MO0307MWDAC8MV.000	Analytical-LA-Coarse Ventilation Model (Section 6.6.1)
MO0306MWDRTCCV.000	Analytical-LA-Coarse-Wet-vs-Dry-kth Ventilation Model (Section 6.9.2)
MO0406MWDLACVD.001	Analytical-LA-Coarse-Delta-Method Ventilation Model (Section 6.11)
MO0406MWDAC8VD.001	Analytical-LA-Coarse-Delta-Method-800m Ventilation Model (Section 6.11)
MO0410MWDANS30.018	Input/Output and Analysis of ANSYS Post Test Modeling of the Ventilation Test Phase I for Model Validation (Section 7.1.3)
MO0306MWDVTPH2.000	Ventilation Test Phase II Data Analysis (Appendix XI)
MO0306MWDMXCNV.000	Analyses to Support the Mixed Convection Correlation (Appendix X)

8.2.1 Summary of Model Outputs

Given the design parameters and inputs listed in Section 4, the primary outputs of the ventilation model are:

- Ventilation efficiencies as a function of time and location from the inlet of the drift, whose trend is to increase with time, but decrease with distance from the drift inlet (DTN: MO0307MWDAC8MV.000, from the Analytical-LA-Coarse results. Note that the results of the ANSYS-LA-Coarse model may also be used).
- Integrated ventilation efficiencies and standard deviations for 600 and 800 meter long drifts (Table 8-2, integrated efficiencies from Analytical-LA-Coarse results and standard deviations, from the Analytical-LA-Coarse-Delta-Method results. Note that the integrated efficiencies are slightly different in the Delta-Method spreadsheet because that spreadsheet uses an average heat transfer coefficient, independent of time and position).
- Waste package, drift wall, and in-drift air preclosure temperatures as function of time and location from the inlet of the drift, whose trend is to decrease with time, but increase with distance from the drift inlet (DTN: MO0307MWDAC8MV.000, from the Analytical-LA-Coarse results. Note that the results of the ANSYS-LA-Coarse model may also be used).

Table 8-2. Integrated Ventilation Efficiency Over 50 Years of Preclosure, and 600 and 800 Meters of Drift

Length of Drift (meters)	Length of Ventilation (years)	Mean	Efficiency Uncertainty
600	50	88%[a]	3%[b]
800	50	86%[a]	3%[c]

[a] DTN: MO0307MWDAC8MV.000, worksheet "Ventilation Efficiency" of Analytical-LA-Coarse-800m.xls, rounded.
[b] DTN: MO0406MWDLACVD.001, worksheet "Delta Method" of Analytical-LA-Coarse-Delta-Method.xls, rounded.
[c] DTN: MO0406MWDAC8VD.001, worksheet "Delta Method" of Analytical-LA-Coarse-Delta-Method-800m.xls, rounded.

8.2.2 Recommendations for Downstream Use of the Model Outputs

Use of the ventilation model outputs, specifically the ventilation efficiency, is recommended for downstream thermal models that do not explicitly model in-drift behavior, such as waste package temperature, during the preclosure period. Such models include the multiscale thermohydrologic model, the drift degradation model, and the UZ coupled processes models. Either the ANSYS-LA-Coarse or the Analytical-LA-Coarse results may be used. The ventilation efficiency can be used to reduce the thermal energy produced by the waste package during the preclosure period as a means of initializing postclosure conditions in the host rock. If the intent of the initialization of the downstream postclosure thermal model is only to account for the correct amount of heat energy supplied to the host rock during the preclosure period, then the use of the ventilation efficiency in this manner (either as a function of time and distance from the drift inlet, or the integrated efficiency) is appropriate. However, if the intent is also to predict drift wall temperature at the start of postclosure, then the use of the ventilation efficiency as described above is inadequate.

8.2.3 Output Uncertainty

Uncertainty in the model output, specifically the integrated ventilation efficiency, is characterized using the mean and standard deviation listed in Table 8-3. Key input data and parameter uncertainties are also characterized using the means and standard deviations identified in Table 6-9. Input data and parameter uncertainties were propagated through the ventilation analysis using the Delta Method (see Section 6.11). The most influential design inputs and parameters on the uncertainty of the model output are the inlet air temperature, the air flow rate, the host-rock wet bulk thermal conductivity and specific heat (as a function of matrix saturation), and the convection heat transfer coefficients.

The uncertainties associated with the model and methods of analyses are characterized by comparing the results of the implementations of the conceptual model to the results of the implementations of the alternative conceptual model, and by comparing the results of the actual methods themselves to each other (i.e., comparing the ANSYS results to the analytical results). Two examples demonstrate these points. First, the uncertainty associated with including, or not including, water and water vapor mass transport in the ventilation analysis is shown to be minimal when comparing the results of both models (Section 6.9.1). Second, there is some uncertainty associated with linearizing the radiation heat transfer in the analytical method. When

comparing the temperature results of the analytical method to the results of the ANSYS method which explicitly treats the fourth order radiation heat transfer equation, there is little difference and hence no impact (Section 6.6.2). These same arguments may be made for other sources of model uncertainty such as: substituting the thermal pulse methodology in the analytical method for the transient conduction heat transfer analysis performed by ANSYS; the insensitivity of the length of well mixed volume elements in which the coupled heat transfer occurs, as addressed in the discretization study; or using finite element numerical iteration techniques in the ANSYS method compared to exact solutions obtained by the analytical approach.

The uncertainty in the output of the ventilation model is propagated through downstream models that use this output by taking the standard deviation of the integrated ventilation efficiency about the mean, and comparing the sensitivity of the downstream results to the results obtained by the mean.

8.3 YUCCA MOUNTAIN REVIEW PLAN CRITERIA ASSESSMENT

This model and analysis report provides preclosure information on ventilation efficiency that other models and analyses use to establish initial conditions for postclosure thermohydrologic calculations. The postclosure calculations feed into the model abstraction of the quantity and chemistry of water contacting engineered barriers and waste forms. This section summarizes the contents of this report as they apply to NRC criteria for a detailed review of that abstraction. These are the relevant criteria from *Yucca Mountain Review Plan, Final Report* (NRC 2003 [DIRS 163274], Section 2.2.1.3.3.3), which are based on meeting the requirements of 10 CFR 63.114(a)-(c) and (e)-(g) [DIRS 156605].

- **Acceptance Criterion 1** – System Description and Model Integration Are Adequate.

  (1) Total system performance assessment adequately incorporates important design features, physical phenomena, and couplings, and uses consistent and appropriate assumptions throughout the quantity and chemistry of water contacting engineered barriers and waste forms abstraction process.

For the ventilation calculations, inputs relevant to the design of the EBS, including ventilation, are almost entirely from current IEDs, except for minor changes to the design subsequent to completion of the calculations (Sections 4.1.7, 4.1.9, and 4.1.10). The input properties of the rock and the EBS materials, as well as the initial conditions in the rock and ventilating air (Sections 4.1.1 through 4.1.6, 4.1.9, and 4.1.15) are from DTNs and controlled engineering calculations that are specific to the site, except for one outside source for emissivity (Tables 4-8 and 4-21) that is qualified and justified in Appendix XVIII.

Section 6.3 describes the physical phenomena and couplings incorporated in the ventilation model. Heat transfer in the EBS couples radiative energy transfer with convective heat transfer. Convective heat transfer is modeled as a coupling of forced convection and natural convection. Coupling of additional moisture-related processes is omitted as not important on the basis of analyses in Section 6.9.

The limitations stated in Section 1 are applicable to the current EBS design and are therefore appropriate. The assumptions are shown in Section 5 to be appropriate for the preclosure period and the EBS and ventilation design. The ventilation efficiency is used by downstream thermohydrologic models that recalculate the details of the preclosure period before proceeding to the postclosure period. Because the processes in the postclosure period differ from those during preclosure and must be projected over a much longer time frame, the assumptions in the downstream models may differ from those in the ventilation model.

Therefore, the ventilation efficiency incorporates important design features, physical phenomena and couplings, and uses appropriate assumptions.

(3) Important design features, such as waste package design and material selection, backfill, drip shield, ground support, thermal loading strategy, and degradation processes, are adequate to determine the initial and boundary conditions for calculations of the quantity and chemistry of water contacting engineered barriers and waste forms.

The inputs to the ventilation analysis include details of the EBS features, including waste package dimensions and material properties (Section 4.1.9), waste package heat decay (Section 4.1.7), drift dimensions, and ventilation design parameters (Section 4.1.10). During the preclosure period, there is no drip shield. Therefore, the ventilation analysis incorporates the important design features that are adequate to determine the ventilation efficiency, which modifies the heat-generation boundary conditions for coupled process models.

(6) The expected ranges of environmental conditions within the waste package emplacement drifts, inside of breached waste packages, and contacting the waste forms and their evolution with time are identified. These ranges may be developed to include: (i) the effects of the drip shield and backfill on the quantity and chemistry of water (e.g., the potential for condensate formation and dripping from the underside of the shield); (ii) conditions that promote corrosion of engineered barriers and degradation of waste forms; (iii) irregular wet and dry cycles; (iv) gamma-radiolysis; and (v) size and distribution of penetrations of engineered barriers.

The ventilation model and analysis predicts heat transfer only during the preclosure period. The calculated ventilation efficiency can be applied in coupled process models to identify the expected range of saturation in the host rock at closure and the expected range of environmental conditions in the host rock, within the emplacement drifts, inside of breached waste packages, and contacting the waste forms and their evolution with time.

- **Acceptance Criterion 2** – Data Are Sufficient for Model Justification.

(2) Sufficient data were collected on the characteristics of the natural system and engineered materials to establish initial and boundary conditions for conceptual models of thermal-hydrologic-mechanical-chemical coupled processes, that affect seepage and flow and the engineered barrier chemical environment.

The ventilation model does not couple thermal processes with hydrologic, mechanical, or chemical processes. However, the ventilation analysis provides information that affects boundary conditions for conceptual models of thermal-hydrologic-mechanical-chemical coupled processes. Specifically, the ventilation analysis provides time- and position-dependent ventilation efficiencies that modify the thermal output of the waste package, which may be treated as a boundary. Section 6.11 shows that the most important parameters for determining ventilation efficiency are inlet air temperature, air flow rate, and the wet bulk thermal conductivity of the rock. The inlet air temperature is assumed to be equal to the ambient host rock temperature, which is calculated (Section 6.5.6) primarily from the boundary conditions at the surface and the water table (Section 6.5.5), with consideration of the thermophysical properties of the rock layers (Section 6.5.2). The boundary temperatures are supported by ample data, as described in Section 4.1.6.

The air flow rate is a design parameter, as described in Section 4.1.10. The thermal conductivity is developed from qualified project data, as described in Section 4.1.5. The collected data are sufficient that the standard deviations in wet bulk thermal conductivity are less than 15 percent of the values. Therefore, sufficient data were collected to establish initial and boundary conditions for the ventilation model. In turn, the calculated ventilation efficiency is sufficient to establish the effect of ventilation on boundary conditions for conceptual models of thermal-hydrologic-mechanical-chemical coupled processes.

- **Acceptance Criterion 3** – Data Uncertainty Is Characterized and Propagated Through the Model Abstraction.

  (1) Models use parameter values, assumed ranges, probability distributions, and bounding assumptions that are technically defensible, reasonably account for uncertainties and variabilities, and do not result in an under-representation of the risk estimate.

Section 6.11 demonstrates that the ventilation model uncertainty analysis uses parameter values, assumed ranges, probability distributions, and bounding assumptions that are technically defensible and reasonably account for uncertainties and variabilities. Section 7.2.2.5 shows that the model does not result in an overestimate of ventilation efficiency, which would tend to under-represent the risk estimate by under-representing the perturbations of pre-emplacement conditions due to repository heating.

  (2) Parameter values, assumed ranges, probability distributions, and bounding assumptions used in the total system performance assessment calculations of quantity and chemistry of water contacting engineered barriers and waste forms are technically defensible and reasonable, based on data from the Yucca Mountain region (e.g., results from large block and drift-scale heater and niche tests), and a combination of techniques that may include laboratory experiments, field measurements, natural analog research, and process-level modeling studies.

Sections 4.1, 6.6.1, and 6.11 provide assurances that the parameter values, assumed ranges, probability distributions and bounding assumptions used in the ventilation calculations are

technically defensible and reasonable, based on data from field measurements in the Yucca Mountain region and on process-level modeling studies.

(3) Input values used in the total system performance assessment calculations of quantity and chemistry of water contacting engineered barriers (e.g., drip shield and waste package) are consistent with the initial and boundary conditions and the assumptions of the conceptual models and design concepts for the Yucca Mountain site. Correlations between input values are appropriately established in the U.S. Department of Energy total system performance assessment. Parameters used to define initial conditions, boundary conditions, and computational domain in sensitivity analyses involving coupled thermal-hydrologic-mechanical-chemical effects on seepage and flow, the waste package chemical environment, and the chemical environment for radionuclide release, are consistent with available data. Reasonable or conservative ranges of parameters or functional relations are established.

Sections 4.1 and 5 show that the input values used in the ventilation calculations are consistent with the initial and boundary conditions and the assumptions of the conceptual models and design concepts for the Yucca Mountain site. Section 6.5.6 explains how correlation between ambient temperatures and inlet air temperature was appropriately established. Sections 6.6.1 and 6.11 demonstrate that parameters used to define initial conditions, boundary conditions, and computational domain in sensitivity analyses are consistent with available data and that reasonable or conservative ranges of parameters were established.

8.4 REQUIRED DOCUMENTATION OF LEVEL OF ACCURACY

Table 8-3 includes the uncertainty in ventilation efficiency. Section 6.11 explains how the uncertainty was determined, thereby meeting the requirement for documentation for level of accuracy (BSC 2004 [DIRS 170950], Section 3.3).

8.5 COMPLETION CRITERIA

This evaluation is consistent with the activities performed as part of *Technical Work Plan: Regulatory Integration Evaluation of Analysis and Model Reports Supporting the TSPA-LA* (BSC 2004 [DIRS 169653]) and fulfills a portion of the Phase 2 work identified in that plan. That is, the work addresses the prioritized list of actions selected in Phase 1 for disposition in Phase 2 (BSC 2004 [DIRS 169653], Section 1.3).

INTENTIONALLY LEFT BLANK

9. INPUTS AND REFERENCES

9.1 DOCUMENTS CITED

Alenitsyn, A.; Butikov, E.I.; and Kondratyev, A.S. 1997. *Concise Handbook of Mathematics and Physics.* Boca Raton, Florida: CRC Press. TIC: 233486. 171443

Azizi, S.; Moyne, C.; and Degiovanni, A. 1988. "Approche Experimentale et Theorique de la Conductivite Thermique des Milieux Poreux Humides—I. Experimentation." *International Journal of Heat and Mass Transfer, 31,* (11), 2305-2317. New York, New York: Pergamon Press. TIC: 243729. 154108

Bird, R.B.; Stewart, W.E.; and Lightfoot, E.N. 1960. *Transport Phenomena.* New York, New York: John Wiley & Sons. TIC: 208957. 103524

Birkholzer, J.T. and Tsang, Y.W. 2000. "Modeling the Thermal-Hydrologic Processes in a Large-Scale Underground Heater Test in Partially Saturated Fractured Tuff." *Water Resources Research, 36,* (6), 1431-1447. Washington, D.C.: American Geophysical Union. TIC: 248278. 154608

BSC (Bechtel SAIC Company) 2001. *ANSYS Calculations in Support of Natural Ventilation Parametric Study for SR.* CAL-SVS-HV-000003 REV 00 ICN 01. Las Vegas, Nevada: Bechtel SAIC Company. ACC: MOL.20010613.0250. 155246

BSC 2001. *Repository Multiple Waste Package Thermal Calculation.* CAL-WIS-TH-000010 REV 00. Las Vegas, Nevada: Bechtel SAIC Company. ACC: MOL.20010814.0330. 156276

BSC 2002. *Properties of Air Entering Emplacement Drifts Calculation.* 800-P0C-VU00-00200-000-00A. Las Vegas, Nevada: Bechtel SAIC Company. ACC: MOL.20030106.0302. 161233

BSC 2003. *Design and Engineering, D&E/PA/C IED Typical Waste Package Components Assembly 1 of 9.* 800-IED-WIS0-00201-000-00C. Las Vegas, Nevada: Bechtel SAIC Company. ACC: ENG.20030917.0002. 165406

BSC 2003. *Repository Design Project, Repository/PA IED Emplacement Drift Committed Materials (2).* 800-IED-WIS0-00302-000-00A. Las Vegas, Nevada: Bechtel SAIC Company. ACC: ENG.20030627.0004. 164101

BSC 2003. *Repository Design Project, Repository/PA IED Emplacement Drift Configuration 1 of 2.* 800-IED-EBS0-00201-000-00A. Las Vegas, Nevada: Bechtel SAIC Company. ACC: ENG.20030630.0002. 164069

BSC 2003. *Technical Work Plan for: Engineered Barrier System Department Modeling and Testing FY03 Work Activities.* TWP-MGR-MD-000015 REV 04 ICN 02. Las Vegas, Nevada: Bechtel SAIC Company. ACC: DOC.20031001.0008. 165601

BSC 2003. *Testing to Provide Data for Ventilation System Design: Phase 1.* TDR-EBS-MD-000021 REV 00. Las Vegas, Nevada: Bechtel SAIC Company. ACC: DOC.20030711.0001. 160724

BSC 2004. *D&E / PA/C IED Emplacement Drift Configuration and Environment.* 800-IED-MGR0-00201-000-00B. Las Vegas, Nevada: Bechtel SAIC Company. ACC: ENG.20040326.0001. 168489

BSC 2004. *D&E / PA/C IED Subsurface Facilities.* 800-IED-WIS0-00101-000-00A. Las Vegas, Nevada: Bechtel SAIC Company. ACC: ENG.20040309.0026. 164519

BSC 2004. *D&E / PA/C IED Typical Waste Package Components Assembly.* 800-IED-WIS0-00203-000-00B. Las Vegas, Nevada: Bechtel SAIC Company. ACC: ENG.20040202.0011. 167754

BSC 2004. *D&E/PA/C IED Typical Waste Package Components Assembly.* 800-IED-WIS0-00202-000-00C. Las Vegas, Nevada: Bechtel SAIC Company. ACC: ENG.20040517.0008. 169472

BSC 2004. *Development of Numerical Grids for UZ Flow and Transport Modeling.* ANL-NBS-HS-000015 REV 02. Las Vegas, Nevada: Bechtel SAIC Company. ACC: DOC.20040901.0001. 169855

BSC 2004. *Multiscale Thermohydrologic Model.* ANL-EBS-MD-000049 REV 02. Las Vegas, Nevada: Bechtel SAIC Company. ACC: DOC.20041014.0008. 169565

BSC 2004. *Q-List.* 000-30R-MGR0-00500-000-000 REV 00. Las Vegas, Nevada: Bechtel SAIC Company. ACC: ENG.20040721.0007. 168361

BSC 2004. *Repository Subsurface Emplacement Drifts Steel Invert Structure Plan & Elevation.* 800-SS0-SSE0-00101-000-00B. Las Vegas, Nevada: Bechtel SAIC Company. ACC: ENG.20040520.0004. 169503

BSC 2004. *Technical Work Plan for: Near-Field Environment and Transport In-Drift Heat and Mass Transfer Model and Analysis Reports Integration.* TWP-MGR-PA-000018 REV 01. Las Vegas, Nevada: Bechtel SAIC Company. ACC: DOC.20040729.0006. 170950

BSC 2004. *Technical Work Plan for: Regulatory Integration Evaluation of Analysis and Model Reports Supporting the TSPA-LA.* TWP-MGR-PA-000014 REV 00 ICN 01. Las Vegas, Nevada: Bechtel SAIC Company. ACC: DOC.20040603.0001. 169653

BSC 2004. *UZ Flow Models and Submodels.* MDL-NBS-HS-000006, Rev. 02. Las Vegas, Nevada: Bechtel SAIC Company. 169861

Carslaw, H.S. and Jaeger, J.C. 1959. *Conduction of Heat in Solids.* 2nd Edition. Oxford, Great Britain: Oxford University Press. TIC: 206085. 100968

CertainTeed. 1996. Submittal Sheet, Standard Fiber Glass Duct Wrap. Valley Forge, Pennsylvania: CertainTeed Corporation. TIC: 249257. 153512

Cho, Y.I.; Ganic, E.N.; Hartnett, J.P.; and Rohsenow, W.M. 1998. "Basic Concepts of Heat Transfer." Chapter 1 of *Handbook of Heat Transfer.* 3rd Edition. Rohsenow, W.M.; Hartnett, J.P.; and Cho, Y.I., eds. New York, New York: McGraw-Hill. TIC: 253612. 160802

Conte, S.D. and de Boor, C. 1972. *Elementary Numerical Analysis, An Algorithmic Approach.* 2nd Edition. New York, New York: McGraw-Hill. TIC: 224146. 159800

CRWMS (Civilian Radioactive Waste Management System) M&O (Management and Operating Contractor) 2000. *Conceptual Arrangement Simulated Emplacement Ventilation Test.* Las Vegas, Nevada: CRWMS M&O. ACC: MOL.20001219.0107. 153503

CRWMS M&O 2001. *Software Validation Test Report ANSYS Version 5.6.2 Software.* SAN: LV-2000-169. SDN: 10145-VTR-5.6.2-00. Las Vegas, Nevada: CRWMS M&O. ACC: MOL.20010323.0064. 155138

DOE (U.S. Department of Energy) 2003. *Software Management Report: ymesh Version 1.54.* Software Document Number: 10172-SMR-1.54-00. Las Vegas, Nevada: U.S. Department of Energy, Office of Repository Development. ACC: MOL.20030529.0026. 171332

DOE 2003. *Software Management Report: rme6 Version 1.2.* Software Document Number: 10617-SMR-1.2-00. Las Vegas, Nevada: U.S. Department of Energy, Office of Repository Development. ACC: MOL.20030523.0042. 171333

Doraswamy, N. 2001. *Validation Test Report for ANSYS Version 5.6.2 Software.* Document Number: 10145-VTR-5.6.2-01. Las Vegas, Nevada: Bechtel SAIC Company. ACC: MOL.20020219.0076. 171331

Ebadian, M.A. and Dong, Z.F. 1998. "Forced Convection, Internal Flow in Ducts." Chapter 5 of *Handbook of Heat Transfer.* 3rd Edition. Rohsenow, W.M.; Hartnett, J.P.; and Cho, Y.I., eds. New York, New York: McGraw-Hill. TIC: 253612. 160728

Fetter, C.W. 1993. *Contaminant Hydrogeology.* Upper Saddle River, New Jersey: Prentice Hall. TIC: 240691. 102009

Gebhart, B.; Jaluria, Y.; Mahajan, R.L.; and Sammakia, B. 1988. *Buoyancy-Induced Flows and Transport.* Textbook Edition. New York, New York: Hemisphere Publishing. TIC: 102802. 152234

Haar, L.; Gallagher, J.S.; and Kell, G.S. 1984. *NBS/NRC Steam Tables: Thermodynamic and Transport Properties and Computer Programs for Vapor and Liquid States of Water in SI Units.* New York, New York: Hemisphere Publishing Corporation. TIC: 241793. 105175

Hahn, G.J. and Shapiro, S.S. 1967. *Statistical Models in Engineering.* New York, New York: John Wiley & Sons. TIC: 247729. 146529

Hartman, H.L. 1982. *Mine Ventilation and Air Conditioning.* Mutmansky, J.M. and Wang, Y.J., eds. 2nd Edition. New York, New York: John Wiley & Sons. TIC: 210152. 128009

Hillel, D. 1998. *Environmental Soil Physics.* San Diego, California: Academic Press. TIC: 254422. 165404

Holman, J.P. 1997. *Heat Transfer.* 8th Edition. New York, New York: McGraw-Hill. TIC: 239954. 101978

Incropera, F.P. and DeWitt, D.P. 1985. *Fundamentals of Heat and Mass Transfer.* 2nd Edition. New York, New York: John Wiley & Sons. TIC: 208420. 114109

Incropera, F.P. and DeWitt, D.P. 1996. *Fundamentals of Heat and Mass Transfer.* 4th Edition. New York, New York: John Wiley & Sons. TIC: 243950. 108184

Jury, W.A.; Gardner, W.R.; and Gardner, W.H. 1991. *Soil Physics.* 5th Edition. New York, New York: John Wiley & Sons. TIC: 241000. 102010

Kays, W.M. and Leung, E.Y. 1963. "Heat Transfer in Annular Passages—Hydrodynamically Developed Turbulent Flow with Arbitrarily Prescribed Heat Flux." *International Journal of Heat and Mass Transfer, 6,* (7), 537-557. New York, New York: Pergamon. TIC: 253626. 160763

Kays, W.M. and Perkins, H.C. 1973. "Forced Convection, Internal Flow in Ducts." Section 7 of *Handbook of Heat Transfer.* Rohsenow, W.M. and Hartnett, J.P., eds. New York, New York: McGraw-Hill. TIC: 253611. 160782

Kern, D.Q. 1950. *Process Heat Transfer.* New York, New York: McGraw-Hill. TIC: 248066. 130111

Knudsen, J.G.; Bell, K.J.; Holt, A.D.; Hottel, H.C.; Sarofim, A.F.; Standiford, F.C.; Stuhlbarg, D.; and Uhl, V.W. 1984. "Heat Transmission." Section 10 of *Perry's Chemical Engineers' Handbook.* 6th Edition. Perry, R.H.; Green, D.W.; and Maloney, J.O., eds. New York, New York: McGraw-Hill. TIC: 246473. 170057

Kuehn, T.H. and Goldstein, R.J. 1976. "Correlating Equations for Natural Convection Heat Transfer Between Horizontal Circular Cylinders." *International Journal of Heat and Mass Transfer, 19,* (10), 1127-1134. New York, New York: Pergamon Press. TIC: 238411. 100675

Kuehn, T.H. and Goldstein, R.J. 1978. "An Experimental Study of Natural Convection Heat Transfer in Concentric and Eccentric Horizontal Cylindrical Annuli." *Journal of Heat Transfer, 100,* (4), 635-640. New York, New York: American Society of Mechanical Engineers. TIC: 244433. 130084

Levenspiel, O. 1972. *Chemical Reaction Engineering.* 2nd Edition. New York, New York: John Wiley & Sons. TIC: 224877. 156839

McAdams, W.H. 1954. *Heat Transmission.* 3rd Edition. New York, New York: McGraw-Hill. TIC: 242359. 161435

Morgan, V.T. 1975. "The Overall Convective Heat Transfer from Smooth Circular Cylinders." *Advances in Heat Transfer.* Volume 11. Irvine, T.F., Jr. and Hartnett, J.P., eds. Pages 199-264. New York, New York: Academic Press. TIC: 254306. 160791

Moyne, C.; Batsale, J-C.; and Degiovanni, A. 1988. "Approche Experimentale et Theorique de la Conductivite Thermique des Milieux Poreux Humides—II. Theorie." *International Journal of Heat and Mass Transfer, 31,* (11), 2319-2329. New York, New York: Pergamon Press. TIC: 249402. 154107

Moyne, C.; Batsale, J.C.; Degiovanni, A.; and Maillet, D. 1990. "Thermal Conductivity of Wet Porous Media: Theoretical Analysis and Experimental Measurements." *Thermal Conductivity 21, Proceedings of the Twenty-First International Thermal Conductivity Conference, October 15-18, 1989, Lexington, Kentucky.* Cremers, C.J. and Fine, H.A., eds. Pages 109-120. New York, New York: Plenum Press. TIC: 249322. 153164

Nagle, R.K. and Saff, E.B. 1994. *Fundamentals of Differential Equations and Boundary Value Problems.* Reading, Massachusetts: Addison-Wesley Publishing. TIC: 238891. 100922

NRC (U.S. Nuclear Regulatory Commission) 2003. *Yucca Mountain Review Plan, Final Report.* NUREG-1804, Rev. 2. Washington, D.C.: U.S. Nuclear Regulatory Commission, Office of Nuclear Material Safety and Safeguards. TIC: 254568. 163274

Perry, R.H.; Green, D.W.; and Maloney, J.O., eds. 1984. *Perry's Chemical Engineers' Handbook.* 6th Edition. New York, New York: McGraw-Hill. TIC: 246473. 125806

Raithby, G.D. and Hollands, K.G.T. 1998. "Natural Convection." Chapter 4 of *Handbook of Heat Transfer.* 3rd Edition. Rohsenow, W.M.; Hartnett, J.P.; and Cho, Y.I., eds. New York, New York: McGraw-Hill. TIC: 253612. 160764

Reid, R.C.; Prausnitz, J.M.; and Sherwood, T.K. 1977. *The Properties of Liquids and Gases.* New York, New York: McGraw-Hill Book Company. TIC: 240958. 130310

Reynolds, W.C.; Lundberg, R.E.; and McCuen, P.A. 1963. "Heat Transfer in Annular Passages. General Formulation of the Problem for Arbitrarily Prescribed Wall Temperatures or Heat Fluxes." *International Journal of Heat and Mass Transfer, 6,* (6), 483-493. New York, New York: Pergamon Press. TIC: 253625. 160770

Rohsenow, W.M.; Hartnett, J.P.; and Cho, Y.I. 1998. *Handbook of Heat Transfer*. 3rd Edition. New York, New York: McGraw-Hill. TIC: 253612. 169241

Sass, J.H.; Lachenbruch, A.H.; Dudley, W.W., Jr.; Priest, S.S.; and Munroe, R.J. 1988. *Temperature, Thermal Conductivity, and Heat Flow Near Yucca Mountain, Nevada: Some Tectonic and Hydrologic Implications.* Open-File Report 87-649. Denver, Colorado: U.S. Geological Survey. TIC: 203195. 100644

Stroe, D.E. 2001. "PO#: A18763CM0A, Transmittal of Test Results." Letter from D.E. Stroe (Anter Laboratories) to M. Knudsen (CRWMS M&O), January 31, 2001, PR20939-51554c, with attachment. ACC: MOL.20010220.0057. 155633

Sutherland, W.A. and Kays, W.M. 1964. "Heat Transfer in an Annulus with Variable Circumferential Heat Flux." *International Journal of Heat and Mass Transfer, 7,* (11), 1187-1194. New York, New York: Pergamon. TIC: 253693. 160789

Weast, R.C., ed. 1977. *CRC Handbook of Chemistry and Physics.* 58th Edition. Cleveland, Ohio: CRC Press. TIC: 242376. 106266

Weinberger, H.F. 1965. *A First Course in Partial Differential Equations.* New York, New York: John Wiley & Sons. TIC: 254310. 163216

White, F.M. 1986. *Fluid Mechanics.* 2nd Edition. New York, New York: McGraw-Hill. TIC: 243415. 111015

Wildenschild, D. and Roberts, J.J. 1999. *Experimental Tests of Enhancement of Vapor Diffusion in Topopah Spring Tuff.* UCRL-JC-134850. Livermore, California: Lawrence Livermore National Laboratory. TIC: 246923. 131055

Yovanovich, M.M. 1998. "Conduction and Thermal Contact Resistances (Conductances)." Chapter 3 of *Handbook of Heat Transfer.* 3rd Edition. Rohsenow, W.M.; Hartnett, J.P.; and Cho, Y.I., eds. New York, New York: McGraw-Hill. TIC: 253612. 171591

Zwillinger, D., ed. 1996. *CRC Standard Mathematical Tables and Formulae.* 30th Edition. Boca Raton, Florida: CRC Press. TIC: 233960. 152179

9.2 CODES, STANDARDS, REGULATIONS, AND PROCEDURES

10 CFR 63. Energy: Disposal of High-Level Radioactive Wastes in a Geologic Repository at Yucca Mountain, Nevada. Readily available 156605

ANSI/NCSL Z540-2-1997. *American National Standard for Calibration — U.S. Guide to the Expression of Uncertainty in Measurement*. Boulder, Colorado: NCSL International. TIC: 251472. 157394

AP-2.14Q, Rev. 3, ICN 0. *Document Review*. Washington, D.C.: U.S. Department of Energy, Office of Civilian Radioactive Waste Management. ACC: DOC.20030827.0018.

AP-2.27Q, Rev. 1, ICN 4. *Planning for Science Activities.* Washington, D.C.: U.S. Department of Energy, Office of Civilian Radioactive Waste Management. ACC: DOC.20040610.0006.

AP-3.15Q, Rev. 4, ICN 5. *Managing Technical Product Inputs*. Washington, D.C.: U.S. Department of Energy, Office of Civilian Radioactive Waste Management. ACC: DOC.20040812.0004.

AP-SIII.10Q, Rev. 2, ICN 7. *Models.* Washington, D.C.: U.S. Department of Energy, Office of Civilian Radioactive Waste Management. ACC: DOC.20040920.0002.

AP-SV.1Q, Rev. 1, ICN 1. *Control of the Electronic Management of Information*. Washington, D.C.: U.S. Department of Energy, Office of Civilian Radioactive Waste Management. ACC: DOC.20040308.0001.

ASME PTC 19.1-1998. *Test Uncertainty, Instruments and Apparatus*. New York, New York: American Society of Mechanical Engineers. TIC: 249327. 153195

LP-SI.11Q-BSC Rev 0, ICN 1. *Software Management*. Washington, D.C.: U.S. Department of Energy, Office of Civilian Radioactive Waste Management. ACC: DOC.20041005.0008.

9.3 SOURCE DATA, LISTED BY DATA TRACKING NUMBER

GS000383351030.002. Angle of Repose, Particle Density, and Uncompacted Bulk Density Data for Analyses Performed on Potential Candidate Backfill Materials. Submittal date: 03/24/00. 148445

GS000483351030.003. Thermal Properties Measured 12/01/99 to 12/02/99 Using the Thermolink Soil Multimeter and Thermal Properties Sensor on Selected Potential Candidate Backfill Materials Used in the Engineered Barrier System. Submittal date: 11/09/2000. 152932

GS000508312231.006. Physical Properties and Water Content from Borehole USW NRG-6, 3/19/94 to 3/27/95. Submittal date: 05/23/2000. 153237

GS020183351030.001. Uncompacted Bulk Density for Analyses Performed 02/02/00 to 05/23/00 on Potential Backfill Materials Used in the Engineered Barrier System. Submittal date: 01/22/2002. 163107

GS950408312231.004. Physical Properties and Water Potentials of Core from Borehole USW SD-9. Submittal date: 03/01/1995. 108986

GS951108312231.009. Physical Properties, Water Content, and Water Potential for Borehole USW SD-7. Submittal date: 09/26/1995. 108984

GS951108312231.010. Physical Properties and Water Content for Borehole USW NRG-7/7A. Submittal date: 09/26/1995. 108983

GS951108312231.011. Physical Properties, Water Content, and Water Potential for Borehole USW UZ-7A. Submittal date: 09/26/1995. 108992

LB0110ECRBH2OP.001. Water Potential Data from Three Locations in the ECRB. Submittal date: 11/12/2001. 156883

LB0208UZDSCPMI.002. Drift-Scale Calibrated Property Sets: Mean Infiltration Data Summary. Submittal date: 08/26/2002. 161243

LB0302PTNTSW9I.001. PTN/TSW Interface Percolation Flux Maps for 9 Infiltration Scenarios. Submittal date: 02/28/2003. 162277

LB0303THERMSIM.001. UZ Thermal Modeling: Simulations. Submittal date: 03/28/2003. 165167

LB990901233124.006. Moisture Data from the ECRB Cross Drift for AMR U0015, “In Situ Testing of Field Processes”. Submittal date: 11/01/1999. 135137

MO0106RIB00038.001. Water-Level Data and the Potentiometric Surface. Submittal date: 06/22/2001. 155631

MO0406SEPTVDST.000. Temperature and Volume Water Content for Drift Scale Test (DST) Heating Phase for Boreholes 79 and 80. Submittal date: 06/29/2004. 170616

MO0407SEPFEPLA.000. LA FEP List. Submittal date: 07/20/2004. 170760

SN0208F3409100.007. Preclosure Ventilation Test: 1/4 Scale, Including Data from Cases 1 through 6 (with Results from 10/05/2000 through 12/22/2000), Final Data Revised August 2002. Submittal date: 08/27/2002. 161729

SN0208F3409100.009. Preclosure Ventilation Test: 1/4 Scale, Phase 2, Including Data from Tests 1 through 16 (with Results from 4/25/01 to 10/01/2001), Final Data Revised August 2002. Submittal date: 08/27/2002. 163079

SN0303T0503102.008. Revised Thermal Conductivity of the Non-Repository Layers of Yucca Mountain. Submittal date: 03/19/2003. 162401

SN0307T0510902.003. Updated Heat Capacity of Yucca Mountain Stratigraphic Units. Submittal date: 07/15/2003. 164196

SN0404T0503102.011. Thermal Conductivity of the Potential Repository Horizon Rev 3. Submittal date: 04/27/2004. 169129

SNL22100196001.006. Laboratory Measurements of Thermal Conductivity as a Function of Saturation State for Welded and Nonwelded Tuff Specimens. Submittal date: 06/08/1998. 158213

9.4 SOFTWARE CODES

BSC 2001. *Software Code: ANSYS.* V5.6.2. Sun, Solaris 2.6 and Solaris 2.7. 10145-5.6.2-01. 164464

CRWMS M&O 2001. *Software Code: ANSYS.* V5.6.2. IRIX 6.5. 10145-5.6.2-00. 154671

LLNL (Lawrence Livermore National Laboratory) 2003. *Software Code: rme6.* v1.2. SUN, SOLARIS 8. 10617-1.2-00. 163892

LLNL 2003. *Software Code: YMESH.* v1.54. SUN, SOLARIS 8. 10172-1.54-00. 163894

INTENTIONALLY LEFT BLANK

APPENDIX I

USING THE GEOLOGIC FRAMEWORK MODEL AND MINERALOGIC HYDROSTRATIGRAPHIC UNITS TO ASSIGN THERMOPHYSICAL PROPERTIES TO THE UZ UNITS

This appendix documents the calculation of thermophysical properties of the UZ model layers based on the thermophysical properties of the lithostratigraphic units. The inputs (thermophysical properties of the lithostratigraphic units) are presented in Tables I-1 and I-2. The outputs (thermophysical properties of the UZ model layers) are presented in Table I-3. The formulae used in the calculation are listed in Table I-4. Table I-5 provides the nomenclature correlation between lithostratigraphic units and UZ model layers.

Table I-1

Sources: DTNs: SN0303T0503102.008 and SN0404T0503102.011

Stratigraphic Unit	Dry Bulk Thermal Conductivity (W/m·K)	Wet Bulk Thermal Conductivity (W/m·K)	Matrix Porosity	Lithophysal Porosity	Dry Bulk Density (kg/m^3)
Tpcp	1.3000	1.8100	0.1190	0.0000	2190
TpcLD	1.3000	1.8100	0.1190	0.0000	2190
Tpcpv3	0.6880	0.7960	0.0360	0.0000	2310
Tpcpv2	0.4900	1.0600	0.3850	0.0000	1460
Tpcpv1	0.4900	1.0600	0.3850	0.0000	1460
Tpbt4	0.4900	1.0600	0.3850	0.0000	1460
Tpy	0.4900	1.0600	0.3850	0.0000	1460
Tpbt3	0.4900	1.0600	0.3850	0.0000	1460
Tpp	0.4900	1.0600	0.3850	0.0000	1460
Tpb2	0.4900	1.0600	0.3850	0.0000	1460
Tptrv3	0.4900	1.0600	0.3850	0.0000	1460
Tptrv2	0.4900	1.0600	0.3850	0.0000	1460
Tptrv1	0.6880	0.7960	0.0360	0.0000	2310
Tptrn	1.3000	1.8100	0.1190	0.0000	2190
Tptrl, Tptf	1.3000	1.8100	0.1190	0.0000	2190
Tptpul RHHtop	1.1829	1.7749	0.1667	0.1228	1834
Tptpmn	1.4189	2.0741	0.1287	0.0254	2148
Tptpll	1.2784	1.8895	0.1486	0.0883	1979
Tptpln	1.4900	2.1303	0.1058	0.0302	2211
Tptpv3	0.6880	0.7960	0.0360	0.0000	2310
Tptpv2	0.4900	1.0600	0.3850	0.0000	1460
Tptpv1	0.4900	1.0600	0.3850	0.0000	1460
Tpbt1	0.4900	1.0600	0.3850	0.0000	1460
Tac (Calico)	0.5950	1.2600	0.3330	0.0000	1670
Tacbt (Calicobt)	0.5950	1.2600	0.3330	0.0000	1670
Tcpuv (Prowuv)	0.5690	1.1300	0.3000	0.0000	1790
Tcpuc (Prowuc)	0.5690	1.1300	0.3000	0.0000	1790
Tcpmd (Prowmd)	1.0600	1.6300	0.2090	0.0000	2070
Tcplc (Prowlc)	0.5690	1.1300	0.3000	0.0000	1790

Table I-2

Source: DTN: SN0307T0510902.003

Mineralogic Unit	Specific Heat (J/g·K)
Tpc	0.930
Tpcpv23	0.950
pTn	0.960
Tptrv1	0.950
Tptrnf	0.930
Tptpul	0.930
Tptpmn	0.930
Tptpll	0.930
Tptpln	0.930
Tptpv3	0.980
Tptpv2	0.980
Tptpv1-Tpbt1	1.080
Tac4	1.070
Tac3	1.070
Tac2	1.070
Tac1	1.070
Tacbt	1.020
Tcpuv	1.040
Tcpuc-Tcplc	0.930

Table I-3 Calculated Values Based on Tables I-1 and I-2 (Formulae Used Are Listed in Table I-4)

UZ UNIT	Dry Bulk Thermal Conductivity (W/m·K)	Wet Bulk Thermal Conductivity (W/m·K)	Matrix Porosity	Lithophysal Porosity	Dry Bulk Density (kg/m^3)	Specific Heat (J/g·K)
tcw12	1.300	1.810	0.119	0.000	2190	0.930
tcw13	0.589	0.928	0.211	0.000	1885	0.950
ptn21	0.490	1.060	0.385	0.000	1460	0.960
ptn22	0.490	1.060	0.385	0.000	1460	0.960
ptn23	0.490	1.060	0.385	0.000	1460	0.960
ptn24	0.490	1.060	0.385	0.000	1460	0.960
ptn25	0.490	1.060	0.385	0.000	1460	0.960
ptn26	0.490	1.060	0.385	0.000	1460	0.960
tsw31	0.994	1.303	0.078	0.000	2250	0.940
tsw32	1.300	1.810	0.119	0.000	2190	0.930
tsw33	1.241	1.792	0.143	0.061	2012	0.930
tsw34	1.419	2.074	0.129	0.025	2148	0.930
tsw35	1.278	1.890	0.149	0.088	1979	0.930
tsw36	1.490	2.130	0.106	0.030	2211	0.930
tsw37	1.490	2.130	0.106	0.030	2211	0.930
tsw38	0.688	0.796	0.036	0.000	2310	0.980
tsw39	0.490	1.060	0.385	0.000	1460	0.980
ch1	0.490	1.060	0.385	0.000	1460	1.080
ch2	0.595	1.260	0.333	0.000	1670	1.070
ch3	0.595	1.260	0.333	0.000	1670	1.070
ch4	0.595	1.260	0.333	0.000	1670	1.070
ch5	0.595	1.260	0.333	0.000	1670	1.070
ch6	0.595	1.260	0.333	0.000	1670	1.020
pp4	0.569	1.130	0.300	0.000	1790	1.040
pp3	0.569	1.130	0.300	0.000	1790	0.930
pp2	0.815	1.380	0.255	0.000	1930	0.930

Table I-4 Formulae Used to Calculate Values Listed in Table I-3

UZ UNIT	Dry Bulk Thermal Conductivity (W/m·K)	Wet Bulk Thermal Conductivity (W/m·K)	Matrix Porosity	Lithophysal Porosity	Dry Bulk Density (kg/m^3)	Specific Heat (J/g·K)
tcw12	=AVERAGE(D5:D6)	=AVERAGE(E5:E6)	=AVERAGE(F5:F6)	=AVERAGE(G5:G6)	=AVERAGE(H5:H6)	=D37
tcw13	=AVERAGE(D7:D8)	=AVERAGE(E7:E8)	=AVERAGE(F7:F8)	=AVERAGE(G7:G8)	=AVERAGE(H7:H8)	=D38
ptn21	=D9	=E9	=F9	=G9	=H9	=D39
ptn22	=AVERAGE(D10:D11)	=AVERAGE(E10:E11)	=AVERAGE(F10:F11)	=AVERAGE(G10:G11)	=AVERAGE(H10:H11)	=D39
ptn23	=D11	=E11	=F11	=G11	=H11	=D39
ptn24	=AVERAGE(D11:D12)	=AVERAGE(E11:E12)	=AVERAGE(F11:F12)	=AVERAGE(G11:G12)	=AVERAGE(H11:H12)	=D39
ptn25	=D13	=E13	=F13	=G13	=H13	=D39
ptn26	=AVERAGE(D14:D16)	=AVERAGE(E14:E16)	=AVERAGE(F14:F16)	=AVERAGE(G14:G16)	=AVERAGE(H14:H16)	=D39
tsw31	=AVERAGE(D17:D18)	=AVERAGE(E17:E18)	=AVERAGE(F17:F18)	=AVERAGE(G17:G18)	=AVERAGE(H17:H18)	=AVERAGE(D40:D41)
tsw32	=D18	=E18	=F18	=G18	=H18	=D41
tsw33	=AVERAGE(D19:D20)	=AVERAGE(E19:E20)	=AVERAGE(F19:F20)	=AVERAGE(G19:G20)	=AVERAGE(H19:H20)	=AVERAGE(D41:D42)
tsw34	=D21	=E21	=F21	=G21	=H21	=D43
tsw35	=D22	=E22	=F22	=G22	=H22	=D44
tsw36	=D23	=E23	=F23	=G23	=H23	=D45
tsw37	=D23	=E23	=F23	=G23	=H23	=D45
tsw38	=D24	=E24	=F24	=G24	=H24	=D46
tsw39	=D25	=E25	=F25	=G25	=H25	=D47
ch1	=AVERAGE(D26:D27)	=AVERAGE(E26:E27)	=AVERAGE(F26:F27)	=AVERAGE(G26:G27)	=AVERAGE(H26:H27)	=D48
ch2	=D28	=E28	=F28	=G28	=H28	=D49
ch3	=D28	=E28	=F28	=G28	=H28	=D50
ch4	=D28	=E28	=F28	=G28	=H28	=D51
ch5	=D28	=E28	=F28	=G28	=H28	=D52
ch6	=D29	=E29	=F29	=G29	=H29	=D53
pp4	=D30	=E30	=F30	=G30	=H30	=D54
pp3	=D31	=E31	=F31	=G31	=H31	=D55
pp2	=AVERAGE(D32:D33)	=AVERAGE(E32:E33)	=AVERAGE(F32:F33)	=AVERAGE(G32:G33)	=AVERAGE(H32:H33)	=D55

Table I-5. Nomenclature Correlation Between Lithostratigraphic Unit and UZ Model Layer

Lithostratigraphic Unit	UZ Model Layer
Tpcr	tcw11
Tpcp	tcw12
TpcLD	
Tpcpv3	tcw13
Tpcpv2	
Tpcpv1	ptn21
Tpbt4	ptn22
Tpy (Yucca)	ptn23
	ptn24
Tpbt3	
Tpp (Pah)	ptn25
Tpbt2	ptn26
Tptrv3	
Tptrv2	
Tptrv1	tsw31
Tptrn	
	tsw32
Tptrl, Tptf	tsw33
Tptpul, RHHtop	
Tptpmn	tsw34
Tptpll	tsw35
Tptpln	tsw36
	tsw37
Tptpv3	tsw38
Tptpv2	tsw39
Tptpv1	ch1
Tpbt1	
Tac (Calico)	ch2
	ch3
	ch4
	ch5
Tacbt (Calicobt)	ch6
Tcpuv (Prowuv)	pp4
Tcpuc (Prowuc)	pp3
Tcpm (Prowmd)	pp2
Tcplc (Prowlc)	
Tcplv (Prowlv)	pp1
Tcpbt (Prowbt)	
Tcbuv (Bullfroguv)	
Tcbuc (Bullfroguc)	bf3
Tcbm (Bullfrogmd)	
Tcblc (Bullfroglc)	
Tcblv (Bullfroglv)	bf2
Tcbbt (Bullfrogbt)	
Tctuv (Tramuv)	
Tctuc (Tramuc)	tr3
Tctm (Trammd)	
Tctlc (Tramlc)	
Tctlv (Tramlv)	tr2
Tctbt (Trambt)	

Source: BSC 2004 [DIRS 169855], Table 6-11.

APPENDIX II

CALCULATING EFFECTIVE THERMOPHYSICAL PROPERTIES FOR THE ANSYS-BASED MODELS

This appendix documents the calculation of effective thermophysical properties used in the ANSYS model discussed in Section 6 of this report. For geologic media composed of air, water, and rock, the heat capacity per unit volume of the composite material is the sum of the heat capacities of the constituents weighted by volume fractions. Jury et al. (1991 [DIRS 102010], p. 179) express this capacity as:

$$C_{soil} = \chi_a \cdot C_a + \chi_w \cdot C_{vw} + \sum_{j=1}^{N} \chi_{sj} \cdot C_{sj} \qquad \text{(Eq. II-1)}$$

where

χ_a = volume fraction of the air
χ_w = volume fraction of the water
χ_{sj} = volume fraction of jth component of the solids
C_a = volumetric heat capacity of the air
C_{vw} = volumetric heat capacity of the water
C_{sj} = volumetric heat capacity of the jth component of the solids

More specifically for the geologic units at Yucca Mountain, Equation II-1 can be written:

$$C_{rock} = \chi_{am} \cdot C_a + \chi_{al} \cdot C_a + \chi_w \cdot C_{vw} + \chi_s \cdot C_s \qquad \text{(Eq. II-2)}$$

where

χ_{am} = volume fraction of the air in the matrix
χ_{al} = volume fraction of the air in the lithophysae
χ_w = volume fraction of the water in the matrix and
χ_s = volume fraction of the solids

The various volume fractions can be written as:

$$\chi_{al} = \frac{V_{al}}{V_s + V_{wm} + V_{am} + V_{al}} \qquad \text{(Eq. II-3)}$$

$$\chi_{am} = \frac{V_{am}}{V_s + V_{wm} + V_{am} + V_{al}} \qquad \text{(Eq. II-4)}$$

$$\chi_w = \frac{V_w}{V_s + V_{wm} + V_{am} + V_{al}} \qquad \text{(Eq. II-5)}$$

$$\chi_s = \frac{V_s}{V_s + V_{wm} + V_{am} + V_{al}} \qquad \text{(Eq. II-6)}$$

Substituting these equations into Equation II-2 and using the identity that the product of the density and the specific heat of a material is the volumetric heat capacity (Incropera and DeWitt 1996 [DIRS 108184], Section 2.2.2) results in the following:

$$(V_s + V_{wm} + V_{am} + V_{al}) \cdot C_{rock} = V_{am} \cdot C_a + V_{al} \cdot C_a + V_w \cdot C_{vw} + V_s \cdot \rho_g \cdot C_p \qquad \text{(Eq. II-7)}$$

where

V_{al}	=	volume of the air in the lithophysae
V_{am}	=	volume of the air in the matrix
V_{wm}	=	volume of the water in the matrix
V_s	=	volume of the solids (which is set to 1)
C_p	=	specific heat of the solids
ρ_g	=	grain density of the solids

Now consider the definitions for the matrix porosity and the lithophysal porosity. The matrix porosity is defined as the ratio of the void volume of the matrix to the total matrix volume (of solids):

$$\phi_m = \frac{V_m}{V_s + V_m} \qquad \text{(Eq. II-8)}$$

where $V_m = V_{am} + V_{wm}$.

Solving for the matrix void volume in terms of the matrix porosity:

$$V_m = \frac{\phi_m}{1 - \phi_m} \cdot V_s \qquad \text{(Eq. II-9)}$$

The lithophysal porosity is defined as the ratio of the volume of the lithophysae to the total volume:

$$\phi_l = \frac{V_{al}}{V_s + V_m + V_{al}} \qquad \text{(Eq. II-10)}$$

Solving for the volume of lithophysae:

$$V_{al} = \phi_l \cdot (V_s + V_m + V_{al}) \qquad \text{(Eq. II-11)}$$

Substituting Equation II-9 into Equation II-11 yields:

$$V_{al} = \frac{\phi_l}{1 - \phi_l} \cdot (1 + \frac{\phi_m}{1 - \phi_m}) \cdot V_s \qquad \text{(Eq. II-12)}$$

The matrix saturation (S) is used to estimate the volume occupied by water:

$$V_w = S \cdot \frac{\phi_m}{1 - \phi_m} \cdot V_s \qquad \text{(Eq. II-13)}$$

Substituting Equation II-12 into Equation II-7, and neglecting the heat capacity of the air (C_a<<C_{vw}) (Jury et al. 1991 [DIRS 102010], p. 180), the following equation is obtained:

$$\left(V_s + \frac{\phi_m V_s}{1-\phi_m} + \frac{\phi_l}{1-\phi_l}\cdot\left(1+\frac{\phi_m}{1-\phi_m}\right)\cdot V_s\right)\cdot C_{rock} = S\cdot\frac{\phi_m}{1-\phi_m}C_{vw}V_s + \rho_g\cdot C_p V_s \qquad \text{(Eq. II-14)}$$

Solving for C_{rock} and canceling out the volume of the solids, V_s, the volumetric heat capacity is expressed as (with $V_s = 1$):

$$C_{rock} = \frac{S\cdot\frac{\phi_m}{1-\phi_m}C_{vw} + \rho_g\cdot C_p}{\left[1+\frac{\phi_m}{1-\phi_m} + \frac{\phi_l}{1-\phi_l}\cdot\left(1+\frac{\phi_m}{1-\phi_m}\right)\right]} \qquad \text{(Eq. II-15)}$$

This methodology is implemented in the following spreadsheet to calculate effective thermophysical properties for the ANSYS models.

An example calculation of the volumetric heat capacity of tsw35 layer is presented below.

Given: S=0.9; ϕ_m=0.15; C_{vw}=4179×997=4.1665×10^6; ρ_g=2593; C_p=930; ϕ_l=0.09

$$C_{rock} = \frac{S\cdot\frac{\phi_m}{1-\phi_m}C_{vw} + \rho_g\cdot C_p}{\left[1+\frac{\phi_m}{1-\phi_m} + \frac{\phi_l}{1-\phi_l}\cdot\left(1+\frac{\phi_m}{1-\phi_m}\right)\right]} = \frac{0.9\cdot\frac{0.15}{1-0.15}\cdot 4.1665\times 10^6 + 2593\cdot 930}{\left[1+\frac{0.15}{1-0.15} + \frac{0.09}{1-0.09}\cdot\left(1+\frac{0.15}{1-0.15}\right)\right]} = 2377188$$

Details of the calculation of volumetric heat capacities of UZ model layers are presented in Table II-1, and the formulae used are listed in Tables II-2 and II-3.

Table II-1. Calculation of Volumetric Heat Capacity of Rock

	C	D	E	F	G	H	I	J	K	L	M
3	Assumed Saturation =		90.5%								
4	Density of Water =		997	kg/m3 at	300	K					
5	Specifici Heat of Water =		4179	J/kg·K at	300	K					
7	**UZ UNIT**	**Dry Bulk Thermal Conductivity (W/m·K)**	**Wet Bulk Thermal Conductivity (W/m·K)**	**ANSYS Thermal Conductivity (W/m·K)**	**Matrix Porosity**	**Lithophysal Porosity**	**ANSYS Specific Heat (J/kg·K)**	**Dry Bulk Density (kg/m^3)**	**Rock Grain Density (kg/m^3)**	**Volumetric Heat Capacity ($J/m^3·K$)**	**ANSYS Density (kg/m^3)**
8	tcw12	1.30	1.81	1.76	0.12	0.00	930	2190	2486	2485606	2673
9	tcw13	0.59	0.93	0.90	0.21	0.00	950	1885	2388	2584822	2721
10	ptn21	0.49	1.06	1.01	0.39	0.00	960	1460	2374	2853942	2973
11	ptn22	0.49	1.06	1.01	0.39	0.00	960	1460	2374	2853942	2973
12	ptn23	0.49	1.06	1.01	0.39	0.00	960	1460	2374	2853942	2973
13	ptn24	0.49	1.06	1.01	0.39	0.00	960	1460	2374	2853942	2973
14	ptn25	0.49	1.06	1.01	0.39	0.00	960	1460	2374	2853942	2973
15	ptn26	0.49	1.06	1.01	0.39	0.00	960	1460	2374	2853942	2973
16	tsw31	0.99	1.30	1.27	0.08	0.00	940	2250	2439	2407354	2561
17	tsw32	1.30	1.81	1.76	0.12	0.00	930	2190	2486	2485606	2673
18	tsw33	1.24	1.79	1.74	0.14	0.06	930	2012	2528	2397573	2578
19	tsw34	1.42	2.07	2.01	0.13	0.03	930	2148	2539	2478525	2665
20	tsw35	1.28	1.89	1.83	0.15	0.09	930	1979	2593	2383185	2563
21	tsw36	1.49	2.13	2.07	0.11	0.03	930	2211	2559	2450892	2635
22	tsw37	1.49	2.13	2.07	0.11	0.03	930	2211	2559	2450892	2635
23	tsw38	0.69	0.80	0.79	0.04	0.00	980	2310	2396	2399603	2449
24	tsw39	0.49	1.06	1.01	0.39	0.00	980	1460	2374	2883142	2942
25	ch1	0.49	1.06	1.01	0.39	0.00	1080	1460	2374	3029142	2805
26	ch2	0.60	1.26	1.20	0.33	0.00	1070	1670	2504	3043081	2844
27	ch3	0.60	1.26	1.20	0.33	0.00	1070	1670	2504	3043081	2844
28	ch4	0.60	1.26	1.20	0.33	0.00	1070	1670	2504	3043081	2844
29	ch5	0.60	1.26	1.20	0.33	0.00	1070	1670	2504	3043081	2844
30	ch6	0.60	1.26	1.20	0.33	0.00	1020	1670	2504	2959581	2902
31	pp4	0.57	1.13	1.08	0.30	0.00	1040	1790	2557	2993295	2878
32	pp3	0.57	1.13	1.08	0.30	0.00	930	1790	2557	2796395	3007
33	pp2	0.81	1.38	1.33	0.25	0.00	930	1930	2589	2754954	2962

Note: Formulae used are listed in Tables II-2 and II-3.

Table II-2. Formulae Used in Calculation Presented in Table II-1

K	L	M	N	O	P
2					
3					
4					
5					
6					
7	**Dry Bulk Density (kg/m^3)**	**Rock Grain Density (kg/m^3)**	**Volumetric Heat Capacity ($J/m^3 \cdot K$)**	**ANSYS Density (kg/m^3)**	
8	2190	=L8*(1+((G8+H8)/(1-(G8+H8))))	=(E3*(G8/(1-G8))*E4*E5+M8*I8)/((1+(G8/(1-G8)))*(1+(H8/(1-H8))))	=N8/I8	
9	1885	=L9*(1+((G9+H9)/(1-(G9+H9))))	=(E3*(G9/(1-G9))*E4*E5+M9*I9)/((1+(G9/(1-G9)))*(1+(H9/(1-H9))))	=N9/I9	
10	1460	=L10*(1+((G10+H10)/(1-(G10+H10))))	=(E3*(G10/(1-G10))*E4*E5+M10*I10)/((1+(G10/(1-G10)))*(1+(H10/(1-H10))))	=N10/I10	
11	1460	=L11*(1+((G11+H11)/(1-(G11+H11))))	=(E3*(G11/(1-G11))*E4*E5+M11*I11)/((1+(G11/(1-G11)))*(1+(H11/(1-H11))))	=N11/I11	
12	1460	=L12*(1+((G12+H12)/(1-(G12+H12))))	=(E3*(G12/(1-G12))*E4*E5+M12*I12)/((1+(G12/(1-G12)))*(1+(H12/(1-H12))))	=N12/I12	
13	1460	=L13*(1+((G13+H13)/(1-(G13+H13))))	=(E3*(G13/(1-G13))*E4*E5+M13*I13)/((1+(G13/(1-G13)))*(1+(H13/(1-H13))))	=N13/I13	
14	1460	=L14*(1+((G14+H14)/(1-(G14+H14))))	=(E3*(G14/(1-G14))*E4*E5+M14*I14)/((1+(G14/(1-G14)))*(1+(H14/(1-H14))))	=N14/I14	
15	1460	=L15*(1+((G15+H15)/(1-(G15+H15))))	=(E3*(G15/(1-G15))*E4*E5+M15*I15)/((1+(G15/(1-G15)))*(1+(H15/(1-H15))))	=N15/I15	
16	2250	=L16*(1+((G16+H16)/(1-(G16+H16))))	=(E3*(G16/(1-G16))*E4*E5+M16*I16)/((1+(G16/(1-G16)))*(1+(H16/(1-H16))))	=N16/I16	
17	2190	=L17*(1+((G17+H17)/(1-(G17+H17))))	=(E3*(G17/(1-G17))*E4*E5+M17*I17)/((1+(G17/(1-G17)))*(1+(H17/(1-H17))))	=N17/I17	
18	2012	=L18*(1+((G18+H18)/(1-(G18+H18))))	=(E3*(G18/(1-G18))*E4*E5+M18*I18)/((1+(G18/(1-G18)))*(1+(H18/(1-H18))))	=N18/I18	
19	2148	=L19*(1+((G19+H19)/(1-(G19+H19))))	=(E3*(G19/(1-G19))*E4*E5+M19*I19)/((1+(G19/(1-G19)))*(1+(H19/(1-H19))))	=N19/I19	
20	1979	=L20*(1+((G20+H20)/(1-(G20+H20))))	=(E3*(G20/(1-G20))*E4*E5+M20*I20)/((1+(G20/(1-G20)))*(1+(H20/(1-H20))))	=N20/I20	
21	2211	=L21*(1+((G21+H21)/(1-(G21+H21))))	=(E3*(G21/(1-G21))*E4*E5+M21*I21)/((1+(G21/(1-G21)))*(1+(H21/(1-H21))))	=N21/I21	
22	2211	=L22*(1+((G22+H22)/(1-(G22+H22))))	=(E3*(G22/(1-G22))*E4*E5+M22*I22)/((1+(G22/(1-G22)))*(1+(H22/(1-H22))))	=N22/I22	
23	2310	=L23*(1+((G23+H23)/(1-(G23+H23))))	=(E3*(G23/(1-G23))*E4*E5+M23*I23)/((1+(G23/(1-G23)))*(1+(H23/(1-H23))))	=N23/I23	
24	1460	=L24*(1+((G24+H24)/(1-(G24+H24))))	=(E3*(G24/(1-G24))*E4*E5+M24*I24)/((1+(G24/(1-G24)))*(1+(H24/(1-H24))))	=N24/I24	
25	1460	=L25*(1+((G25+H25)/(1-(G25+H25))))	=(E3*(G25/(1-G25))*E4*E5+M25*I25)/((1+(G25/(1-G25)))*(1+(H25/(1-H25))))	=N25/I25	
26	1670	=L26*(1+((G26+H26)/(1-(G26+H26))))	=(E3*(G26/(1-G26))*E4*E5+M26*I26)/((1+(G26/(1-G26)))*(1+(H26/(1-H26))))	=N26/I26	
27	1670	=L27*(1+((G27+H27)/(1-(G27+H27))))	=(E3*(G27/(1-G27))*E4*E5+M27*I27)/((1+(G27/(1-G27)))*(1+(H27/(1-H27))))	=N27/I27	
28	1670	=L28*(1+((G28+H28)/(1-(G28+H28))))	=(E3*(G28/(1-G28))*E4*E5+M28*I28)/((1+(G28/(1-G28)))*(1+(H28/(1-H28))))	=N28/I28	
29	1670	=L29*(1+((G29+H29)/(1-(G29+H29))))	=(E3*(G29/(1-G29))*E4*E5+M29*I29)/((1+(G29/(1-G29)))*(1+(H29/(1-H29))))	=N29/I29	
30	1670	=L30*(1+((G30+H30)/(1-(G30+H30))))	=(E3*(G30/(1-G30))*E4*E5+M30*I30)/((1+(G30/(1-G30)))*(1+(H30/(1-H30))))	=N30/I30	
31	1790	=L31*(1+((G31+H31)/(1-(G31+H31))))	=(E3*(G31/(1-G31))*E4*E5+M31*I31)/((1+(G31/(1-G31)))*(1+(H31/(1-H31))))	=N31/I31	
32	1790	=L32*(1+((G32+H32)/(1-(G32+H32))))	=(E3*(G32/(1-G32))*E4*E5+M32*I32)/((1+(G32/(1-G32)))*(1+(H32/(1-H32))))	=N32/I32	
33	1930	=L33*(1+((G33+H33)/(1-(G33+H33))))	=(E3*(G33/(1-G33))*E4*E5+M33*I33)/((1+(G33/(1-G33)))*(1+(H33/(1-H33))))	=N33/I33	
34					

Table II-3. Formulae Used in Calculation Presented in Table II-1

	B	C	D	E	F	G	H	I	J
2									
3		Assumed Saturation =		0.9054					
4		Density of Water =		997	kg/m3 at	300	K		
5		Specifici Heat of Water =		4179	J/kg·K at	300	K		
6									
7		**UZ UNIT**	**Dry Bulk Thermal Conductivity (W/m·K)**	**Wet Bulk Thermal Conductivity (W/m·K)**	**ANSYS Thermal Conductivity (W/m·K)**	**Matrix Porosity**	**Lithophysal Porosity**	**ANSYS Specific Heat (J/kg·K)**	
8		tcw12	1.3	1.81	=D8+((E8-D8)/100)*E3*100	0.119	0	='GFM to UZ Raw Data'!I58*1000	
9		tcw13	0.589	0.928	=D9+((E9-D9)/100)*E3*100	0.2105	0	='GFM to UZ Raw Data'!I59*1000	
10		ptn21	0.49	1.06	=D10+((E10-D10)/100)*E3*100	0.385	0	='GFM to UZ Raw Data'!I60*1000	
11		ptn22	0.49	1.06	=D11+((E11-D11)/100)*E3*100	0.385	0	='GFM to UZ Raw Data'!I61*1000	
12		ptn23	0.49	1.06	=D12+((E12-D12)/100)*E3*100	0.385	0	='GFM to UZ Raw Data'!I62*1000	
13		ptn24	0.49	1.06	=D13+((E13-D13)/100)*E3*100	0.385	0	='GFM to UZ Raw Data'!I63*1000	
14		ptn25	0.49	1.06	=D14+((E14-D14)/100)*E3*100	0.385	0	='GFM to UZ Raw Data'!I64*1000	
15		ptn26	0.49	1.06	=D15+((E15-D15)/100)*E3*100	0.385	0	='GFM to UZ Raw Data'!I65*1000	
16		tsw31	0.994	1.303	=D16+((E16-D16)/100)*E3*100	0.0775	0	='GFM to UZ Raw Data'!I66*1000	
17		tsw32	1.3	1.81	=D17+((E17-D17)/100)*E3*100	0.119	0	='GFM to UZ Raw Data'!I67*1000	
18		tsw33	1.24145	1.79245	=D18+((E18-D18)/100)*E3*100	0.14285	0.0614	='GFM to UZ Raw Data'!I68*1000	
19		tsw34	1.4189	2.0741	=D19+((E19-D19)/100)*E3*100	0.1287	0.0254	='GFM to UZ Raw Data'!I69*1000	
20		tsw35	1.2784	1.8895	=D20+((E20-D20)/100)*E3*100	0.1486	0.0883	='GFM to UZ Raw Data'!I70*1000	
21		tsw36	1.49	2.1303	=D21+((E21-D21)/100)*E3*100	0.1058	0.0302	='GFM to UZ Raw Data'!I71*1000	
22		tsw37	1.49	2.1303	=D22+((E22-D22)/100)*E3*100	0.1058	0.0302	='GFM to UZ Raw Data'!I72*1000	
23		tsw38	0.688	0.796	=D23+((E23-D23)/100)*E3*100	0.036	0	='GFM to UZ Raw Data'!I73*1000	
24		tsw39	0.49	1.06	=D24+((E24-D24)/100)*E3*100	0.385	0	='GFM to UZ Raw Data'!I74*1000	
25		ch1	0.49	1.06	=D25+((E25-D25)/100)*E3*100	0.385	0	='GFM to UZ Raw Data'!I75*1000	
26		ch2	0.595	1.26	=D26+((E26-D26)/100)*E3*100	0.333	0	='GFM to UZ Raw Data'!I76*1000	
27		ch3	0.595	1.26	=D27+((E27-D27)/100)*E3*100	0.333	0	='GFM to UZ Raw Data'!I77*1000	
28		ch4	0.595	1.26	=D28+((E28-D28)/100)*E3*100	0.333	0	='GFM to UZ Raw Data'!I78*1000	
29		ch5	0.595	1.26	=D29+((E29-D29)/100)*E3*100	0.333	0	='GFM to UZ Raw Data'!I79*1000	
30		ch6	0.595	1.26	=D30+((E30-D30)/100)*E3*100	0.333	0	='GFM to UZ Raw Data'!I80*1000	
31		pp4	0.569	1.13	=D31+((E31-D31)/100)*E3*100	0.3	0	='GFM to UZ Raw Data'!I81*1000	
32		pp3	0.569	1.13	=D32+((E32-D32)/100)*E3*100	0.3	0	='GFM to UZ Raw Data'!I82*1000	
33		pp2	0.8145	1.38	=D33+((E33-D33)/100)*E3*100	0.2545	0	='GFM to UZ Raw Data'!I83*1000	
34									

APPENDIX III

DOCUMENTATION OF THE DIMENSIONLESS PULSE RESPONSE CALCULATION

This appendix documents a Mathcad calculation to develop the dimensionless pulse response used in the analytical ventilation calculations.

Develop a calculation of the dimensionless wall-temperature response due to a pulse for a region bounded internally by a cylinder for an arbitrary radius and thermal physical properties. Using Equation 6-62:

$$F(\xi,\tau) := -\left(1 - e^{-\xi^2\cdot\tau}\right)\cdot\frac{\left[\left(J0(\xi)\right)\cdot Y1(\xi) - Y0(\xi)\cdot J1(\xi)\right]}{\xi^2\cdot\left(J1(\xi)^2 + Y1(\xi)^2\right)}$$

where

ξ	=	Integration variable
τ	=	Dimensionless time
J0(ξ)	=	Bessel function of zero order of the first kind
J1(ξ)	=	Bessel function of first order of the first kind
Y0(ξ)	=	Bessel function of zero order of the second

In order to develop a lookup table for a range of dimensionless times, consider a radius of 10 m, a thermal diffusivity of 20 m^2/yr, and a time of 1 year. These properties develop a lower bound for the dimensionless time parameter. Consider then a radius of 2 m, a thermal diffusivity of 30 m^2/yr, and a time of 1,000 years. These properties develop an upper bound for the dimensionless time parameter.

$$\alpha := 20\frac{m^2}{yr}$$

$$a := 10\ m$$

$$t := 1\ yr$$

$$\tau := \frac{\alpha\cdot t}{a^2}$$

$$\tau := 0.2$$

$$\alpha := 30\frac{m^2}{yr}$$

$$a := 2\ m$$

$$t := 1000\ yr$$

$$\tau := \frac{\alpha\cdot t}{a^2}$$

$$\tau := 7.5 \times 10^{3}$$

The dimensionless time ranges from 0.2 to 7500. Use a value of τ as 10, 20, 50, 100, 200, 400, 1000, and 5000, which lie within the previously established bounds of 0.2 to 7500 presented above. Plot the dimensionless function.

$$\xi := 0, 0.1, ..., 100$$

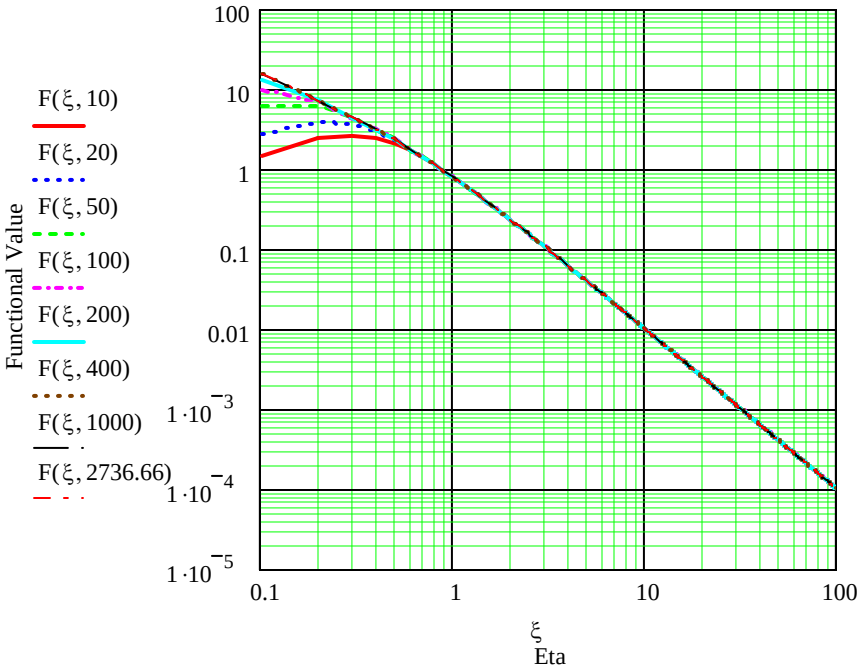

Now consider the close form solution for an internally bounded cylinder (Carslaw and Jaeger, 1959, [DIRS 100968] p. 338):

$$\Theta(\tau) := \frac{2}{\pi} \cdot \int_{0}^{\infty} F(\xi, \tau)\, d\xi$$

$$\tau := 0.01, 0.02, ..., 10.0$$

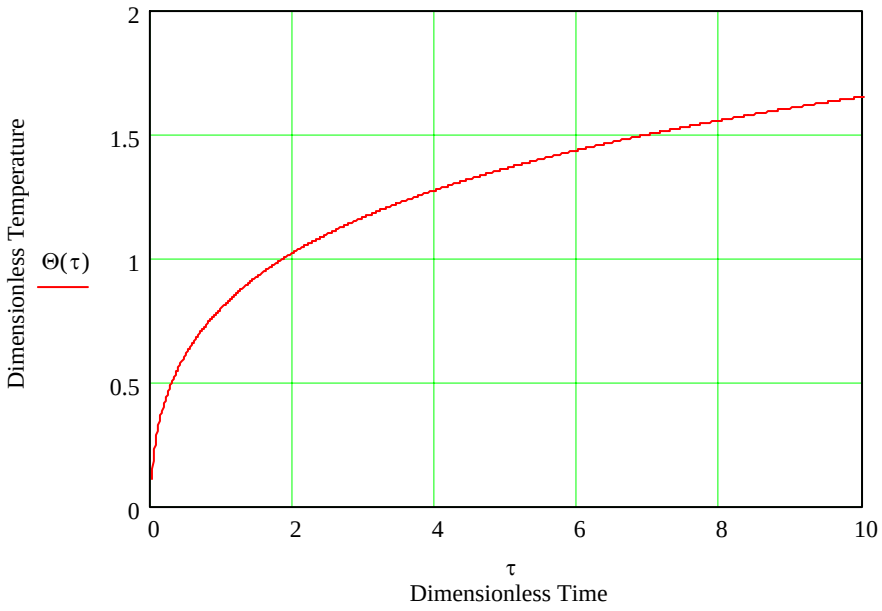

This is the relationship presented by Carslaw and Jaeger (1959 [DIRS 100968], p. 338).

$$\tau := 1, 2, ..., 7500$$

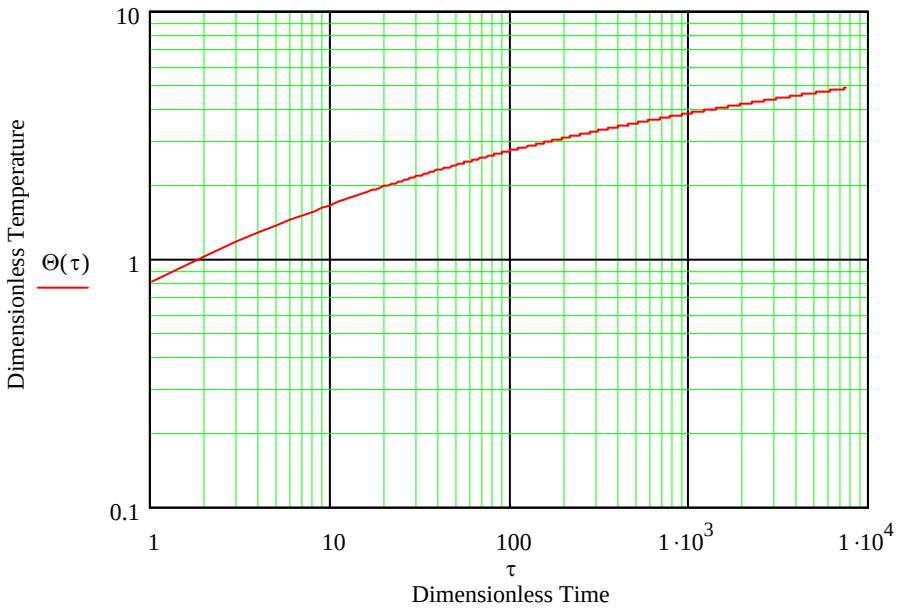

Define an interpolation array and an interpolation function for the "working" equation.

$$i := 1 .. 100$$

$$\tau_i := 0.0 + (i - 1) \cdot 0.1$$

$$Kv_{i,1} := \tau_i$$

$$Kv_{i,2} := \Theta(\tau_i)$$

$$i := 1, 2, ..., 15000$$

$$\tau_i := 10.0 + (i - 1) \cdot 0.5$$

$$Kv1_{i,1} := \tau_i$$

$$Kv1_{i,2} := \Theta(\tau_i)$$

$$A := stack(Kv, Kv1)$$

WRITEPRN ("DIMPULSE2.TXT") := A

A =

	0	1	2
0	0	0	0
1	0	0	0
2	0	0.1	0.314
3	0	0.2	0.424
4	0	0.3	0.502
5	0	0.4	0.565
6	0	0.5	0.617
7	0	0.6	0.662
8	0	0.7	0.702
9	0	0.8	0.739
10	0	0.9	0.772
11	0	1	0.802
12	0	1.1	0.83
13	0	1.2	0.857
14	0	1.3	0.881
15	0	1.4	0.905

Write out a pulse to 10,000 years every year.

$$i := 1, 2, ..., 10000$$

$$\tau_i := i$$

$$Kv2_{i,1} := \tau_i$$

$$Kv2_{i,2} := \Theta(\tau_i)$$

$$B := Kv2$$

WRITEPRN ("DIMPULSE2.TXT") := B

Note that the pulse calculation is developed in the EXCEL spreadsheet Analytical-LA-800m.xls on worksheet Cylinder_Pulse using the methodology presented in Section 6.4.2.4.1.

INTENTIONALLY LEFT BLANK

APPENDIX IV

DOCUMENTATION OF THE ANSYS-LA-COARSE VENTILATION MODEL (INPUTS AND OUTPUTS)

This appendix documents the ANSYS-LA-Coarse ventilation model which was developed using the ANSYS software and spreadsheet methods. The input and output files, and Microsoft Excel spreadsheet are contained in the file ANSYS-LA-Coarse.zip (DTN: MO0306MWDASLCV.001). Table IV-1 is a description of the input and output files, and the worksheets contained in the spreadsheet ANSYS-LA-Coarse.xls. Further documentation of the cell formulas and referencing are found within the electronic copy of the file.

Table IV-1. Contents of ANSYS-LA-Coarse.zip

ANSYS Input and Output Files	
File	**Description**
decay_data.input	ANSYS input file containing the waste package heat decay.
th_data.input	ANSYS input file containing the thermal properties of the repository layers and the EBS components.
la800.dat	ANSYS input file which generates the mesh and assigns thermal properties to each cell within the mesh.
la800.db	ANSYS output file.
la800.grph	ANSYS output file.
la800.sub	ANSYS output file.
la800.out	ANSYS output file.
air_temp_c0 through air_temp_c10	ANSYS input files containing the inlet air temperature of the specified segment (from ANSYS-LA-Coarse.xls).
dr_h_c0 through dr_h_c10	ANSYS input file containing the drift wall convection coefficients for the specified segment (from ANSYS-LA-Coarse.xls).
wp_h_c0 through wp_h_c10	ANSYS input files containing the waste package convection coefficients for the specified segment (from ANSYS-LA-Coarse.xls).
la800c0 through la800c10	Main ANSYS input files.
la800c0.db through la800c10.db	ANSYS output files.
la800c0.grph through la800c10.grph	ANSYS output files.
la800c0.dsub through la800c10.dsub	ANSYS output files.
la800c0.mntr through la800c10.mntr	ANSYS output files.
la800c0.osav through la800c10.osav	ANSYS output files.
la800c0.rth through la800c10.rth	ANSYS output files.
la800c0.stat through la800c10.stat	ANSYS output files.
la800c0.s01 to .s21 through la800c10.s01 to .s21	ANSYS output files.
la800c0.out through la800c10.out	Main ANSYS output files.
result_c0 through result_c10	Temperature results that are cut from the end of the .out files and imported to ANSYS-LA-Coarse.xls.
ANSYS-LA-Coarse.xls	
Worksheet	**Description**
0-800m data	Contains the calculations of the heat removal by convection for each segment given the waste package, drift wall, and air temperatures, and waste package and drift wall convection coefficients. Calculates the exit air temperatures for the inlet conditions of the next segment.

Table IV-1. Contents of ANSYS-LA-Coarse.zip (Continued)

ANSYS Input and Output Files	
Worksheet	**Description**
Transposed 0-800m data	Contains the waste package, drift wall, and air temperature and efficiencies copied from worksheet 0-800m data into a more usable format.
Efficiency data	Contains the integrated ventilation efficiency calculation for 600 m and 800 m.
Efficiency vs. Time	Plots the ventilation efficiency versus time.
Efficiency vs. Length	Plots the ventilation efficiency versus distance from the drift inlet.
WP Temp vs. Length	Plots the waste package temperature versus distance from the drift inlet for each time step.
DW Temp vs. Length	Plots the drift wall temperature versus distance from the drift inlet for each time step.
Inlet Air Temp vs. Length	Plots the air temperature versus distance from the drift inlet for each time step.
0m through 800m	Plots the waste package, drift wall, and air temperatures versus time.
c0-t0-19 through c10-t0-19	Contains the temperature results from the result_c0 through result_c10 ANSYS output files. Performs a circumferential weighted average given the temperatures of each element of the drift wall and waste package.
c0-h through c10-h	Contains the calculation of convection heat transfer coefficients using the Mixed Convection Correlation (Appendix IX).
Matl prop and constants	Contains the inputs needed to calculate mixed convection heat transfer coefficients. These inputs are obtained from Table 4-17 and Table 4-19.

APPENDIX V

DOCUMENTATION OF THE ANSYS-LA-FINE VENTILATION MODEL (INPUTS AND OUTPUTS)

This appendix documents the ANSYS-LA-Fine ventilation model which was developed using the ANSYS software and spreadsheet methods. The input and output files, and Microsoft Excel spreadsheet, are contained in the file ANSYS-LA-Fine.zip (DTN: MO0306MWDALAFV.000). Table V-1 is a description of the input and output files, and the worksheets contained in the spreadsheet ANSYS-LA-Fine.xls. Further documentation of the cell formulas and referencing are found within the electronic copy of the file.

Table V-1. Contents of ANSYS-LA-Fine.zip

ANSYS Input and Output Files	
File	**Description**
decay_data.input	ANSYS input file containing the waste package heat decay.
th_data.input	ANSYS input file containing the thermal properties of the repository layers and the EBS components.
la600.dat	ANSYS input file which generates the mesh and assigns thermal properties to each cell within the mesh.
la600.db	ANSYS output file.
la600.grph	ANSYS output file.
la600.sub	ANSYS output file.
la600.out	ANSYS output file.
air_temp_c0 through air_temp_c24	ANSYS input files containing the inlet air temperature of the specified segment (from ANSYS-LA-Coarse.xls).
dr_h_c0 through dr_h_c24	ANSYS input file containing the drift wall convection coefficients for the specified segment (from ANSYS-LA-Coarse.xls).
wp_h_c0 through wp_h_c24	ANSYS input files containing the waste package convection coefficients for the specified segment (from ANSYS-LA-Coarse.xls).
la600c0 through la600c24	Main ANSYS input files.
la600c0.db through la600c24.db	ANSYS output files.
la600c0.grph through la600c24.grph	ANSYS output files.
la600c0.dsub through la600c24.dsub	ANSYS output files.
la600c0.mntr through la600c24.mntr	ANSYS output files.
la600c0.osav through la600c24.osav	ANSYS output files.
la600c0.rth through la600c24.rth	ANSYS output files.
la600c0.stat through la600c24.stat	ANSYS output files.
la600c0.s01 to .s21 through la600c24.s01 to .s21	ANSYS output files.
la600c0.out through la600c24.out	Main ANSYS output files.
result_c0 through result_c24	Temperature results that are cut from the end of the .out files and imported to ANSYS-LA-Coarse.xls.
ANSYS-LA-Coarse.xls	
Worksheet	**Description**
0-600m data	Contains the calculations of the heat removal by convection for each segment given the waste package, drift wall, and air temperatures, and waste package and drift wall convection coefficients. Calculates the exit air temperatures for the inlet conditions of the next segment.

Table V-1. Contents of ANSYS-LA-Fine.zip (Continued)

ANSYS Input and Output Files	
Worksheet	**Description**
Transposed 0-600m data	Contains the waste package, drift wall, and air temperature and efficiencies copied from worksheet 0-800m data into a more usable format.
Efficiency data	Contains the integrated ventilation efficiency calculation.
Efficiency vs. Time	Plots the ventilation efficiency versus time.
Efficiency vs. Length	Plots the ventilation efficiency versus distance from the drift inlet.
WP Temp vs. Length	Plots the waste package temperature versus distance from the drift inlet for each time step.
DW Temp vs. Length	Plots the drift wall temperature versus distance from the drift inlet for each time step.
Inlet Air Temp vs. Length	Plots the air temperature versus distance from the drift inlet for each time step.
0m through 600m	Plots the waste package, drift wall, and air temperatures versus time.
c0-t0-19 through c24-t0-19	Contains the temperature results from the result_c0 through result_c24 ANSYS output files. Performs a circumferential weighted average given the temperatures of each element of the drift wall and waste package.
c0-h through c24-h	Contains the calculation of convection heat transfer coefficients using the Mixed Convection Correlation (Appendix IX).
Matl prop and constants	Contains the inputs needed to calculate mixed convection heat transfer coefficients. These inputs are obtained from Table 4-17 and Table 4-19.

APPENDIX VI

DOCUMENTATION OF THE ANALYTICAL-LA-COARSE VENTILATION MODEL (SPREADSHEET METHODS)

This appendix documents the Analytical-LA-Coarse ventilation model, which was developed using spreadsheet methods. The Microsoft Excel spreadsheet model is contained in the file Analytical-LA-Coarse-800m.xls (DTN: MO0307MWDAC8MV.000). Table VI-1 is a description of each worksheet contained in the spreadsheet Analytical-LA-Coarse.xls. Further documentation of the cell formulas and referencing are found within the electronic copy of the file.

Table VI-1. Contents of Analytical-LA-Coarse-800m.xls

Worksheet	Description
Input	Contains the inputs needed for other worksheets to calculate the ventilation efficiency and the preclosure temperatures of the waste package, drift wall, and in-drift air. These inputs are obtained from Section 4 and 6.5 of this report. More specific references to subsections of Section 4 and 6.5 are documented in Column G. The input values listed in Column E are cell referenced throughout the spreadsheet. No calculations are made in this worksheet.
WP Decay	Contains the power source (waste package) decay history for the preclosure period obtained from Table 4-13. This information is used if the Waste Emplacement Power History Flag ('Input!E25') is set to 2.
3 Component Exponential WP Decay	Fits the waste package power decay to a 3 component exponential equation by defining pre-exponential power constants and exponential decay constants.
Mixed Convection Inputs	Contains the inputs needed to calculate mixed convection heat transfer coefficients. These inputs are obtained from Table 4-17 and Table 4-19.
Thermal Model	Contains the calculation of the bulk thermal conductivity (which takes into account solids, and air- and water-filled voids), which is linear function of the water saturation of the rock. Also contains the a calculation of volumetric heat capacity and associated effective bulk density.
Dimensionless Pulse Calculation	Contains the output of the MathCad file, Dimensionless Pulse Response.mcd. The MathCad file generates a text file, DIMPULSE2.txt, which is copied into this worksheet.
Cylinder Pulse	Contains the calculation of the drift wall temperature response due to a dimensionless pulse (worksheet Dimensionless Pulse Response) for a region bounded internally by a cylinder. This worksheet uses the drift dimensions and the thermal physical properties listed in worksheet Input. The mathematical equations for this calculation are also documented in Section 6.4.2.4.1.
Slab Pulse	Contains the calculation of the drift wall temperature response due to a dimensionless pulse (worksheet Dimensionless Pulse Response) applied at the surface of a semi-infinite homogeneous slab. The mathematical equations for this calculation are also documented in Section 6.4.2.4.2.
Composite Pulse	Builds the drift wall temperature response which is a composite of the Cylinder Pulse and the Slab Pulse worksheets.
CSTR Analysis	Contains preparatory or initial calculations used in the CSTR01 through CSTR08 worksheets. These calculations use the inputs listed on worksheet Input to calculate Equations 6-18, 6-45, 6-32, 6-31, 6-38, 6-29, 6-30, and 6-56. This worksheet also contains a summary of the convection heat transfer coefficients used in the CSTR01 through CSTR08 worksheets. A user-defined heat transfer coefficient, or the mixed convection correlation, (described in Appendix VIII) may be used here, depending on the value of a flag set on worksheet Input.

Table VI-1. Contents of Analytical-LA-Coarse-800m.xls (Continued)

Worksheet	Description
CSTR01	Contains the heat transfer analysis for the first 100-m section. These calculations use the results of the CSTR Analysis worksheet and iterative calculations of Equations 6-18, 6-45, 6-32, 6-31, 6-38, 6-29, 6-30, 6-56, and 6-39. The methodology is described in Section 6.4.2. The output of this worksheet includes waste package, drift wall, and drift air temperatures, an energy balance, and initial conditions for CSTR02.
CSTR01-h	Contains the calculation of convection heat transfer coefficients using the Mixed Convection Correlation (Appendix VIII) for CSTR01.
CSTR02	Contains the heat transfer analysis for the second 100-m section (200-m). These calculations use the results of the CSTR01 worksheet and iterative calculations of Equations 6-18, 6-45, 6-32, 6-31, 6-38, 6-29, 6-30, 6-56, and 6-39. The methodology is described in Section 6.4.2. The output of this worksheet includes waste package, drift wall, and drift air temperatures, an energy balance, and initial conditions for CSTR03.
CSTR02-h	Contains the calculation of convection heat transfer coefficients using the Mixed Convection Correlation (Appendix VIII) for CSTR02.
CSTR03	Contains the heat transfer analysis for the third 100-m section (300-m). These calculations use the results of the CSTR02 worksheet and iterative calculations of Equations 6-18, 6-45, 6-32, 6-31, 6-38, 6-29, 6-30, 6-56, and 6-39. The methodology is described in Section 6.4.2. The output of this worksheet includes waste package, drift wall, and drift air temperatures, an energy balance, and initial conditions for CSTR04.
CSTR03-h	Contains the calculation of convection heat transfer coefficients using the Mixed Convection Correlation (Appendix VIII) for CSTR03.
CSTR04	Contains the heat transfer analysis for the fourth 100-m section (400-m). These calculations use the results of the CSTR03 worksheet and iterative calculations of Equations 6-18, 6-45, 6-32, 6-31, 6-38, 6-29, 6-30, 6-56, and 6-39. The methodology is described in Section 6.4.2. The output of this worksheet includes waste package, drift wall, and drift air temperatures, an energy balance, and initial conditions for CSTR05.
CSTR04-h	Contains the calculation of convection heat transfer coefficients using the Mixed Convection Correlation (Appendix VIII) for CSTR04.
CSTR05	Contains the heat transfer analysis for the fifth 100-m section (500-m). These calculations use the results of the CSTR04 worksheet and iterative calculations of Equations 6-18, 6-45, 6-32, 6-31, 6-38, 6-29, 6-30, 6-56, and6-39. The methodology is described in Section 6.4.2. The output of this worksheet includes waste package, drift wall, and drift air temperatures, an energy balance, and initial conditions for CSTR06.
CSTR05-h	Contains the calculation of convection heat transfer coefficients using the Mixed Convection Correlation (Appendix VIII) for CSTR05.
CSTR06	Contains the heat transfer analysis for the sixth 100-m section (600-m). These calculations use the results of the CSTR05 worksheet and iterative calculations of Equations 6-18, 6-45, 6-32, 6-31, 6-38, 6-29, 6-30, 6-56, and 6-39. The methodology is described in Section 6.4.2. The output of this worksheet includes waste package, drift wall, and drift air temperatures, and an energy balance, and initial conditions for CSTR07.
CSTR06-h	Contains the calculation of convection heat transfer coefficients using the Mixed Convection Correlation (Appendix VIII) for CSTR06.
CSTR07	Contains the heat transfer analysis for the seventh 100-m section (500-m). These calculations use the results of the CSTR06 worksheet and iterative calculations of Equations 6-18, 6-45, 6-32, 6-31, 6-38, 6-29, 6-30, 6-56, and 6-39. The methodology is described in Section 6.4.2. The output of this worksheet includes waste package, drift wall, and drift air temperatures, an energy balance, and initial conditions for CSTR08.

Table VI-1. Contents of Analytical-LA-Coarse-800m.xls (Continued)

Worksheet	Description
CSTR07-h	Contains the calculation of convection heat transfer coefficients using the Mixed Convection Correlation (Appendix VIII) for CSTR07.
CSTR08	Contains the heat transfer analysis for the eighth 100-m section (600-m). These calculations use the results of the CSTR07 worksheet and iterative calculations of Equations 6-18, 6-45, 6-32, 6-31, 6-38, 6-29, 6-30, 6-56, and 6-39. The methodology is described in Section 6.4.2. The output of this worksheet includes waste package, drift wall, and drift air temperatures, and an energy balance.
CSTR08-h	Contains the calculation of convection heat transfer coefficients using the Mixed Convection Correlation (Appendix VIII) for CSTR06.
CSTR01 Plot	Plots the waste package, drift wall, and drift air temperature results versus time for CSTR01.
CSTR02 Plot	Plots the waste package, drift wall, and drift air temperature results versus time for CSTR02.
CSTR03 Plot	Plots the waste package, drift wall, and drift air temperature results versus time for CSTR03.
CSTR04 Plot	Plots the waste package, drift wall, and drift air temperature results versus time for CSTR04.
CSTR05 Plot	Plots the waste package, drift wall, and drift air temperature results versus time for CSTR05.
CSTR06 Plot	Plots the waste package, drift wall, and drift air temperature results versus time for CSTR06.
CSTR07 Plot	Plots the waste package, drift wall, and drift air temperature results versus time for CSTR07.
CSTR08 Plot	Plots the waste package, drift wall, and drift air temperature results versus time for CSTR08.
Ventilation Efficiency	Contains the calculations of both integrated and instantaneous ventilation efficiency described by Equations 6-6 and 6-5.

INTENTIONALLY LEFT BLANK

APPENDIX VII

DOCUMENTATION OF DELTA METHOD USING THE ANALYTICAL VENTILATION MODEL (SPREADSHEET METHODS)

This appendix documents the use of the Delta Method (Section 6-11) to quantify the sensitivity of the integrated ventilation efficiency to uncertainties in key input parameters. The Delta Method uses the analytical or spreadsheet approach to ventilation. The electronic copy of this Microsoft Excel spreadsheet is contained in the file Rev4-Analytical-LA-Coarse-Delta-Method.xls (DTN: MO0406MWDLACVD.001) and Rev4-Analytical-LA-Coarse-Delta-Method-800m.xls (DTN: MO0406MWDAC8VD.001). Table VII-1 and Table VII-2 are descriptions of each worksheet contained in the spreadsheets. Further documentation of the cell formulas and referencing are found within the electronic copy of the file.

Table VII-1. Rev4-Contents of Analytical-LA-Coarse-Delta-Method.xls

Worksheet	Description
Input	Contains the inputs needed for other worksheets to calculate the ventilation efficiency and the preclosure temperatures of the waste package, drift wall, and in-drift air. These inputs are obtained from Sections 4 and 6.5 of this report. More specific references to subsections of Sections 4 and 6.5 are documented in Column G. The input values listed in Column E are cell referenced throughout the spreadsheet. This worksheet also contains the key input parameters and their respective standard deviations used for the Delta Method (Table 6-9). No calculations are made in this worksheet.
Delta Method	Contains the calculation to determine the mean system performance (i.e., mean integrated ventilation efficiency) and its standard deviation based on the means and standard deviations of the component variables (key input parameters). This worksheet manually implements Equations 6-89 and 6-90 described in Section 6.11.
Plot Delta Method	Qualitatively plots the results of the Delta Method to show the influence of the key input parameters on the mean and standard deviation of the integrated ventilation efficiency.
WP Decay	Contains the power source (waste package) decay history for the preclosure period obtained from Table 4-13. This information is used if the Waste Emplacement Power History Flag ('Input!E25') is set to 2.
3 Component Exponential WP Decay	Fits the waste package power decay to a 3 component exponential equation by defining pre-exponential power constants and exponential decay constants.
Mixed Convection Inputs	Contains the inputs needed to calculate mixed convection heat transfer coefficients. These inputs are obtained from Tables 4-17 and 4-19.
Thermal Model	Contains the calculation of the bulk thermal conductivity (which takes into account solids, and air and water filled voids), which is linear function of the water saturation of the rock. Also contains the a calculation of volumetric heat capacity and associated effective bulk density.
Dimensionless Pulse Calculation	Contains the output of the MathCad file, Dimensionless Pulse Response.mcd. The MathCad file generates a text file, DIMPULSE2.txt, which is copied into this worksheet.
Cylinder Pulse	Contains the calculation of the drift wall temperature response due to a dimensionless pulse (worksheet Dimensionless Pulse Response) for a region bounded internally by a cylinder. This worksheet uses the drift dimensions and the thermal physical properties listed in worksheet Input. The mathematical equations for this calculation are also documented in Section 6.4.2.4.1.
Slab Pulse	Contains the calculation of the drift wall temperature response due to a dimensionless pulse (worksheet Dimensionless Pulse Response) applied at the surface of a semi-infinite homogeneous slab. The mathematical equations for this calculation are also documented in Section 6.4.2.4.2.

Table VII-1. Contents of Rev4-Analytical-LA-Coarse-Delta-Method.xls (Continued)

Worksheet	Description
Composite Pulse	Builds the drift wall temperature response which is a composite of the Cylinder Pulse and the Slab Pulse worksheets.
CSTR Analysis	Contains preparatory or initial calculations used in the CSTR01 through CSTR06 worksheets. These calculations use the inputs listed on worksheet Input to calculate Equations 6-18, 6-45, 6-32, 6-31, 6-38, 6-29, 6-30, and 6-56. This worksheet also contains a summary of the convection heat transfer coefficients used in the CSTR01 through CSTR06 worksheets. A user-defined heat transfer coefficient, or the mixed convection correlation, (described in Appendix VIII) may be used here, depending on the value of a flag set on worksheet Input.
CSTR01	Contains the heat transfer analysis for the first 100-m section. These calculations use the results of the CSTR Analysis worksheet and iterative calculations of Equations 6-18, 6-45, 6-32, 6-31, 6-38, 6-29, 6-30, 6-56, and 6-39. The methodology is described in Section 6.4.2. The output of this worksheet includes waste package, drift wall, and drift air temperatures, an energy balance, and initial conditions for CSTR02.
CSTR01-h	Contains the calculation of convection heat transfer coefficients using the Mixed Convection Correlation (Appendix VIII) for CSTR01.
CSTR02	Contains the heat transfer analysis for the second 100-m section (200-m). These calculations use the results of the CSTR01 worksheet and iterative calculations of Equations 6-18, 6-45, 6-32, 6-31, 6-38, 6-29, 6-30, 6-56, and 6-39. The methodology is described in Section 6.4.2. The output of this worksheet includes waste package, drift wall, and drift air temperatures, an energy balance, and initial conditions for CSTR03.
CSTR02-h	Contains the calculation of convection heat transfer coefficients using the Mixed Convection Correlation (Appendix VIII) for CSTR02.
CSTR03	Contains the heat transfer analysis for the third 100-m section (300-m). These calculations use the results of the CSTR02 worksheet and iterative calculations of Equations 6-18, 6-45, 6-32, 6-31, 6-38, 6-29, 6-30, 6-56, and 6-39. The methodology is described in Section 6.4.2. The output of this worksheet includes waste package, drift wall, and drift air temperatures, an energy balance, and initial conditions for CSTR04.
CSTR03-h	Contains the calculation of convection heat transfer coefficients using the Mixed Convection Correlation (Appendix VIII) for CSTR03.
CSTR04	Contains the heat transfer analysis for the fourth 100-m section (400-m). These calculations use the results of the CSTR03 worksheet and iterative calculations of Equations 6-18, 6-45, 6-32, 6-31, 6-38, 6-29, 6-30, 6-56, and 6-39. The methodology is described in Section 6.4.2. The output of this worksheet includes waste package, drift wall, and drift air temperatures, an energy balance, and initial conditions for CSTR05.
CSTR04-h	Contains the calculation of convection heat transfer coefficients using the Mixed Convection Correlation (Appendix VIII) for CSTR04.
CSTR05	Contains the heat transfer analysis for the fifth 100-m section (500-m). These calculations use the results of the CSTR04 worksheet and iterative calculations of Equations 6-18, 6-45, 6-32, 6-31, 6-38, 6-29, 6-30, 6-56, and 6-39. The methodology is described in Section 6.4.2. The output of this worksheet includes waste package, drift wall, and drift air temperatures, an energy balance, and initial conditions for CSTR06.
CSTR05-h	Contains the calculation of convection heat transfer coefficients using the Mixed Convection Correlation (Appendix VIII) for CSTR05.

Table VII-1. Rev4-Contents of Analytical-LA-Coarse-Delta-Method.xls (Continued)

Worksheet	Description
CSTR06	Contains the heat transfer analysis for the sixth 100-m section (600-m). These calculations use the results of the CSTR05 worksheet and iterative calculations of Equations 6-18, 6-45, 6-32, 6-31, 6-38, 6-29, 6-30, 6-56, and 6-39. The methodology is described in Section 6.4.2. The output of this worksheet includes waste package, drift wall, and drift air temperatures, and an energy balance.
CSTR06-h	Contains the calculation of convection heat transfer coefficients using the Mixed Convection Correlation (Appendix VIII) for CSTR06.
CSTR01 Plot	Plots the waste package, drift wall, and drift air temperature results versus time for CSTR01.
CSTR02 Plot	Plots the waste package, drift wall, and drift air temperature results versus time for CSTR02.
CSTR03 Plot	Plots the waste package, drift wall, and drift air temperature results versus time for CSTR03.
CSTR04 Plot	Plots the waste package, drift wall, and drift air temperature results versus time for CSTR04.
CSTR05 Plot	Plots the waste package, drift wall, and drift air temperature results versus time for CSTR05.
CSTR06 Plot	Plots the waste package, drift wall, and drift air temperature results versus time for CSTR06.
Ventilation Efficiency	Contains the calculations of both integrated and instantaneous ventilation efficiency described by Eq. 6-6 and Eq. 6-5.

Table VII-2. Contents of Rev4-Analytical-LA-Coarse-Delta-Method-800m.xls

Worksheet	Description
Input	Contains the inputs needed for other worksheets to calculate the ventilation efficiency and the preclosure temperatures of the waste package, drift wall, and in-drift air. These inputs are obtained from Sections 4 and 6.5 of this report. More specific references to subsections of Sections 4 and 6.5 are documented in Column G. The input values listed in Column E are cell referenced throughout the spreadsheet. This worksheet also contains the key input parameters and their respective standard deviations used for the Delta Method (Table 6-9). No calculations are made in this worksheet.
Delta Method	Contains the calculation to determine the mean system performance (i.e., mean integrated ventilation efficiency) and its standard deviation based on the means and standard deviations of the component variables (key input parameters). This worksheet manually implements Equatons 6-89 and 6-90 described in Section 6-11.
Plot Delta Method	Qualitatively plots the results of the Delta Method to show the influence of the key input parameters on the mean and standard deviation of the integrated ventilation efficiency.
WP Decay	Contains the power source (waste package) decay history for the preclosure period obtained from Table 4-13. This information is used if the Waste Emplacement Power History Flag ('Input!E25') is set to 2.
3 Component Exponential WP Decay	Fits the waste package power decay to a 3 component exponential equation by defining pre-exponential power constants and exponential decay constants.
Mixed Convection Inputs	Contains the inputs needed to calculate mixed convection heat transfer coefficients. These inputs are obtained from Tables 4-17 and 4-19.
Thermal Model	Contains the calculation of the bulk thermal conductivity (which takes into account solids, and air and water filled voids), which is linear function of the water saturation of the rock. Also contains a calculation of volumetric heat capacity and associated effective bulk density.

Table VII-2. Contents of Rev4-Analytical-LA-Coarse-Delta-Method-800m.xls (Continued)

Worksheet	Description
Dimensionless Pulse Calculation	Contains the output of the MathCad file, Dimensionless Pulse Response.mcd. The MathCad file generates a text file, DIMPULSE2.txt, which is copied into this worksheet.
Cylinder Pulse	Contains the calculation of the drift wall temperature response due to a dimensionless pulse (worksheet Dimensionless Pulse Response) for a region bounded internally by a cylinder. This worksheet uses the drift dimensions and the thermal physical properties listed in worksheet Input. The mathematical equations for this calculation are also documented in Section 6.4.2.4.1.
Slab Pulse	Contains the calculation of the drift wall temperature response due to a dimensionless pulse (worksheet Dimensionless Pulse Response) applied at the surface of a semi-infinite homogeneous slab. The mathematical equations for this calculation are also documented in Section 6.4.2.4.2.
Composite Pulse	Builds the drift wall temperature response, which is a composite of the Cylinder Pulse and the Slab Pulse worksheets.
CSTR Analysis	Contains preparatory or initial calculations used in the CSTR01 through CSTR06 worksheets. These calculations use the inputs listed on worksheet Input to calculate Equations 6-18, 6-45, 6-32, 6-31, 6-38, 6-29, 6-30, and 6-56. This worksheet also contains a summary of the convection heat transfer coefficients used in the CSTR01 through CSTR06 worksheets. A user-defined heat transfer coefficient, or the mixed convection correlation, (described in Appendix VIII) may be used here, depending on the value of a flag set on worksheet Input.
CSTR01	Contains the heat transfer analysis for the first 100-m section. These calculations use the results of the CSTR Analysis worksheet and iterative calculations of Equations 6-18, 6-45, 6-32, 6-31, 6-38, 6-29, 6-30, 6-56, and 6-39. The methodology is described in Section 6.4.2. The output of this worksheet includes waste package, drift wall, and drift air temperatures, an energy balance, and initial conditions for CSTR02.
CSTR01-h	Contains the calculation of convection heat transfer coefficients using the Mixed Convection Correlation (Appendix VIII) for CSTR01.
CSTR02	Contains the heat transfer analysis for the second 100-m section (200-m). These calculations use the results of the CSTR01 worksheet and iterative calculations of Equations 6-18, 6-45, 6-32, 6-31, 6-38, 6-29, 6-30, 6-56, and 6-39. The methodology is described in Section 6.4.2. The output of this worksheet includes waste package, drift wall, and drift air temperatures, an energy balance, and initial conditions for CSTR03.
CSTR02-h	Contains the calculation of convection heat transfer coefficients using the Mixed Convection Correlation (Appendix VIII) for CSTR02.
CSTR03	Contains the heat transfer analysis for the third 100-m section (300-m). These calculations use the results of the CSTR02 worksheet and iterative calculations of Equations 6-18, 6-45, 6-32, 6-31, 6-38, 6-29, 6-30, 6-56, and 6-39. The methodology is described in Section 6.4.2. The output of this worksheet includes waste package, drift wall, and drift air temperatures, an energy balance, and initial conditions for CSTR04.
CSTR03-h	Contains the calculation of convection heat transfer coefficients using the Mixed Convection Correlation (Appendix VIII) for CSTR03.
CSTR04	Contains the heat transfer analysis for the fourth 100-m section (400-m). These calculations use the results of the CSTR03 worksheet and iterative calculations of Equations 6-18, 6-45, 6-32, 6-31, 6-38, 6-29, 6-30, 6-56, and 6-39. The methodology is described in Section 6.4.2. The output of this worksheet includes waste package, drift wall, and drift air temperatures, an energy balance, and initial conditions for CSTR05.
CSTR04-h	Contains the calculation of convection heat transfer coefficients using the Mixed Convection Correlation (Appendix VIII) for CSTR04.

Table VII-2. Contents of Rev4-Analytical-LA-Coarse-Delta-Method-800m.xls (Continued)

Worksheet	Description
CSTR05	Contains the heat transfer analysis for the fifth 100-m section (500-m). These calculations use the results of the CSTR04 worksheet and iterative calculations of Equations 6-18, 6-45, 6-32, 6-31, 6-38, 6-29, 6-30, 6-56, and 6-39. The methodology is described in Section 6.4.2. The output of this worksheet includes waste package, drift wall, and drift air temperatures, an energy balance, and initial conditions for CSTR06.
CSTR05-h	Contains the calculation of convection heat transfer coefficients using the Mixed Convection Correlation (Appendix VIII) for CSTR05.
CSTR06	Contains the heat transfer analysis for the sixth 100-m section (600-m). These calculations use the results of the CSTR05 worksheet and iterative calculations of Equations 6-18, 6-45, 6-32, 6-31, 6-38, 6-29, 6-30, 6-56, and 6-39. The methodology is described in Section 6.4.2. The output of this worksheet includes waste package, drift wall, and drift air temperatures, and an energy balance, and initial conditions for CSTR07.
CSTR06-h	Contains the calculation of convection heat transfer coefficients using the Mixed Convection Correlation (Appendix VIII) for CSTR06.
CSTR07	Contains the heat transfer analysis for the seventh 100-m section (500-m). These calculations use the results of the CSTR06 worksheet and iterative calculations of Equations 6-18, 6-45, 6-32, 6-31, 6-38, 6-29, 6-30, 6-56, and 6-39. The methodology is described in Section 6.4.2. The output of this worksheet includes waste package, drift wall, and drift air temperatures, an energy balance, and initial conditions for CSTR08.
CSTR07-h	Contains the calculation of convection heat transfer coefficients using the Mixed Convection Correlation (Appendix VIII) for CSTR07.
CSTR08	Contains the heat transfer analysis for the eighth 100-m section (600-m). These calculations use the results of the CSTR07 worksheet and iterative calculations of Equations 6-18, 6-45, 6-32, 6-31, 6-38, 6-29, 6-30, 6-56, and 6-39. The methodology is described in Section 6.4.2. The output of this worksheet includes waste package, drift wall, and drift air temperatures, and an energy balance.
CSTR08-h	Contains the calculation of convection heat transfer coefficients using the Mixed Convection Correlation (Appendix VIII) for CSTR06.
CSTR01 Plot	Plots the waste package, drift wall, and drift air temperature results versus time for CSTR01.
CSTR02 Plot	Plots the waste package, drift wall, and drift air temperature results versus time for CSTR02.
CSTR03 Plot	Plots the waste package, drift wall, and drift air temperature results versus time for CSTR03.
CSTR04 Plot	Plots the waste package, drift wall, and drift air temperature results versus time for CSTR04.
CSTR05 Plot	Plots the waste package, drift wall, and drift air temperature results versus time for CSTR05.
CSTR06 Plot	Plots the waste package, drift wall, and drift air temperature results versus time for CSTR06.
CSTR07 Plot	Plots the waste package, drift wall, and drift air temperature results versus time for CSTR07.
CSTR08 Plot	Plots the waste package, drift wall, and drift air temperature results versus time for CSTR08.
Ventilation Efficiency	Contains the calculations of both integrated and instantaneous ventilation efficiency described by Equations 6-6 and 6-5.

INTENTIONALLY LEFT BLANK

APPENDIX VIII

DOCUMENTATION OF THE EFFECT OF WATER SATURATION ON THE INTEGRATED VENTILATION EFFICIENCY USING THE ANALYTICAL VENTILATION MODEL (SPREADSHEET METHODS)

This appendix documents the use of the effect of water saturation on the integrated ventilation efficiency (Section 6.9.2). The electronic copy of this Microsoft Excel spreadsheet is contained in the file Analytical-LA-Coarse-Wet-vs-Dry-kth.xls (DTN: MO0306MWDRTCCV.000). Table VIII-1 is a description of each worksheet contained in the spreadsheet Analytical-LA-Coarse-Delta-Method.xls. Further documentation of the cell formulas and referencing are found within the electronic copy of the file.

Table VIII-1. Contents of Analytical-LA-Coarse-Wet-vs-Dry-kth.xls

Worksheet	Description
Input	Contains the inputs needed for other worksheets to calculate the ventilation efficiency and the preclosure temperatures of the waste package, drift wall, and in-drift air. These inputs are obtained from Sections 4 and 6.5 of this report. More specific references to subsections of Sections 4 and 6.5 are documented in Column G. The input values listed in Column E are cell referenced throughout the spreadsheet. This worksheet also contains the key input parameters and their respective standard deviations used for the Delta Method (Table 6-9). No calculations are made in this worksheet.
Wet vs. Dry	Contains the results of varying the water saturation on the integrated ventilation efficiency and waste package, drift wall, and drift air temperatures. This calculation is made by changing the water saturation input on worksheet Input and manually pasting the results into the Wet vs. Dry worksheet.
WP Decay	Contains the power source (waste package) decay history for the preclosure period obtained from Table 4-13. This information is used if the Waste Emplacement Power History Flag ('Input!E25') is set to 2.
3 Component Exponential WP Decay	Fits the waste package power decay to a 3 component exponential equation by defining pre-exponential power constants and exponential decay constants.
Mixed Convection Inputs	Contains the inputs needed to calculate mixed convection heat transfer coefficients. These inputs are obtained from Tables 4-17 and 4-19.
Thermal Model	Contains the calculation of the bulk thermal conductivity (which takes into account solids, and air and water filled voids), which is linear function of the water saturation of the rock. Also contains the a calculation of volumetric heat capacity and associated effective bulk density.
Dimensionless Pulse Calculation	Contains the output of the MathCad file, Dimensionless Pulse Response.mcd. The MathCad file generates a text file, DIMPULSE2.txt, which is copied into this worksheet.
Cylinder Pulse	Contains the calculation of the drift wall temperature response due to a dimensionless pulse (worksheet Dimensionless Pulse Response) for a region bounded internally by a cylinder. This worksheet uses the drift dimensions and the thermal physical properties listed in worksheet Input. The mathematical equations for this calculation are also documented in Section 6.4.2.4.1.
Slab Pulse	Contains the calculation of the drift wall temperature response due to a dimensionless pulse (worksheet Dimensionless Pulse Response) applied at the surface of a semi-infinite homogeneous slab. The mathematical equations for this calculation are also documented in Section 6.4.2.4.2.
Composite Pulse	Builds the drift wall temperature response which is a composite of the Cylinder Pulse and the Slab Pulse worksheets.

Table VIII-1. Contents of Analytical-LA-Coarse-Wet-vs-Dry-kth.xls (Continued)

Worksheet	Description
CSTR Analysis	Contains preparatory or initial calculations used in the CSTR01 through CSTR06 worksheets. These calculations use the inputs listed on worksheet Input to calculate Equations 6-18, 6-45, 6-32, 6-31, 6-38, 6-29, 6-30, and 6-56. This worksheet also contains a summary of the convection heat transfer coefficients used in the CSTR01 through CSTR06 worksheets. A user-defined heat transfer coefficient, or the mixed convection correlation, (described in Appendix VIII) may be used here, depending on the value of a flag set on worksheet Input.
CSTR01	Contains the heat transfer analysis for the first 100-m section. These calculations use the results of the CSTR Analysis worksheet and iterative calculations of Equations 6-18, 6-45, 6-32, 6-31, 6-38, 6-29, 6-30, 6-56, and E6-39. The methodology is described in Section 6.4.2. The output of this worksheet includes waste package, drift wall, and drift air temperatures, an energy balance, and initial conditions for CSTR02.
CSTR01-h	Contains the calculation of convection heat transfer coefficients using the Mixed Convection Correlation (Appendix VIII) for CSTR01.
CSTR02	Contains the heat transfer analysis for the second 100-m section (200-m). These calculations use the results of the CSTR01 worksheet and iterative calculations of Equations 6-18, 6-45, 6-32, 6-31, 6-38, 6-29, 6-30, 6-56, and 6-39. The methodology is described in Section 6.4.2. The output of this worksheet includes waste package, drift wall, and drift air temperatures, an energy balance, and initial conditions for CSTR03.
CSTR02-h	Contains the calculation of convection heat transfer coefficients using the Mixed Convection Correlation (Appendix VIII) for CSTR02.
CSTR03	Contains the heat transfer analysis for the third 100-m section (300-m). These calculations use the results of the CSTR02 worksheet and iterative calculations of Equations 6-18, 6-45, 6-32, 6-31, 6-38, 6-29, 6-30, 6-56, and 6-39. The methodology is described in Section 6.4.2. The output of this worksheet includes waste package, drift wall, and drift air temperatures, an energy balance, and initial conditions for CSTR04.
CSTR03-h	Contains the calculation of convection heat transfer coefficients using the Mixed Convection Correlation (Appendix VIII) for CSTR03.
CSTR04	Contains the heat transfer analysis for the fourth 100-m section (400-m). These calculations use the results of the CSTR03 worksheet and iterative calculations of Equations 6-18, 6-45, 6-32, 6-31, 6-38, 6-29, 6-30, 6-56, and 6-39. The methodology is described in Section 6.4.2. The output of this worksheet includes waste package, drift wall, and drift air temperatures, an energy balance, and initial conditions for CSTR05.
CSTR04-h	Contains the calculation of convection heat transfer coefficients using the Mixed Convection Correlation (Appendix VIII) for CSTR04.
CSTR05	Contains the heat transfer analysis for the fifth 100-m section (500-m). These calculations use the results of the CSTR04 worksheet and iterative calculations of Equations 6-18, 6-45, 6-32, 6-31, 6-38, 6-29, 6-30, 6-56, and 6-39. The methodology is described in Section 6.4.2. The output of this worksheet includes waste package, drift wall, and drift air temperatures, an energy balance, and initial conditions for CSTR06.
CSTR05-h	Contains the calculation of convection heat transfer coefficients using the Mixed Convection Correlation (Appendix VIII) for CSTR05.

Table VIII-1. Contents of Analytical-LA-Coarse-Wet-vs-Dry-kth.xls (Continued)

Worksheet	Description
CSTR06	Contains the heat transfer analysis for the sixth 100-m section (600-m). These calculations use the results of the CSTR05 worksheet and iterative calculations of Equations 6-18, 6-45, 6-32, 6-31, 6-38, 6-29, 6-30, 6-56, and 6-39. The methodology is described in Section 6.4.2. The output of this worksheet includes waste package, drift wall, and drift air temperatures, and an energy balance.
CSTR06-h	Contains the calculation of convection heat transfer coefficients using the Mixed Convection Correlation (Appendix VIII) for CSTR06.
CSTR01 Plot	Plots the waste package, drift wall, and drift air temperature results versus time for CSTR01.
CSTR02 Plot	Plots the waste package, drift wall, and drift air temperature results versus time for CSTR02.
CSTR03 Plot	Plots the waste package, drift wall, and drift air temperature results versus time for CSTR03.
CSTR04 Plot	Plots the waste package, drift wall, and drift air temperature results versus time for CSTR04.
CSTR05 Plot	Plots the waste package, drift wall, and drift air temperature results versus time for CSTR05.
CSTR06 Plot	Plots the waste package, drift wall, and drift air temperature results versus time for CSTR06.
Ventilation Efficiency	Contains the calculations of both integrated and instantaneous ventilation efficiency described by Equations 6-6 and 6-5.

INTENTIONALLY LEFT BLANK

APPENDIX IX

DOCUMENTATION OF THE MIXED CONVECTION CORRELATION METHODOLOGY

SYMBOLS

a	coefficient in Fourier series for $q''(x,\theta)$
b	coefficient in Fourier series for $q''(x,\theta)$
c	Nusselt number coefficient for laminar natural convection
$\overline{C}$	Nusselt number coefficient for turbulent natural convection
D	diameter
D_h	hydraulic diameter D_o - D_i
e*	dimensionless eccentricity, $2\varepsilon/(D_o - D_i)$, positive upward
g	gravitational acceleration
$h(x,\theta)$	local convective heat transfer coefficient
$\overline{h}(x)$	effective circumferential convective heat transfer coefficient
h_{cond}	overall conductive heat transfer coefficient for the combined concrete and insulation.
$\tilde{h}$	error in convection coefficient
k	thermal conductivity of the fluid
L_i	combined length of the waste packages
m	exponent for blending laminar and turbulent forms for Nusselt numbers
M	value of the second derivative of y with respect to x somewhere in (x_0, x_1)
$\overline{Nu}(x)$	effective circumferential Nusselt number, $\overline{h}(x)(D_o - D_i)/k$
Nu_{conv}	Nusselt number for overall natural convection between the cylinders, $\frac{D_i\overline{q}''}{k(\overline{T}_i - \overline{T}_o)}$
Nu_i'	Kuehn-Goldstein Nusselt number, $\overline{h}_i D_i/k$
Nu_{ii}	forced-convection Nusselt number of inner cylinder when it alone is heated
Nu_{oo}	forced-convection Nusselt number of outer cylinder when it alone is heated
Nu_o'	Kuehn-Goldstein Nusselt number for the outer cylinder, $\overline{h}_o D_o/k$
Pr	Prandtl number, ν/α
$q''(x,\theta)$	convective heat flux (positive into the fluid)
$\overline{q}''(x)$	circumferential average convective heat flux (positive into the fluid)
$\overline{q}''_{rad,i}(x)$	circumferential average radiative flux from the waste packages at location x
q_{in}	24-hour average power generated in the waste packages
r^*	ratio of the diameters, D_i/D_o
R_n	eigenfunction for nth harmonic of axial variation in heat flux on one wall (the next subscript is the affected wall; the last subscript is the heated wall)
$Ra(x)$	Rayleigh number, $\frac{g\beta D^3}{\nu\alpha}\left\|\overline{T}(x) - T_f(x)\right\|$
Re	dimensionless Reynolds number, $\frac{u_m(D_o - D_i)}{\nu}$
Re_0	Reynolds number at the lower end of an interpolation interval
Re_1	Reynolds number at the upper end of an interpolation interval

Re_M	equivalent Reynolds number for mixed convection
Re_N	equivalent Reynolds number for natural convection
$T(x,\theta)$	surface temperature
$\overline{T}(x)$	circumferential average surface temperature
$\overline{\overline{T^4}}(x)$	24-hour and circumferential average of the 4th power of the absolute temperature
$T_f(x)$	mean fluid temperature
$u(x)$	standard uncertainty in a predicted value x
$u_c(y)$	combined standard uncertainty in a predicted value y
u_m	mean axial fluid velocity
x	longitudinal coordinate along the cylinder in the direction of flow or input variable for an interpolation
x_0	lower boundary of an interpolation interval
x_1	upper boundary of an interpolation interval
$y(x)$	surrogate for any parameter being interpolated in a table

GREEK SYMBOLS

α	thermal diffusivity
β	fluid coefficient of thermal expansion
ε	distance between the central axes of the cylinders
ε_i	measured emissivity of the waste package
ε_o	measured emissivity of the concrete pipe
$\overline{\Phi}_b$	average dimensionless fluid temperature
ϕ	angle between the vertical direction and the direction of forced flow
v	kinematic viscosity
$\tau(x)$	dimensionless temperature parameter, $\frac{\overline{T}_i(x)-T_f(x)}{\overline{T}_o(x)-T_f(x)}$
θ	angle from the zenith relative to the axis of a cylinder
σ	Stefan-Boltzmann constant
θ^*	influence coefficient in forced-convection correlation

SUBSCRIPTS

a	average external ambient
b	bottom
F	forced convection
i	inner cylinder surface
L	laminar
l	left
M	mixed convection
N	natural convection
n	harmonic of Fourier expansion
o	outer cylinder surface
r	right
T	turbulent
t	top

Heat transfer coefficients are classically predicted by the use of equations that are called correlations. The use of equations or correlations for the prediction not only of heat transfer coefficients, but also for mass and momentum transfer, is commonly accepted engineering practice that has been in successful use for over 50 years. The terminology of correlations or equations is not universal (for an example of the use of the word "correlation" as it refers to heat transfer, see Ebadian and Dong 1998 [DIRS 160728], p. 5.26, Table 5.11). However, Kern (1950 [DIRS 130111], pp. 43 to 57) appears to use the words "correlation," "equation," and "evaluation" interchangeably. Thus, even though various word usages will appear in the textbook literature when referring to correlations, equations, and evaluations, the meanings are all the same.

Obtaining a heat-transfer correlation is common practice in the process industry, and usually involves a very limited set of data for a particular configuration of the heat transfer surfaces. The reason a "very limited set of data" is available is because it is not practical to have measurements of heat transfer (or mass or momentum) for every combination of independent variables. However, the final heat-transfer correlation is not based on just any equation form, but is based on the correlating parameters of Reynolds number, Prandtl number, and a few other dimensionless groups (Kern 1950 [DIRS 130111], pp. 38 to 40). The fact that these correlating parameters do work is based on dimensional analysis and experience.

The test that follows evaluates heat transfer coefficients and results in a correlation for the case of mixed convection in an internally heated pipe. Mixed convection is the situation where the forced flow rate is so small that natural convection contributes to the overall rate of heat transfer. It must be emphasized that the relative importance to the overall rate of heat transfer does not always depend on just the heat transfer coefficients, but also on what is on the other side of the surface where the heat transfer coefficient is being applied.

The efficiency of the ventilating air can be defined as the percentage of the total energy generated from the waste packages that is removed by the ventilating air. The energy is transferred to the ventilating air by a combination of forced and natural convection, defined as mixed convection. A temperature-dependent correlation of the mixed convection within the emplacement drifts has been developed. The correlation provides a measure of the convection heat transfer occurring at the waste package and drift wall surfaces in the form of a parameter equal to the dimensionless temperature gradient, the Nusselt number. From the Nusselt number, convective heat transfer coefficients dependent on temperatures of the waste package, the emplacement drift wall, and the ventilation air due to the decay of the nuclear waste can be determined.

Section IX.1 of this appendix describes the development of the mixed-convection methodology. Sections IX.2 and IX.3 present a sensitivity study and a discussion of the uncertainty associated with the methodology. Section IX.4 examines the methodology for YMP specific conditions using experimental data from the EBS Ventilation Test Series.

Results of the following activities are included:

- Development of a methodology to calculate the effective heat transfer coefficients for convection within the EBS based on mixed convection.

- Determine the sensitivity of the methodology to each of its parameters.
- Estimate the uncertainty in the heat transfer coefficients predicted by the methodology.
- Comparison of methodology results with data from the ventilation tests.

IX.1 METHODOLOGY DEVELOPMENT

As a means of general introduction, the next few sections (IX.1.1 through IX.1.3) provide an overview of mixed convection, including:

- A conceptual picture of the processes involved
- Definitions of dimensionless groups used in describing the processes
- Underlying engineering principles.

Prior to developing a mathematical methodology to quantitatively define mixed convection, a literature search was performed to determine if any applicable models appropriate for mixed convection in the YMP emplacement drifts existed. None was found, although a general methodology for combining forced and natural convection models into a mixed-convection methodology was documented. Sections IX.1.4 through IX.1.6 summarize the results of the literature search, first covering correlations for natural convection, then for forced convection, and finally the methodology for mixed convection. The summary includes correlations and methods that were not used and the rationale for not selecting them. The discussion also details the idealizations inherent in the correlations chosen for the methodology. This section refers to Section 4 of the main document for information about inputs.

IX.1.1 Concept for Mixed Convection

A concept for mixed convection can be constructed by determining the flow patterns that will be established within the emplacement drifts.

In the absence of forced ventilation, and when the inner cylinder is hotter than the outer, air adjacent to the inner cylinder will be heated, expanding and rising from buoyancy effects. When it reaches the outer cylinder, it will begin to cool as it transfers heat. The density of the air will increase as it falls along the outer wall, continuing to transfer heat to the outer cylinder. Figure IX-1a shows the resulting two-dimensional flow pattern from pure natural convection.

At sufficiently high ventilation speeds, forced convection will dominate. The flow will be exclusively axial, as shown in Figure IX-1b.

At low ventilation speeds, the forced flow is modified by the buoyancy effect. If there were no significant radiation to the outer cylinder, so that its temperature remained below the air temperature, the flow would be as in Figure IX-1c. Heat transfer from this flow pattern is called mixed convection. The mixed flow velocity at many locations is approximately the vector sum of the natural convection flow velocity and the forced convection flow velocity.

At the temperatures anticipated in the EBS, radiation causes the outer cylinder to be hotter than the fluid, which will modify the mixed-convection flow patterns described above. Buoyancy

effects will tend to make the air rise in the boundary layer along the outer wall as well as along the inner cylinder. The return downward flow must occur away from the walls, within the annulus. This mixed-convection flow, suggested by Figure IX-1d, is reflective of the YMP emplacement drifts.

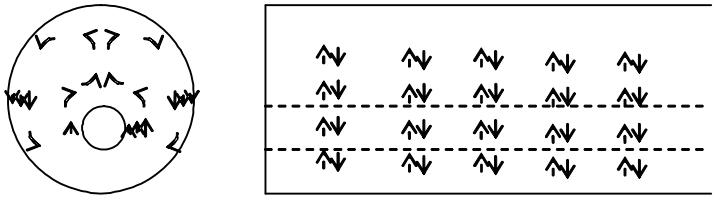

(a) Flow in natural convection

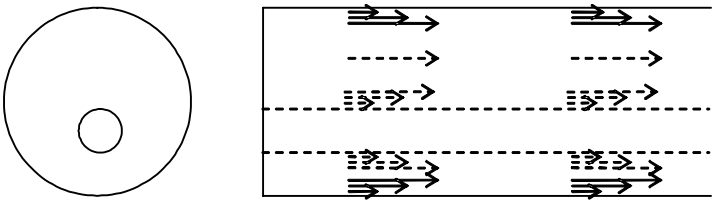

(b) Flow in forced convection

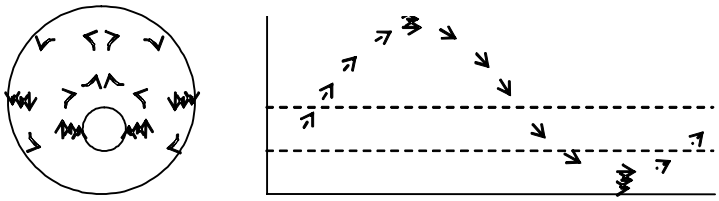

(c) Flow in mixed convection without significant radiation

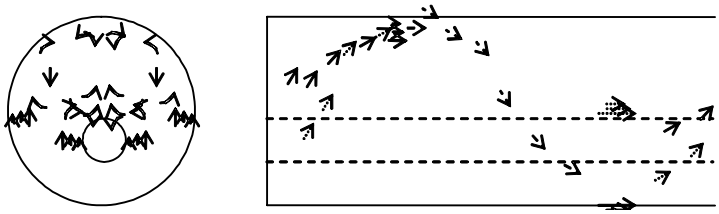

(d) Flow in mixed convection with outer wall hotter than fluid

NOTE: Boundary layer thickness exaggerated.

Figure IX-1. Flow Patterns for Various Modes of Convection

IX.1.2 Dimensionless Groups

Papers in refereed journals usually express correlations of experimental heat transfer data as relationships between certain dimensionless groups, such as the Reynolds, Nusselt, Prandtl and Rayleigh numbers. The definitions of the dimensionless groups are not uniform in the literature. This section presents the definitions used in this appendix.

The driver for forced convection is the mean axial fluid velocity, u_m (m/s). Its surrogate is the dimensionless Reynolds number, *Re*, a measure of the ratio of inertial to viscous forces. It is usually defined for the opening between cylinders as (Ebadian and Dong 1998 [DIRS 160728], p. 5.3, Eq. 5.3):

$$Re = \frac{u_m (D_o - D_i)}{\nu} = \frac{u_m D_h}{\nu} \qquad \text{(Eq. IX-1)}$$

where ν is the kinematic viscosity (m^2/s), D_o the outer cylinder diameter, and D_i the inner cylinder diameter.

The dimensionless surrogate for the heat transfer coefficient is the Nusselt number. Corresponding to each convection coefficient $\overline{h}(x)$ is the effective circumferential Nusselt number, $\overline{Nu}(x)$, defined in this appendix by (Kays and Leung 1963 [DIRS 160763], p. 537).

$$\overline{Nu_i}(x) = \overline{h_i}(x)(D_o - D_i)/k \qquad \text{(Eq. IX-2)}$$

$$\overline{Nu_o}(x) = \overline{h_o}(x)(D_o - D_i)/k \qquad \text{(Eq. IX-3)}$$

where *k* is the thermal conductivity of the fluid and the subscripts indicate the inner or outer cylinder. Here the arbitrary distance parameter has been chosen as the hydraulic diameter, equal to four times the ratio of the orifice area to its perimeter (Ebadian and Dong 1998 [DIRS 160728], Equation 5.1).

Another dimensionless group is the Prandtl number, which is a property of the fluid, defined by:

$$Pr = \nu / \alpha \qquad \text{(Eq. IX-4)}$$

where α is the thermal diffusivity (m^2/s) (Raithby and Hollands 1998 [DIRS 160764], pp. 4.83 to 4.86). The methodology documented here is limited to $Pr = 0.7$.

Natural convection is driven by buoyancy forces, which are caused by temperature gradients in the fluid. The Rayleigh number, *Ra* , includes the ratio of buoyancy to viscous forces. The Rayleigh numbers for the cylinders are conventionally defined by (Raithby and Hollands 1998 [DIRS 160764], p. 4.21, Figure 4.16a):

$$Ra_i(x) = \frac{g\beta D_i^{\,3}}{\nu\alpha}\left|\overline{T_i}(x) - T_f(x)\right| \qquad \text{(Eq. IX-5)}$$

$$Ra_o(x) = \frac{g\beta D_o^{\,3}}{\nu\alpha}\left|\overline{T_o}(x) - T_f(x)\right| \qquad \text{(Eq. IX-6)}$$

where *g* is the gravitational acceleration (m/s^2) and β is the fluid coefficient of thermal expansion (K^{-1}). For gases such as air, β is evaluated as $1/T_f$, as for a perfect gas (Raithby and Hollands 1998 [DIRS 160764], p. 4.2).

The mixed-convection methodology documented here considers each cylinder separately. It does not attempt to predict the Nusselt number for radial convective heat transfer at each position on a surface. Rather, it predicts a circumferential average at each axial location. That is, it predicts an effective circumferential Nusselt number at each axial location that is directly related to the effective circumferential heat transfer coefficient for radial convection (Equation IX-2 or IX-3). That heat transfer coefficient is defined in terms of the following properties of that axial location:

- The mean surface temperature
- The mean heat flux
- The cross-sectional mean fluid temperature.

Therefore, the predicted Nusselt number and the two average temperatures are sufficient to predict the circumferential average heat flux (by definition).

IX.1.3 Underlying Engineering Principles

Incropera and DeWitt (1985 [DIRS 114109], p. 296) describe two approaches to determine convection coefficients, one theoretical and one empirical. The empirical approach involves performing heat transfer measurements under controlled conditions and correlating the data in terms of appropriate dimensionless parameters. The theoretical approach involves solving the boundary layer equations for the particular geometry. No completely theoretical solution is available for turbulent flow in an annulus; the mathematical methodology documented here incorporates empirical correlations.

The available correlations are for experiments in which the boundary conditions are uniform over the circumference of each cylinder. The correlations apply to the total or mean heat flux on each surface. They do not provide information on the variation of heat flux with position around the circumference.

The fluid temperature away from the boundary layers is sufficiently uniform such that any central temperature is a good approximation to the mean fluid temperature. A user of the methodology can obtain the average heat fluxes from the predicted Nusselt numbers and the average temperatures.

Because the Nusselt number is dimensionless, it must depend on dimensionless groups (Cho et al. 1998 [DIRS 160802], p. 1.24). The methodology documented here is based on correlations of experimental data that relate the Nusselt number to the Reynolds number, the Rayleigh number, the Prandtl number, and temperature ratios.

The mixed-convection concept suggests that the mixed flow velocity at any point be approximated as the vector sum of the natural convection flow velocity and the forced convection flow velocity. For horizontal ventilation, ignoring end effects, the forced flow is always orthogonal to the natural flow. Therefore, the square of the mixed velocity would be the sum of the squares of the natural and forced components. Rather than make such a postulation explicitly, the mathematical methodology documented here uses the method of Morgan (1975 [DIRS 160791]).

IX.1.4 Natural Convection

The Kuehn-Goldstein (1978 [DIRS 130084]) correlation is the basis for the natural convection correlation documented here. A search of the engineering literature regarding natural convection in an annulus determined that the Kuehn-Goldstein correlation is generally accepted as the best available. For example, Raithby and Hollands (1998 [DIRS 160764], p. 4.59) discuss their own correlation, but recommend the Kuehn-Goldstein correlation if turbulence effects may be important. Kuehn and Goldstein (1978 [DIRS 130084], p. 639) report that their correlation fits the data better than the general correlation given in their earlier paper (Kuehn and Goldstein 1976 [DIRS 100675]).

The Kuehn-Goldstein correlation is for idealized configurations that differ from the EBS in the following respects. The correlation is:

- For situations in which the outer cylinder is colder than the air (Figures IX-1a and IX-1c).
- For cylinders that each have a uniform temperature (are isothermal).
- For a configuration with concentric cylinders.
- For a configuration in which the inner cylinder extends the full length of the outer cylinder (coextensive).
- For cylinders with fully insulated ends.

For local natural convection at the inner and outer cylinders, the Kuehn-Goldstein correlation is:

$$Nu_i' = \frac{2}{\ln\left[1 + \frac{2}{\left[\left(c_i Ra_i^{1/4}\right)^m + \left(\overline{C}_i Ra_i^{1/3}\right)^m\right]^{\frac{1}{m}}}\right]} \qquad \text{(Eq. IX-7)}$$

$$Nu_o' = \frac{-2}{\ln\left[1 - \frac{2}{\left[\left(c_o Ra_o^{1/4}\right)^m + \left(\overline{C}_o Ra_o^{1/3}\right)^m\right]^{\frac{1}{m}}}\right]} \qquad \text{(Eq. IX-8)}$$

where $Nu_i' = \overline{h}_i D_i / k$, $Nu_o' = \overline{h}_o D_o / k$, the constants are listed in Table IX-1, and the parameters are taken to be independent of *x*. These Nusselt numbers use the cylinder diameters as the arbitrary distance parameters instead of the hydraulic diameter chosen for this mixed-convection methodology. To restate the correlation in terms of the Nusselt numbers defined in Equations IX-2 and IX-3, the parameter r^* (defined as D_i/D_o) is used, so that:

$$D_h = D_o - D_i = D_o\left(1 - r^*\right) = D_i\left(1/r^* - 1\right) \quad \text{(Eq. IX-9)}$$

$$\overline{Nu_{Ni}}(x) = \frac{2\left(1/r^* - 1\right)}{\ln\left[1 + \frac{2}{\left(\left\{c_i\left[Ra_i(x)\right]^{1/4}\right\}^m + \left\{\overline{C_i}\left[Ra_i(x)\right]^{1/3}\right\}^m\right)^{\frac{1}{m}}}\right]} \quad \text{(Eq. IX-10)}$$

$$\overline{Nu_{No}}(x) = \frac{-2\left(1 - r^*\right)}{\ln\left[1 - \frac{2}{\left(\left\{c_o\left[Ra_o(x)\right]^{1/4}\right\}^m + \left\{\overline{C_o}\left[Ra_o(x)\right]^{1/3}\right\}^m\right)^{\frac{1}{m}}}\right]} \quad \text{(Eq. IX-11)}$$

Table IX-1. Values of Constants for Large Ra in the Correlations of Kuehn and Goldstein

Constant	Value (dimensionless)
c_i	0.5
$\overline{C_i}$	0.12
c_o	1
$\overline{C_o}$	0.12
m	15

Source: Kuehn and Goldstein 1978 [DIRS 130084]

The effects of the idealized configuration of the Kuehn-Goldstein correlation when applied to the more complex YMP geometry are considered in the uncertainty analysis presented later in this appendix.

IX.1.5 Forced Convection

For forced convection, the Kays-Leung (1963 [DIRS 160763]) correlation underlies the methodology presented in this appendix. The correlation is specific for fully developed turbulent forced convection through an annulus and makes extensive use of theoretical solutions. The results cover a wide range of annulus radius ratio and Reynolds number. Their paper is cited by Ebadian and Dong (1998 [DIRS 160728], p. 5.51 and Table 5.27).

Some modelers have used the Dittus-Boelter correlation rather than the Kays-Leung correlation. The Dittus-Boelter formula gives the asymptotic Nusselt number for fully developed turbulent flow (Re > 10,000) in circular tubes (r^* = 0). For air (Pr = 0.70), and the tube hotter than the fluid, the correlation is (Incropera and DeWitt 1985 [DIRS 114109], p. 394, Eq. 8.58):

$$Nu = 0.020\,Re^{0.8} \quad \text{(Eq. IX-12)}$$

This formula was used for the Nusselt number at the outer wall in earlier ventilation model calculations with fully developed turbulent flow. Incropera and DeWitt (1985 [DIRS 114109], p. 400) consider the Dittus-Boelter equation to be a first approximation, in which the inner and outer convection coefficients are assumed to be equal.

For concentric circular cylinders with a uniform heat rate on each cylinder, Kays and Leung (1963 [DIRS 160763], p. 539, Eqs. 15 and 16) derived the following expressions:

$$\overline{Nu}_i(x) = \frac{Nu_{ii}(x)}{1-\theta_i^*(x)(q_o''/q_i'')} \quad \text{(Eq. IX-13)}$$

$$\overline{Nu}_o(x) = \frac{Nu_{oo}(x)}{1-\theta_o^*(x)(q_i''/q_o'')} \quad \text{(Eq. IX-14)}$$

where

$Nu_{ii}(x)$ = the Nusselt number of the inner cylinder when it alone is heated

$Nu_{oo}(x)$ = the Nusselt number of the outer cylinder when it alone is heated

$\theta_i^*(x)$ and $\theta_o^*(x)$ = influence coefficients

Using empirical velocity and eddy distribution profiles, Kays and Leung (1963 [DIRS 160763]) evaluated the parameters by obtaining asymptotic solutions of the energy differential equations, using fluid properties evaluated at $T_f(x)$ and empirical equations for turbulent region diffusivity.

Kays and Leung (1963 [DIRS 160763], Table 1) tabulated the asymptotic values of the parameters, θ_i^*, θ_o^*, Nu_{ii}, and Nu_{oo} as functions of r^*, the Reynolds number, and the Prandtl number. Table IX-2 contains the values for Pr=0.7 and r^* of 0.2 and 0.5, which are used in Section IX.1.6. The methodology is limited to values of r^* between 0.2 and 0.5, which includes the design value for the EBS.

Table IX-2. Parameters for Forced Convection Correlation for Fully Developed Flow and Pr = 0.7

r^*:	0.2				
Re:	10000	30000	100000	300000	1000000
Nu_{ii}:	38.6	79.8	196	473	1270
θ_I:	0.412	0.338	0.286	0.260	0.235
Nu_{oo}:	29.4	64.3	165	397	1070
θ_o:	0.063	0.055	0.049	0.044	0.040
r^*:	0.5				
Re:	10000	30000	100000	300000	1000000
Nu_{ii}:	30.9	66	166	400	1080
θ_I:	0.3	0.258	0.225	0.206	0.185
Nu_{oo}:	28.3	62	158	380	1040
θ_o:	0.137	0.119	0.107	0.097	0.090

Source: Kays and Leung 1963 [DIRS 160763], Table 1

However, Equations IX-13 and IX-14 do not provide an explicit form for the calculation of heat transfer coefficients for models that have known boundary temperatures rather than known fluxes. In convective processes involving heat transfer from a boundary surface exposed to a relatively low-velocity fluid stream, it is convenient to introduce a local convective heat transfer coefficient, $h(x,\theta)$ (W/m^2·K), defined implicitly by Newton's law of cooling, which is:

$$q''(x,\theta) = h(x,\theta)\left[T(x,\theta) - T_f(x)\right] \quad \text{(Eq. IX-15)}$$

where $q''(x,\theta)$ is the convective heat flux (W/m^2) (positive into the fluid) and $T(x,\theta)$ is the surface temperature (K) (Incropera and DeWitt 1985 [DIRS 114109], p. 8, Eq. 1.3). If the temperature difference is zero, then $q''(x,\theta)$ is zero, and $h(x,\theta)$ is not defined.

Because the methodology does not permit heat transfer coefficients that vary around the circumference, a nominal value, the "effective circumferential" convective heat transfer coefficient $\bar{h}(x)$ (W/m^2·K), is defined such that:

$$\bar{q}''(x) = \bar{h}(x)\left[\bar{T}(x) - T_f(x)\right] \quad \text{(Eq. IX-16)}$$

where $\bar{q}''(x)$ is the circumferential average convective heat flux (W/m^2) and $\bar{T}(x)$ is the circumferential average surface temperature (K). If the cylinder has a uniform temperature around its circumference, then $\bar{h}(x)$ is the circumferential average of $h(x,\theta)$, but if the temperature varies around the circumference, $\bar{h}(x)$ may differ from the average of $h(x,\theta)$.

From Equations IX-16, IX-2, and IX-3, the ratio of heat fluxes is:

$$\frac{\bar{q}_i''(x)}{\bar{q}_o''(x)} = \frac{\overline{Nu}_i(x)}{\overline{Nu}_o(x)}\tau(x) \quad \text{(Eq. IX-17)}$$

where

$$\tau(x) = \frac{\overline{T_i}(x) - T_f(x)}{\overline{T_o}(x) - T_f(x)} \quad \text{(Eq. IX-18)}$$

Substituting for the ratio in Equations IX-13 and IX-14, using the asymptotic values of the parameters, yields the following two solutions for the asymptotic Nusselt numbers:

$$\overline{Nu}_i(x) = \frac{Nu_{ii}}{1 - \frac{\theta_i^*}{\tau(x)} \frac{\overline{Nu}_o(x)}{\overline{Nu}_i(x)}} \quad \text{(Eq. IX-19)}$$

$$\overline{Nu}_o(x) = \frac{Nu_{oo}}{1 - \theta_o^* \frac{\overline{Nu}_i(x)}{\overline{Nu}_o(x)} \tau(x)} \quad \text{(Eq. IX-20)}$$

The forced-convection correlation is valid only for fully developed flows. This permits replacing the asymptotic limits with the local values. Solving the above simultaneous equations yields the following formulas for explicit calculation of the effective circumferential Nusselt numbers from the temperatures:

$$\overline{Nu_{Fi}}(x) = \frac{Nu_{ii}(Re) + Nu_{oo}(Re)\theta_i^*(Re)/\tau(x)}{1 - \theta_o^*(Re)\theta_i^*(Re)} \quad \text{(Eq. IX-21)}$$

$$\overline{Nu_{Fo}}(x) = \frac{Nu_{oo}(Re) + Nu_{ii}(Re)\theta_o^*(Re)\tau(x)}{1 - \theta_o^*(Re)\theta_i^*(Re)} \quad \text{(Eq. IX-22)}$$

In comparing experimental data with their correlations, Kays and Leung (1963 [DIRS 160763], pp. 544-545, Figures 6 through 8) did not correct the experimental data for *Re* effects of natural convection. Because the flow was vertically upward, so that buoyancy effects were longitudinal rather than transverse, the effects of natural convection are minimized.

The Kays-Leung correlations are for idealized configurations that differ from the EBS in that the cylinders are concentric. The effects of this idealization are considered in the uncertainty analysis presented later in this appendix.

IX.1.6 Mixed Convection

Review of the literature shows little research has been completed for mixed convection conditions, and no information was found for configurations similar to the YMP drifts. For internal flows, Incropera and DeWitt (1985 [DIRS 114109], p. 445) and Raithby and Hollands (1998 [DIRS 160764], pp. 4.78 to 4.79) limit consideration of mixed convection to laminar flows within heated cylinders. Earlier ventilation model calculations neglected natural convection, using only a model for forced convection. The method used for mixed convection in the

methodology documented here is based on the method of Morgan (1975 [DIRS 160791], p. 244, Eq. 21).

The literature search found no published correlations of experimental data for the flow pattern of Figure IX-1d. In order to use published correlations, the following statements need to be true:

- Mixed-convection in the EBS configuration is approximately the same as mixed-convection in an idealized configuration in which a hotter cylinder is inside a cooler cylinder.

- The effective circumferential Nusselt number at each surface is related to the Reynolds number and dimensionless temperature difference across the boundary layer, but is independent of the conditions at the other surface. This relation is given by the correlation of Kays and Leung (1963 [DIRS 160763], p. 539, Eqs. 15 and 16) for natural convection.

- Natural convection in the EBS may be predicted by the correlation of Kuehn and Goldstein (1978 [DIRS 130084], p. 639, Eq. 1). In particular, the Kuehn-Goldstein correlation must remain valid when the outer surface is hotter than the air.

- The effective Reynolds number for natural convection at a surface depends only on the circumferential Nusselt number at that surface, as predicted by the Kuehn-Goldstein correlation. In particular, the effective Reynolds number is approximately the same as the Reynolds number for the particular forced flow at that surface that would give the same effective Nusselt number.

- As proposed by Morgan (1975 [DIRS 160791]) for configurations in which the direction for natural convection is 90º from the direction for forced convection, the effective Reynolds number for mixed convection is the square root of the sum of the square of the Reynolds number for forced convection and the square of the effective Reynolds number for natural convection.

The validity of these statements is demonstrated in comparison of the methodology to experimental data.

IX.1.6.1 Methodology

Morgan (1975 [DIRS 160791]) proposed a method for calculating the Nusselt number when both natural and forced modes of convection are present. He considered an equivalent Reynolds number for natural convection, Re_N, such that the Nusselt number for natural convection would be equal to the Nusselt number for a forced convection that had a Reynolds number of Re_N.

In other words, for the forced-convection flow pattern of Figure IX-1b, Equations IX-21 and IX-22 provide relationships among the Reynolds number and the two effective circumferential Nusselt numbers. The Morgan approach applies these relationships to the natural-convection flow pattern of Figure IX-1a to obtain effective Reynolds numbers for natural convection. The

equations are similar, with the Nusselt numbers and Reynolds number replaced by $\overline{Nu_{Ni}}(x)$, $\overline{Nu_{Ni}}(x)$, Re_{Ni}, and Re_{No}.

For the natural-convection flow pattern of Figure IX-1a, the two surfaces need not have the same effective Reynolds number. By conservation of mass, the mass flow rates must be related, but the channel widths are not known. For example, the flow speed may be higher when the air is rising past the inner cylinder, because the motion is in the direction of buoyancy. At the outer cylinder the flow may be slower and occupy a wider channel. Therefore, in applying Equations IX-21 and IX-22 to natural convection (or mixed convection) each equation uses the Reynolds number appropriate to the surface.

For steady pure natural convection, with or without radiation, energy conservation requires that the ratio of the convective fluxes at the two surfaces be related to the inverse of their circumferences. This additional relationship might have permitted simultaneous solution of Equations IX-21 and IX-22 in the case of natural convection. However, the appearance of an additional variable, the second Reynolds number, precludes solving the equations simultaneously. Therefore, each surface must be treated separately.

Once the effective Reynolds number for natural convection at a surface is available, the Morgan procedure defines the effective Reynolds number for the mixed flow to be Re_M, such that (Morgan 1975 [DIRS 160791], p. 244, Eq. 21):

$$(Re_M)^2 = (Re_N)^2 + (Re)^2 + 2(Re_N)(Re)\cos\phi \qquad \text{(Eq. IX-23)}$$

where Re is the Reynolds number for forced convection and ϕ is the angle between the direction of gravity and the direction of forced flow. The total heat transfer is found by using Re_M in place of Re in the forced convection correlation. Section IX.1.6.2 uses Equation IX-23, in the special case that $\phi = 90^o$, ($\cos\phi = 0$), for prediction of mixed convection in the EBS during ventilation.

Morgan (1975 [DIRS 160791]) applied the mixed-convection technique to predict the effective Reynolds number for mixed convection in external horizontal flow that is transverse to a horizontal cylinder. He compared the predicted ratio of effective Nusselt number to forced-flow Nusselt number to the experimental values from two data sets (Morgan 1975 [DIRS 160791], p. 249, Figure 10). Section IX.3.5 uses this comparison as a sound basis for estimating the additional uncertainty that arises when Equation IX-23 is used.

The mixed-convection methodology incorporates correlations of experimental data. The correlations are for idealized configurations that are not the same as the EBS configuration. With one exception, methodology development recognizes that the idealizations are not true and considers their effects in the uncertainty analysis (Section IX.3). The one exception applies to natural convection when the outer surface is hotter than the air. During forced ventilation, the ventilating air removes heat. Because the outer cylinder is heated by thermal radiation from the inner cylinder, the outer surface will be hotter than the air. As discussed in Section 5, the development of the mixed-convection methodology assumes that the Kuehn-Goldstein correlation remains valid when the outer surface is hotter than the air.

IX.1.6.2 Mathematical Methodology

The methodology documented here combines the natural and forced convection formulas into mixed convection formulas. The following formulas give the effective circumferential Nusselt number for mixed convection at each surface:

$$\overline{Nu_{Mi}}(x) = \frac{Nu_{ii}(Re_{Mo}(x)) + Nu_{oo}(Re_{Mo}(x))\theta_i^*(Re_{Mo}(x))/\tau(x)}{1-\theta_o^*(Re_{Mo}(x))\theta_i^*(Re_{Mo}(x))} \quad \text{(Eq. IX-24)}$$

$$\overline{Nu_{Mo}}(x) = \frac{Nu_{oo}(Re_{Mi}(x)) + Nu_{ii}(Re_{Mi}(x))\theta_o^*(Re_{Mi}(x))\tau(x)}{1-\theta_o^*(Re_{Mi}(x))\theta_i^*(Re_{Mi}(x))} \quad \text{(Eq. IX-25)}$$

where the parameters are interpolated linearly between Reynolds numbers and values of r^* in Table IX-2,

$$Re_{Mi}(x) = \sqrt{Re^2 + [Re_{Ni}(x)]^2} \quad \text{(Eq. IX-26)}$$

$$Re_{Mo}(x) = \sqrt{Re^2 + [Re_{No}(x)]^2} \quad \text{(Eq. IX-27)}$$

The Morgan procedure entails finding the equivalent natural-convection Reynolds numbers, Re_{Ni} and Re_{No}, such that Equations IX-24 and IX-25 are satisfied with the subscript $_M$ replaced by the subscript $_N$. To simplify the implicit equations to be solved, the methodology documented here makes the following approximations:

$$\overline{Nu_{Ni}}(x) = \mathrm{Nu}_{ii}(Re_{Ni}(x)) \quad \text{(Eq. IX-28)}$$

$$\overline{Nu_{No}}(x) = \mathrm{Nu}_{oo}(Re_{No}(x)) \quad \text{(Eq. IX-29)}$$

with $\overline{Nu_{Ni}}(x)$ and $\overline{Nu_{No}}(x)$ given by Equations IX-10, IX-11 and Table IX-1 and with linear interpolations with respect to Reynolds number and r^* in Table IX-2. The uncertainty analysis of Section IX.3.5 includes the effects of these approximations.

Equations IX-10 and IX-11 are appropriate to the flow patterns of Figures IX-1a and IX-1c. The methodology documented here applies those correlations to the general case, including the flow pattern of Figure IX-1d.

An application of the methodology may be represented as an algorithm, with a preparation phase to establish the dimensionless groups that are input to the methodology, a Nusselt number prediction phase that accords with the methodology, and a phase for interpretation of the calculated Nusselt numbers. The *preparation* phase consists of the following steps:

Step P1. (Geometry) Calculate D_i/D_o, which is r^*. Also calculate the hydraulic diameter, D_o-D_i.

Step P2. (Reynolds Number) Choose the axial position of interest, *x*. Determine the mass flow rate, $u_m(x)$, and the mean fluid temperature, $T_f(x)$. Calculate *Re*, using Equation IX-1.

Step P3. (Rayleigh Numbers) Estimate the local value of *g*. Determine the circumferential average temperature on each surface, $\overline{T}_i(x)$ and $\overline{T}_o(x)$. Calculate $\overline{T}_i(x) - T_f(x)$ and $\overline{T}_o(x) - T_f(x)$. Calculate $\tau(x)$ using Equation IX-18. Calculate $Ra_i(x)$ and $Ra_o(x)$, using Equations IX-5 and IX-6.

The following steps apply the methodology to predict the mixed-convection *Nusselt* numbers:

Step N1. (Forced-Convection Parameters) Using linear interpolation for r^* in Table IX-2, establish tables for $\mathrm{Nu}_{\mathrm{ii}}$, $\mathrm{Nu}_{\mathrm{oo}}$, θ_i^*, and θ_o^* as functions of *Re*.

Step N2. (Natural Convection) Using Equations IX-10 and IX-11 with Table IX-1, calculate $\overline{Nu_{Ni}}(x)$ and $\overline{Nu_{No}}(x)$. Using the table created in Step N1, and using linear dependence on *Re* between table values, find $Re_{Ni}(x)$ to satisfy Equation IX-28 and $Re_{No}(x)$ to satisfy Equation IX-29.

Step N3. (Inner-Surface Nusselt Number) Using Equation IX-26, calculate $Re_{Mi}(x)$. Using linear interpolation in the table created in Step N1, look up the values of $Nu_{ii}(Re_{Mi}(x))$, $Nu_{oo}(Re_{Mi}(x))$, $\theta_i^*(Re_{Mi}(x))$, and $\theta_o^*(Re_{Mi}(x))$. Using Equation IX-24, calculate $\overline{Nu_{Mi}}(x)$.

Step N4. (Outer-Surface Nusselt Number) Using Equation IX-27, calculate $Re_{Mo}(x)$. Using linear interpolation in the table created in Step N1, look up the values of $Nu_{ii}(Re_{Mo}(x))$, $Nu_{oo}(Re_{Mo}(x))$, $\theta_i^*(Re_{Mo}(x))$, and $\theta_o^*(Re_{Mo}(x))$. Using Equation IX-25, calculate $\overline{Nu_{Mo}}(x)$.

The development of the methodology supports the following *interpretation* of the mixed-convection Nusselt numbers:

Step I1. Using Equations IX-2 and IX-3, calculate $\overline{h_i}(x)$ and $\overline{h_o}(x)$.

Step I1. Using Equation IX-16, calculate the two circumferential average heat fluxes and apply them uniformly over each surface.

Appendix X contains an Excel spreadsheet that may be used for this algorithm.

IX.1.6.3 Methodology Limitations

This section summarizes the limitations of the ventilation methodology discussed in the above sections of the appendix. The impacts of these limitations are addressed in Section IX.3. Sentences describing the limitations appear in italics.

Although forced ventilation is proposed during the preclosure period, the anticipated flow rate is low enough that both natural and forced convection play a significant role in the transfer of energy. This combination increases the complexity of predicting heat transfer. Review of the literature showed that little research has been completed for mixed convection conditions, with no information found for configurations similar to the YMP drifts.

The available correlations are based on measurements of stationary processes. Therefore, the mixed-convection methodology documented here applies only when the temperatures at the surfaces are varying so slowly with time that the convective processes are nearly stationary. The ventilating fluid must be air, and its velocity and other properties at every location must be varying slowly enough that processes are nearly stationary.

Also, the methodology documented here uses a forced-convection correlation that is valid only for fully developed flows. Therefore, the methodology is limited to situations in which the flow is fully developed over most of the length of the drift.

The EBS drift configuration is similar to an air-filled horizontal cylinder (the drift) with an interior cylindrical solid (the train of waste packages), as shown in Figure IX-2. The methodology documented here is limited to configurations in which the waste packages are spaced in the drift such that the heat generation per unit length will be nearly uniform throughout the drift.

The cylinders are neither concentric nor of equal length (coextensive). The diameters of the inner and outer cylinders are D_i and D_o, respectively. Because the core of the methodology uses only dimensionless parameters, any consistent system of units is acceptable. The applications discussed in this appendix use SI units, so the diameters are in meters. To improve readability, this appendix indicates the SI units for each variable.

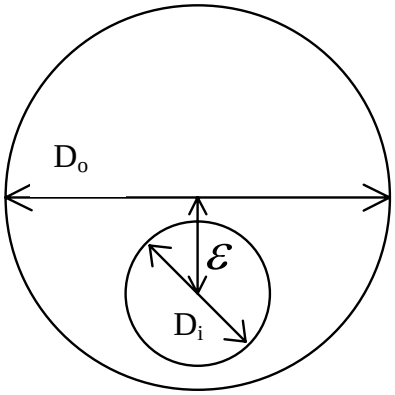

Figure IX-2. Configuration Treated by Methodology of Mixed-Convection Heat Transfer

The parameter r^* is the ratio of the diameters, D_i/D_o. *The methodology documented here has the limitation that* $0.5 \geq r^* \geq 0.2$.

The distance between the central axes of the cylinders is ε. The dimensionless eccentricity, e^*, is $2\varepsilon/(D_o - D_i)$, positive upward. *Another methodology limitation is that* $0 \geq e^* > -2/3$. That is the range covered by the experimental data for natural convection.

The driver for forced convection is the mean axial fluid velocity, u_m (m/s). Its surrogate is the dimensionless Reynolds number, *Re*, a measure of the ratio of inertial to viscous forces. *A limitation of the mixed convection methodology is that the Reynolds number be at least 15,000 (turbulent).* This is the range in which both the natural convection correlation and the forced convection correlation are valid.

The coordinate pair (x, θ_o) specifies positions on the inner surface of the outer cylinder, with x being the longitudinal coordinate along the cylinder in the direction of flow and θ_o being the angle from the vertically upward direction (zenith) relative to the axis of the outer cylinder. Similarly, (x, θ_i) specifies positions on the outer surface of the inner cylinder, with θ_i being the angle from the zenith relative to the axis of the inner cylinder. If a statement applies to either surface, the subscript on θ is omitted.

A thermal boundary layer must develop whenever the surface temperature differs from the fluid free-stream temperature (Incropera and DeWitt 1985 [DIRS 114109], p. 251). At each longitudinal position along the annulus, the central region of the fluid has a mean temperature $T_f(x)$ (K). *The current methodology is limited to air, with a Prandtl number of 0.7 and all other properties evaluated at* $T_f(x)$.

In convective processes involving heat transfer from a boundary surface exposed to a relatively low-velocity fluid stream, it is convenient to introduce a local convective heat transfer coefficient, $h(x,\theta)$ (W/m^2·K), defined implicitly by *Newton's law of cooling*, Equation IX-15.

The mixed-convection methodology documented here addresses the heat transfer coefficients used to predict convection in the EBS and in scaled tests of EBS designs. *Therefore, another limitation of the methodology is that the inner cylinder be hotter than the outer cylinder.*

The methodology does not predict local heat transfer coefficients. Rather, it leads to an effective circumferential convective heat transfer coefficient $\overline{h}(x)$ (W/m^2·K), defined by Equation IX-16.

IX.2 SENSITIVITY STUDY

Table IX-3 presents the results of a simple sensitivity study for the algorithm, Steps N1 through N3. The table shows how the values of the two Nusselt numbers change as each of the five inputs are varied. Each sensitivity for each input is the ratio of the change in Nusselt number to the change in the dimensionless input.

Appendix X contains the Excel spreadsheet that produced this sensitivity study.

Table IX-3. Sensitivity Study

Case		Ra_i	Ra_o	τ	Re	r^*	Nu_{Mi}	Nu_{Mo}	Sensitivity Nu_{Mi}	Sensitivity Nu_{Mo}
Base Values		1.E+08	7.E+08	6	45,000	0.3	165	202		
Re	low	1.E+08	7.E+08	6	15,000	0.3	145	177	1E-03	1E-03
	high	1.E+08	7.E+08	6	150,000	0.3	285	348		
τ	low	1.E+08	7.E+08	3	45,000	0.3	171	169	-9E-01	1E+01
	high	1.E+08	7.E+08	15	45,000	0.3	161	301		
Ra_i	low	5.E+07	7.E+08	6	45,000	0.3	144	202	3E-07	—
	high	2.E+08	7.E+08	6	45,000	0.3	195	202		
Ra_o	low	1.E+08	2.E+08	6	45,000	0.3	165	168	—	4E-08
	high	1.E+08	2.E+09	6	45,000	0.3	165	243		
r^*	low	1.E+08	7.E+08	6	45,000	0.2	253	203	-5E+02	-5E+01
	high	1.E+08	7.E+08	6	45,000	0.5	103	189		

IX.3 UNCERTAINTY ANALYSIS

Both the forced and the natural convection correlations used in developing the mixed convection methodology are empirical or semi-empirical in nature. Thus, there is some inherent uncertainty associated with each correlation separately. Combining these equations into a mixed convection equation further increases the uncertainty. This section describes a comprehensive analysis of the overall uncertainty in the mixed convection equations.

This analysis discusses the uncertainty in the predictions without reference to any particular application. Therefore, it does not consider uncertainties in the dimensionless groups that are inputs to the methodology. Those uncertainties must be addressed by making use of the sensitivity study of Section IX.2. Section IX.4 provides examples of quantifying uncertainty from all sources using data from the EBS Ventilation Test Series.

IX.3.1 Definitions

There is no standard for the expression of uncertainty in predictions made with algorithms. However, algorithms are used to predict measurements. The treatment of uncertainty in this appendix is based on ANSI/NCSL Z540-2-1997, *American National Standard for Calibration — U.S. Guide to the Expression of Uncertainty in Measurement* [DIRS 157394]. The following are adapted from definitions that appear in the standard:

1. The **measurand** is the particular quantity subject to measurement and therefore to prediction. Its definition may require specification of the conditions under which the quantity is measured. The standard avoids the phrase “true value of the measurand” because the word “true” is viewed as redundant. The “true value of the measurand” is simply the value of the measurand (ANSI/NCSL Z540-2-1997 [DIRS 157394], p. 41).

2. The **measurement error** is the result of the measurement minus the value of the measurand (ANSI/NCSL Z540-2-1997 [DIRS 157394], p. 34). As used in this

appendix, the **prediction error** is the result of the prediction minus the value of the measurand.

3. A **random component** of prediction error is an effect that, for multiple predictions with varying inputs, produces a mean error that is small relative to the standard deviation of the error from that effect. An example of a random component is the residual error after a formula has been adjusted to correlate with data.

4. A **systematic component** of prediction error is an effect that is not a random component.

5. If the systematic component of prediction error includes a systematic effect that is quantifiable, one may add a **correction** to the prediction to compensate for that effect. However, the necessary correction may not be practical in the intended application of the prediction.

6. The **uncertainty** of the result of a prediction is an estimate of the likelihood of nearness to the best value that is consistent with presently available knowledge (adapted from ANSI/NCSL Z540-2-1997 [DIRS 157394], p. 41). Components of uncertainty include estimates of random error, uncertainties in corrections, and estimates of uncorrected or unrecognized systematic effects.

7. **Standard uncertainty** $u(x)$, of a predicted value x is the uncertainty of the result of a prediction expressed as a standard deviation. It does not correspond to a high level of confidence.

8. A **Type A evaluation** of uncertainty is an evaluation by statistical analysis of a series of observations. A **Type B evaluation** of uncertainty is an evaluation by any other method. A Type B evaluation is founded on an *a priori* distribution of the possible values (ANSI/NCSL Z540-2-1997 [DIRS 157394], p. 3).

9. If the result of a prediction is a function of the values of a number of other quantities, the standard uncertainty in the prediction is the **combined standard uncertainty**.

10. For contributions to uncertainty that are independent, the **law of propagation of uncertainty** (ANSI/NCSL Z540-2-1997 [DIRS 157394], p. 19) determines the combined standard uncertainty. For $y = f(x_i \ldots, x_n)$, the combined standard uncertainty $u_c(y)$ is given by:

$$u_c^2(y) = \sum_{i=1}^{N} \left(\frac{\delta f}{\delta x_i} \right)^2 u^2(x_i) \qquad \text{(Eq. IX-30)}$$

11. In some applications, it may be necessary to have a measure of uncertainty that encompasses a large fraction of the values that one could reasonably attribute to the measurand. If necessary, the user may multiply the standard uncertainty by a **coverage factor** to obtain an **expanded uncertainty**. In general, the coverage factor will be in the range 2 to 3 (ANSI/NCSL Z540-2-1997 [DIRS 157394], p. 24). This

appendix uses a coverage factor of 2 to approximate a 95% confidence interval (ASME PTC 19.1-1998 [DIRS 153195], p. 95).

12. The **relative combined standard uncertainty** in a predicted positive value y is $u_c(y)/y$ (ANSI/NCSL Z540-2-1997 [DIRS 157394], p. 25, Sect. 7.2.1).

13. For non-zero values of the x_i, Equation IX-30 may be rewritten for propagation of relative uncertainty:

$$\left[\frac{u_c(y)}{y}\right]^2 = \sum_{i=1}^{N}\left(\frac{x_i}{y}\frac{\partial f}{\partial x_i}\right)^2\left[\frac{u(x_i)}{x_i}\right]^2 \qquad \text{(Eq. IX-31)}$$

IX.3.2 Interpolation Errors

The uncertainty analysis considers errors arising from interpolation in Table IX-2.

Consider one variable at a time. Let x be the variable and y be a parameter defined by $f(x)$. The error in linear interpolation for y is (Conte and de Boor 1972 [DIRS 159800], pp. 211-212, Example 4.5):

$$\frac{(x-x_1)(x-x_2)}{2} f''(\xi)$$

where x is the input variable, (x_1, x_2) is the interpolation interval, and $f''(\xi)$ is a value of the second derivative of y with respect to x at some point ξ in the interval (x_1, x_2). The relative error is:

$$\frac{(x-x_1)(x-x_2)}{2} M'$$

The maximum value of $(x-x_1)(x-x_2)/2$ in the interval (x_1, x_2) is $(x_2-x_1)^2/8$. Therefore, the maximum relative error in the interval is $(x_2-x_1)^2 M'/8$.

Suppose the interpolation interval is not at the edge of the table, so that for $x_0 < x_1 < x_2 < x_3$ we have the values y_0, y_1, y_2, and y_3. By the mean value theorem for derivatives (Conte and de Boor 1972 [DIRS 159800], p. 23, Theorem 1.6), there is x_a in (x_0, x_1) where

$$f'(x_a) = \frac{y_1 - y_0}{x_1 - x_0} \qquad \text{(Eq. IX-32)}$$

Similarly, there is x_b in (x_2, x_3) where

$$f'(x_b) = \frac{y_3 - y_2}{x_3 - x_2} \qquad \text{(Eq. IX-33)}$$

Applying the mean value theorem for derivatives one more time, there is x_m in (x_a, x_b) where

$$f''(x_m) = \frac{f'(x_b) - f'(x_a)}{x_b - x_a} \qquad \text{(Eq. IX-34)}$$

Because the smallest possible value of $x_b - x_a$ is $x_2 - x_1$,

$$\left|\frac{d^2 y}{dx^2}(x_m)\right| \le \frac{\left|\frac{y_3 - y_2}{x_3 - x_2} - \frac{y_1 - y_0}{x_1 - x_0}\right|}{x_2 - x_1} \qquad \text{(Eq. IX-35)}$$

so that the right hand side is a high estimate of the second derivative somewhere in (x_0, x_3). We use it as though it were a high estimate of the magnitude of $f''(\xi)$. Therefore, a high estimate for the magnitude of M' is:

$$\frac{1}{(x_2 - x_1)\text{Min}(y_1, y_2)}\left|\frac{y_3 - y_2}{x_3 - x_2} - \frac{y_1 - y_0}{x_1 - x_0}\right|$$

where Min (y_1, y_2) is the minimum value of y between x_1 and x_2.

We now address interpolation with respect to r^*. Table IX-4 provides the parameter table for r^* values of 0.1, 0.2, 0.5, and 0.8 (Kays and Leung 1963 [DIRS 160763], pp. 552 to 554) and the calculation of M'. All calculations in this appendix were performed to many significant digits, with the results being rounded for presentation in tables.

Consider, for example, the parameter Nu_{ii} as a function of r^*, with Re fixed at 10,000. The values of x_0, x_1, x_2, and x_3 are 0.1, 0.2, 0.5, and 0.8. The values of y_0, y_1, y_2, and y_3 are 48.5, 38.6, 30.9, and 28.5. At some unknown location x_a between 0.1 and 0.2, the derivative of the function is (38.6 – 48.5)/(0.2 – 0.1), which is –99. Similarly, there is a location x_b between 0.5 and 0.8 where the derivative of the function is (28.5 – 30.9)/(0.8 – 0.5), or –8.0.

Therefore, there is some x_m between x_a and x_b, where the second derivative is [–8.0 – (–99]/(x_b – x_a), or 91/(x_b – x_a). We do not know the value of either x_a or x_b, but we know that one is not larger than 0.2 and the other is no smaller than 0.5, so that their difference must be at least 0.3. Therefore, we know that there is some point between 0.1 and 0.8 where the second derivative is less than 303 (about 91 divided by 0.3).

If the function is sufficiently smooth, x_m will be between x_1 and x_2. To get a high estimate of M', we divide by the smallest value of y between x_1 and x_2, which is 30.9. Therefore, the high estimate of M' is 9.8 (303 divided by 30.9). In fact, this is the largest value for any function in Table IX-4, so for interpolation with respect to r^*, we take the upper bound on M' to be 10.

Table IX-4. High Estimate of Second Derivative with Respect to r^*

Re	10,000				
	r^*	Nu_{ii}	θ_i	Nu_{oo}	θ_o
	0.1	48.5	0.512	29.8	0.032
	0.2	38.6	0.412	29.4	0.063
	0.5	30.9	0.300	28.3	0.137
	0.8	28.5	0.224	28.0	0.192
	$\delta y/\delta x(x_a)$	-99.0	-1.0	-4.0	0.3
	$\delta y/\delta x(x_b)$	-8.0	-0.3	-1.0	0.2
	$\delta^2 y/\delta x^2(x_m)$	303.3	2.5	10.0	0.4
	M'	9.8	8.296	0.4	6.702
Re	30,000				
	r^*	Nu_{ii}	θ_i	Nu_{oo}	θ_o
	0.1	98.0	0.407	66.0	0.028
	0.2	79.8	0.338	64.3	0.055
	0.5	66.0	0.258	62.0	0.119
	0.8	62.3	0.212	61.0	0.166
	$\delta y/\delta x(x_a)$	-182.0	-0.7	-17.0	0.3
	$\delta y/\delta x(x_b)$	-12.3	-0.2	-3.3	0.2
	$\delta^2 y/\delta x^2(x_m)$	565.6	1.8	45.6	0.4
	M'	8.6	6.934	0.7	6.869
Re	100,000				
	r^*	Nu_{ii}	θ_i	Nu_{oo}	θ_o
	0.1	235.0	0.338	167.0	0.024
	0.2	196.0	0.286	165.0	0.049
	0.5	166.0	0.225	158.0	0.107
	0.8	157.0	0.186	156.0	0.150
	$\delta y/\delta x(x_a)$	-390.0	-0.5	-20.0	0.3
	$\delta y/\delta x(x_b)$	-30.0	-0.1	-6.7	0.1
	$\delta^2 y/\delta x^2(x_m)$	1200.0	1.3	44.4	0.4
	M'	7.2	5.778	0.3	7.256

Now consider interpolation with respect to Reynolds numbers. For each interval (Re_n, Re_{n+1}) in the table, Re_{n+1} is approximately $3Re_n$. Therefore, the maximum relative error, $(Re_{n+1} - Re_n)^2 M'/8$, is $0.5(Re_n)^2 M'$.

For the EBS Ventilation Test Series, the inner and outer diameters were 40.64 cm and 1.37 m (BSC 2003 [DIRS 160724], Sections 2.2.2.1 and 2.2.2.2), so that $r^* = 0.297$. Table IX-5 contains the parameter table after interpolation to $r^* = 0.297$. In order to have four values of *Re*, we take the values for 300,000 from Kays and Leung (1963 [DIRS 160763], pp. 552 to 554).

Table IX-5 shows the derivation of M' and the values of $0.5(Re_1)^2 M'$. Again consider the calculation for the parameter Nu_{ii}, this time as a function of *Re*, with r^* fixed at 0.297. Now the

values of x_0, x_1, x_2, and x_3 are 10,000, 30,000, 100,000, and 300,000, and the values of y_0, y_1, y_2, and y_3 are 36.1, 75.4, 186.3, and 449.5. At some unknown Reynolds number x_a between 10,000 and 30,000, the derivative of the function is (75.4 – 36.1)/(30000 – 10000), which is 1.96×10^{-3}. Similarly, there is a Reynold number x_b between 100,000 and 300,000 where the derivative of the function is (449.5 – 186.3)/(300000 – 100000), or 1.32×10^{-3}.

Therefore, there is some x_m between x_a and x_b, where the second derivative is $(1.32 \times 10^{-3} - 1.96\times10^{-3})/(x_b - x_a)$, or $-6.4\times10^{-4}/(x_b - x_a)$. We do not know the value of either x_a or x_b, but we know that one is not larger than 30,000 and the other is no smaller than 100,000, so that their difference must be at least 70,000. Therefore, we know that there is some Reynolds number between 10,000 and 300,000 where the magnitude of the second derivative is less than 9.23×10^{-9} (about 6.4×10^{-4} divided by 70,000).

If the function is sufficiently smooth, x_m will be between x_1 and x_2. To get a high estimate of M', we divide by the smallest value of y between x_1 and x_2, which is 75.4. Therefore, the high estimate of M' is 1.22×10^{-10} (about 9.2×10^{-9} divided by 75.4) and the maximum relative error for Reynolds numbers between 30,000 and 100,000 is 5.5%, which is $0.5 \times (30{,}000)^2 \times 1.22 \times 10^{-10}$. The results in Table IX-5 indicate that the relative error should be no more than about 7%.

Table IX-5. High Estimate of Second Derivative with Respect to *Re*

r^* 0.297				
Re	Nu_{ii}	θ_i	Nu_{oo}	θ_o
10,000	36.1	0.376	29.0	0.087
30,000	75.4	0.312	63.6	0.076
100,000	186.3	0.266	162.7	0.068
300,000	449.5	0.243	391.5	0.061
$\delta y/\delta x\,(x_a)$	1.96E-03	-3.18E-06	1.73E-03	-5.61E-07
$\delta y/\delta x\,(x_b)$	1.32E-03	-1.19E-07	1.14E-03	-3.31E-08
$\delta^2 y/\delta x^2\,(x_m)$	9.23E-09	4.38E-11	8.31E-09	7.54E-12
M'	1.22E-10	1.64E-10	1.31E-10	1.11E-10
$0.5M'(30{,}000)^{\wedge 2}$	5.5%	7.4%	5.9%	5.0%
$\delta x/\delta y\,(y_a)$	5.10E+02		5.79E+02	
$\delta x/\delta y\,(y_b)$	7.60E+02		8.74E+02	
$\delta^2 x/\delta y^2\,(y_m)$	2.26E+00		2.97E+00	
M'	7.52E-05		9.90E-05	
$M'(y_2-y_1)^2/8$	11.6%		12.2%	

At the bottom of Table IX-5 is an error analysis for the reverse interpolation for $Re_{Ni}(x)$ or $Re_{No}(x)$, starting from Nu_{ii} or Nu_{oo}. The roles of the variables are reversed.

For example, the first derivative of *Re* with respect to Nu_{ii}, at some value of Nu_{ii} between 36.1 and 75.4, is 509 [=(30,000 – 10,000)/(75.4 – 36.1)]. Similarly, the value of the derivative is 760 somewhere between 186 and 450.

Therefore, the value of the second derivative is less than (760 – 509)/(186.3 – 75.4), which is about 2.26, at some value of Nu_{ii} between 36.1 and 450. Dividing by the smallest value of Re in the intermediate interval, 30,000, yields 7.5×10^{-5} as a high estimate for M'.

Therefore, the relative error should be no more than 11.6%, which is the result of $M' \times (186.3 - 75.4)^2/8$. Table IX-5 shows that a similar analysis for reverse interpolation from Nu_{oo} gives 12.2% as a high estimate of the relative error.

IX.3.3 Uncertainty in Nusselt Numbers from the Natural Convection Methodology

This section evaluates the following sources of uncertainty in effective circumferential Nusselt numbers calculated from the natural convection correlation:

1. The extent to which measured Nusselt numbers for concentric, coextensive, isothermal cylinders deviate from the effective circumferential Nusselt numbers predicted by the correlation.

2. The uncertainty arising from applying a correlation for a diameter ratio of 0.38 to configurations with other diameter ratios in the range 0.2 to 0.5.

3. Uncertainty in the effective circumferential Nusselt numbers arising from temperature variation along the lengths of the cylinders.

This section also discusses the following sources of uncertainty, which must be evaluated for each particular application:

1. The uncertainty in effective circumferential Nusselt numbers for coextensive, isothermal cylinders arising from eccentric location of the inner cylinder.

2. The uncertainty in effective circumferential Nusselt numbers for isothermal cylinders arising from unequal cylinder lengths.

3. Uncertainty in the effective circumferential Nusselt numbers arising from temperature variation along the circumferences of the cylinders.

This uncertainty analysis does not estimate the error from applying the natural convection correlation to situations in which the outer surface is hotter than the air (Figure IX-1d).

IX.3.3.1 Deviations in Measured $\overline{Nu_N}$ for Concentric, Coextensive, and Isothermal Cylinders

This section estimates the uncertainty inherent in the Kuehn-Goldstein correlation, even when applied to idealized configurations.

One definition of a Nusselt number for *overall* convection between the two cylinders is:

$$\overline{Nu}_{conv} = \frac{D_i \overline{q}_i''}{k\left(\overline{T}_i - \overline{T}_o\right)} \qquad \text{(Eq. IX-36)}$$

As suggested by Kuehn and Goldstein (1978 [DIRS 130084], p. 639), the three Nusselt numbers are related by:

$$\overline{Nu}_{conv}(x) = \left(\frac{1}{Nu_i'} + \frac{1}{Nu_o'}\right)^{-1} = \left[\frac{\left(1/r^* - 1\right)}{\overline{Nu}_i(x)} + \frac{\left(1 - r^*\right)}{\overline{Nu}_o(x)}\right]^{-1} \qquad \text{(Eq. IX-37)}$$

Kuehn and Goldstein (1978 [DIRS 130084]) correlated results of 40 tests for which *Pr* was 0.7, r^* was 0.38, and the Rayleigh number ranged widely. After correcting test data for end losses and radiation, they determined that their correlation fit $\overline{Nu}_{conv}$ for *Ra* > 5,000 (33 tests) with a standard deviation of 1.7% (Kuehn and Goldstein 1978 [DIRS 130084], p. 639).

However, a fit to $\overline{Nu}_{conv}$ does not require a fit to each of the values of $\overline{Nu}_{Ni}$ and $\overline{Nu}_{No}$. For example, $\overline{Nu}_{Ni}$ could be too large and $\overline{Nu}_{No}$ too small. These could combine to produce the correct value of $\overline{Nu}_{conv}$, but the predicted value of T_f would be too large.

Kuehn and Goldstein (1978 [DIRS 130084], p. 636) define an average dimensionless fluid temperature, $\overline{\Phi}_b$, by

$$\overline{\Phi}_b = \left(T_f - \overline{T}_o\right) / \left(\overline{T}_i - \overline{T}_o\right) \qquad \text{(Eq. IX-38)}$$

They report that the dimensionless average fluid temperature near the center of the gap obtained from the correlation agrees "fairly well" with the experimental results. They give only one example, for which the experimental result is 0.25 compared to 0.28 given by the correlation (Kuehn and Goldstein 1978 [DIRS 130084], p. 639).

In steady natural convection, the total heat flux at the two cylinders must be equal and opposite. That is:

$$\overline{q_i''}\ D_i = -\overline{q_0''}\ D_0 \qquad \text{(Eq. IX-39)}$$

The average dimensionless fluid temperature, $\overline{\Phi}_b$, is related to the ratio $\overline{Nu}_{conv} / \overline{Nu}_0$, or alternatively to the ratio $\overline{Nu}_{conv} / \overline{Nu}_i$. A derivation of the relationship between $\overline{\Phi}_b$ and $\overline{Nu}_{conv} / \overline{Nu}_0$ starts with Equation IX-28, first substitutes for the temperature differences from Equations IX-16 and IX-36, and then uses Equations IX-39 and IX-3 to simplify. The resulting expression can be converted to use $\overline{Nu}_{conv} / \overline{Nu}_i$ by applying Equation IX-37. The result is:

$$\overline{\Phi}_b = \frac{-\overline{q}_o''/\overline{h}_o}{D_i \overline{q}_i''/k\overline{Nu}_{conv}} = \frac{(D_o - D_i)\overline{Nu}_{conv}}{D_0 \overline{Nu}_o} = \left(1 - r^*\right)\frac{\overline{Nu}_{conv}}{\overline{Nu}_o} = 1 - \left(\frac{1}{r^*} - 1\right)\frac{\overline{Nu}_{conv}}{\overline{Nu}_i} \qquad \text{(Eq. IX-40)}$$

Therefore, if $\overline{Nu_{\text{conv}}}$ is relatively accurate, an error of +12% in $\overline{\phi}_b$ corresponds to a value of $\overline{Nu_{Ni}}$ that is about 12% too high and a value of $\overline{Nu_{No}}$ that is about 12% too low.

This appendix uses an *a priori* normal distribution for a Type B evaluation of the uncertainty inherent in the Kuehn-Goldstein correlation. This analysis assigns a relative standard uncertainty of 12% to predictions of $\overline{Nu_{Ni}}$ and $\overline{Nu_{No}}$ for concentric, coextensive, isothermal cylinders with r^* = 0.38. The smaller error for $\overline{Nu}_{conv}$ indicates that the errors in $\overline{Nu_{Ni}}$ and $\overline{Nu_{No}}$ tend to be equal and opposite. With only one data point available, this uncertainty analysis treats the error as random rather than systematic.

IX.3.3.2 Uncertainty in $\overline{Nu_N}$ from Diameter Ratio

For $Ra > 10^8$, Pr = 0.7, and r^* = 0.33 or 0.5, the agreement between the Kuehn-Goldstein correlation for natural convection was within 5% of the experimental data (Kuehn and Goldstein 1976 [DIRS 100675], Figure 2). Kuehn and Goldstein (1978 [DIRS 130084], p. 639, Eq. 1) presented a modified correlation for the same data which provided an even better fit. Therefore, this appendix neglects any additional uncertainty for r^* between 0.2 and 0.5.

IX.3.3.3 Uncertainty in $\overline{Nu_N}$ from Longitudinal Temperature Variation

In natural convection, there should be no longitudinal gradient. To the extent that there are longitudinal gradients in a natural convection test, they are considered to be the result of end effects, and the test results are corrected for these effects. Therefore, there is no uncertainty associated with longitudinal temperature gradients in natural convection.

In mixed convection, there is a longitudinal gradient that is expected from forced convection. In this appendix, any effects on the natural convection Nusselt number from a longitudinal temperature gradient are included in the uncertainties inherent in combining the two correlations into a mixed convection model.

IX.3.3.4 Uncertainty in $\overline{Nu_N}$ from Eccentricity

Kuehn and Goldstein (1978 [DIRS 130084], p. 637) reported the effects of eccentricity on heat transfer coefficients. The *overall* heat transfer coefficients tend to increase by 10 percent as the inner cylinder is moved downward from the concentric position to an e^* of –2/3.

The methodology is limited to values between 0 and –2/3 (Section IX.1.6.3). This appendix uses that information for a Type B evaluation of uncertainty by assuming that the error is linear with the eccentricity. That is, the use of the concentric correlation systematically underestimates the heat transfer coefficients. The fractional error is about $-0.15\,|e^*|$, so that it would be zero if the cylinders were concentric and is –0.1 when the value of e^* is –2/3.

IX.3.3.5 Uncertainty in $\overline{Nu_N}$ from Unequal Cylinder Lengths

In a particular configuration, the outer cylinder may be longer than the inner cylinder. The inner cylinder may be a series of waste packages with gaps between them, reducing the heated length of the inner cylinder. The additional area of the outer cylinder may permit more convective heat transfer from the air to the outer cylinder. Therefore, the air temperature may be closer to the temperature of the outer cylinder than it would be if the inner cylinder extended the entire length of the outer cylinder.

The contribution to uncertainty from the length difference may be neglected if the following conditions hold:

1. The greater length of the outer cylinder does not cause a qualitative change in the flow from natural convection other than mild divergence and convergence along the axis.

2. The change in the Rayleigh numbers appearing in the correlation, caused by the change in air temperature, properly accounts for most of the changes in the circumferential average Nusselt numbers.

3. The remaining effects of the longer outer cylinder are not significant compared to the other contributions to uncertainty.

IX.3.3.6 Uncertainty in $\overline{Nu_N}$ from Circumferential Temperature Variation

It may be that heat transfer by thermal conductivity within one or both cylinders is not sufficient to maintain a cylinder at nearly uniform temperature. In such a case, one must consider how accurately the natural convection correlation predicts an effective circumferential Nusselt number.

Kuehn and Goldstein (1978 [DIRS 130084], p. 637) observed that moving a heated inner cylinder below its concentric position results in more uniform local coefficients on the outer cylinder. However, this uncertainty analysis uses results for concentric cylinders.

Because the inner cylinder is hotter than the outer cylinder and the flow develops as shown in Figure IX-1a, natural convection cools the bottom of the inner cylinder more effectively than the top and transfers heat to the top of the outer cylinder more effectively than to the bottom. Therefore, both cylinders are hotter at the top than at the bottom. For pure natural convection, in which T_f is between the temperatures of the cylinders, the magnitude of the temperature difference between the inner cylinder and the fluid is smallest at the bottom. For the outer cylinder, on the other hand, the difference is smallest at the top.

Kuehn and Goldstein (1978 [DIRS 130084]) obtained temperature distributions and local heat transfer coefficients using time-averaged interferograms. For four Rayleigh numbers, they plotted local equivalent conductivities (which are proportional to the local heat transfer coefficients) for isothermal cylinders as a function of angular position numbers (Kuehn and Goldstein 1978 [DIRS 130084], Figure 8).

First, consider the inner cylinder. Because the inner cylinder is hotter than the outer cylinder and the flow develops as shown in Figure IX-1a, natural convection cools the bottom of the inner cylinder more effectively than the top. Therefore, if conduction within the cylinder is not sufficient to maintain a uniform temperature, the inner cylinder is hotter at the top than at the bottom. The magnitude of the temperature difference between the inner cylinder and the fluid is *smallest* at the bottom.

For four Rayleigh numbers, Kuehn and Goldstein (1978 [DIRS 130084], Figure 8) plotted local heat transfer coefficients for concentric isothermal cylinders as a function of angular position. Their plot shows that h_i is smallest at the top of the cylinder, may increase by a factor of five or more at the sides, and stays within 50% of that value along the bottom half of the cylinder.

To estimate the effect of deviations from temperature uniformity around the inner cylinder, we use the approximation that the heat transfer coefficients are not affected. We let h_T be the heat transfer coefficient around the top quarter of the cylinder and assign $5h_T$ as the heat transfer coefficient around the rest of the circumference.

For an isothermal inner cylinder, the effective circumferential heat transfer coefficient is the same as the average, which is $4h_t$. For varying temperatures at the top, left, bottom, and right, each representing the average over one-quarter of the circumference, we have:

$$\bar{h}_i[\bar{T}_i - T_f] = \frac{h_t[T_t - T_f] + 5h_t[T_l - T_f] + 5h_t[T_r - T_f] + 5h_t[T_b - T_f]}{4} \qquad \text{(Eq. IX-41)}$$

Adding and subtracting $h_t\ [T_t - T_f]$ on the right and letting $\bar{T}_i$ be the average of the four temperatures, we obtain:

$$\bar{h}_i[\bar{T}_i - T_f] = 5h_t[\bar{T}_i - T_f] - h_t[T_t - T_f] \qquad \text{(Eq. IX-42)}$$

$$\bar{h}_i = 5h_t - \frac{h_t[T_t - T_f]}{[\bar{T}_i - T_f]} = 4h_t + \frac{h_t[\bar{T}_i - T_f]}{[\bar{T}_i - T_f]} - \frac{h_t[T_t - T_f]}{[\bar{T}_i - T_f]} \qquad \text{(Eq. IX-43)}$$

$$\bar{h}_i = 4h_t - \frac{h_t[T_t - \bar{T}_i]}{[\bar{T}_i - T_f]} \qquad \text{(Eq. IX-44)}$$

The error from using the average,

$$\tilde{h}_i = \frac{h_t + 5h_t + 5h_t + 5h_t}{4} = 4h_t \qquad \text{(Eq. IX-45)}$$

is

$$\tilde{h}_i - \bar{h}_i = \frac{\bar{h}_i[T_t - \bar{T}_i]}{[\bar{T}_i - T_f]} = +0.25\frac{\tilde{h}_i[T_t - \bar{T}_i]}{[\bar{T}_i - T_f]} \qquad \text{(Eq. IX-46)}$$

so that the relative error is about $+0.25[T_t - \overline{T}_i]/[\overline{T}_i - T_f]$. This is also the relative error in the inner-cylinder Nusselt number.

Now, consider the outer cylinder. As shown in Figure IX-1a, natural convection transfers heat to the top of the outer cylinder more effectively than to the bottom. Therefore, if conduction within the cylinder is not sufficient to maintain a uniform temperature, the outer cylinder is hotter at the top than at the bottom. For pure natural convection, in which T_f is between the temperatures of the cylinders, the magnitude of the temperature difference between the inner cylinder and the fluid is *smallest* at the top.

The Kuehn and Goldstein chart (1978 [DIRS 130084], Figure 8) shows that h_o is largest at the top of the outer cylinder, drops by a factor of three or more at the sides, and drops to zero along the bottom of the cylinder.

To estimate the effect of deviations from temperature uniformity around the outer cylinder, we again use the approximation that the heat transfer coefficients are not affected. We let h_t be the heat transfer coefficient around the top quarter of the cylinder and assign $h_t/3$ as the heat transfer coefficient at the sides. As in the application to the EBS tests, we exclude the bottom quarter from the analysis.

For an isothermal outer cylinder, the effective circumferential heat transfer coefficient is the same as the average of the three coefficients, which is $5h_t/9$. For varying temperatures at the top, left, and right, each representing the average over one-quarter of the circumference, and using the relative heat transfer coefficients from the previous paragraph, we have

$$\overline{h}_o[T_f - \overline{T}_o] = \frac{h_t[T_f - T_t] + \frac{1}{3}h_t[T_f - T_l] + \frac{1}{3}h_t[T_f - T_R]}{3} \qquad \text{(Eq. IX-47)}$$

In this case, we subtract and add $\frac{2}{9}h_t\left[T_f - T_t\right]$ on the right and let $\overline{T}_o$ be the average of these temperatures to obtain

$$\overline{h}_o[T_f - \overline{T}_o] = \frac{1}{3}h_t[T_f - \overline{T}_o] + \frac{2}{9}h_t[T_f - T_t] \qquad \text{(Eq. IX-48)}$$

$$\overline{h}_o = \frac{1}{3}h_t + \frac{2}{9}h_t\frac{[T_f - T_t]}{[T_f - \overline{T}_o]} = \frac{5}{9}h_t - \frac{2}{9}h_t\frac{[T_f - \overline{T}_o]}{[T_f - \overline{T}_o]} + \frac{2}{9}h_t\frac{[T_f - T_t]}{[T_f - \overline{T}_o]} \qquad \text{(Eq. IX-49)}$$

$$\overline{h}_o = \frac{5}{9}h_t - \frac{2}{9}h_t\frac{[T_t - \overline{T}_o]}{[T_f - \overline{T}_o]} \qquad \text{(Eq. IX-50)}$$

The error from using the average,

$$\tilde{h}_o = \frac{h_t + \frac{1}{3}h_t + \frac{1}{3}h_t}{3} = \frac{5}{9}h_t \qquad \text{(Eq. IX-51)}$$

is

$$\tilde{h}_o - \bar{h}_o = +\frac{2}{9}\frac{h_t[T_t - \bar{T}_o]}{[T_f - \bar{T}_o]} = +\frac{2}{5}\frac{\tilde{h}_o[T_t - \bar{T}_o]}{[T_f - \bar{T}_o]} \qquad \text{(Eq. IX-52)}$$

so that the relative error is about $+0.4[T_t - \bar{T}_o]/[T_f - \bar{T}_o]$. This is also the relative error in the outer-cylinder Nusselt number.

IX.3.4 Uncertainty in Nusselt Numbers from the Forced Convection Correlation

This uncertainty analysis evaluates the following sources of uncertainty in effective circumferential Nusselt numbers calculated from the forced convection correlation:

1. Uncertainty in the Nusselt numbers arising from flux variation along the lengths of the cylinders.

2. Uncertainty in the effective circumferential Nusselt numbers arising from flux variation along the circumferences of the cylinders.

This section also discusses the following sources of uncertainty, which must be evaluated for each particular application:

1. The extent to which measured Nusselt numbers for fully developed flow in concentric, coextensive, uniform-flux cylinders deviate from the Nusselt numbers predicted by the correlation.

2. Uncertainty from linear interpolation of the Kays-Leung parameters to the diameter ratio of 0.3.

3. Uncertainty from linear interpolation of the Kays-Leung parameters to the appropriate Reynolds number.

4. The uncertainty in effective circumferential Nusselt numbers for fully developed flow in uniform-flux cylinders arising from unequal cylinder lengths.

5. The uncertainty in effective circumferential Nusselt numbers for fully developed flow in coextensive, uniform-flux cylinders arising from eccentric location of the inner cylinder.

6. Uncertainty arising from deviations from fully developed flow.

IX.3.4.1 Uncertainty in Measured $\overline{Nu_F}$ from Flux Variation along the Lengths of the Cylinders

The methodology documented here is limited to configurations in which the waste packages are spaced in the drift such that the heat generation will be roughly constant per unit length of drift. Therefore, the surface flux should vary sufficiently slowly in the axial direction that the flow at each location is approximately the same as if that flux were uniform over the length of the cylinder. Consequently, this analysis neglects that source of error.

IX.3.4.2 Uncertainty in Measured $\overline{Nu_F}$ from Flux Variation along the Circumferences of the Cylinders

In pure forced convection with uniform boundary conditions, there is no dependence on the angle θ. Sutherland and Kays (1964 [DIRS 160789], p. 1189) considered fully developed flow in a concentric annulus with heat flux varying circumferentially, but not axially. They represented the heat fluxes at each surface as a Fourier series of the form:

$$q''(\theta) = \sum_{n=0}^{\infty} \left[a_n \sin(n\theta) + b_n \cos(n\theta) \right] \qquad \text{(Eq. IX-53)}$$

Neglecting thermal conduction in the walls, they derived (Sutherland and Kays 1964 [DIRS 160789], p. 1189, Eqs. 3a and 3b):

$$\begin{aligned} T_i(\theta) - T_f &= \frac{D_o - D_i}{k} \sum_{n=0}^{\infty} R_{n_{ii}} \left[a_{n_i} \sin(n\theta) + b_{n_i} \cos(n\theta) \right] \\ &+ \frac{D_o - D_i}{k} \sum_{n=0}^{\infty} R_{n_{io}} \left[a_{n_o} \sin(n\theta) + b_{n_o} \cos(n\theta) \right] \end{aligned} \qquad \text{(Eq. IX-54)}$$

$$\begin{aligned} T_0(\theta) - T_f &= \frac{D_o - D_i}{k} \sum_{n=0}^{\infty} R_{n_{oi}} \left[a_{n_i} \sin(n\theta) + b_{n_i} \cos(n\theta) \right] \\ &+ \frac{D_o - D_i}{k} \sum_{n=0}^{\infty} R_{n_{oo}} \left[a_{n_o} \sin(n\theta) + b_{n_o} \cos(n\theta) \right] \end{aligned} \qquad \text{(Eq. IX-55)}$$

where the R_n are the eigenfunctions when only one wall is heated. The index n indicates the harmonic of the Fourier expansion, its first subscript is the affected wall, and its second subscript is the heated wall.

Integration of those equations over θ (over 2π) yields:

$$\overline{q}_i'' = 2\pi b_{0i} \qquad \text{(Eq. IX-56)}$$

$$\overline{q}_o'' = 2\pi b_{0_0} \qquad \text{(Eq. IX-57)}$$

$$\frac{k\left(\overline{T}_i - T_f\right)}{D_o - D_i} = R_{0_{ii}}\, 2\pi\, b_{0_i} + R_{0_{io}}\, 2\pi\, b_{0_o} = R_{0_{ii}}\, \overline{q}_i'' + R_{0_{io}}\, \overline{q}_o'' \qquad \text{(Eq. IX-58)}$$

$$\frac{k\left(\overline{T}_0 - T_f\right)}{D_o - D_i} = R_{0_{oi}}\, 2\pi\, b_{0_i} + R_{0_{oo}}\, 2\pi\, b_{0_o} = R_{0_{oi}}\, \overline{q}_i' + R_{0_{oo}}\, \overline{q}_o'' \qquad \text{(Eq. IX-59)}$$

Therefore, the relationships between the mean heat fluxes and the mean temperatures are independent of any axial variation. Consequently, this appendix neglects the uncertainty arising from flux variation around the circumference.

IX.3.4.3 Deviations in Measured $\overline{Nu_F}$ for Concentric, Coextensive, Uniform-Flux Cylinders

The concentric tubes were mounted vertically with airflow from the bottom upward (Reynolds et al. 1963 [DIRS 160770], p. 489). The reported experimental data reflect correction for radiative heat transfer (Kays and Leung 1963 [DIRS 160763], p. 540). Correction for the effects of natural convection were not necessary (as explained previously). They reported measurement uncertainties of about 3% in Nu_{ii} and Nu_{oo} after correction for radiative heat transfer (Kays and Leung 1963 [DIRS 160763], p. 541). They presented the asymptotic Nusselt numbers, both analytical and experimental, for various values of r^*, including 0.255, 0.376, and 0.5 (Kays and Leung 1963 [DIRS 160763], pp. 544-545, Figures 6 to 8).

The measurements were consistently within 3% of the correlation, except that Nu_{ii} tended to deviate from the experimental data at Reynolds numbers below 20,000. At Re = 15,000 and r^* = 0.255, for instance, the correlation predicts a value for Nu_{ii} that is about 10% high (the two labels for "Present analysis" in their Figure 8 having been transposed inadvertently). The mixed-convection methodology is limited to Reynolds numbers greater than 15,000 (Section IX.1.6.3).

Because the contributions of natural convection to the experimental results can be neglected (Section IX.1.5), this appendix uses an *a priori* normal distribution for a Type B evaluation of the uncertainty inherent in the Kays-Leung correlation. For concentric, coextensive, uniform-flux cylinders, this appendix assigns a relative uncertainty of 3% as the random component and an additional systematic error in $\overline{Nu_{Fi}}(x)$ that decreases linearly from 10% to zero as Re increases from 15,000 to 20,000.

IX.3.4.4 Uncertainty in $\overline{Nu_F}$ from Linear Interpolation in Diameter Ratio

The error in linear interpolation for y is (Conte and de Boor 1972 [DIRS 159800], pp. 211-212, Example 4.5).

$$(x - x_0)(x - x_1)M / 2$$

where x is the input variable, (x_0, x_1) is the interpolation interval, and M is a value of the second derivative of y with respect to x somewhere in (x_0, x_1). The analysis in Section IX.3.2 suggests

that the absolute value of M is no more than 10 times the value of the parameters. For $0.5 \geq r^* \geq 0.2$, and letting the worst case value of M correspond to the 95% confidence limit, one may take:

$$5(r^* - 0.2)(0.5 - r^*)$$

as the upper 95% confidence limit in the relative error caused by interpolation in r^*, so that the standard relative uncertainty would be one-half of that value.

IX.3.4.5 Uncertainty in $\overline{Nu_F}$ from Linear Interpolation in Reynolds Number

The maximum error in an interpolation interval is (Conte and de Boor 1972 [DIRS 159800], pp. 211-212, Example 4.5):

$$(x_1 - x_0)^2 M / 8$$

where x is the input variable, (x_0, x_1) is the interpolation interval, and M is a value of the second derivative of y with respect to x somewhere in (x_0, x_1). For the Kays-Leung tables, in which $Re_1 = 3Re_0$, the maximum error is $0.5(Re_0)^2 M$. Section IX.3.2 provides an example demonstrating the evaluation of M from the table developed in Step P2. One may take $0.5(Re_0)^2 M$ as the upper 95% confidence limit in the error caused by interpolation in Re.

IX.3.4.6 Uncertainty in $\overline{Nu_F}$ from Eccentric Location of the Inner Cylinder

Here we estimate the error caused by using a correlation developed for concentric cylinders to predict forced-convection Nusselt numbers for eccentric configurations. Our analysis is based on a review of experimental results for the turbulent flow of air in an eccentric annulus with fully developed constant heat rate (Kays and Perkins 1973 [DIRS 160782], pp. 7-109 to 7-110, Figures 89 and 90).

Although the Nusselt number is uniform around the cylinder for the concentric configuration, eccentricity introduces circumferential variation in the Nusselt numbers. The cited charts provide the ratio of the local Nusselt number to the concentric value, as a function of positive eccentricity, for two opposite locations on the cylinder and two values of r^*. For pure forced convection, there is no difference between positive and negative eccentricity. The locations where the cylinders are most separated (labeled A in the figures) correspond to the tops of the cylinders in a configuration with negative eccentricity.

First, we consider the inner cylinder. We take the effect on Nu_{ii} as an estimate of the effect on $\overline{Nu_{Fi}}(x)$. We consider only the effect at the bottom, where the local heat transfer coefficient may be greater by about a factor of 5 (from natural convection; see Kuehn and Goldstein 1978 [DIRS 130084], Figure 8). For the two values of r^*, with heating from the inner surface and the outer surface insulated, piecewise linear fits (by inspection) to the data in the region of interest (Kays and Perkins 1973 [DIRS 160782], pp. 7-109, Figure 89, "B") result in the following approximations:

$$\frac{\overline{Nu_{Fi}}(x)}{\mathrm{Nu}_{ii}(Re)} = 1 + 0.15e^{*}, \quad r^{*} = 0.255,\ 0 \geq e^{*} \geq -0.67 \qquad \text{(Eq. IX-60)}$$

$$\frac{\overline{Nu_{Fi}}(x)}{\mathrm{Nu}_{ii}(Re)} = 1, \quad r^{*} = 0.5,\ 0 \geq e^{*} \geq -0.27 \qquad \text{(Eq. IX-61)}$$

$$\frac{\overline{Nu_{Fi}}(x)}{\mathrm{Nu}_{ii}(Re)} = 1 + 0.5\left(e^{*} + 0.27\right), \quad r^{*} = 0.5,\ -0.27 \geq e^{*} \geq -0.67 \qquad \text{(Eq. IX-62)}$$

The following general form for the relative error, $1 - \frac{\overline{Nu_{Fi}}(x)}{\mathrm{Nu}_{ii}(Re)}$, covers the range $0.5 \geq r^{*} \geq 0.2$ and matches the above equations at $r^{*} = 0.255$ and $r^{*} = 0.5$:

$$1 - \frac{\overline{Nu_{Fi}}(x)}{\mathrm{Nu}_{ii}(Re)} = -\frac{r^{*} - 0.15}{0.7}e^{*}, \quad 0.3 \geq r^{*} \geq 0.2,\ 0 \geq e^{*} \geq -0.67 \qquad \text{(Eq. IX-63)}$$

$$1 - \frac{\overline{Nu_{Fi}}(x)}{\mathrm{Nu}_{ii}(Re)} = 0, \quad 0.5 \geq r^{*} \geq 0.3,\ 0 \geq e^{*} \geq 0.405\text{-}1.35r^{*} \qquad \text{(Eq. IX-64)}$$

$$1 - \frac{\overline{Nu_{Fi}}(x)}{\mathrm{Nu}_{ii}(Re)} = -\frac{r^{*} - 0.15}{0.7}\left(e^{*} + 1.35r^{*} - 0.405\right),$$

$$0.5 \geq r^{*} \geq 0.3,\ 0.405\text{-}1.35r^{*} \geq e^{*} \geq -0.67 \qquad \text{(Eq. IX-65)}$$

For the outer cylinder, we take the effect on Nu_{oo} as representative of the effect on $\overline{Nu_{Fo}}(x)$. We consider only the effect at the top, because the local heat transfer coefficient may drop to zero at the bottom (from natural convection; see Section IX.3.3). For the two values of r^{*}, with heating from the outer surface and the inner surface insulated, the ratio is approximately (Kays and Perkins 1973 [DIRS 160782], p. 7-110, Figure 90, "A"):

$$\frac{\overline{Nu_{Fo}}(x)}{\mathrm{Nu}_{oo}(Re)} = 1, \quad r^{*} = 0.255,\ 0 \geq e^{*} \geq -0.4 \qquad \text{(Eq. IX-66)}$$

$$\frac{\overline{Nu_{Fo}}(x)}{\mathrm{Nu}_{oo}(Re)} = 1 + 0.15\left(e^{*} + 0.4\right), \quad r^{*} = 0.255,\ -0.4 \geq e^{*} \geq -0.67 \qquad \text{(Eq. IX-67)}$$

$$\frac{\overline{Nu_{Fo}}(x)}{\mathrm{Nu}_{oo}(Re)} = 1, \quad r^{*} = 0.5,\ 0 \geq e^{*} \geq -0.53 \qquad \text{(Eq. IX-68)}$$

$$\frac{\overline{Nu_{Fo}}(x)}{\mathrm{Nu}_{oo}(Re)} = 1 + 0.35\left(e^{*} + 0.53\right), \quad r^{*} = 0.5,\ -0.53 \geq e^{*} \geq -0.67 \qquad \text{(Eq. IX-69)}$$

The following is the linear form for the relative error, $1 - \frac{\overline{Nu_{Fo}}(x)}{\mathrm{Nu}_{oo}(Re)}$, $0.5 \geq r^{*} \geq 0.2$, that matches the above equations at $r^{*} = 0.255$ and $r^{*} = 0.5$:

$$1 - \frac{\overline{Nu_{Fo}}(x)}{\mathrm{Nu}_{oo}(Re)} = 0, \quad 0.5 \geq r^{*} \geq 0.2,\ 0 \geq e^{*} \geq -\frac{26r^{*} + 12.97}{49} \qquad \text{(Eq. IX-70)}$$

$$1 - \frac{\overline{Nu_{Fo}}(x)}{\mathrm{Nu}_{oo}(Re)} = -\frac{r^{*} - 0.07125}{1.225}\left(e^{*} + \frac{26r^{*} + 12.97}{49}\right), \quad 0.5 \geq r^{*} \geq 0.2,$$

$$-\frac{26r^{*} + 12.97}{49} \geq e^{*} \geq -0.67 \qquad \text{(Eq. IX-71)}$$

That is, the error in $\overline{Nu_{Fi}}(x)$ is positive, with a formula that depends on the value of r^{*}. If $0.3 \geq r^{*} \geq 0.2$ and $0 \geq e^{*} \geq -0.67$, Equation IX-63 shows that there is a systematic relative error in $\overline{Nu_{Fi}}(x)$ of about $\left(-e^{*}\right)\frac{r^{*} - 0.15}{0.7}$.

For $0.5 \geq r^{*} \geq 0.3$, the error in $\overline{Nu_{Fi}}(x)$ is not significant if $0 \geq e^{*} \geq 0.405 - 1.35r^{*}$; otherwise, there is a systematic relative error in $\overline{Nu_{Fi}}(x)$ of about (Equation IX-65) $+\left(-e^{*} + 0.405 - 1.35r^{*}\right)\frac{r^{*} - 0.15}{0.7}$.

The error in $\overline{Nu_{Fo}}(x)$ is negligible if $0 \geq e^{*} \geq -\frac{26r^{*} + 12.97}{49}$. Otherwise, Equation IX-71 shows that there is a systematic relative error in $\overline{Nu_{Fo}}(x)$ of about $+\frac{r^{*} - 0.07125}{1.225}\left(-e^{*} - \frac{26r^{*} + 12.97}{49}\right)$.

IX.3.4.7 Uncertainty in Measured $\overline{Nu_{F}}$ from Unequal Cylinder Lengths

As in natural convection, any additional area in the outer cylinder may permit more convective heat transfer from the air to the outer cylinder. Also, where the inner cylinder is not present, the orifice area increases from $\pi\,(D_o - D_i)^2/4$ to $\pi\,D_o^2/4$, by a factor of $1/(1-r^{*})^2$. Because the mass flow rate must be the same and density does not change significantly, air velocity must drop by a factor of $(1-r^{*})^2$. If the additional length of the cylinder is sufficiently small, the contribution to uncertainty from the length difference may be neglected. Alternatively, if r^{*} is sufficiently small, the effect of the greater length of the outer cylinder may be accounted for by applying the predicted Nusselt number to the additional area.

IX.3.4.8 Uncertainty in Measured $\overline{Nu_F}$ from Deviations from Fully Developed Flow

Kays and Leung also considered thermally developing annular flow. They presented non-dimensional fluid temperatures, including parameters labeled θ_{ii} and θ_{oo}, for thermally developing annular flow with r^*=0.255 (Kays and Leung 1963 [DIRS 160763], p. 542, Figure 2). The parameters Nu_{ii} and Nu_{oo} are approximately the inverses of θ_{ii} and θ_{oo}, respectively. The Nusselt numbers start out at about twice their asymptotic value but decay to within 10% of their asymptote in a distance of about ten hydraulic diameters. For $x \le 11$ (D_o-D_i), this uncertainty analysis assigns systematic errors in predictions of $\overline{Nu_{Fi}}(x)$ and $\overline{Nu_{Fo}}(x)$, based on a linear fit to the errors at x = 0 and x = 10 (D_o-D_i), that amount to

$$+\left[1-\frac{x}{11(D_o-D_i)}\right]100\%$$

IX.3.5 Uncertainty in Nusselt Numbers from the Mixed Convection Methodology

The uncertainty in the mixed-convection methodology is affected by the uncertainties in natural convection and forced convection in accordance with the Law of Propagation of Uncertainty (ANSI/NCSL Z540-2-1997 [DIRS 157394], p. 19). Because the preliminary steps are not part of the methodology, this section considers only the uncertainties in Steps N1 through N4. In addition to the uncertainty contributed by the underlying convection correlations, this uncertainty analysis considers two sources of uncertainty in the mixed convection methodology. One is the error from using an approximation to the forced convection correlation (Equations IX-28 and IX-29) to find the equivalent Reynolds number for natural convection. The second source of uncertainty is the variation of measured mixed convection results from the Morgan approximation.

As noted at the beginning of Section IX.3, uncertainties in the input dimensionless groups must be evaluated by using the sensitivity analysis of Section IX.2. In addition, the uncertainty inherent in the methodology depends on the input parameters. Therefore, the prediction uncertainty is not quantified in this section. Section IX.4 provides examples of the evaluation of uncertainty in specific applications.

Step N1 uses interpolation in r^* to create a table of forced-convection parameters that are functions of *Re* only. As discussed in Section IX.3.4, the standard relative uncertainty is

$$2.5(r^* - 0.2)(0.5 - r^*)$$

Step N2 produces the equivalent Reynolds numbers for natural convection, $Re_{Ni}(x)$ and $Re_{No}(x)$. The uncertainty in each of these equivalent Reynolds numbers is a combined relative uncertainty, composed of the following contributions:

1. Relative uncertainty in the appropriate Nusselt number for natural convection, calculated in accordance with Section IX.3.3.

2. Relative uncertainty in the values for $\mathrm{Nu}_{\mathrm{ii}}$ and $\mathrm{Nu}_{\mathrm{oo}}$ produced by Step N1, calculated as described above.

3. Relative uncertainty in the reverse linear interpolation to get $Re_{Ni}(x)$ and $Re_{No}(x)$, calculated in accordance with the discussion of forward interpolation in Section IX.3.4.

4. Relative uncertainty introduced by the approximations represented by Equations IX-28 and IX-29.

The errors from using Equation IX-28 for $Re_{Ni}(x)$ and Equation IX-29 for $Re_{No}(x)$, instead of Equations IX-24 and IX-25, depend on the value of $\tau(x)$ and must therefore be evaluated separately for each application.

In Step N3, the equivalent Reynolds number for inner surface natural convection combines with the Reynolds number for forced convection to produce an equivalent Reynolds numbers for mixed convection. The uncertainty in $Re_{Ni}(x)$ propagates through Equation IX-23 (specialized to the inner surface by adding the subscript *i*). Taking the partial derivative of that equation with respect to $Re_{Ni}(x)$ and multiplying by $Re_{Ni}(x)/Re_{Mi}(x)$ yields:

$$\frac{Re_{Ni}(x)}{Re_{Mi}(x)}\frac{\partial Re_{Mi}(x)}{\partial Re_{Ni}(x)} = \left(\frac{Re_{Ni}(x)}{Re_{Mi}(x)}\right)^2 \qquad \text{(Eq. IX-72)}$$

This factor, applied to the relative uncertainty in $Re_{Ni}(x)$, produces its contribution to the combined relative uncertainty in $Re_{Mi}(x)$ (see Equation IX-31).

Next, Step N3 produces the Nusselt number for the inner surface. There are three contributors to the uncertainty in the Nusselt number:

1. The uncertainty in $Re_{Mi}(x)$, propagated according to the Law of Propagation of Uncertainty and making use of the sensitivity study (Section IX.2)

2. The uncertainty in the forced convection methodology when the input Reynolds number is known, calculated in accordance with Section IX.3.4

3. The uncertainty in mixed-convection Nusselt numbers inherent in the Morgan approximation.

Morgan (1975 [DIRS 160791], p. 249, Figure 10) compared the experimental values from two data sets to the predicted ratio of effective Nusselt number to forced-flow Nusselt number. The experimental value for the ratio was consistently within 15% of the theoretical value. Taking 15% as the 95% confidence limit of an *a priori* normal distribution for a Type B evaluation of the uncertainty, this appendix assigns a standard uncertainty of 7.5% as the relative error inherent in the Morgan approximation for mixed convection.

Step N4 is the same as Step N3, except that it applies to the outer surface. The uncertainty considerations are the same as those for Step N3.

IX.4 COMPARISON OF METHODOLOGY RESULTS TO TEST DATA

This section evaluates the methodology under YMP specific conditions by corroboration of methodology results with data acquired from the EBS Ventilation Test series. Uncertainties in both the measurements and the predictions are considered.

The calculated uncertainties in the previous section determine the accuracy of the predictions for the EBS forced ventilation test configuration, taking into consideration that the cylinders in the EBS model were of different lengths, were not held to either constant temperature or constant flux conditions, and were not concentric. However, the invert and waste package support systems make the EBS test geometry more complex than that for which the uncertainty was evaluated. To determine how appropriate the methodology is for the EBS configuration, it was applied to the EBS ventilation tests. A description of how this was done and the overall results are given below.

IX.4.1 Test Data of Ventilation Test Phase 1 and 2

The Ventilation Test Phase 1 report, *Testing to Provide Data for Ventilation System Design: Phase 1* (BSC 2003 [DIRS 160724], Sections 2.2.4 and 3) presents 24-hour averages of measurements taken at the rate of four per hour. For the Phase 1 tests, the time period chosen was the last full day of data in cases where quasi steady-state conditions were achieved, or the last 24 hours of data collected in cases where recorded temperatures were still increasing with time. For the Phase 2 tests, the averaging period was chosen as the last 24-hour period of the test where the design test conditions were maintained. Appendix XI describes the averaging process, starting from the raw data in DTN: SN0208F3409100.009 [DIRS 163079]. A brief description of the phase 1 and phase 2 ventilation tests is presented in Section 7.1.2 of this report.

A volume flow rate for each test within each phase was calculated using measured differential pressure, relative humidity, barometric pressure, and air temperatures at both the inlet (designated Station A) and the outlet (designated Station D) (BSC 2003 [DIRS 160724], Section 5.2). The 24-hour average flow rates for each of the forced ventilation tests were within 10% of the nominally desired values, as shown in Tables IX-6 and IX-7. No flow rate measurements were reported at Station D for Tests 15 or 16 of Phase 2.

Tables IX-6 and IX-7 also show the 24-hour average line load for each test, which is the total power input divided by the total heated length of the test train, 33.9 m (BSC 2003 [DIRS 160724], Section 2.2.2.2). The standard uncertainty in the 24-hour-average total load was 5.8 W (BSC 2003 [DIRS 160724], Section 3.3.2.4), which is equivalent to a standard uncertainty of 0.2 W/m ($5.8W \div 33.9m \approx 0.2W/m$) in the average line load, much less than 1% ($0.2W/m \div 179W/m \approx 0.1\%$) of the measured average.

The test reports also tabulate average temperatures for 24-hour periods. Tables IX-8 through IX-10 present the calculated average temperatures at a point midway along the heated portion of the test train (Station 3). Values in the tables are reported by quadrant (top, right, bottom, and left) for sensors located on the external surface of the waste package, the internal and external

surfaces of the concrete pipe, the external surface of the insulation, and within the annulus between the waste package and concrete pipe (ventilation air).

Table IX-6. Averaged Flow Rates and Line Loads and Their Standard Uncertainties for EBS Ventilation Tests, Phase 1

Test No.	Nominal Flow Rate (m^3/s)	Station A, Flow Rate (m^3/s)	Station D, Flow Rate (m^3/s)	Flow Rate Uncertainty (m^3/sec)	Nominal Line Load (W/m)	Avg. Line Load (W/m)
1	1	0.997	1.001	0.014	180	182
2	0.5	0.501	0.495	0.03	180	179
3	1	0.998	1.016	0.014	360	359
4	2	1.990	1.990	0.008	360	362
5	0.5	0.519	0.525	0.03	360	362
6	3	3.048	3.052	0.02	360	364
NC1	—	—	—	—	120	120
NC2	—	—	—	—	240	242

Source: BSC 2003 [DIRS 160724], Tables 3-16 and 5-6.

NC1=Natural Convection Test 1; NC2=Natural Convection Test 2.

Table IX-7. Averaged Flow Rates and Line Loads and Their Standard Uncertainties for EBS Ventilation Tests, Phase 2

Test No.	Nominal Flow Rate (m^3/s)	Station A, Flow Rate (m^3/s)	Station D, Flow Rate (m^3/s)	Flow Rate Uncertainty (m^3/sec)	Nominal Line Load (W/m)	Avg. Line Load (W/m)
1	1	1.021	0.972	0.014	220	218
2	1	1.037	0.986	0.014	220	218
3	1	1.058	1.012	0.014	220	216
4	1	1.054	1.003	0.014	220	215
5	1	1.024	0.989	0.014	360	360
6	1	1.041	1.005	0.014	360	359
7	1	1.053	1.011	0.014	360	357
8	1	1.055	1.013	0.014	360	358
9	0.5	0.516	0.506	0.03	220	215
10	0.5	0.552	0.544	0.03	220	215
11	0.5	0.554	0.530	0.03	220	216
12	0.5	0.547	0.553	0.03	360	360
13	0.5	0.553	0.550	0.03	360	360
14	0.5	0.553	0.537	0.03	360	361
15	1	0.993	N/A	0.014	360	360
16	1	0.991	N/A	0.014	360	364

Source: Appendix XI of this document.

Table IX-8. Averaged Temperature Values (C) at Station 3 for EBS Ventilation Tests, Phase 1

		Ventilating Air (°C)	WP Surface (°C)	Concrete Pipe Wall (°C)	Concrete/ Insulation Interface (°C)	Outside Insulation Surface (°C)
Test 1	top	—	47.4	30.5	30.7	30.3
	right	27.8	42.0	29.8	30.0	27.5
	bottom	—	39.1	28.4	28.2	26.7
	left	27.4	40.8	30.2	30.1	27.9
Test 2	top	—	51.6	33.6	33.1	28.8
	right	31.4	45.9	32.8	32.7	28.4
	bottom	—	42.9	30.5	30.1	27.1
	left	31.4	44.7	33.4	32.8	27.6
Test 3	top	—	63.4	33.8	33.5	27.8
	right	29.3	54.6	32.7	33.0	26.5
	bottom	—	50.3	30.6	30.0	25.1
	left	29.2	53.3	33.5	33.0	25.9
Test 4	top	—	57.4	29.9	30.0	27.0
	right	27.2	49.4	30.0	30.2	26.0
	bottom	—	45.3	28.8	28.3	25.2
	left	26.8	48.0	29.9	29.9	25.7
Test 5	top		65.6	34.6	33.7	24.5
	right	31.0	56.7	33.5	33.3	23.6
	bottom	—	52.0	29.2	28.4	22.6
	left	31.0	55.0	34.6	33.6	23.6
Test 6	top	—	48.0	23.4	23.5	21.2
	right	21.7	40.6	23.5	23.7	20.6
	bottom	—	36.8	23.3	23.0	20.0
	left	21.7	39.8	23.7	23.7	20.1
Test NC1	top	—	60.9	46.3	43.8	28.2
	right	48.7	56.9	45.7	43.6	28.3
	bottom	—	55.0	38.0	36.7	25.5
	left	48.4	56.3	45.5	43.3	27.4
Test NC2	top	—	93.2	69.4	64.4	33.0
	right	73.4	87.4	68.6	64.2	32.8
	bottom	—	84.9	56.1	51.6	29.0
	left	72.9	86.3	68.3	63.8	31.8

Source: BSC 2003 [DIRS 160724], Tables 5-7 through 5-14.

WP = waste package; NC1=Natural Convection Test 1; NC2=Natural Convection Test 2.

Table IX-9. Averaged Temperature Values (C) at Station 3 for EBS Ventilation Tests, Phase 2, Tests 1 through 8

		Ventilating Air (°C)	WP Surface (°C)	Concrete Pipe Wall (°C)	Concrete/ Insulation Interface (°C)	Outside Insulation Surface (°C)
Test 1	top	—	50.5	30.8	30.8	28.5
	right	27.5	44.3	30.2	30.6	28.5
	bottom	—	41.1	29.4	30.7	28.0
	left	27.3	43.5	30.6	30.5	28.3
Test 2	top	—	59.3	38.8	37.9	30.0
	right	36.9	52.8	38.5	37.8	29.2
	bottom	—	49.9	35.3	35.8	28.4
	left	36.7	51.9	38.6	37.6	28.4
Test 3	top	—	68.4	48.4	47.1	36.6
	right	47.0	62.2	48.2	47.2	36.6
	bottom	—	59.6	44.2	44.7	35.1
	left	46.7	61.3	48.2	46.9	35.8
Test 4	top	—	67.9	48.0	46.6	35.9
	right	46.7	61.7	47.8	46.8	36.3
	bottom	—	59.1	43.8	44.2	34.4
	left	46.5	60.9	47.9	46.6	36.0
Test 5	top	—	64.1	34.4	34.4	31.1
	right	29.8	55.2	33.4	33.8	30.1
	bottom	—	50.8	31.8	33.0	28.7
	left	29.7	54.0	34.1	34.0	30.4
Test 6	top	—	73.6	43.8	43.4	37.2
	right	39.6	64.4	42.9	43.0	36.3
	bottom	—	60.4	39.8	40.9	34.4
	left	39.4	63.1	43.6	43.1	36.5
Test 7	top	—	81.4	51.8	50.3	37.8
	right	49.1	72.7	51.3	50.4	37.9
	bottom	—	69.0	46.4	47.0	35.4
	left	48.7	71.4	51.8	50.4	38.2
Test 8	top	—	81.4	51.6	50.1	37.2
	right	49.0	72.7	51.2	50.2	37.3
	bottom	—	69.0	46.4	46.9	34.8
	left	48.7	71.4	51.6	50.1	37.1

Source: Appendix XI of this document.

WP = waste package.

Table IX-10. Averaged Temperature Values (C) at Station 3 for EBS Ventilation Tests, Phase 2, Tests 9 through 16

		Ventilating Air (°C)	WP Surface (°C)	Concrete Pipe Wall (°C)	Concrete/ Insulation Interface (°C)	Outside Insulation Surface (°C)
Test 9	top	—	55.2	35.3	35.3	33.0
	right	31.6	48.5	34.5	34.8	32.3
	bottom	—	45.1	33.1	34.8	31.0
	left	31.6	47.6	35.0	35.0	32.7
Test 10	top	—	63.5	43.0	42.4	36.2
	right	40.4	56.5	42.5	42.2	36.0
	bottom	—	53.5	39.5	40.9	34.2
	left	40.3	55.7	42.9	42.2	36.2
Test 11	top	—	71.7	51.0	49.7	39.6
	right	49.7	65.1	50.6	49.7	39.4
	bottom	—	62.3	46.1	47.1	36.9
	left	49.6	64.3	50.9	49.7	39.9
Test 12	top	—	71.2	41.0	40.9	35.6
	right	35.9	61.5	40.0	40.4	35.2
	bottom	—	56.9	38.0	39.6	33.8
	left	35.9	60.1	40.8	40.5	35.1
Test 13	top	—	78.0	47.3	46.3	34.8
	right	44.0	68.4	46.9	46.2	35.0
	bottom	—	64.4	42.3	43.1	33.1
	left	43.9	67.2	47.3	46.1	34.5
Test 14	top	—	86.1	55.6	53.7	38.4
	right	53.4	77.0	55.2	53.8	38.2
	bottom	—	73.2	48.3	48.9	35.1
	left	53.3	75.7	55.7	53.9	38.8
Test 15	top	—	68.6	38.4	37.8	29.4
	right	34.6	59.7	37.7	37.7	30.4
	bottom	—	55.4	35.0	36.4	28.8
	left	34.4	58.4	38.3	37.5	28.7
Test 16	top	—	68.6	37.9	37.2	27.9
	right	34.3	59.5	37.2	37.0	28.2
	bottom	—	55.2	34.8	36.1	27.4
	left	34.1	58.2	37.8	36.9	27.1

Source: Appendix XI of this document.

WP = waste package.

IX.4.2 Prediction of Nusselt numbers

This section describes the prediction of Nusselt numbers for the EBS Ventilation Tests, in accordance with the algorithm of Section IX.1.6.

Step P1. (Geometry) For D_i = 0.4064 m and D_o = 1.37 m (Tables 7-4 and 7-5), r^* = 0.297. The predictions ignore the effect of the invert, so that they use a hydraulic diameter of 0.96 m. The effect of the invert would be to reduce the hydraulic diameter to about 0.93 m.

Step P2. (Reynolds Number) To minimize the influence of end effects, the axial position of interest is the most centrally located measurement station (Station 3). The cross-sectional area is 1.34 m^2. For each test, the mean fluid temperature at Station 3, T_f, is the average of the two reported measurements (Tables IX-8 through IX-10). Table 4-17 contains the properties of air at temperatures relevant to the EBS Ventilation Test Series. For each test, Table IX-11 or IX-12 shows the value of T_f, the kinematic viscosity, ν, of air at T_f, linearly interpolated in Table 4-17, the average of the two reported flow rates (Tables IX-6 and IX-7), the mean axial flow velocity calculated by dividing the flow rate by the annulus cross-sectional area, and the value of *Re* calculated using Equation IX-1.

Step P3. (Rayleigh Numbers) The value for g is 9.8 m/s^2 (Table 4-20). For each test (at Station 3), Table IX-13 or IX-14 gives the circumferential average temperature on each surface, based on the measurements in Tables IX-8 through Table IX-10. On the inner surface (the waste package), $\overline{T}_i$ is the average of the four reported measurements. However, because the bottom of the outer surface is covered by the invert, the circumferential average temperature on the outer surface, $\overline{T}_o$, is the average of only the top and side measurements. Tables IX-13 and IX-14 also show the amount that each average differs from its associated T_f, as well as the Rayleigh numbers calculated from Equations IX-5 and IX-6 and the relevant air properties.

Step N1. (Forced-Convection Parameters) Table IX-15 contains the forced-convection parameters as a function of *Re*, for *Pr*=0.7 and r^*=0.297, linearly interpolated from Table IX-2.

Step N2. (Natural Convection) For each test (at Station 3), Table IX-16 or IX-17 gives the effective circumferential Nusselt numbers for natural convection, on the inner and outer surfaces. The tables also show the equivalent Reynolds numbers, calculated in accordance with Equations IX-28 and IX-29.

Step N3. (Inner-Surface Nusselt Number) Tables IX-18 and IX-19 report the mixed-convection Reynolds number at the inner surface for each test, calculated in accordance with Equation IX-26. These tables also report the forced-convection parameters associated with each such Reynolds number, from interpolation in Table IX-11. The last column contains the effective

circumferential Nusselt number convection at the inner surface, from the mixed-convection methodology, Equation IX-24.

Step N4. (Outer-Surface Nusselt Number) Tables IX-20 and IX-21 report the mixed-convection Reynolds number at the outer surface for each test, calculated in accordance with Equation IX-27. These tables also report the forced-convection parameters associated with each such Reynolds number, from interpolation in Table IX-11. The last column contains the effective circumferential Nusselt number for mixed convection at the outer surface, from the mixed-convection methodology, Equation IX-25.

Table IX-11. Reynolds Numbers for EBS Ventilation Test Series, Phase 1

Location	T_f (ºC)	T_f (K)	ν (m^2/s)	V (m^3/s)	u_m (m/s)	Re (Thousands)
Test 1, Station 3	27.60	300.75	1.597E-05	0.999	0.74	44.8
Test 2, Station 3	31.40	304.55	1.635E-05	0.498	0.37	21.8
Test 3, Station 3	29.25	302.40	1.613E-05	1.007	0.75	44.7
Test 4, Station 3	27.00	300.15	1.591E-05	1.990	1.48	89.7
Test 5, Station 3	31.00	304.15	1.631E-05	0.522	0.39	22.9
Test 6, Station 3	21.70	294.85	1.543E-05	3.050	2.27	141.7

Output DTN: MO0306MWDMXCNV.000, worksheet “Dimensionless Inputs” of Phase 1 Supporting Calculations for Mixed Convection.xls.

Table IX-12. Reynolds Numbers for EBS Ventilation Test Series, Phase 2

Location	T_f (ºC)	T_f (K)	ν (m^2/s)	V (m^3/s)	u_m (m/s)	Re (Thousands)
Test 1, Station 3	27.40	300.55	1.595E-05	0.996	0.74	44.8
Test 2, Station 3	36.80	309.95	1.689E-05	1.012	0.75	42.9
Test 3, Station 3	46.85	320.00	1.790E-05	1.035	0.77	41.4
Test 4, Station 3	46.60	319.75	1.788E-05	1.028	0.76	41.2
Test 5, Station 3	29.75	302.90	1.618E-05	1.006	0.75	44.6
Test 6, Station 3	39.50	312.65	1.716E-05	1.023	0.76	42.7
Test 7, Station 3	48.90	322.05	1.811E-05	1.032	0.77	40.8
Test 8, Station 3	48.85	322.00	1.810E-05	1.034	0.77	40.9
Test 9, Station 3	31.60	304.75	1.637E-05	0.511	0.38	22.4
Test 10, Station 3	40.35	313.50	1.725E-05	0.548	0.41	22.8
Test 11, Station 3	49.65	322.80	1.818E-05	0.542	0.40	21.4
Test 12, Station 3	36.15	309.30	1.683E-05	0.550	0.41	23.4
Test 13, Station 3	43.95	317.10	1.761E-05	0.552	0.41	22.5
Test 14, Station 3	53.35	326.50	1.856E-05	0.545	0.41	21.1
Test 15, Station 3	34.50	307.65	1.666E-05	0.993	0.74	42.7
Test 16, Station 3	34.20	307.35	1.663E-05	0.991	0.74	42.7

Output DTN: MO0306MWDMXCNV.000, worksheet “Dimensionless Inputs” of Phase 2 Supporting Calculations for Mixed Convection.xls.

Table IX-13. Rayleigh Numbers for EBS Ventilation Test Series, Phase 1

Location	Avg T_i (ºC)	Avg T_o (ºC)	(T_i-T_f) (ºC)	(T_o-T_f) (ºC)	τ	α (m^2/s)	Ra_i (Millions)	Ra_o (Millions)
Test 1, Station 3	42.33	30.17	14.73	2.567	5.74	2.26E-05	89	596
Test 2, Station 3	46.28	33.27	14.88	1.867	7.97	2.32E-05	85	408
Test 3, Station 3	55.40	33.33	26.15	4.083	6.40	2.29E-05	154	923
Test 4, Station 3	50.03	29.93	23.03	2.933	7.85	2.25E-05	141	687
Test 5, Station 3	57.33	34.23	26.33	3.233	8.14	2.31E-05	151	711
Test 6, Station 3	41.30	23.53	19.60	1.833	10.69	2.18E-05	130	465

Output DTN: MO0306MWDMXCNV.000, worksheet "Dimensionless Inputs" of Phase 1 Supporting Calculations for Mixed Convection.xls.

Table IX-14. Rayleigh Numbers for EBS Ventilation Test Series, Phase 2

Location	Avg T_i (ºC)	Avg T_o (ºC)	(T_i-T_f) (ºC)	(T_o-T_f) (ºC)	τ	α (m^2/s)	Ra_i (Millions)	Ra_o (Millions)
Test 1, Station 3	44.85	30.53	17.45	3.133	5.57	2.26E-05	106	730
Test 2, Station 3	53.48	38.63	16.68	1.833	9.10	2.40E-05	87	368
Test 3, Station 3	62.88	48.27	16.03	1.417	11.31	2.55E-05	72	245
Test 4, Station 3	62.40	47.90	15.80	1.300	12.15	2.54E-05	72	225
Test 5, Station 3	56.03	33.97	26.28	4.217	6.23	2.29E-05	154	945
Test 6, Station 3	65.38	43.43	25.88	3.933	6.58	2.44E-05	130	758
Test 7, Station 3	73.63	51.63	24.73	2.733	9.05	2.58E-05	108	458
Test 8, Station 3	73.63	51.47	24.78	2.617	9.47	2.58E-05	109	439
Test 9, Station 3	49.10	34.93	17.50	3.333	5.25	2.32E-05	99	726
Test 10, Station 3	57.30	42.80	16.95	2.450	6.92	2.45E-05	84	466
Test 11, Station 3	65.85	50.83	16.20	1.183	13.69	2.59E-05	70	196
Test 12, Station 3	62.43	40.60	26.28	4.450	5.90	2.39E-05	139	902
Test 13, Station 3	69.50	47.17	25.55	3.217	7.94	2.50E-05	120	580
Test 14, Station 3	78.00	55.50	24.65	2.150	11.47	2.64E-05	101	338
Test 15, Station 3	60.53	38.13	26.03	3.633	7.16	2.36E-05	141	756
Test 16, Station 3	60.38	37.63	26.18	3.433	7.62	2.36E-05	143	718

Output DTN: MO0306MWDMXCNV.000, worksheet "Dimensionless Inputs" of Phase 2 Supporting Calculations for Mixed Convection.xls.

Table IX-15. Parameters for Annular Forced Convection at Pr = 0.7 and $r^* = 0.297$

Re:	10000	30000	100000	300000	1000000
Nu_{ii}:	36.1	75.4	186.3	449.5	1208.8
θ_i:	0.376	0.312	0.266	0.243	0.219
Nu_{oo}:	29.0	63.6	162.7	391.5	1060.3
θ_o:	0.087	0.076	0.068	0.061	0.056

Output DTN: MO0306MWDMXCNV.000, worksheet "Predicted Nusselt Numbers" of Phase 1 Supporting Calculations for Mixed Convection.xls.

Table IX-16. Natural Convection Nusselt Numbers for EBS Ventilation Test Series, Phase 1

Location	Nu_{Ni}	Nu_{No}	Re_{Ni} (Thousands)	Re_{No} (Thousands)
Test 1, Station 3	131	109	65	62
Test 2, Station 3	129	99	64	55
Test 3, Station 3	156	122	81	71
Test 4, Station 3	152	113	78	65
Test 5, Station 3	155	114	80	66
Test 6, Station 3	148	103	76	58

Output DTN: MO0306MWDMXCNV.000, worksheet "Predicted Nusselt Numbers" of Phase 1 Supporting Calculations for Mixed Convection.xls.

Table IX-17. Natural Convection Nusselt Numbers for EBS Ventilation Test Series, Phase 2

Location	Nu_{Ni}	Nu_{No}	Re_{Ni} (Thousands)	Re_{No} (Thousands)
Test 1, Station 3	139	115	70	66
Test 2, Station 3	130	97	65	53
Test 3, Station 3	123	87	60	47
Test 4, Station 3	123	85	60	45
Test 5, Station 3	156	123	81	72
Test 6, Station 3	148	116	76	67
Test 7, Station 3	139	102	70	57
Test 8, Station 3	140	101	71	57
Test 9, Station 3	136	115	68	66
Test 10, Station 3	129	103	64	58
Test 11, Station 3	122	83	59	43
Test 12, Station 3	151	121	78	71
Test 13, Station 3	144	108	73	62
Test 14, Station 3	137	95	69	52
Test 15, Station 3	152	116	78	67
Test 16, Station 3	152	114	79	66

Output DTN: MO0306MWDMXCNV.000, worksheet "Predicted Nusselt Numbers" of Phase 2 Supporting Calculations for Mixed Convection.xls.

Table IX-18. Predicted Inner-Surface Nusselt Numbers for EBS Ventilation Test Series, Phase 1

Location	Re_{Mi} (Thousands)	$Nu_{ii}(Re_{Mi})$	$Nu_{oo}(Re_{Mi})$	$\theta_i(Re_{Mi})$	$\theta_o(Re_{Mi})$	Nu_{Mi}
Test 1, Station 3	79	153	133	0.280	0.070	163
Test 2, Station 3	68	135	117	0.288	0.071	142
Test 3, Station 3	92	174	152	0.271	0.069	184
Test 4, Station 3	119	211	184	0.264	0.067	221
Test 5, Station 3	83	160	139	0.277	0.070	168
Test 6, Station 3	161	266	232	0.259	0.066	276

Output DTN: MO0306MWDMXCNV.000, worksheet "Predicted Nusselt Numbers" of Phase 1 Supporting Calculations for Mixed Convection.xls.

Table IX-19. Predicted Inner-Surface Nusselt Numbers for EBS Ventilation Test Series, Phase 2

Location	Re_{Mi} (thousands)	$Nu_{ii}(Re_{Mi})$	$Nu_{oo}(Re_{Mi})$	$\theta_i(Re_{Mi})$	$\theta_o(Re_{Mi})$	Nu_{Mi}
Test 1, Station 3	83	159	139	0.278	0.070	170
Test 2, Station 3	78	151	131	0.281	0.070	158
Test 3, Station 3	73	143	124	0.284	0.071	150
Test 4, Station 3	73	143	124	0.284	0.071	149
Test 5, Station 3	92	174	152	0.271	0.069	184
Test 6, Station 3	87	166	144	0.275	0.069	175
Test 7, Station 3	81	157	136	0.279	0.070	164
Test 8, Station 3	82	157	137	0.278	0.070	164
Test 9, Station 3	72	141	123	0.285	0.071	151
Test 10, Station 3	68	135	117	0.288	0.071	143
Test 11, Station 3	63	128	110	0.291	0.072	133
Test 12, Station 3	81	156	136	0.279	0.070	166
Test 13, Station 3	77	149	130	0.282	0.070	157
Test 14, Station 3	72	142	123	0.285	0.071	148
Test 15, Station 3	89	169	147	0.273	0.069	178
Test 16, Station 3	89	170	148	0.273	0.069	178

Output DTN: MO0306MWDMXCNV.000, worksheet "Predicted Nusselt Numbers" of Phase 2 Supporting Calculations for Mixed Convection.xls.

Table IX-20. Predicted Outer-Surface Nusselt Numbers for EBS Ventilation Test Series, Phase 1

Location	Re_{Mo} (thousands)	$Nu_{ii}(Re_{Mo})$	$Nu_{oo}(Re_{Mo})$	$\theta_i(Re_{Mo})$	$\theta_o(Re_{Mo})$	Nu_{Mo}
Test 1, Station 3	77	149	130	0.282	0.070	194
Test 2, Station 3	59	122	105	0.293	0.072	179
Test 3, Station 3	84	161	140	0.277	0.069	216
Test 4, Station 3	111	201	175	0.265	0.067	286
Test 5, Station 3	70	138	120	0.286	0.071	204
Test 6, Station 3	153	256	223	0.260	0.066	411

Output DTN: MO0306MWDMXCNV.000, worksheet "Predicted Nusselt Numbers" of Phase 1 Supporting Calculations for Mixed Convection.xls.

Table IX-21. Predicted Outer-Surface Nusselt Numbers for EBS Ventilation Test Series, Phase 2

Location	Re_{Mo} (thousands)	$Nu_{ii}(Re_{Mo})$	$Nu_{oo}(Re_{Mo})$	$\theta_i(Re_{Mo})$	$\theta_o(Re_{Mo})$	Nu_{Mo}
Test 1, Station 3	80	155	134	0.279	0.070	198
Test 2, Station 3	69	136	118	0.287	0.071	211
Test 3, Station 3	62	127	110	0.291	0.072	217
Test 4, Station 3	61	125	108	0.292	0.072	222
Test 5, Station 3	84	162	141	0.277	0.069	215
Test 6, Station 3	79	154	134	0.280	0.070	209
Test 7, Station 3	70	139	121	0.286	0.071	215
Test 8, Station 3	70	138	120	0.286	0.071	218
Test 9, Station 3	70	138	120	0.286	0.071	175
Test 10, Station 3	62	126	109	0.291	0.072	175
Test 11, Station 3	48	104	90	0.300	0.074	199
Test 12, Station 3	74	146	127	0.283	0.071	191
Test 13, Station 3	66	132	114	0.289	0.072	193
Test 14, Station 3	56	117	101	0.295	0.073	202
Test 15, Station 3	79	154	134	0.280	0.070	215
Test 16, Station 3	79	152	132	0.280	0.070	218

Output DTN: MO0306MWDMXCNV.000, worksheet "Predicted Nusselt Numbers" of Phase 2 Supporting Calculations for Mixed Convection.xls.

IX.4.3 Uncertainty in Predicted Nusselt Numbers

This section evaluates the sources of uncertainty that have a quantitative dependence on the configuration or environment. These are the sources for which Section IX.3 does not provide a numerical uncertainty. The sources of uncertainty, both those evaluated here and those evaluated in Section IX.3, become inputs to the combined uncertainty.

IX.4.3.1 Uncertainty in the Predicted Nusselt Numbers for Natural Convection

For natural convection, Section IX.3.3 evaluates the deviation of measured Nusselt numbers from the Kuehn-Goldstein correlation of those measurements. The Type B evaluation gives a

random relative standard uncertainty of 12%. It also finds that the contribution from the effects of diameter ratio are negligible for the value in the EBS Ventilation Test Series, $r^* = 0.3$.

This section evaluates the following sources of uncertainty for the particular configuration and conditions of the EBS Ventilation Tests, based on the discussions in Section IX.3.3:

1. The uncertainty in predicted effective circumferential Nusselt numbers for coextensive, isothermal cylinders arising from eccentric location of the inner cylinder

2. The uncertainty in predicted effective circumferential Nusselt numbers for isothermal cylinders arising from unequal cylinder lengths

3. Uncertainty in the effective circumferential Nusselt numbers arising from temperature variation along the circumferences of the cylinders.

As described in Section IX.3.3, the use of the concentric correlation for natural convection systematically underestimates the natural convection heat transfer by $-0.15|e^*|$. For the EBS Ventilation Test Series configuration, with an e^* of –0.42, this source of uncertainty causes a systematic error of about –6%.

The use of data from Station 3 minimizes the effects of the extra length of wall beyond the ends of the waste package train. As suggested in Section IX.3.3, this analysis neglects the error caused by those extensions and by the gaps between the waste packages, because the following conditions hold:

1. The greater length of the outer cylinder does not cause a qualitative change in the flow from natural convection other than mild divergence and convergence along the axis.

2. The changes in the Rayleigh numbers appearing in the correlation, caused by the change in air temperature, account for most of the changes in the circumferential average Nusselt numbers.

3. The remaining effects of the longer outer cylinder are not significant compared to the other contributions to uncertainty.

The following is an evaluation of the effects of the circumferential temperature variations in the EBS Ventilation Tests. From Section IX.3.3, the relative error in the inner-cylinder Nusselt number is about $+0.25[T_t - \overline{T_i}]/[\overline{T_i} - T_f]$ and the relative error in the outer-cylinder Nusselt number is about $+0.4[T_t - \overline{T_o}]/[T_f - \overline{T_o}]$.

Table IX-22 provides an evaluation of the errors for each test in the EBS Ventilation Test Series. The average is a Type A evaluation of the effects of the circumferential temperature variations. The predictions for $\overline{Nu_{Ni}}(x)$ have a systematic error of +8% with a random standard uncertainty that is 0.5% of $\overline{Nu_{Ni}}(x)$.

At the outer surface, the values are negative, because unlike the situation for pure natural convection, the ventilation tests have $\overline{T}_o > T_f$. The negative error is reasonable because the magnitude of the temperature difference is *largest* at the top. The predictions have a systematic error of –3% in $\overline{Nu_{No}}(x)$ with a random standard uncertainty of 2%.

Table IX-22. Errors in $\overline{Nu_N}(x)$ for EBS Ventilation Test Series

Location		NU_{NI} Error	NU_{NO} Error
Phase 1	Test 1, Station 3	8.6%	–5.2%
	Test 2, Station 3	8.9%	–7.1%
	Test 3, Station 3	7.6%	–4.6%
	Test 4, Station 3	8.0%	0.5%
	Test 5, Station 3	7.9%	–4.5%
	Test 6, Station 3	8.5%	2.9%
Phase 2	Test 1, Station 3	8.1%	–3.4%
	Test 2, Station 3	8.7%	–3.6%
	Test 3, Station 3	8.6%	–3.8%
	Test 4, Station 3	8.7%	–3.1%
	Test 5, Station 3	7.4%	–3.4%
	Test 6, Station 3	7.9%	–3.7%
	Test 7, Station 3	7.9%	–2.4%
	Test 8, Station 3	7.8%	–2.0%
	Test 9, Station 3	8.7%	–4.4%
	Test 10, Station 3	9.1%	–3.3%
	Test 11, Station 3	9.0%	–5.6%
	Test 12, Station 3	8.3%	–3.6%
	Test 13, Station 3	8.3%	3.3%
	Test 14, Station 3	8.2%	–1.9%
	Test 15, Station 3	7.8%	–2.9%
	Test 16, Station 3	7.9%	–3.1%
	mean	8.3%	–3.0%
	std dev	0.5%	2.46%

Output DTN: MO0306MWDMXCNV.000, file: "Phase 1 Supporting Calculations for Mixed Convection.xls," spreadsheet: "Circum.T Vartn," col. F; and file: "Phase 2 Supporting Calculations for Mixed Convection.xls," spreadsheet: "Circum.T Vartn," col. F.

In all of the EBS ventilation tests, the outer surface was hotter than the air (Tables IX-13 and IX-14). Therefore, the flow patterns were more like Figure IX-1d than Figure IX-1c. There may be an unknown error from applying the Kuehn-Goldstein correlation to the flow pattern of Figure IX-1d.

Table IX-23 presents the contributions to $\overline{Nu_N}$ uncertainty from other causes and their combined standard uncertainty. Systematic effects are shown as corrections, which have the opposite signs

from the errors. The 95% confidence interval for $\overline{Nu_{Ni}}(x)$ is from –26% to +22%. At the outer surface, the systematic effects are in the same direction, so that the 95% confidences limit is from –15% to +33%. Of the effects considered in Table IX-23, the dominant source of uncertainty is the deviation of measured Nusselt numbers reported by Kuehn and Goldstein (1976 [DIRS 100675]) from their correlation of those measurements.

Table IX-23. Uncertainty Budget, Predicted $\overline{Nu_N}$

Source of Uncertainty	Relative Standard Uncertainties from Random Effects		Corrections for Systematic Effects	
	Type A Evaluation	Type B Evaluation	Type A Evaluation	Type B Evaluation
Correlation for concentric, coextensive, isothermal cylinders	—	12%	—	—
Eccentricity	—	—	—	+6%
Circumferential temperature variation	$\overline{Nu_{Ni}}$: 0.6% $\overline{Nu_{No}}$: 2%	—	—	$\overline{Nu_{Ni}}$: –8% $\overline{Nu_{No}}$: +3%

NOTES: $\overline{Nu_{Ni}}$: Correction for systematic effects: -2%
Combined standard uncertainty from random effects: 12%
95% confidence interval: -26% to +22%

$\overline{Nu_{No}}$: Correction for systematic effects: +9%
Combined standard uncertainty from random effects: 12%
95% confidence interval: -15% to +33%

IX.4.3.2 Uncertainty in the Predicted Nusselt Numbers for Forced Convection

For forced convection, Section IX.3.4 finds that the contribution from the effects of flux variations along the lengths and the circumferences of the cylinder are negligible. This section evaluates the following sources of uncertainty for the particular configuration and conditions of the EBS Ventilation Tests, based on the discussions in Section IX.3.4:

1. The extent to which measured circumferential average Nusselt numbers for fully developed flow in concentric, coextensive, uniform-flux cylinders deviate from the circumferential average Nusselt numbers predicted by the correlation.

2. Uncertainty from linear interpolation of the Kays-Leung parameters to the diameter ratio of 0.3.

3. Uncertainty from linear interpolation of the Kays-Leung parameters to the appropriate Reynolds number.

4. The uncertainty in effective circumferential Nusselt numbers for fully developed flow in uniform-flux cylinders arising from unequal cylinder lengths.

5. The uncertainty in effective circumferential Nusselt numbers for fully developed flow in coextensive, uniform-flux cylinders arising from eccentric location of the inner cylinder.

6. Uncertainty arising from deviations from fully developed flow.

For the uncertainty inherent in the Kays-Leung correlation, the Type B evaluation in Section IX.3.4 assigns a relative uncertainty of 3% as the random component. Because all of the ventilation tests had *Re* greater than 20,000, the systematic component is negligible.

For $0.2 < r^* < 0.5$, one may take $5(r^* - 0.2)(0.5 - r^*)$ as the upper 95% confidence limit in the relative error caused by interpolation of r^* (Section IX.3.4). For interpolation to r^*=0.3, the 95% confidence limit is 10%. This appendix uses an *a priori* normal distribution for a Type B evaluation of the uncertainty, with a standard uncertainty of 5%, for the relative error caused by interpolation in r^*.

The maximum error in an interpolation in *Re* is $0.5(Re_0)^2 M$, where Re_0 is the value at the lower end of the interval and *M* is a second derivative (Section IX.3.2). The analysis in Section IX.3.2 indicates that for $r^* = 0.3$, the relative error should be no more than 7%. Taking 7% as the 95% confidence limit of an *a priori* normal distribution for a Type B evaluation of the uncertainty, this appendix assigns a standard uncertainty of 3.5% as the relative error caused by interpolation in *Re*.

Section IX.3.4 derived expressions for the relative systematic errors in the Nusselt numbers arising from the eccentricity of the configuration. For the configuration of the EBS Ventilation Test Series, $r^* = 0.3$ and $e^* = -0.4$. Applying these values to the expressions, the relative systematic errors for the inner and outer Nusselt numbers are:

$$1 - \frac{\overline{Nu_{Fi}}(x)}{\mathrm{Nu}_{ii}(Re)} = +8.6\% \qquad \text{(Eq. IX-73)}$$

and

$$1 - \frac{\overline{Nu_{Fo}}(x)}{\mathrm{Nu}_{oo}(Re)} = 0 \qquad \text{(Eq. IX-74)}$$

As suggested in Section IX.3.4, this analysis neglects the error caused by the difference in total lengths of the cylinders, because the necessary conditions hold. That is, the additional length of the cylinder is sufficiently small.

Section IX.3.4 provides an estimate of the systematic error arising from applying Nusselt numbers predicted for fully developed flow to regions of thermally developing flow. According to that estimate, the systematic error becomes negligible at a distance of 10 (D_i - D_o) into the flow. For the EBS Ventilation Test configuration, that distance is 10 m. Because Station 3 is about 20 m from the inlet (BSC 2003 [DIRS 160724], Section 2), this analysis neglects that source of uncertainty.

Table IX-24 presents the contributions to $\overline{Nu_F}$ uncertainty from various causes and the combined standard uncertainty. Systematic effects are shown as corrections and therefore have opposite signs. There are three major random effects that are approximately equal in significance, causing the 95% confidence limit for $\overline{Nu_{Fo}}$ to range from –14% to +14%. $\overline{Nu_{Fi}}$ also has a systematic effect from eccentricity, so that its 95% confidence limit extends from –23% to +5%.

Table IX-24. Uncertainty Budget, Predicted $\overline{Nu_F}$

Source of Uncertainty	Relative Uncertainties from Random Effects		Corrections for Systematic Effects	
	Type A Evaluation	Type B Evaluation	Type A Evaluation	Type B Evaluation
Correlation for fully-developed flow in concentric, coextensive, uniform-flux cylinders	—	3%	—	—
Linear interpolation in r^*	—	5%	—	—
Linear interpolation in *Re*	—	3.5%	—	—
Eccentricity	—	—	—	$\overline{Nu_{Fi}}$: -9%

NOTES: Correction for systematic effects, $\overline{Nu_{Fi}}$ only: -9%
Combined standard uncertainty from random effects: 7%
$\overline{Nu_{Fi}}$ 95% confidence interval: –23% to +5%
$\overline{Nu_{Fo}}$ 95% confidence interval: –14% to +14%

IX.4.3.3 Uncertainty in the Predicted Nusselt Numbers for Mixed Convection

This section evaluates the uncertainties in the predicted Nusselt numbers by propagating uncertainty through the calculations of Step N1 through Step N3 that were reported in Section IX.4.2. The uncertainty analysis reflects the discussion in Section IX.3.5. Uncertainties in measured temperatures and flow rates are neglected.

Step N1 uses interpolation in r^* to create Table IX-15, in which the forced-convection parameters are functions of *Re* only. As discussed above, the standard uncertainty in each interpolated parameter, such as Nu_{ii} or Nu_{oo}, is 5%.

Step N2 begins with the calculation of the two natural convection Nusselt numbers, $\overline{Nu_{Ni}}(x)$ and $\overline{Nu_{No}}(x)$, reported in Tables IX-16 and IX-17. As reported in Table IX-23, each is missing a correction for systematic effects and has a combined standard uncertainty of 12% from random effects. These combine with the 5% standard uncertainties in Nu_{ii} and Nu_{oo} to produce the total uncertainty in the Nusselt numbers that $Re_{Ni}(x)$ and $Re_{No}(x)$ are supposed to represent. That is, the total uncertainty before the reverse interpolation consists of a combined standard uncertainty of 13% from random effects, as well as a systematic error. This does not include the error arising from having the flow pattern of Figure IX-1d instead of the pattern of Figure IX-1c.

The factor for propagating relative uncertainty is $(Nu_{ii}/Re)\partial Re/\partial Nu_{ii}$ or $(Nu_{oo}/Re)\partial Re/\partial Nu_{oo}$ (see Equation IX-31). For the interval between *Re* of 30,000 and *Re* of 100,000 in Table IX-15, for example, the last two weighting factors are both about 1.3. Taking 1.3 as a representative propagation factor, the uncertainty in Nu_N contributes 17% to the random standard uncertainty in Re_N from random effects. The corrections of –2% and +9% in the $\overline{Nu_{Ni}}(x)$ and $\overline{Nu_{No}}(x)$ become corrections of –3% and +12% in $Re_{Ni}(x)$ and $Re_{No}(x)$, respectively.

Another source of uncertainty in $Re_{Ni}(x)$ and $Re_{No}(x)$ is the interpolation in Reynolds number. The analysis in Section IX.3.2 shows that the error may range up to 12%. That result is the basis for a Type B evaluation of the uncertainty and an assignment of 6% as the standard relative uncertainty from the reverse interpolation. Together with the 17% of the previous paragraph, this yields 18% as the combined standard uncertainty from random effects (applying Equation IX-30).

A final source of uncertainty in $Re_{Ni}(x)$ and $Re_{No}(x)$ is the use of the approximations represented by Equations IX-28 and IX-29. For purposes of this appendix, Tables IX-25 and IX-26 present the values of $Re_{Ni}(x)$ and $Re_{No}(x)$ that would have been obtained without the approximation. These "correct" values are the result of applying the bisection method (Conte and de Boor 1972 [DIRS 159800], p. 28, Algorithm 2.1) until the interval in Re was less than 50.0.

Tables IX-25 and IX-26 also contain the percentage corrections that are implied for the values of $Re_{Ni}(x)$ and $Re_{No}(x)$ appearing in Tables IX-16 and IX-17, the random uncertainties, and the 95% confidence limits. For the confidence limits, the percentage of random uncertainty was applied *after* the correction. For Test 1 of Phase 1, for example, the correction is –15%, the random standard uncertainty is 14%, and the lower confidence limit of –39% is the value of the expression (100% – 28%) (100% – 15%) – 100%. The confidence limits do not include the error from the approximation that the effects of the Figure IX-1d flow pattern are negligible.

Of the evaluated sources of uncertainty in $Re_{Ni}(x)$ the dominant source is the uncertainty in $\overline{Nu_{Ni}}(x)$, which stems from the deviation of measured Nusselt numbers reported by Kuehn and Goldstein (1976 [DIRS 100675]) from their correlation of those measurements. The dominant contribution to the evaluated uncertainty in $Re_{No}(x)$ is the approximation represented by Equation IX-29.

Table IX-25. Combined Uncertainty in Re_{Ni} and Re_{No} for EBS Ventilation Test Series, Phase 1

Location	Re_N from Eq. IX-28 or IX-29 (Simplified) (Thousands)	Re_N from Eq. IX-24 or IX-25 (Not Simplified) (Thousands)	To Correct for Simplified Equation	Correction for Systematic Effect in Nu_N	Combined Correction for Systematic Effects	Standard Uncertainty from Random Effects	95% Confidence Interval	
							Lower	Upper
Re_{Ni}								
Test 1, Station 3	65	60	–8%	–3%	–11%	18%	–43%	21%
Test 2, Station 3	64	60	–7%	–3%	–10%	18%	–42%	22%
Test 3, Station 3	81	76	–7%	–3%	–10%	18%	–42%	23%
Test 4, Station 3	78	74	–6%	–3%	–9%	18%	–42%	24%
Test 5, Station 3	80	76	–6%	–3%	–9%	18%	–42%	24%
Test 6, Station 3	76	72	–5%	–3%	–8%	18%	–41%	25%
Re_{No}								
Test 1, Station 3	62	35	–44%	12%	–32%	18%	–56%	–7%
Test 2, Station 3	55	25	–54%	12%	–42%	18%	–63%	–21%
Test 3, Station 3	71	39	–45%	12%	–33%	18%	–57%	–9%
Test 4, Station 3	65	31	–52%	12%	–40%	18%	–62%	–19%
Test 5, Station 3	66	31	–54%	12%	–42%	18%	–63%	–21%
Test 6, Station 3	58	22	–62%	12%	–50%	18%	–68%	–32%

Output DTN: MO0306MWDMXCNV.000, worksheet “Uncertainties” of Phase 1 Supporting Calculations for Mixed Convection.xls.

Table IX-26. Combined Uncertainty in Re_{Ni} and Re_{No} for EBS Ventilation Test Series, Phase 2

Location	Re_N from Eq. IX-28 or IX-29 (Simplified) (Thousands)	Re_N from Eq. IX-24 or IX-25 (Not Simplified) (Thousands)	To Correct for Simplified Equation	Correction for Systematic Effect in Nu_N	Combined Correction for Systematic Effects	Standard Uncertainty from Random Effects	95% Confidence Interval	
							Lower	Upper
Re_{Ni}								
Test 1, Station 3	70	65	–8%	–3%	–11%	18%	–43%	21%
Test 2, Station 3	65	61	–7%	–3%	–10%	18%	–42%	23%
Test 3, Station 3	60	57	–6%	–3%	–9%	18%	–42%	24%
Test 4, Station 3	60	57	–5%	–3%	–8%	18%	–41%	26%
Test 5, Station 3	81	75	–8%	–3%	–11%	18%	–43%	21%
Test 6, Station 3	76	71	–7%	–3%	–10%	18%	–42%	23%
Test 7, Station 3	70	66	–6%	–3%	–9%	18%	–42%	23%
Test 8, Station 3	71	67	–6%	–3%	–9%	18%	–42%	24%
Test 9, Station 3	68	63	–8%	–3%	–11%	18%	–43%	21%
Test 10, Station 3	64	60	–7%	–3%	–10%	18%	–42%	23%
Test 11, Station 3	59	57	–5%	–3%	–8%	18%	–41%	25%
Test 12, Station 3	78	72	–7%	–3%	–10%	18%	–43%	22%
Test 13, Station 3	73	69	–6%	–3%	–9%	18%	–42%	24%
Test 14, Station 3	69	65	–5%	–3%	–8%	18%	–41%	25%
Test 15, Station 3	78	74	–6%	–3%	–9%	18%	–42%	24%
Test 16, Station 3	79	74	–6%	–3%	–9%	18%	–42%	23%
Re_{No}								
Test 1, Station 3	66	39	–42%	12%	–30%	18%	–55%	–5%
Test 2, Station 3	53	23	–58%	12%	–46%	18%	–65%	–26%
Test 3, Station 3	47	16	–66%	12%	–54%	18%	–70%	–37%
Test 4, Station 3	45	15	–68%	12%	–56%	18%	–72%	–40%
Test 5, Station 3	72	41	–44%	12%	–32%	18%	–56%	–7%
Test 6, Station 3	67	36	–47%	12%	–35%	18%	–58%	–12%
Test 7, Station 3	57	24	–58%	12%	–46%	18%	–65%	–26%
Test 8, Station 3	57	23	–59%	12%	–47%	18%	–66%	–28%
Test 9, Station 3	66	40	–40%	12%	–28%	18%	–54%	–2%

Table IX-26. Combined Uncertainty in Re_{Ni} and Re_{No} for EBS Ventilation Test Series, Phase 2 (Continued)

Location	Re_N from Eq. IX-28 or IX-29 (Simplified) (Thousands)	Re_N from Eq. IX-24 or IX-25 (Not Simplified) (Thousands)	To Correct for Simplified Equation	Correction for Systematic Effect in Nu_N	Combined Correction for Systematic Effects	Standard Uncertainty from Random Effects	95% Confidence Interval	
				Re_{No}				
Test 10, Station 3	58	29	–50%	12%	–38%	18%	–60%	–15%
Test 11, Station 3	43	12	–72%	12%	–60%	18%	–74%	–45%
Test 12, Station 3	71	40	–43%	12%	–31%	18%	–56%	–7%
Test 13, Station 3	62	29	–54%	12%	–42%	18%	–63%	–21%
Test 14, Station 3	52	18	–65%	12%	–53%	18%	–70%	–36%
Test 15, Station 3	67	34	–49%	12%	–37%	18%	–60%	–15%
Test 16, Station 3	66	32	–51%	12%	–39%	18%	–61%	–18%

Output DTN: MO0306MWDMXCNV.000, worksheet “Uncertainties” of Phase 2 Supporting Calculations for Mixed Convection.xls.

Steps N3 and N4 begin with calculations of $Re_{Mi}(x)$ and $Re_{Mo}(x)$, for which the only uncertainty is from the uncertainty in $Re_{Ni}(x)$ and $Re_{No}(x)$. As explained in Section IX.3.5, the relative uncertainty in Re_N propagates into Re_M with a factor of $[Re_N/Re_M]^2$. Tables IX-27 and IX-28 show that propagation for the EBS Ventilation Test Series, still omitting the error from the qualitatively different flow pattern.

Finally, steps N3 and N4 calculate $\overline{Nu_{Mi}}(x)$ and $\overline{Nu_{Mo}}(x)$. Tables IX-27 and IX-28 show the factor $(Re_M/Nu_M)\partial Nu_M/\partial Re_M$ by which the relative uncertainty in Re_M propagates into $\overline{Nu_M}$. For purposes of this appendix, the derivatives were estimated by taking a small increment in Re_M and evaluating $\overline{Nu_M}$ again.

Table IX-27. Combined Uncertainty in Re_{Mi} and Re_{Mo} for EBS Ventilation Test Series, Phase 1

Location	$(Re_N/Re_M)^2$	Combined Correction for Systematic Effects	Standard Uncertainty from Random Effects	(Re_M/Nu_M) Times Partial of Nu_M with Respect to Re_M
Re_{Mi}				
Test 1, Station 3	0.68	–8%	12%	0.80
Test 2, Station 3	0.90	–9%	16%	0.78
Test 3, Station 3	0.77	–7%	14%	0.80
Test 4, Station 3	0.43	–4%	8%	0.74
Test 5, Station 3	0.92	–8%	17%	0.81
Test 6, Station 3	0.22	–2%	4%	0.79
Re_{Mo}				
Test 1, Station 3	0.66	–21%	12%	0.78
Test 2, Station 3	0.86	–36%	16%	0.74
Test 3, Station 3	0.72	–24%	13%	0.78
Test 4, Station 3	0.34	–14%	6%	0.70
Test 5, Station 3	0.89	–37%	16%	0.76
Test 6, Station 3	0.14	–7%	3%	0.74

Output DTN: MO0306MWDMXCNV.000, worksheet “Uncertainties” of Phase 1 Supporting Calculations for Mixed Convection.xls, rows 34 to 37, columns B, D, E, and J.

Table IX-28. Combined Uncertainty in Re_{Mi} and Re_{Mo} for EBS Ventilation Test Series, Phase 2

Location	$(Re_N/Re_M)^2$	Combined Correction for Systematic Effects	Standard Uncertainty from Random Effects	(Re_M/Nu_M) Times Partial of Nu_M with Respect to Re_M
Re_{Mi}				
Test 1, Station 3	0.71	−8%	13%	0.81
Test 2, Station 3	0.69	−7%	12%	0.80
Test 3, Station 3	0.68	−6%	12%	0.80
Test 4, Station 3	0.68	−5%	12%	0.80
Test 5, Station 3	0.77	−8%	14%	0.80
Test 6, Station 3	0.76	−8%	14%	0.82
Test 7, Station 3	0.75	−7%	13%	0.81
Test 8, Station 3	0.75	−6%	13%	0.81
Test 9, Station 3	0.90	−10%	16%	0.79
Test 10, Station 3	0.89	−9%	16%	0.78
Test 11, Station 3	0.89	−7%	16%	0.77
Test 12, Station 3	0.92	−9%	17%	0.81
Test 13, Station 3	0.91	−8%	16%	0.80
Test 14, Station 3	0.91	−8%	16%	0.79
Test 15, Station 3	0.77	−7%	14%	0.82
Test 16, Station 3	0.77	−7%	14%	0.82
Re_{Mo}				
Test 1, Station 3	0.69	−21%	12%	0.79
Test 2, Station 3	0.61	−28%	11%	0.75
Test 3, Station 3	0.56	−30%	10%	0.74
Test 4, Station 3	0.55	−31%	10%	0.73
Test 5, Station 3	0.72	−23%	13%	0.79
Test 6, Station 3	0.71	−25%	13%	0.78
Test 7, Station 3	0.66	−30%	12%	0.76
Test 8, Station 3	0.66	−31%	12%	0.75
Test 9, Station 3	0.90	−25%	16%	0.77
Test 10, Station 3	0.86	−33%	16%	0.75
Test 11, Station 3	0.80	−48%	14%	0.70
Test 12, Station 3	0.90	−28%	16%	0.78
Test 13, Station 3	0.88	−37%	16%	0.75
Test 14, Station 3	0.86	−46%	15%	0.73
Test 15, Station 3	0.71	−26%	13%	0.78
Test 16, Station 3	0.70	−28%	13%	0.77

Output DTN: MO0306MWDMXCNV.000, worksheet “Uncertainties” of Phase 2 Supporting Calculations for Mixed Convection.xls, rows 54 to 87, columns B, D, E, F, and J.

The other contributors to the uncertainty in each mixed-convection Nusselt number are:

1. The uncertainty in the forced convection correlation when the input Reynolds number is known, which is a correction of -9% for systematic effects, at the inner surface only, and a standard uncertainty of 7% from random effects at both surfaces (Table IX-24).

2. The 7.5% standard uncertainty in mixed-convection Nusselt numbers inherent in the Morgan approximation (Section IX.3.5).

Tables IX-29 and IX-30 present the combined uncertainties in $\overline{Nu_{Mi}}(x)$ and $\overline{Nu_{Mo}}(x)$, with the various contributors to those uncertainties. As before, this does not include the effect of the qualitatively different flow pattern.

Of the evaluated sources of uncertainty in each mixed-convection Nusselt number, the dominant source is the uncertainty in the effective Reynolds number. For the inner surface Nusselt number, the root source is the deviation of measured Nusselt numbers reported by Kuehn and Goldstein (1976 [DIRS 100675]) from their correlation of those measurements. At the outer surface, the root source is the approximation represented by Equation IX-29.

Table IX-29. Uncertainty in Predicted $\overline{Nu_M}$ for EBS Ventilation Test Series, Phase 1

Location	From Uncertainty in Re_M		From Nu_F Uncertainty		From Morgan Approx.	Combined Uncertainty		95% Confidence Interval	
	Correction for Systematic Effects	Random Standard Uncert.	Correction for Systematic Effects	Random Standard Uncert.	Random Standard Uncert.	Correction for Systematic Effects	Random Standard Uncert.	Lower	Upper
				Nu_{Mi}					
Test 1, Station 3	–6%	10%	–9%	7%	7.5%	–15%	14%	–39%	9%
Test 2, Station 3	–7%	13%	–9%	7%	7.5%	–16%	16%	–43%	11%
Test 3, Station 3	–6%	11%	–9%	7%	7.5%	–15%	15%	–41%	11%
Test 4, Station 3	–3%	6%	–9%	7%	7.5%	–12%	12%	–33%	9%
Test 5, Station 3	–7%	14%	–9%	7%	7.5%	–16%	17%	–44%	13%
Test 6, Station 3	–1%	3%	–9%	7%	7.5%	–10%	11%	–30%	9%
				Nu_{Mo}					
Test 1, Station 3	–16%	9%	0%	7%	7.5%	–16%	14%	–39%	7%
Test 2, Station 3	–27%	12%	0%	7%	7.5%	–27%	15%	–50%	–5%
Test 3, Station 3	–19%	10%	0%	7%	7.5%	–19%	14%	–42%	5%
Test 4, Station 3	–10%	4%	0%	7%	7.5%	–10%	11%	–30%	10%
Test 5, Station 3	–28%	12%	0%	7%	7.5%	–28%	16%	–51%	–5%
Test 6, Station 3	–5%	2%	0%	7%	7.5%	–5%	10%	–25%	14%

Output DTN: MO0306MWDMXCNV.000, worksheet “Uncertainties” of Phase 1 Supporting Calculations for Mixed Convection.xls, rows 54 to 67, columns B through K.

Table IX-30. Uncertainty in Predicted $\overline{Nu_M}$ for EBS Ventilation Test Series, Phase 2

Location	From Uncertainty in Re_M		From Nu_F Uncertainty		From Morgan Approx.	Combined Uncertainty		95% Confidence Interval	
	Correction for Systematic Effects	Random Standard Uncert.	Correction for Systematic Effects	Random Standard Uncert.	Random Standard Uncert.	Correction for Systematic Effects	Random Standard Uncert.	Lower	Upper
					Nu_{Mi}				
Test 1, Station 3	–6%	10%	–9%	7%	7.5%	–15%	15%	–40%	10%
Test 2, Station 3	–5%	10%	–9%	7%	7.5%	–14%	14%	–39%	10%
Test 3, Station 3	–5%	10%	–9%	7%	7.5%	–14%	14%	–38%	11%
Test 4, Station 3	–4%	10%	–9%	7%	7.5%	–13%	14%	–38%	11%
Test 5, Station 3	–7%	11%	–9%	7%	7.5%	–16%	15%	–41%	10%
Test 6, Station 3	–6%	11%	–9%	7%	7.5%	–15%	15%	–41%	11%
Test 7, Station 3	–6%	11%	–9%	7%	7.5%	–15%	15%	–40%	11%
Test 8, Station 3	–5%	11%	–9%	7%	7.5%	–14%	15%	–40%	11%
Test 9, Station 3	–8%	13%	–9%	7%	7.5%	–17%	16%	–44%	10%
Test 10, Station 3	–7%	13%	–9%	7%	7.5%	–16%	16%	–43%	12%
Test 11, Station 3	–5%	12%	–9%	7%	7.5%	–14%	16%	–42%	13%
Test 12, Station 3	–8%	13%	–9%	7%	7.5%	–17%	17%	–45%	11%
Test 13, Station 3	–7%	13%	–9%	7%	7.5%	–16%	17%	–44%	13%
Test 14, Station 3	–6%	13%	–9%	7%	7.5%	–15%	17%	–43%	13%
Test 15, Station 3	–6%	11%	–9%	7%	7.5%	–15%	15%	–41%	11%
Test 16, Station 3	–6%	11%	–9%	7%	7.5%	–15%	15%	–41%	11%
					Nu_{Mo}				
Test 1, Station 3	–16%	10%	0%	7%	7.5%	–16%	14%	–40%	8%
Test 2, Station 3	–21%	8%	0%	7%	7.5%	–21%	13%	–42%	0%
Test 3, Station 3	–22%	7%	0%	7%	7.5%	–22%	13%	–42%	–2%
Test 4, Station 3	–23%	7%	0%	7%	7.5%	–23%	13%	–42%	–3%
Test 5, Station 3	–18%	10%	0%	7%	7.5%	–18%	14%	–42%	6%
Test 6, Station 3	–19%	10%	0%	7%	7.5%	–19%	14%	–42%	4%
Test 7, Station 3	–23%	9%	0%	7%	7.5%	–23%	14%	–44%	–2%
Test 8, Station 3	–23%	9%	0%	7%	7.5%	–23%	14%	–44%	–3%
Test 9, Station 3	–20%	13%	0%	7%	7.5%	–20%	16%	–46%	6%
Test 10, Station 3	–25%	12%	0%	7%	7.5%	–25%	16%	–48%	–1%
Test 11, Station 3	–34%	10%	0%	7%	7.5%	–34%	14%	–53%	–15%
Test 12, Station 3	–22%	13%	0%	7%	7.5%	–22%	16%	–47%	3%

Table IX-30. Uncertainty in Predicted $\overline{Nu_M}$ for EBS Ventilation Test Series, Phase 2 (Continued)

Location	From Uncertainty in Re_M		From Nu_F Uncertainty		From Morgan Approx.	Combined Uncertainty		95% Confidence Interval	
	Correction for Systematic Effects	Random Standard Uncert.	Correction for Systematic Effects	Random Standard Uncert.	Random Standard Uncert.	Correction for Systematic Effects	Random Standard Uncert.	Lower	Upper
					Nu_{Mo}				
Test 13, Station 3	–28%	12%	0%	7%	7.5%	–28%	16%	–51%	–5%
Test 14, Station 3	–33%	11%	0%	7%	7.5%	–33%	15%	–53%	–13%
Test 15, Station 3	–21%	10%	0%	7%	7.5%	–21%	14%	–43%	2%
Test 16, Station 3	–21%	10%	0%	7%	7.5%	–21%	14%	–44%	1%

Output DTN: MO0306MWDMXCNV.000, worksheet “Uncertainties” of Phase 2 Supporting Calculations for Mixed Convection.xls, rows 94 to 127, columns B through K.

IX.4.4 Measurement of Nusselt Numbers

This appendix follows the practice in the open literature on convective heat transfer, such as Kuehn and Goldstein (1978 [DIRS 130084]). "Measured" circumferential average Nusselt numbers are based on measured heat input and measured temperatures, with corrections for non-convective mechanisms, such as radiative heat transfer and conductive heat transfer. At the Rayleigh numbers and Reynolds numbers in the EBS Ventilation Test Series, conduction to the air is not a significant mechanism.

Therefore, a measured value for circumferential average convective heat flux from the inner surface at a central location (Station 3) is:

$$\overline{q''}(x) = \frac{q_{in}}{\pi D_i L_i} - \overline{q''}_{ad,i}(x) \qquad \text{(Eq. IX-75)}$$

where q_{in} is the 24-hour average power generated in the waste packages, L_i is the combined length of the waste packages, and $\overline{q''}_{ad,i}(x)$ is the circumferential average radiative flux from the waste packages at location *x*. For each ventilation test, Table IX-6 or IX-7 gives the value of the average line load, $\frac{q_{in}}{L_i}$.

For transparent air between concentric cylinders (Incropera and DeWitt 1985 [DIRS 114109], p. 647, Eq. 13.25):

$$\overline{q''}_{ad,i}(x) = \frac{\sigma\left[\overline{\overline{T^4}}_i(x) - \overline{\overline{T^4}}_o(x)\right]}{\frac{1}{\varepsilon_i} + \frac{1-\varepsilon_o}{\varepsilon_o} r^*} \qquad \text{(Eq. IX-76)}$$

where σ is the Stefan-Boltzmann constant (Table 4-28), ε_i and ε_o are the measured emissivity of the waste package steel and concrete pipe (Tables 7-4 and 7-5), and each $\overline{\overline{T^4}}(x)$ is the 24-hour and circumferential average of the fourth power of the absolute temperature (K). This appendix approximates the averages of the fourth powers from the 24-hour averages, $\overline{T}(x)$, of absolute temperatures (K) at the top (t), left (l), bottom (b), and right (r) positions on the surfaces as follows:

$$\overline{\overline{T^4}}_i(x) \cong \left\{\overline{\overline{T}}_i(x)\right\}^4 = \left\{\left[\overline{T}_{ti}(x) + \overline{T}_{bi}(x) + \overline{T}_{li}(x) + \overline{T}_{ri}(x)\right]/4\right\}^4 \qquad \text{(Eq. IX-77)}$$

$$\overline{\overline{T^4}}_o(x) \cong \left\{\overline{\overline{T}}_o(x)\right\}^4 = \left\{\left[\overline{T}_{to}(x) + \overline{T}_{lo}(x) + \overline{T}_{ro}(x)\right]/3\right\}^4 \qquad \text{(Eq. IX-78)}$$

Because the bottom of the concrete pipe is covered by the invert, its bottom temperature is not included for radiation.

By factoring, Equation IX-78 may be put in the form:

$$\overline{q}''_{rad,i}(x) \cong \frac{\sigma}{\frac{1}{\varepsilon_i}+\frac{1-\varepsilon_o}{\varepsilon_o}r^*}\left\{\left[\overline{\overline{T_i}}(x)\right]^3+\left[\overline{\overline{T_i}}(x)\right]^2\left[\overline{\overline{T_o}}(x)\right]+\left[\overline{\overline{T_i}}(x)\right]\left[\overline{\overline{T_o}}(x)\right]^2+\left[\overline{\overline{T_o}}(x)\right]^3\right\}\left[\overline{\overline{T_i}}(x)-\overline{\overline{T_o}}(x)\right]$$

$$=\frac{0.5\sigma}{\frac{1}{\varepsilon_i}+\frac{1-\varepsilon_o}{\varepsilon_o}r^*}\left\{\left[\overline{\overline{T_i}}(x)+\overline{\overline{T_o}}(x)\right]^3\left[\overline{\overline{T_i}}(x)-\overline{\overline{T_o}}(x)\right]+\left[\overline{\overline{T_i}}(x)+\overline{\overline{T_o}}(x)\right]\left[\overline{\overline{T_i}}(x)-\overline{\overline{T_o}}(x)\right]^3\right\}$$

(Eq. IX-79)

Ignoring the term containing the cube of the temperature difference, the approximation becomes:

$$\overline{q}''_{rad,i}(x) \cong \frac{0.5\sigma}{\frac{1}{\varepsilon_i}+\frac{1-\varepsilon_o}{\varepsilon_o}r^*}\left[\overline{\overline{T_i}}(x)+\overline{\overline{T_o}}(x)\right]^3\left[\overline{\overline{T_i}}(x)-\overline{\overline{T_o}}(x)\right] \quad \text{(Eq. IX-80)}$$

For each ventilation test, Table IX-31 or IX-32 shows $\overline{q}''_{rad,i}(x)$ calculated in accordance with Equation IX-80, the measured $\overline{q}''_i(x)$, the value of $\overline{h_i}(x)$ from Equation IX-16, and the value of $\overline{Nu_i}(x)$ from Equation IX-2, using k = 0.0263 W/mK.

Table IX-31. Inner-Surface Nusselt Number Measurements, EBS Ventilation Test Series, Phase 1

Location	$q_{in}/\pi D_i L$ (W/m^2)	$q''_{rad,©}$ (W/m^2)	$q''_{©}$ (W/m^2)	Effective h_i (W/m^{2}K)	Effective Nu_i
Test 1, Station 3	143	64	78	5.32	195
Test 2, Station 3	140	71	69	4.65	170
Test 3, Station 3	281	126	155	5.94	218
Test 4, Station 3	284	110	174	7.54	276
Test 5, Station 3	284	134	150	5.70	209
Test 6, Station 3	285	90	195	9.94	364

Output DTN: MO0306MWDMXCNV.000, worksheet “Effective Nui” of Phase 1 Supporting Calculations for Mixed Convection.xls.

Table IX-32. Inner-Surface Nusselt Number Measurements, EBS Ventilation Test Series, Phase 2

Location	$q_{in}/\pi D_i L$ (W/m^2)	$q''_{rad,©}$ (W/m^2)	$q''_{©}$ (W/m^2)	Effective h_i (W/m^{2}K)	Effective Nu_i
Test 1, Station 3	171	77	94	5.39	198
Test 2, Station 3	171	86	85	5.08	186
Test 3, Station 3	169	92	77	4.79	175
Test 4, Station 3	168	91	77	4.87	178
Test 5, Station 3	282	127	155	5.91	217
Test 6, Station 3	281	137	144	5.55	204
Test 7, Station 3	280	148	131	5.31	194
Test 8, Station 3	280	149	131	5.29	194
Test 9, Station 3	168	79	89	5.11	187
Test 10, Station 3	168	87	81	4.79	175
Test 11, Station 3	169	98	72	4.42	162
Test 12, Station 3	282	133	149	5.66	208
Test 13, Station 3	282	145	137	5.36	196
Test 14, Station 3	283	157	125	5.08	186
Test 15, Station 3	282	134	148	5.69	209
Test 16, Station 3	285	136	150	5.71	209

Output DTN: MO0306MWDMXCNV.000, worksheet “Effective Nui” of Phase 2 Supporting Calculations for Mixed Convection.xls.

At the outer surface, heat arrives by radiation and leaves by conduction into the wall and by convection into the air. Therefore, the measured value for circumferential average convective flux is:

$$\overline{q''_o}(x) = r^* \overline{q''}_{rad,i}(x) - h_{cond}\left[\overline{\overline{T_o}}(x) - \overline{\overline{T_a}}(x)\right] \qquad \text{(Eq. IX-81)}$$

where the radiative flux at the waste package has been multiplied by r^* to reflect the larger circumference at the outer wall, h_{cond} is the overall conductive heat transfer coefficient for the combined thickness of concrete and insulation, and $\overline{\overline{T_a}}(x)$ is an average ambient temperature external to the insulation, defined by

$$\overline{\overline{T_a}}(x) = \left[\overline{T_{ta}}(x) + \overline{T_{la}}(x) + \overline{T_{ra}}(x)\right]/3 \qquad \text{(Eq. IX-82)}$$

The two natural convection tests conducted at the end of Phase 1 establish a value for h_{cond}. Because there is no heat removed by ventilating air in the natural convection tests, conduction through the wall must be equal to the heat input. That is, neglecting end effects,

$$r^* \frac{q_{in}}{\pi D_i L_i} = h_{cond}\left[\overline{\overline{T_o}}(x) - \overline{\overline{T_a}}(x)\right] \qquad \text{(Eq. IX-83)}$$

where the flux from the heat source has been multiplied by r^* to reflect the larger circumference at the outer wall. Table IX-33 shows that the calculation of h_{cond} from data in Table IX-8 for the two natural convection tests gives an average value of 1.99 W/m^{2}K, with a standard deviation of less than 1%.

For each ventilation test, Table IX-34 or IX-35 shows the measured $\overline{q_o''}(x)$, the value of $\overline{h_o}(x)$ from Equation IX-16, and the value of $\overline{Nu_o}(x)$ from Equation IX-3, with k = 0.0263 W/mK.

For the direct measurements taken during the EBS Ventilation Test Series, the uncertainties are small. Averaging 96 measurements to get a 24-hour average reduces further the effects of random errors. For example, the uncertainty in the average heat input is only 2.6 W out of a total input of 4 kW or more (BSC 2003 [DIRS 160724], Tables 3-15 and 3-16).

The major uncertainty in the measured Nusselt numbers is in the approximation for radiative heat transfer. One source of uncertainty is the absence of measured temperatures below the center of the concrete pipe. Other sources are the approximations that underlie the radiation formula, including:

- Concentric cylinders
- Isothermal surfaces
- Transparent air
- No end effects

The effort documented here did not include a literature search for data regarding deviations from these approximations. This appendix does not provide numerical uncertainties for the measured Nusselt numbers.

Table IX-33. Determination of Conductive Heat Transfer Coefficient from Natural Convection Tests Conducted During EBS Ventilation Test Series

Location	q_{in}/L (W/m)	Source at Wall (W/m^2)	Avg. T_a (°C)	Avg. T_o (°C)	Avg. (T_o-T_a) (°C)	h_{cond} (W/m^2°C)
Test NC1, Station 3	120	27.9	27.97	45.83	17.87	1.561
Test NC2, Station 3	242	56.2	32.53	68.77	36.23	1.552
					average	1.556
					std. dev.	0.006

NC1=Natural Convection Test 1; NC2=Natural Convection Test 2.

Table IX-34. Outer-Surface Nusselt Number Measurements, EBS Ventilation Test Series, Phase 1

Location	$r^* q''_{rad,©}$ (W/m^2)	Avg T_a (°C)	q_{cond} (W/m^2)	q''_o (W/m^2)	Effective h_o (W/m^{2}K)	Effective Nu_o
Test 1, Station 3	19.0	28.57	2.5	16.6	6.45	236
Test 2, Station 3	21.1	28.27	7.8	13.3	7.12	261
Test 3, Station 3	37.4	26.73	10.3	27.1	6.63	243
Test 4, Station 3	32.6	26.23	5.8	26.9	9.16	336
Test 5, Station 3	39.6	23.90	16.1	23.5	7.28	267
Test 6, Station 3	26.8	20.63	4.5	22.3	12.16	445

Output DTN: MO0306MWDMXCNV.000, worksheet "Effective Nui" of Phase 1 Supporting Calculations for Mixed Convection.xls.

Table IX-35. Outer-Surface Nusselt Number Measurements, EBS Ventilation Test Series, Phase 2

Location	$r^* q''_{rad,©}$ (W/m^2)	Avg T_a (°C)	q_{cond} (W/m^2)	q''_o (W/m^2)	Effective h_o (W/m^{2}K)	Effective Nu_o
Test 1, Station 3	22.7	28.43	3.3	19.5	6.21	228
Test 2, Station 3	25.5	29.20	14.7	10.8	5.92	217
Test 3, Station 3	27.4	36.33	18.6	8.9	6.26	229
Test 4, Station 3	27.1	36.07	18.4	8.7	6.71	246
Test 5, Station 3	37.6	30.53	5.3	32.2	7.64	280
Test 6, Station 3	40.8	36.67	10.5	30.2	7.69	282
Test 7, Station 3	44.0	37.97	21.3	22.8	8.33	305
Test 8, Station 3	44.3	37.20	22.2	22.1	8.46	310
Test 9, Station 3	23.5	32.67	3.5	19.9	5.98	219
Test 10, Station 3	25.9	36.13	10.4	15.5	6.33	232
Test 11, Station 3	28.9	39.63	17.4	11.5	9.72	356
Test 12, Station 3	39.5	35.30	8.2	31.2	7.02	257
Test 13, Station 3	43.0	34.77	19.3	23.7	7.37	270
Test 14, Station 3	46.7	38.47	26.5	20.2	9.40	345
Test 15, Station 3	39.7	29.50	13.4	26.3	7.23	265
Test 16, Station 3	40.2	27.73	15.4	24.8	7.22	265

Output DTN: MO0306MWDMXCNV.000, worksheet "Effective Nui" of Phase 2 Supporting Calculations for Mixed Convection.xls.

IX.4.5 Corroboration of Predicted Results With Test Data

Figures IX-3 through IX-6 compare "measured" and predicted Nusselt numbers at Station 3 for the Phase 1 and Phase 2 tests in the EBS Ventilation Test Series. When the prediction agrees with the measurement, the point lies on the diagonal line. These plots show the 95% confidence limits for the predictions. In some cases, because of systematic errors that are not corrected in the methodology, the predicted value is outside of the confidence limits.

The "measured" values of $\overline{Nu_i}$ agree with the predicted values to within the uncertainty (Figures IX-3 and IX-4). However, the "measured" values for $\overline{Nu_o}$ are consistently higher than the predicted values (Figures IX-5 and IX-6).

The predicted values of $\overline{Nu_o}$ (Figures IX-5 and IX-6) could be brought within their own 95% confidence limits by solving Equation IX-25 implicitly, thereby eliminating the systematic error caused by the approximation of Equation IX-29. For each case, one could evaluate the right hand side of Equation IX-25 for two or three values of *Re*, then interpolate in the resulting small table. However, this would not improve the agreement with the measured values.

A striking feature of Figure IX-6, in particular, is that the measured values of $\overline{Nu_o}$ span a factor of three, while the predicted values are relatively constant. Most of the variation in measured $\overline{Nu_o}$ occurred in tests at the lowest flow rate, 0.5 m^3/s. Table IX-36 is a summary of the measured values of $\overline{Nu_o}$ for all tests that had controlled inlet air conditions and a nominal flow rate of 0.5 m^3/s. There appears to be a strong dependence on air inlet temperature that was not seen at higher flow rates. At the lower flow rates, natural convection has a greater influence. The natural convection correlation is based on the flow pattern of Figure IX-1c, but the actual circulation near the outer surface is in the opposite direction, as shown in Figure IX-1d. Because the temperature of the outer surface is near the temperature of the air (Table IX-16 and IX-17), details of the flow pattern may be sensitive to the inlet temperature.

Table IX-36 also contains the predicted Nusselt numbers and the values that would result from the Dittus-Boelter formula. The Dittus-Boelter predictions are the result of applying Equation IX-12, using Reynolds numbers from Table IX-12. Although the predictions are low, the Dittus-Boelter values are even lower, by about a factor of three.

Concentrating attention on the Nusselt numbers tends to exaggerate the significance of the errors with respect to overall energy transfer in the EBS Ventilation Tests. To provide another perspective, an energy balance can be represented by expressing the various components of energy transfer as percentages of the total input energy. A certain percentage was convected from the inner wall to the air, a percentage was convected from the outer wall to the air, and a percentage was conducted through the outer wall. Using measured data, these percentages must sum to 100%.

Figures IX-7 and IX-8 show an energy balance using the methodology for convection to the air and measured conduction losses. All of these plots are based on a vertical section at the center of the configuration (Station 3) and contain no adjustment for longitudinal effects other than the airflow. The figures show the sum, $\pi D_i \overline{q}_i'' + \pi D_o \left(\overline{q}_o'' + q_{\text{cond}}\right)$, as a percentage of the average line load given in Table IX-6 or IX-7. In forming the sum, q_{cond} is from Table IX-34 or IX-35. The convective heat flux at each surface is:

$$\overline{q}'' = \frac{k\,\overline{Nu}\left(\overline{T} - T_f\right)}{D_o - D_i} \qquad \text{(Eq. IX-84)}$$

The Nusselt numbers are from Tables IX-18 through IX-21, each temperature is from Table IX-13 or IX-14, and *k* is 0.0263 W/m K.

The percentages cluster around 85%. Of the energy convected, 75 to 85% was directly from the waste package, with the remaining 15 to 25% being convected from the drift wall. From this perspective, the effects of errors in $\overline{Nu_o}$ are limited because $\overline{T_o} - T_f$ is small. Considered in terms of the effects of the errors in a ventilation model that conserves total energy, the surface temperatures might have to rise enough to remove an additional 10% of the energy. For the ventilation tests, for example, a ventilation model that used the mixed-convection methodology might predict a waste package temperature that was too high by about 2°C and a wall temperature that was too high by about 0.3ºC.

In summary, the results of the EBS Ventilation Tests support the mixed convection methodology for prediction of the Nusselt number at the waste package, which is the dominant source for heat transfer to the air. They also support the use of the methodology, rather than a forced convection formula, at the drift wall. The determination of accuracy and precision followed conventional scientific standards, and used sensitivity analyses and bounding techniques, as appropriate.

This appendix accounts for uncertainties and variabilities in parameter values and provides for the technical basis for parameter ranges, probability distributions, or bounding values that may be used in predictions. Also, this appendix considers alternative conceptual models of processes that are consistent with available data and current scientific understanding and evaluates the effects that alternative conceptual models have on the predictions.

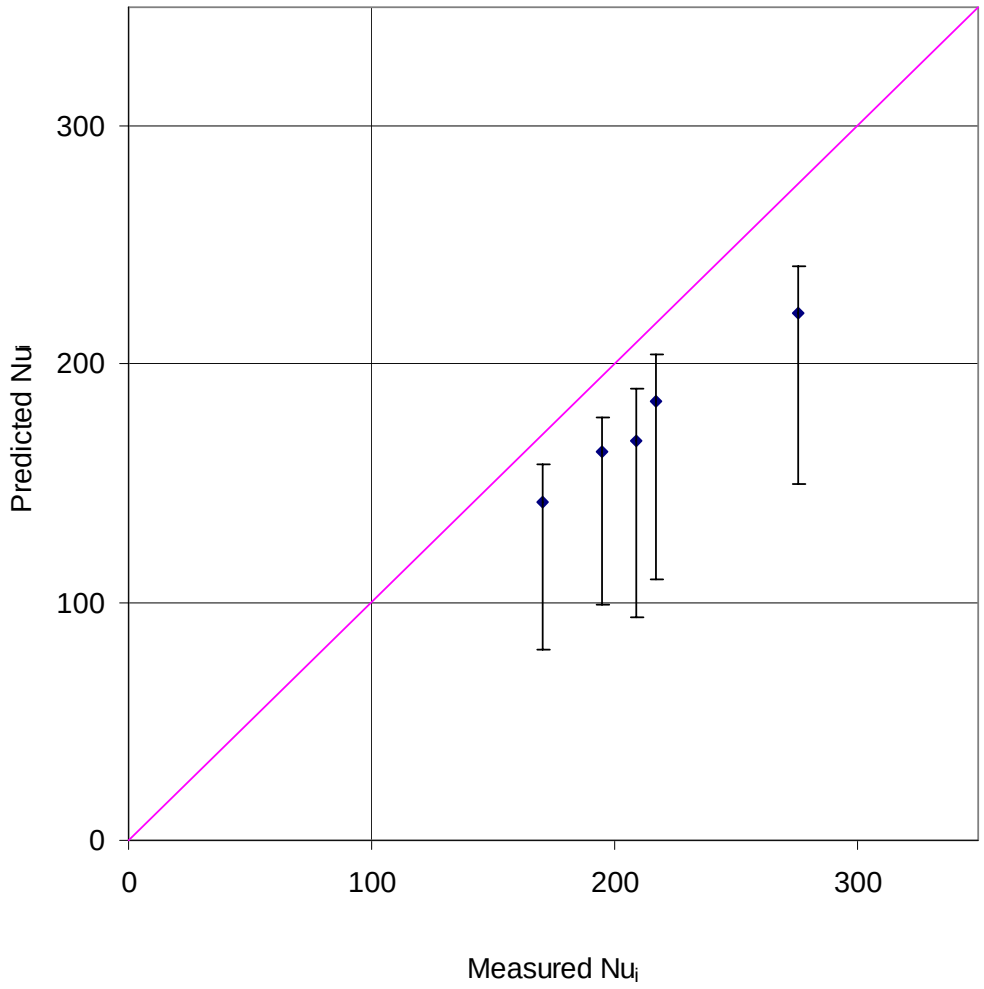

Output DTN: MO0306MWDMXCNV.000, modified from worksheet "Nusselt no. plots sta. 3" of Phase 1 Supporting Calculations for Mixed Convection.xls.

Figure IX-3. Comparison of "Measured" and Predicted Inner Surface Nusselt Numbers for Phase 1 Ventilation Tests

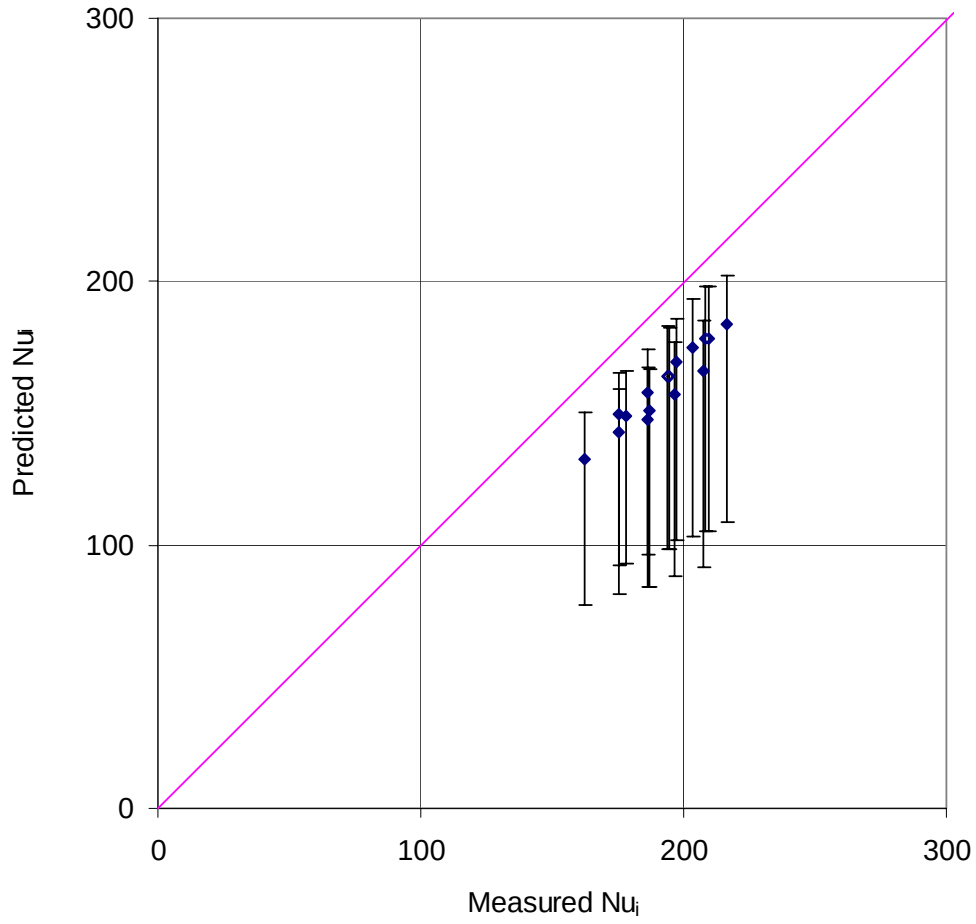

Output DTN: MO0306MWDMXCNV.000, modified from worksheet "Nusselt no. plots sta. 3" of Phase 2 Supporting Calculations for Mixed Convection.xls.

Figure IX-4. Comparison of "Measured" and Predicted Inner Surface Nusselt Numbers for Phase 2 Ventilation Tests

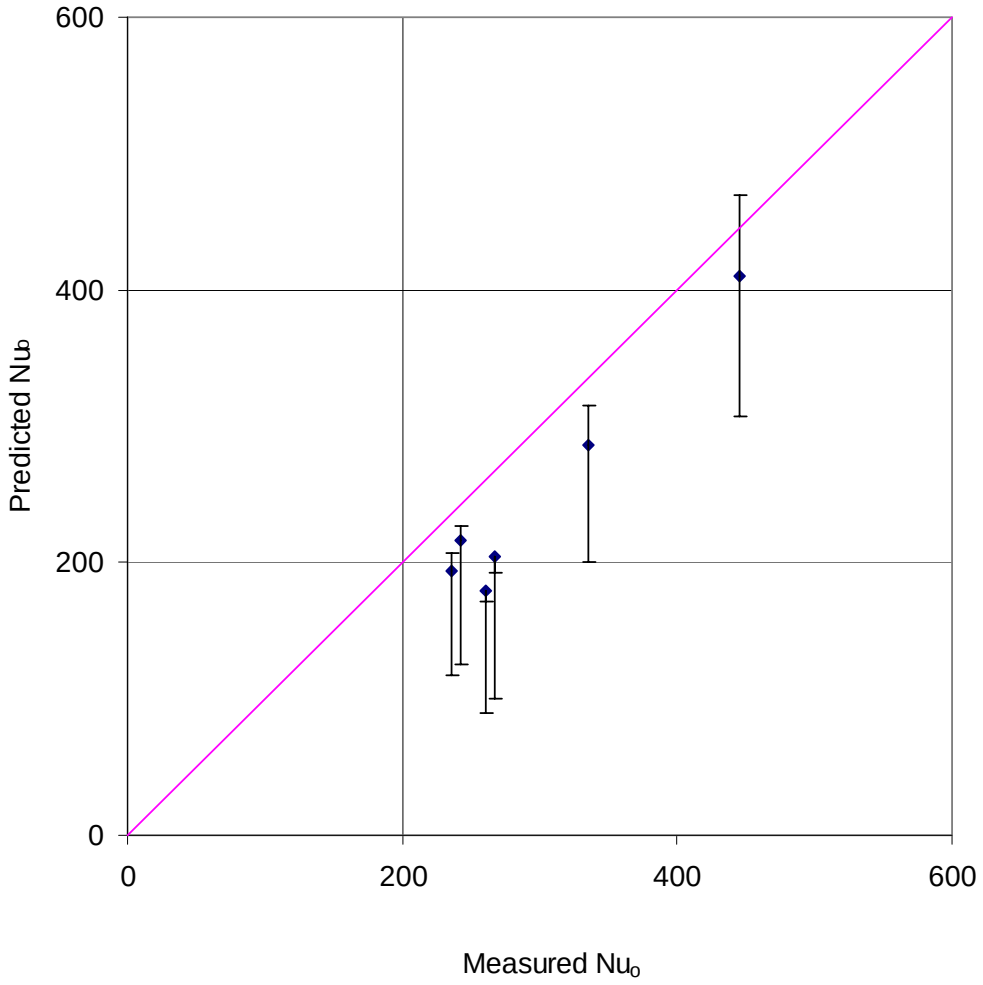

Output DTN: MO0306MWDMXCNV.000, modified from worksheet “Nusselt no. plots sta. 3” of Phase 1 Supporting Calculations for Mixed Convection.xls.

Figure IX-5. Comparison of “Measured” and Predicted Outer Surface Nusselt Numbers for Phase 1 Ventilation Tests

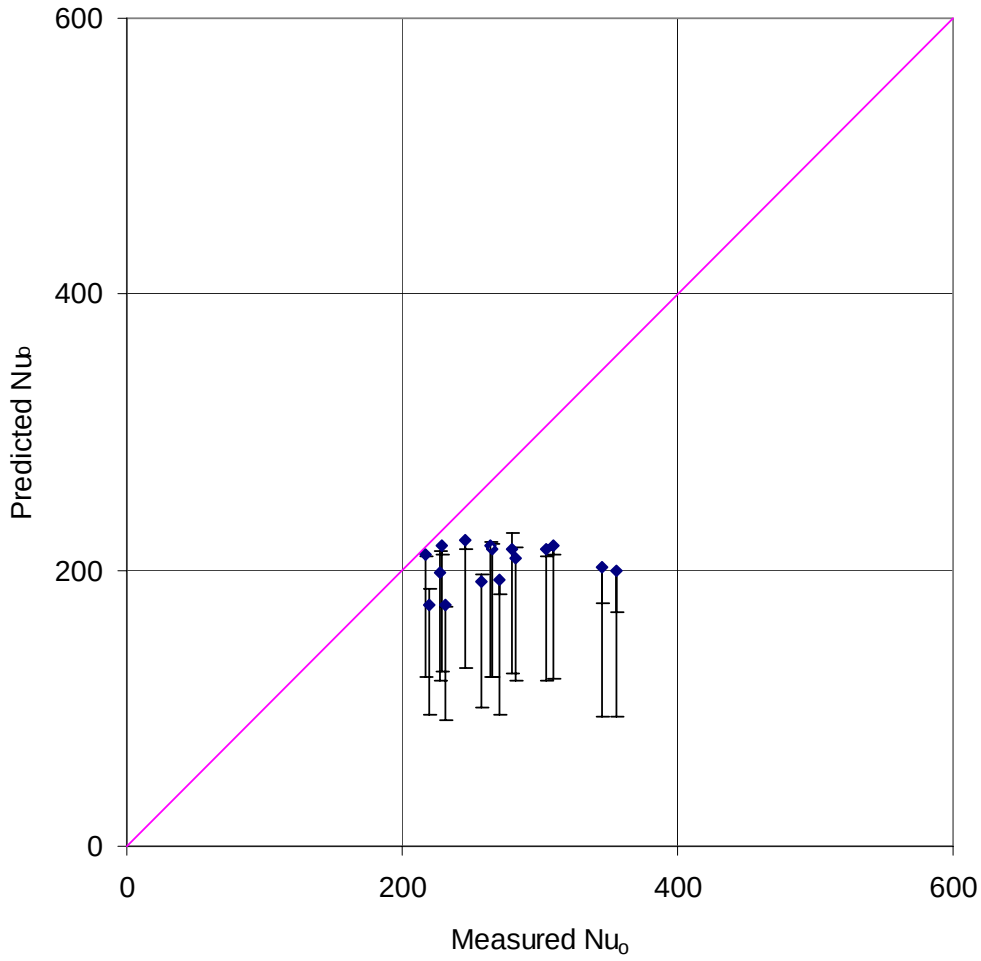

Output DTN: MO0306MWDMXCNV.000, modified from worksheet "Nusselt no. plots sta. 3" of Phase 2 Supporting Calculations for Mixed Convection.xls.

Figure IX-6. Comparison of "Measured" and Predicted Outer Surface Nusselt Numbers for Phase 2 Ventilation Tests

Table IX-36. Outer-Surface Nusselt Number Measurements for Flow Rate of 0.5 m^3/s

Phase	Test	Nominal Line Load (W/m)	Inlet Air Temperature (C)	Measured Nu_o	Predicted Nu_o	*Dittus-Boelter* Nu_o
2	9	220	25	219	175	60
2	10	220	35	232	175	61
2	11	220	45	356	199	58
2	12	360	25	257	191	63
2	13	360	35	270	193	61
2	14	360	45	345	202	58

Source: Tables IX-7, IX-35, and IX-21, and Equation IX-12, using Re from Table IX-12.

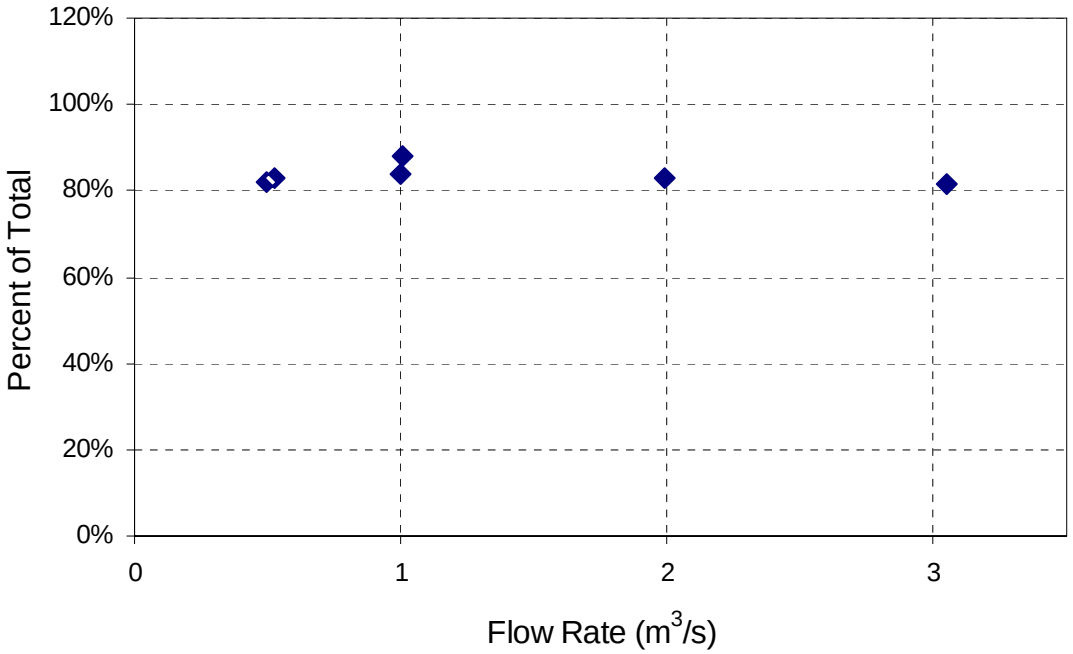

Output DTN: MO0306MWDMXCNV.000, modified from worksheet "Energy balance" of Phase 1 Supporting Calculations for Mixed Convection.xls.

Figure IX-7. Energy Balance Using Convection Prediction for Phase 1 Tests (Heat Convected to Air, Augmented by Heat Conducted Through Concrete, as a Percentage of Input Energy)

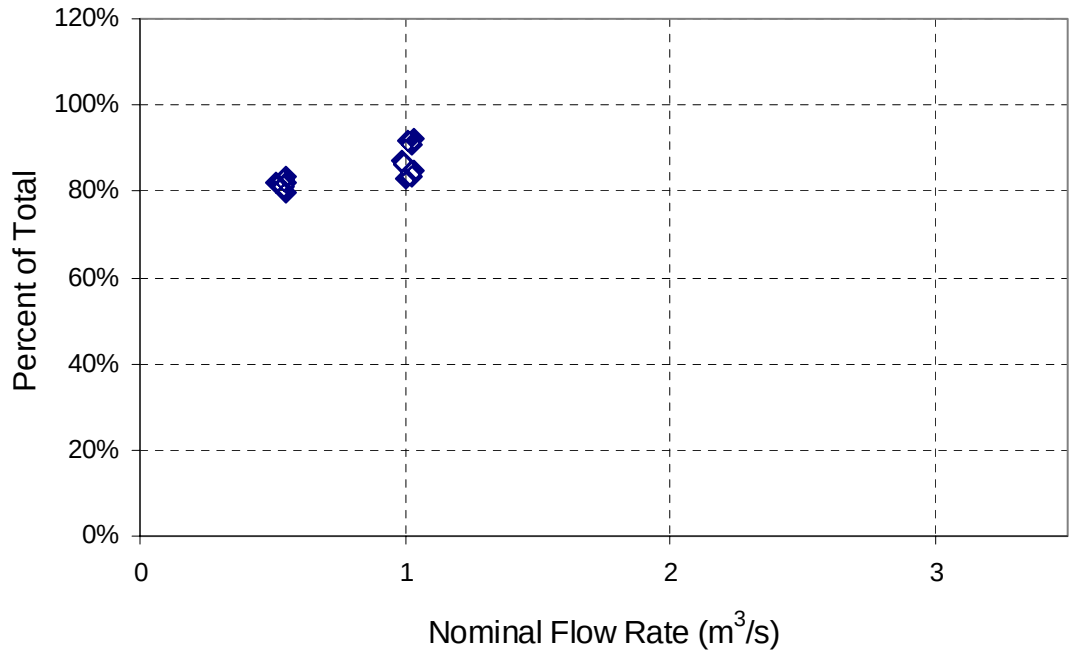

Output DTN: MO0306MWDMXCNV.000, modified from worksheet "Energy balance" of Phase 2 Supporting Calculations for Mixed Convection.xls.

Figure IX-8. Energy Balance Using Convection Prediction for Phase 2 tests (Heat Convected to Air, Augmented by Heat Conducted Through Concrete, as a Percentage of Input Energy)

APPENDIX X

VERIFICATION CALCUATIONS IN SUPPORT OF THE MIXED CONVECTION CORRELATION METHODOLOGY (APPENDIX IX)

This appendix documents the spreadsheets calculations used in Appendix IX. The electronic copies of these Microsoft Excel spreadsheets are contained in Mixed Convection.zip (DTN: MO0306MWDMXCNV.000). Table X-1 summarizes the contents of the spreadsheets. Further documentation of the cell formulas and referencing is found within the electronic copy of the file.

Table X-1. Contents of Spreadsheet used in the Mixed Convection Methodology of Appendix IX

File Name (.xls)	Contents
Phase 1 Supporting Calculations for Mixed Convection	Mixed Convection model applied to the EBS Ventilation Test Series, Phase I; Evaluation of uncertainty for EBS Ventilation Tests Series, Phase I; Determination of measured Nusselt numbers for EBS Ventilation Test Series, Phase I; Calculated Energy Balance for Phase I.
Phase 2 Supporting Calculations for Mixed Convection	Mixed Convection model applied to the EBS Ventilation Test Series, Phase II; Evaluation of uncertainty for EBS Ventilation Tests Series, Phase II; Determination of measured Nusselt numbers for EBS Ventilation Test Series, Phase II; Calculated Energy Balance for Phase II.
h-cond from NC tests	Evaluation of effective heat transfer coefficient for conduction
Mixed Convection Sensitivity	Sensitivity of Mixed Convection model to input parameters

INTENTIONALLY LEFT BLANK

APPENDIX XI

ANALYSIS OF THE VENTILATION TEST PHASE 2 DATA IN SUPPORT OF THE CALCULATIONS PERFORMED IN APPENDIX IX

Results from the Phase 2 Ventilation Tests were used to support validation of the mixed convection correlation in Appendix IX. The raw data is in DTN: SN0208F3409100.009 [DIRS 163079].

The summary data are contained in Vent-Test Phase-II.zip (DTN: MO0306MWDVTPH2.000). There is one file for each test (*Phase II Test 1_Q.xls, Phase II Test 2_Q.xls, Phase II Test 3_Q.xls, Phase II Test 4_Q.xls, Phase II Test 5_Q.xls, Phase II Test 6_Q.xls, Phase II Test 7_Q.xls, Phase II Test 8_Q.xls, Phase II Test 9_Q.xls, Phase II Test 10_Q.xls, Phase II Test 11_Q.xls, Phase II Test 12_Q.xls, Phase II Test 13_Q.xls, Phase II Test 14_Q.xls, Phase II Test 15_Q.xls, and Phase II Test 16_Q.xls*) that contains:

- The data recorded by the datalogger and entered into the Technical Data Management System – sheet name "*raw data*." This sheet also contains simple statistical analysis (average, standard deviation, maximum and minimum) for a defined time period. The time period was chosen as a 24-hour period over which data is representative of steady-state conditions where the ventilating air was at or near the desired temperature and relative humidity.

  The sheet is organized as follows:

  - Cell A14: DTN: SN0208F3409100.009 associated with the data
  - Time period chosen for averaging data: Cells C1 and C2
  - Rows 4 and 5: addresses corresponding to chosen time period for statistical analysis
  - Rows 7, 8, 9 and 10: resulting statistical analysis (average, standard deviation, maximum and minimum) for the chosen time period
  - Row 24: Starting row for the data pulled from the Technical Data Management System

- The calculated total power input (summation of the five stations) and line load (total power input divided by the heated length) – sheet name "*power*."

  The sheet is organized as follows:

  - Columns A through F: Summary of the power data, including the time stamp and recorded power data for the five power stations (taken directly from the "raw data" worksheet)
  - Column H: Summation of the five recorded power inputs for each time stamp
  - Column I: Calculated average line load for the test train, defined as the total power input (column H) divided by the total heated length (111' 4" (33.9 m)), calculated by adding the recorded distance to the leading edge of waste package 25 (98' 2 1/2" + 105 1/2") plus the recorded length of waste package 25 (52") (BSC 2003 [DIRS 160724], p. 2-3).

- The calculated volumetric and mass flow rates – sheet name "*flow.*" The flow rates for each test were calculated based on air velocity probe differential pressure, relative humidity, barometric pressure, and air temperature measurements. Complete details of the calculation can be found in *Testing to Provide Data for Ventilation System Design: Phase 1* (BSC 2003 [DIRS 160724], Section 5.2.1). As a summary, the measured differential pressure was converted to an air velocity. Properties of the ventilating fluid (e.g., the mixture of air and water vapor) were determined using measured relative humidities and temperatures. The air velocity was then combined with the cross-sectional area of the ducting to determine a volume flow rate.

  The sheet is organized as follows:

  - Column A through J: Summary of the data required to calculate flow. At station A, there were two differential pressure gauges (VA-VEL-01 and VA-VEL-02), two relative humidity gauges (VA-HUM-H1 and VA-HUM-H2), and nine RTDs measuring air temperature (VA-RTD-01 through VA-RTD-09), that were used in calculating the flow. Each set of measurements was averaged to create the differential pressure, relative humidity, and air temperature needed for the flow calculations. The flow at station D was calculated using measurements from one differential pressure gauge at station D (VD-VEL-01), two relative humidity gauges at station C (VC-HUM-H1 and VC-HUM-H2), and two RTD air temperature gauges at station C (VC-RTD-01 and VC-RTD-02).

  - Columns L through AD: Calculations of flow rates for Station A

  - Column AI through AY: Calculations of flow rate for Station D

- All constants and dimensions used in the calculation are given in a sheet named "*properties.*" References for these properties are provided.

APPENDIX XII

DOCUMENTATION OF THE VENTILATION PHASE 1 POST-TEST ANSYS ANALYSES FOR MODEL VALIDATION (INPUTS AND OUTPUTS)

This appendix documents the Ventilation Test Phase 1 post-test ANSYS modeling for validation purposes, which was developed using the Ventilation Test Phase 1 data, ANSYS software and spreadsheet methods. The input and output files, and Microsoft Excel spreadsheets are contained in DTN: MO0209MWDANS30.017.

INTENTIONALLY LEFT BLANK

APPENDIX XIII

ANALYTICAL SOLUTION USING MATHCAD FOR THE CONTRIBUTION OF LATENT HEAT TO THE IN-DRIFT AIR OF A VENTILATED EMPLACEMENT DRIFT USING A SOLUTION FOR STEADY-STATE UNSATURATED FLOW TO MOISTURE POTENTIAL BOUNDARY AT THE DRIFT WALL

Note that the symbol := used throughout this appendix means to assign the right hand value or expression to the left hand variable.

Develop a steady solution for radial unsaturated flow to the specified moisture potential conditions. Neglect the gravity component of flow, and consider the van Genuchten constitutive relationships. *Soil Physics* (Jury et al. 1991 [DIRS 102010], Section 3.4) develops the solution for radial flow under saturated conditions. In the case of steady-state flow under saturated conditions, the water conservation equation for a cylindrical coordinate geometry is given by:

$$\frac{1}{r} \cdot \frac{d}{dr}\left(r \cdot J_r\right) = 0 \qquad \text{(Eq. XIII-1)}$$

where

r = Radial Coordinate
J_r = Darcy Flux in the Radial Direction

Equation XIII-1 can be integrated once to produce the result:

$$r \cdot J_r = \phi = constant = \frac{Q}{2\pi \cdot z_0} \qquad \text{(Eq. XIII-2)}$$

where

Q = Steady-state moisture flow
z_0 = Drift length

The radial flux under Darcy's Law is given by:

$$J_r = -K_s \cdot \frac{dp}{dr} \qquad \text{(Eq. XIII-3)}$$

where

K_S = Saturated Hydraulic Conductivity
p = Pressure or Pressure Head Depending on convention adopted for Darcy's Law

Writing Darcy's Law for radial flow to the tunnel surface:

$$-K_s \cdot \frac{dp}{dr} = \frac{Q}{2\pi \cdot z_0 \cdot r} \qquad \text{(Eq. XIII-4)}$$

This equation can be integrated after placing all factors explicitly for r on the same side of the equation:

$$dp = \frac{-Q}{2\pi \cdot K_s \cdot z_0} \cdot \frac{dr}{r} \qquad \text{(Eq. XIII-5)}$$

Since $p(R_1) = p_1$ and $p(R_2) = p_2$ are specified at the boundary, then:

$$\int_{p_1}^{p_2} dp = \frac{-Q}{2\pi \cdot K_s \cdot z_0} \int_{R_1}^{R_2} \frac{dr}{r} \qquad \text{(Eq. XIII-6)}$$

from which we calculate:

$$Q = \frac{2\pi \cdot K_s \cdot z_0 \cdot (p_1 - p_2)}{ln\left(\frac{R_2}{R_1}\right)} \qquad \text{(Eq. XIII-7)}$$

This expression agrees with the formulation presented in *Soil Physics* (Jury et al. 1991 [DIRS 102010], p. 113 Equation 3.92).

Now consider the unsaturated flow case. The pressure gradient becomes a moisture potential gradient. For unsaturated flow, the unsaturated hydraulic conductivity is a strong nonlinear function of the moisture potential $\overline{\psi}$.

Neglecting the elevation head:

$$H_1 = \frac{p_1}{\gamma_w g} + 0 = -\psi_1 \qquad \text{(Eq. XIII-8)}$$

$$H_2 = \frac{p_2}{\gamma_w g} + 0 = -\psi_2 \qquad \text{(Eq. XIII-9)}$$

where

H_1	=	Total Potential at the Drift Surface R1
H_2	=	Total Potential at the Outer Boundary R2
ψ_1	=	Moisture Potential at Radius R1 Set by the RH in the Drift
ψ_2	=	Moisture Potential at Radius R2 Set by Undisturbed State of Capillary Equilibrium
γ_w	=	Unit Weight of Water
g	=	gravitational constant

Writing Darcy's Law for unsaturated radial flow:

$$-K(\psi)\cdot\frac{dH}{dr}=\frac{Q}{2\pi\cdot z_0\cdot r} \qquad \text{(Eq. XIII-10)}$$

Noting that if we neglect the elevation head:

$$H\approx\psi$$

$$-K(\psi)\cdot\frac{d\psi}{dr}=\frac{Q}{2\pi\cdot z_0\cdot r} \qquad \text{(Eq. XIII-11)}$$

The convention is adopted that moisture potential is in units of head (Jury et al. 1991 [DIRS 102010], p. 51). Now the van Genuchten constitutive relation can be invoked. From *Contaminant Hydrogeology* (Fetter 1993 [DIRS 102009], p. 182), the constitutive relation is:

$$K(\psi)=\frac{K_s\left\{1-(\alpha\psi)^{n-1}\left[1+(\alpha\psi)^n\right]^{-m}\right\}^2}{\left[1+(\alpha\psi)^n\right]^{\frac{m}{2}}} \qquad \text{(Eq. XIII-12)}$$

where

n	=	1/(1-m)
α	=	Van Genuchten alpha
m	=	Van Genuchten fitting parameter

Substituting in the constitutive relation into Darcy's Law:

$$-\frac{K_s\left\{1-(\alpha\psi)^{n-1}\left[1+(\alpha\psi)^n\right]^{-m}\right\}^2}{\left[1+(\alpha\psi)^n\right]^{\frac{m}{2}}}\cdot\frac{d\psi}{dr}=\frac{Q}{2\pi\cdot z_0\cdot r} \qquad \text{(Eq. XIII-13)}$$

Equation XIII-13 can be integrated in the same manner:

$$-\int_{\psi_1}^{\psi_2}\frac{K_s\left\{1-(\alpha\psi)^{n-1}\left[1+(\alpha\psi)^n\right]^{-m}\right\}^2}{\left[1+(\alpha\psi)^n\right]^{\frac{m}{2}}}\cdot d\psi=\frac{Q}{2\pi\cdot z_0}\int_{R_1}^{R_2}\frac{dr}{r}=\frac{Q}{2\pi\cdot z_0}\cdot\ln\left(\frac{R_2}{R_1}\right) \qquad \text{(Eq. XIII-14)}$$

Note that the sign convention in the constitutive law is positive while in Darcy's Law it is negative. Note also that ψ_1 and ψ_2 are expressed in units of head consistent with the sign convention presented in *Soil Physics* (Jury et al. 1991 [DIRS 102010], p. 151). Substituting in the definition of hydraulic conductivity (Fetter 1993 [DIRS 102009], p. 181):

$$K_s = \frac{\rho g k}{\mu} \qquad \text{(Eq. XIII-15)}$$

where

k = intrinsic permeability (m^2)
μ = fluid viscosity ($N \cdot s/m^2$)

$$Q = \frac{-2\pi \cdot z_0 \cdot \frac{\rho g k}{\mu} \cdot \int_{\psi_1}^{\psi_2} \frac{\left\{1-(\alpha\psi)^{n-1}\left[1+(\alpha\psi)^n\right]^{-m}\right\}^2}{\left[1+(\alpha\psi)^n\right]^{\frac{m}{2}}} \cdot d\psi}{ln\left(\frac{R_2}{R_1}\right)} \qquad \text{(Eq. XIII-16)}$$

Now consider the boundary conditions, and the geometry for the problem. Use an RH of 30 percent (Section 4.1.2) in the ventilated drift and use the Kelvin Equation to calculate moisture potential (Jury et al. 1991 [DIRS 102010], p. 60):

$$RH = exp\left(\frac{M_w \psi_1}{\rho_w RT}\right) \qquad \text{(Eq. XIII-17)}$$

Input properties for analysis. The properties for water are obtained from Section 4.1.12 at 350 K:

$$\rho_w = 973.7 \text{ kg/m}^3 = 0.9737 \text{ gm/cm}^3$$

From Table 4-20:

M_w = 18 gm/mol
R = 8.315 J/mol·K

Substituting into Equation XIII-17:

$$\psi(RH,T) = \frac{\rho_w RT}{M_w} \cdot ln\left(\frac{RH}{100}\right)$$

$$\psi(30\%,350K) = -1.896 \cdot 10^8 \frac{kg}{m \cdot s^2}$$

The moisture potential is expressed in pressure. Calculate the moisture potential in units of head:

$$\psi_1 = \frac{|\psi(30\%,350K)|}{\rho_w g} = \frac{\left|-1.896\cdot 10^8 \frac{kg}{m\cdot s^2}\right|}{\left(973.7\frac{kg}{m^3}\right)\cdot\left(9.81\frac{m}{s^2}\right)} = 1.985\cdot 10^4 m = 1.985\cdot 10^6 cm$$

From Table 4-6 and Table 4-9, the hydrologic properties for the repository host rock unit surrounding the drift (Tptpll or tsw35) are:

Matrix permeability = k_m = $4.48\cdot10^{-18}$ m^2
Matrix porosity = ϕ_m = 0.1486
Van Genuchten matrix alpha = α = $1.08\cdot10^{-5}$ Pa^{-1}
Van Genuchten matrix fitting parameter = m = 0.216
Residual matrix saturation = θ_r = $s_{lrm}\cdot \phi_m$ = 0.0178
Satiated matrix saturation = θ_s = $s_{lsm}\cdot\phi_m$ = 0.1486

From Table 4-18 at 350 K:

$$\mu_w = 3.65\cdot10^{-4}\ N\cdot s/m^2$$

To convert α from Pa^{-1} to cm^{-1}, multiply by $\rho_w g$:

$$\alpha = \left(\frac{1.08\cdot10^{-5}}{Pa}\right)\left(\frac{1Pa}{1\frac{N}{m^2}}\right)\left(\frac{1N}{1\frac{kg\cdot m}{s^2}}\right)\left(973.7\frac{kg}{m^3}\right)\left(9.81\frac{m}{s^2}\right) = 0.1032m^{-1} = 1.032\cdot10^{-3}cm^{-1}$$

The retention relationship (Fetter 1993 [DIRS 102009], p. 172, Equation 4.9) is used to calculate the moisture potential:

$$\theta = \theta_r + \frac{\theta_s - \theta_r}{\left[1+(\alpha\psi)^n\right]^m} \qquad \text{(Eq. XIII-18)}$$

where

$$n = \frac{1}{1-m} \qquad \text{(Eq. XIII-19)}$$

Solve Equation XIII-18 for moisture potential in terms of volumetric moisture content:

$$\psi = \frac{\left\{-1+\left[\frac{-\left(-\theta_s+\theta_r\right)}{\theta-\theta_r}\right]^{\frac{1}{m}}\right\}^{\frac{1}{n}}}{\alpha} \qquad \text{(Eq. XIII-20)}$$

The average saturation of Tptpll (tsw35) given the saturations measured in USW SD-7, USW SD-9, USW NRG-6, USW NRG-7/7A, and USW UZ-7A in Table 4-4 is 0.74. The average volumetric moisture content is:

$$\theta = 0.74 \cdot \theta_s = 0.1100$$

Solving Equation XIII-20 then yields:

$$\psi = 2908 \text{ cm} = \psi_2$$

The radius of the drift, R_1, is 2.75 m (Table 4-16). Assume a radius of influence, R_2, of 6 m. The drift length, z_0, is 600 m. Calculate the steady-state moisture flow at the drift wall by solving the integral in Equation XIII-16:

$$Q = 2.002 \cdot 10^{-8} \frac{m^3}{s}$$

The steady-state moisture flow, expressed as a liquid flux toward the drift wall, is:

$$\frac{Q}{2\pi \cdot R_1 \cdot z_0} = \frac{2.002 \cdot 10^{-8} \frac{m^3}{s}}{2\pi \cdot 2.75m \cdot 600m} \cdot \frac{31556926s}{1yr} \cdot \frac{1000mm}{1m} = 0.061 \frac{mm}{yr}$$

Calculate the latent heat transfer over the 50-year ventilation period by multiplying the flow by the latent heat of vaporization at 350 K (Table 4-18):

$$\left(2.002 \cdot 10^{-8} \frac{m^3}{s}\right) \cdot \left(973.7 \frac{kg}{m^3}\right) \cdot \left(2317 \frac{kJ}{kg}\right) \cdot \left(\frac{1000J}{1kJ}\right) \cdot (50yr) \cdot \left(\frac{31556926s}{1yr}\right) = 7.130 \cdot 10^{10} J$$

The total waste package heat input over 50 years and 600 meters is 8.60×10^{14} J (DTN: MO0307MWDAC8MV.000, worksheet "Ventilation Efficiency"). The contribution of latent heat expressed as a percentage of the total waste package heat input is:

$$\frac{7.130 \cdot 10^{10} J}{8.605 \cdot 10^{14} J} = 0.01\%$$

Note that the above analysis is based upon a steady state analysis and measured values of moisture potential. At the time of waste emplacement within the repository emplacement drift, a transient flow response will be induced with a higher flow rate that might result in more rapid

dewatering of the saturated matrix pore space than is predicted on the basis of the steady state analysis presented above. However, the results of *Multiscale Thermohydrologic Model* (BSC 2004 [DIRS 169565]) show that at selected locations the matrix saturation remains high during the preclosure period. For example, matrix saturation remains high at locations P2ER8C6, P2WR8C8, P2WR5C10, and P3R7C12 (BSC 2004 [DIRS 169565], Figures 6.3-7 through 6.3-10). Further, the volumetric moisture content versus temperature relation as measured from neutron logging of boreholes 79 and 80 during the Drift Scale Test heating phase shows little reduction in volumetric moisture content below the boiling point of water (DTN: MO0406SEPTVDST.000 [DIRS 170616], file "both.xls"). Since the ventilation analysis predicts below boiling conditions, the latent heat of vaporization from the dewatering of the saturated matrix under transient flow is not expected to be significant.

The calculation of the farfield moisture potential from the saturation on core measurements (Table 4-4) and the van Genuchten retention relationship may be compared with measurements of water potential made in the ECRB Cross-Drift (Table 4-5). At a depth, R_2, of 5.62 m, the measured water potential, ψ_2, is 10 m. The potential at the drift wall was calculated previously to be ψ_1 (30%, 350K) = $1.985 \cdot 10^4$ m. The drift length, z_0, is again 600 m. Calculate the steady-state moisture flow at the drift wall by solving the integral in Equation XIII-16:

$$Q = 9.1196 \cdot 10^{-8} \frac{\mathrm{m}^3}{\mathrm{s}}$$

The steady-state moisture flow, expressed as a liquid flux toward the drift wall, is:

$$\frac{Q}{2\pi \cdot R_1 \cdot z_0} = \frac{9.1196 \cdot 10^{-8} \frac{\mathrm{m}^3}{\mathrm{s}}}{2\pi \cdot 2.75\mathrm{m} \cdot 600\mathrm{m}} \cdot \frac{31556926\mathrm{s}}{1\mathrm{yr}} \cdot \frac{1000\mathrm{mm}}{1\mathrm{m}} = 0.278 \frac{\mathrm{mm}}{\mathrm{yr}}$$

Calculate the latent heat transfer over the 50-year ventilation period by multiplying the flow by the latent heat of vaporization at 350 K (Table 4-18):

$$\left(9.1196 \cdot 10^{-8} \frac{\mathrm{m}^3}{\mathrm{s}}\right) \cdot \left(973.7 \frac{\mathrm{kg}}{\mathrm{m}^3}\right) \cdot \left(2317 \frac{\mathrm{kJ}}{\mathrm{kg}}\right) \cdot \left(\frac{1000\mathrm{J}}{1\mathrm{kJ}}\right) \cdot (50\mathrm{yr}) \cdot \left(\frac{31556926\mathrm{s}}{1\mathrm{yr}}\right) = 3.246 \cdot 10^{11}\,\mathrm{J}$$

The total waste package heat input over 50 years and 600 meters is $8.60 \cdot 10^{14}$ J (DTN: MO0307MWDAC8MV.000, worksheet "Ventilation Efficiency"). The contribution of latent heat expressed as a percentage of the total waste package heat input is:

$$\frac{3.246 \cdot 10^{11}\,\mathrm{J}}{8.605 \cdot 10^{14}\,\mathrm{J}} = 0.04\%$$

INTENTIONALLY LEFT BLANK

APPENDIX XIV

DOCUMENTATION OF THE ANSYS-LA-COARSE-INSTANTANEOUS-EFFICIENCY-APPLICATION (INPUTS AND OUTPUTS)

This appendix documents the ANSYS-LA-Coarse-Instantaneous-Efficiency-Application model which was developed using the ANSYS software and spreadsheet methods. The input and output files, and Microsoft Excel spreadsheet are contained in the file ANSYS-LA-Coarse-Instantaneous-Efficiency-Application.zip (DTN: MO0306MWDCIEAP.000). Table XIV-1 is a description of the input and output files, and the worksheets contained in the spreadsheet ANSYS-LA-Coarse-Instantaneous-Efficiency-Application.xls. Further documentation of the cell formulas and referencing are found within the electronic copy of the file.

Table XIV-1. Contents of ANSYS-LA-Coarse-Instantaneous-Efficiency-Application.zip

ANSYS Input and Output Files	
File	**Description**
decay_data_c3.input	ANSYS input file containing the waste package heat decay for segment 3, reduced by the ventilation efficiency.
decay_data_c8.input	ANSYS input file containing the waste package heat decay for segment 8, reduced by the ventilation efficiency.
th_data.input	ANSYS input file containing the thermal properties of the repository layers and the EBS components.
la800.dat	ANSYS input file which generates the mesh and assigns thermal properties to each cell within the mesh.
la800.db	ANSYS output file.
la800.grph	ANSYS output file.
la800.sub	ANSYS output file.
la800.out	ANSYS output file.
air_temp_c3 and air_temp_c8	ANSYS input files containing the inlet air temperature of the specified segment (from ANSYS-LA-Coarse.xls).
dr_h_c3 and dr_h_c8	ANSYS input file containing the drift wall convection coefficients for the specified segment (from ANSYS-LA-Coarse.xls).
wp_h_c0 through wp_h_c10	ANSYS input files containing the waste package convection coefficients for the specified segment (from ANSYS-LA-Coarse.xls).
la800c3_ev1.dat and la800c8_ev1.dat	Main ANSYS input files.
la800c3_ev1.db and la800c8_ev1.db	ANSYS output files.
la800c3_ev1.grph and la800c8_ev1.grph	ANSYS output files.
la800c3_ev1.dsub and la800c10.dsub	ANSYS output files.
la800c3_ev1.mntr and la800c8_ev1.mntr	ANSYS output files.
la800c3_ev1.osav and la800c8_ev1.osav	ANSYS output files.
la800c3_ev1.rth and la800c8_ev1.rth	ANSYS output files.
la800c3_ev1.stat and la800c8_ev1.stat	ANSYS output files.
la800c3_ev1.s01 to .s21 and la800c8_ev1.s01 to .s21	ANSYS output files.
la800c3_ev1.out and la800c8_ev1.out	Main ANSYS output files.

Table XIV-1. Contents of ANSYS-LA-Coarse-Instantaneous-Efficiency-Application.zip (Continued)

ANSYS Input and Output Files	
File	**Description**
result_c3_ev1 and result_c8_ev1	Temperature results that are cut from the end of the .out files and imported to ANSYS-LA-Coarse.xls.
100m data	Contains the data from ANSYS-LA-Coarse.xls at 100 m (segment 3) used in the instantaneous ventilation efficiency application and the output of the ANSYS model.
Plot 100m	Plots the waste package and drift wall temperatures for ANSYS-LA-Coarse and ANSYS-LA-Coarse-Instantaneous-Efficiency-Application.
c3-t0-19	Contains the temperature results from the result_c3 ANSYS output files. Performs a circumferential weighted average given the temperatures of each element of the drift wall and waste package.
600m data	Contains the data from ANSYS-LA-Coarse.xls at 600 m (segment 8) used in the instantaneous ventilation efficiency application and the output of the ANSYS model.
Plot 600m	Plots the waste package and drift wall temperatures for ANSYS-LA-Coarse and ANSYS-LA-Coarse-Instantaneous-Efficiency-Application.
c8-t0-19	Contains the temperature results from the result_c8 ANSYS output files. Performs a circumferential weighted average given the temperatures of each element of the drift wall and waste package.

APPENDIX XV

DOCUMENTATION OF THE ANSYS-LA-COARSE-INSTANTANEOUS-EFFICIENCY-TWP-APPLICATION (INPUTS AND OUTPUTS)

This appendix documents the ANSYS-LA-Coarse-Instantaneous-Efficiency-Twp-Application model, which was developed using the ANSYS software and spreadsheet methods. The input and output files, and Microsoft Excel spreadsheet are contained in the file ANSYS-LA-Coarse-Intstantaneous-Efficiency-Twp-Application.zip (DTN: MO0306MWDCIETA.000). Table XV-1 is a description of the input and output files, and the worksheets contained in the spreadsheet ANSYS-LA-Coarse-Intstantaneous-Efficiency-Twp-Application.xls. Further documentation of the cell formulas and referencing are found within the electronic copy of the file.

Table XV-1. Contents of ANSYS-LA-Coarse-Intstantaneous-Efficiency-Twp-Application.zip

ANSYS Input and Output Files	
File	**Description**
decay_data_c3.input	ANSYS input file containing the waste package heat decay for segment 3, reduced by the ventilation efficiency.
decay_data_c8.input	ANSYS input file containing the waste package heat decay for segment 8, reduced by the ventilation efficiency.
th_data.input	ANSYS input file containing the thermal properties of the repository layers and the EBS components.
la800.dat	ANSYS input file which generates the mesh and assigns thermal properties to each cell within the mesh.
la800.db	ANSYS output file.
la800.grph	ANSYS output file.
la800.sub	ANSYS output file.
la800.out	ANSYS output file.
air_temp_c3 and air_temp_c8	ANSYS input files containing the inlet air temperature of the specified segment (from ANSYS-LA-Coarse.xls).
dr_h_c3 and dr_h_c8	ANSYS input file containing the drift wall convection coefficients for the specified segment (from ANSYS-LA-Coarse.xls).
wp_h_c0 through wp_h_c10	ANSYS input files containing the waste package convection coefficients for the specified segment (from ANSYS-LA-Coarse.xls).
la800c3_ev2.dat and la800c8_ev2.dat	Main ANSYS input files.
la800c3_ev2.db and la800c8_ev2.db	ANSYS output files.
la800c3_ev2.grph and la800c8_ev2.grph	ANSYS output files.
la800c3_ev2.dsub and la800c10.dsub	ANSYS output files.
la800c3_ev2.mntr and la800c8_ev2.mntr	ANSYS output files.
la800c3_ev2.osav and la800c8_ev2.osav	ANSYS output files.
la800c3_ev2.rth and la800c8_ev2.rth	ANSYS output files.
la800c3_ev2.stat and la800c8_ev2.stat	ANSYS output files.
la800c3_ev2.s01 to .s21 and la800c8_ev2.s01 to .s21	ANSYS output files.

Table XV-1. Contents of ANSYS-LA-Coarse-Intstantaneous-Efficiency-Twp-Application.zip (Continued)

ANSYS Input and Output Files	
File	**Description**
la800c3_ev2.out and la800c8_ev2.out	Main ANSYS output files.
result_c3_ev2 and result_c8_ev2	Temperature results that are cut from the end of the .out files and imported to ANSYS-LA-Coarse.xls.
100m data	Contains the data from ANSYS-LA-Coarse.xls at 100 m (segment 3) used in the instantaneous ventilation efficiency application and the output of the ANSYS model.
Plot 100m	Plots the waste package and drift wall temperatures for ANSYS-LA-Coarse and ANSYS-LA-Coarse-Instantaneous-Efficiency-Application.
c3-t0-19	Contains the temperature results from the result_c3 ANSYS output files. Performs a circumferential weighted average given the temperatures of each element of the drift wall and waste package.
600m data	Contains the data from ANSYS-LA-Coarse.xls at 600 m (segment 8) used in the instantaneous ventilation efficiency application and the output of the ANSYS model.
Plot 600m	Plots the waste package and drift wall temperatures for ANSYS-LA-Coarse and ANSYS-LA-Coarse-Instantaneous-Efficiency-Application.
c8-t0-19	Contains the temperature results from the result_c8 ANSYS output files. Performs a circumferential weighted average given the temperatures of each element of the drift wall and waste package.

APPENDIX XVI

CALCULATION FOR ESTIMATING THE IN-DRIFT CROSS-SECTIONAL AREA AVAILABLE FOR AIR FLOW

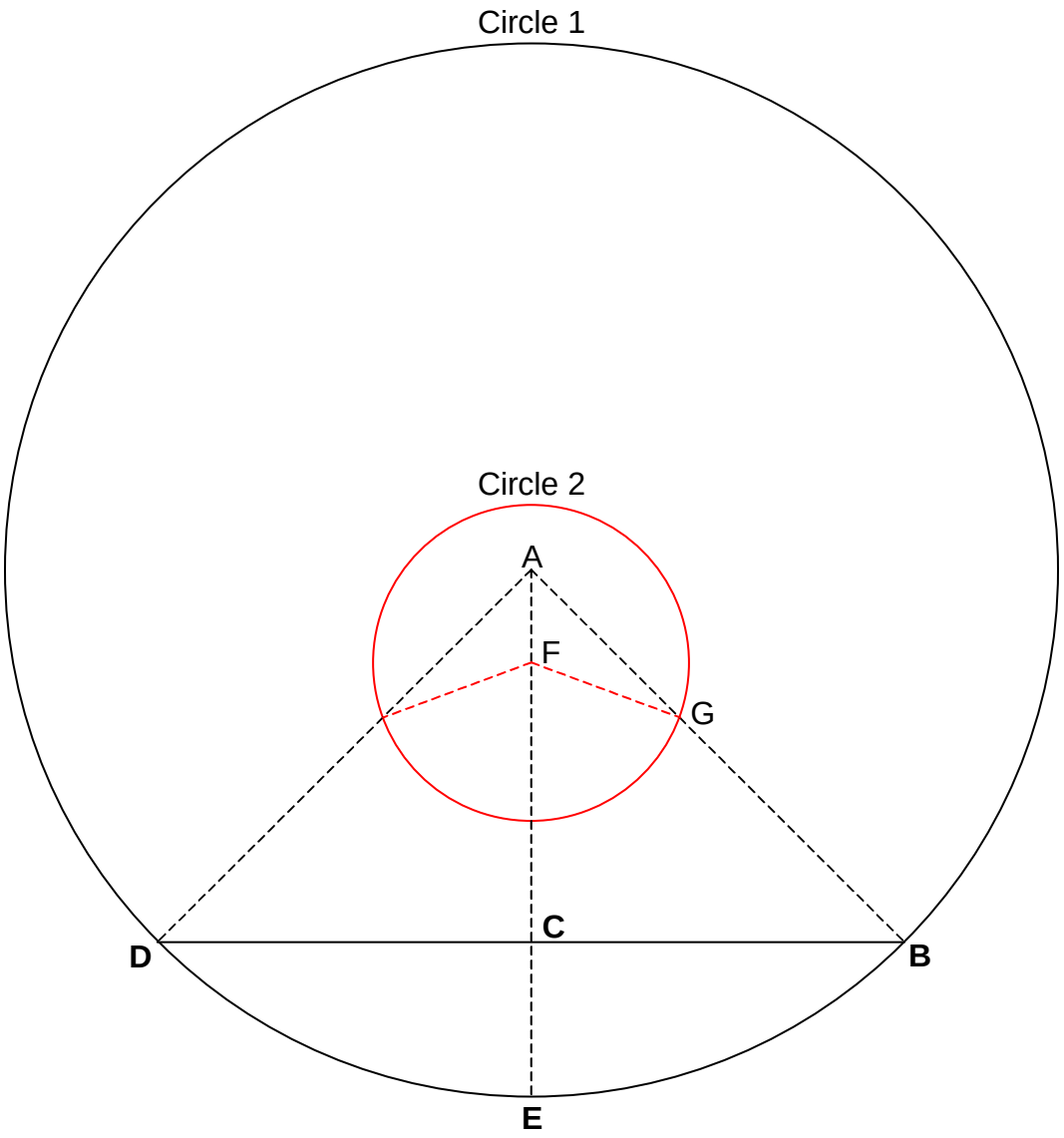

From Table 4-16:

$$AB = ACE = AD = \frac{5.5\text{m}}{2} = 2.75\text{m}$$

$$CE = 0.806\text{m}$$

From Table 4-15:

$$FG = \frac{1.644\text{m}}{2} = 0.822\text{m}$$

Using the Pythagorean Theorem:

$$AC^2 + BC^2 = AB^2$$

Then:

$$\mathrm{BC} = \sqrt{2.75^2 - (2.75 - 0.806)^2} = 1.945\mathrm{m}$$

$\angle$CAB is:

$$cos(\angle \mathrm{CAB}) = \frac{\mathrm{AC}}{\mathrm{AB}} = \frac{2.75 - 0.806}{2.75} = 0.707$$

Or:

$$\angle \mathrm{CAB} = cos^{-1}(0.707) = 45^{\circ}$$

Since ACE bisects BCD, $\angle$DAB is twice $\angle$CAB, or 90°. Since the sum of all internal angles emanating from the center of a circle is 360°, the pie shaped slice composed of points A, B, and D, and arc BED is ¼ the area of the Circle 1.

The area available for flow is: the area of Circle 1; minus the area of the pie shaped slice composed of points A, B, and D, and arc BED; plus the area of the triangle composed of points ABCD; minus the area of the Circle 2.

The area of Circle 1 is:

$$\pi \mathrm{AB}^2 = \pi \cdot 2.75^2 = 23.758\mathrm{m}^2$$

The area of the pie shaped slice composed of points A, B, and D, and arc BED is:

$$\frac{1}{4}\pi \mathrm{AB}^2 = \frac{1}{4}\pi \cdot 2.75^2 = 5.940\mathrm{m}^2$$

The area of the triangle composed of points ABCD is:

$$\frac{1}{2} \cdot \mathrm{BCD} \cdot \mathrm{AC} = \frac{1}{2} \cdot 2 \cdot 1.945 \cdot (2.75 - 0.806) = 3.781\mathrm{m}^2$$

The area of Circle 2 is:

$$\pi \mathrm{FG}^2 = \pi \cdot 0.822^2 = 2.123\mathrm{m}^2$$

Therefore, the area available for flow is:

$$23.758 - 5.940 + 3.781 - 2.123 = 19.476\mathrm{m}^2$$

APPENDIX XVII

CALCULATION OF DITTUS-BOELTER HEAT TRANSFER COEFFICIENTS FOR THE VENTILATION TEST PHASE I CASES 1 THROUGH 5

Table XVII-1 provides details of the calculations of Dittus-Boelter heat transfer coefficients. These coefficients are presented in Table 7-10 for comparison with the mixed convection correlation.

Table XVII-1. Calculating the Convection Heat Transfer Coefficients for the Ventilation Test Phase 1 Cases 1 Through 5 Using the Dittus-Boelter Correlation for Fully Developed Turbulent Flow in a Smooth Cylinder

Input Parameter	Value	Source
Constant (pi), dimensionless	3.14	Universal Constant
Emplacement Drift Diameter (D), m	1.3716	Table 7-5 (convert in to m)
Waste Package Diameter (d), m	0.4064	Table 7-4 (convert in to m)
Wetted Perimeter (P), m	5.6	$P=Pi \cdot (D+d)$
Cross Section Area (A), m^2	1.35	$A=pi/4 \cdot (D^2-d^2)$
Hydraulic Diameter (Dh), m	0.9652	Dh=4A/P=D-d
Air Density (rho), kg/m^3	1.1614	Table 4-17 (for 300K)
Air Thermal Conductivity (k), W/m·K	0.0263	Table 4-17 (for 300K)
Air Specific Heat (Cp), J/kg-K	1007	Table 4-17 (for 300K)
Air Dynamic Viscosity (mu), kg/m-s	1.846E-05	Table 4-17 (for 300K)
Air Prandtl Number (Pr), dimensionless	0.707	Table 4-17 (for 300K)
Case 3 and Case 5		
Air Flow Rate (Q), m^3/s per drift	0.5	Table 7-2
Air Flow Velocity (v), m/s	0.37	v=Q/A
Reynolds Number (Re), dimensionless	22468.25	Re=rho·v·Dh/mu (Incropera and DeWitt 1996 [DIRS 108184], Section 8.1.2)
Nusselt Number (Nu), dimensionless	60.64	$Nu=0.023 \cdot Re^{0.8} \cdot Pr^{0.4}$ (Incropera and DeWitt 1996 [DIRS 108184], Section 8.5)
Conv. Heat Transfer Coef. (h), $W/m^2 \cdot K$	1.65	h=k·Nu/Dh (Incropera and DeWitt 1996 [DIRS 108184], Section 8.5)
Case 1 and Case 4		
Air Flow Rate (Q), m^3/s per drift	1	Table 7-2
Air Flow Velocity (v), m/s	0.74	v=Q/A
Reynolds Number (Re), dimensionless	44936.49	Re=rho·v·Dh/mu (Incropera and DeWitt 1996 [DIRS 108184], Section 8.1.2)
Nusselt Number (Nu), dimensionless	105.58	$Nu=0.023 \cdot Re^{0.8} \cdot Pr^{0.4}$ (Incropera and DeWitt 1996 [DIRS 108184], Section 8.5)
Conv. Heat Transfer Coef. (h), $W/m^2 \cdot K$	2.88	h=k·Nu/Dh (Incropera and DeWitt 1996 [DIRS 108184], Section 8.5)
Case 2		
Air Flow Rate (Q), m^3/s per drift	2	Table 7-2
Air Flow Velocity (v), m/s	1.48	v=Q/A
Reynolds Number (Re), dimensionless	89872.98	Re=rho·v·Dh/mu (Incropera and DeWitt 1996 [DIRS 108184], Section 8.1.2)
Nusselt Number (Nu), dimensionless	183.8	$Nu=0.023 \cdot Re^{0.8} \cdot Pr^{0.4}$ (Incropera and DeWitt 1996 [DIRS 108184], Section 8.5)
Conv. Heat Transfer Coef. (h), $W/m^2 \cdot K$	5.01	h=k·Nu/Dh (Incropera and DeWitt 1996 [DIRS 108184], Section 8.5)

INTENTIONALLY LEFT BLANK

APPENDIX XVIII

QUALIFICATION OF INPUTS OBTAINED FROM OUTSIDE SOURCES

This appendix demonstrates that inputs from outside sources, including those listed in Table 4-22, are suitable for their uses in this report. Handbooks are considered to be compilations of established facts. However, handbooks in themselves derive or present no new information; they only present what has been published in the open literature, either in textbooks or publications. Thus, when a textbook, source, or a publication is referenced (or cited) by a handbook, the textbook, source, or publication becomes reliable because it is part of the handbook, which in its entirety is established fact. Therefore, some of the following sources are demonstrated to be reliable for the intended use identified in Table 4-22 because the reliability of these sources (per AP-SIII.10Q, Section 5.2.1(k)) is demonstrated by being cited as references in the indicated handbook(s) and thus widely used in standard work practices by engineers and scientists. The other sources are demonstrated as being reliable by other specific methods as described. The extent to which the data (information or equations) demonstrate the properties (information or mathematics) of interest is also addressed.

Qualification of the use of information from Bird, R.B.; Stewart, W.E.; and Lightfoot, E.N. 1960 [DIRS 103524]. The referenced source by Bird et al. was first published in 1960 and has been in publication ever since. This source is referenced by handbooks, specifically those by Cho et al. (1998 [DIRS 160802], reference number 10) and Perry et al. (1984 [DIRS 125806], in the general references for Section 10: Heat Transmission). The information from the source by Bird et al. is reliable and qualified for the intended use because it has been in publication for over four decades. This source is cited in two handbooks in the subject area of heat and mass transfer, and thus is widely used in the standard work practices on these topics. The extent to which this source of information addresses the use of equations for annular radiant heat transfer is considered adequate because these topics are well known, as documented here.

Qualification of the use of information from Carslaw, H.S. and Jaeger, J.C. 1959 [DIRS 100968]. The referenced source by Carslaw and Jaeger was first published in 1946. The second edition was first published in 1959 and has been reprinted 13 times. This source is referenced in two handbooks, one by Yovanovich (1998 [DIRS 171591], reference number 11 in Chapter 3: Conduction and Thermal Contact Resistances (Conductances)), and one by and Perry et al. (1984 [DIRS 125806], in the general references for Section 10: Heat Transmission). The information from the source by Carslaw and Jaeger is reliable and qualified for the intended use because it has been in publication for over four decades, it is cited in two handbooks in the subject area of heat conduction, and thus is widely used in the standard work practices on these topics. The extent to which this source of information addresses the linearization of radiant heat transfer and analytical/mathematical results for conduction heat transfer is considered adequate because these topics are well known, as documented here.

Qualification of the use of information from Conte, S.D. and de Boor, D. 1972 [DIRS 159800]. The referenced source by Conte and de Boor is a text on elementary numerical analysis that was published in 1972 as the second edition. The information in this text as used in this report is corroborated from other publications. The error in linear interpolation is also described by Alenitsyn et al. (1997 [DIRS 171443], Section 10.2.2). The mean value theorem and derivatives are described by Weinberger (1965 [DIRS 163216], Chapter IV, Section 24). The bisection method as used for the approximate solutions of equations is also described by Alenitsyn et al. (1997 [DIRS 171443], Section 10.4.1). The information from the source by Conte and de Boor is considered reliable for its intended use because it has been in publication

for over three decades and is in its second edition, and the information is corroborated by other sources as noted. The extent to which this source of information addresses the error in linear interoplation, mean value theorem and derivatives, and the bisection method, is considered adequate because these topics are well known, as documented here.

Qualification of the use of information from Fetter, C.W. 1993 [DIRS 102009]. The referenced source by Fetter on the topics of the theory supporting analytical equations for steady-state unsaturated flow in porous medium and the use of the van Genuchten relation was reviewed by the following individuals: J.M. Bahr at the University of Wisconsin – Madison; R.A. Griffin at the University of Alabama; J.I. Hoffman at Eastern Washington University; M. Th. Van Genuchten at the U.S. Department of Agriculture Salinity Laboratory; S. Kornder at the James River Paper Company; G. Sposito at the University of California – Berkeley; N. Valkenburg at Geraghty and Miller, Inc.; and P. Wierenga at the University of Arizona. Noting that the information of interest from Fetter pertains to unsaturated flow and the van Genuchten relation, and the fact that this source was reviewed by Martinus Th. van Genuchten, among others, the source is considered reliable for its intended use. The extent to which this source of information addresses the supporting analytical equations for steady-state unsaturated flow in porous medium and the use of the van Genuchten relation is considered adequate because these topics were extensively reviewed, as documented here.

Qualification of the use of information from Hahn, G.J. and Shapiro, S.S. 1967 [DIRS 146529]. The referenced source by Hahn and Shapiro is used for the delta method for investigating the sensitivity, or effect of uncertainty, of key input parameters with respect to the dependent variables. This method of investigating the uncertainty of a result is also described by the American Society of Mechanical Engineers (1998 [DIRS 153195], Section 7). The information from the source by Hahn and Shapiro is reliable and qualified for intended use because it also appears in an ASME standard as ASME PTC 19.1-1998 [DIRS 153195], as referenced here. The extent to which this source of information addresses the use of the delta method to investigate the effect of uncertainty is considered adequate because this topic appears in a standard, as documented here.

Qualification of the use of information from Hartman, H.L. 1982 [DIRS 128009]. The referenced source by Hartman for calculating the saturation vapor pressure of water is demonstrated as being reliable by corroborating a value calculated in the report from Hartman. This value is calculated in Section 6.9.1 as a saturation vapor pressure at 42°C of 2.427 in. Hg using equation 21-1 from Hartman. To convert in. Hg to Newton/m^2 (which is the pascal) multiply in. Hg by 3376.9 (Perry et al. 1984 [DIRS 125806], Table 1-5 and Table 1-6). Thus, 2.427 in. Hg is 8195.7 Pa. The saturation vapor pressure is also obtained from Haar et al. (1984 [DIRS 105175], Table 1) at 42°C as P = 0.082054 MPa = 8205 Pa (where M denotes mega as a SI prefix (Perry et al. 1984 [DIRS 125806], Table 1-3). These two values for the saturation vapor pressure of water, 8195.7 and 8205 Pa, are sufficiently close to be considered the same. Therefore, the information from the source by Hartman for calculation of the saturation vapor pressure of water and related psychrometric information is considered reliable for the intended purpose. The extent to which this source of information addresses the use of psychrometric information is considered adequate because these topics are well known, as documented here.

Qualification of the reference by Incropera, F.P. and DeWitt, D.P. 1996 [DIRS 108184]. The referenced source by Incropera and DeWitt is referenced as the third edition in the handbook by Rohsenow et al. (1998 [DIRS 169241], reference number 6 in Chapter 2: Thermophysical Properties). The source cited here is the fourth edition of this publication. The information from this source by Incropera and DeWitt is reliable and qualified for the intended use because it has been in publication through four editions, this source is cited in handbooks, it is a textbook (with exercises), and thus is widely used in the standard work practices on thermophysical properties and heat transfer topics. The extent to which this source of information addresses rock and concrete emissivity, thermophysical properties of air and water, constants, heat transfer correlations, definitions, radiant heat transfer for an annulus, treatment of air as a non-participating medium in radiant heat transfer, identities, boundary layer formation, and radiant heat transfer between concentric cylinders is considered adequate because these topics are well known, as documented here.

Qualification of the use of information from Jury, W.A.; Gardner, W.R.; and Gardner, W.H. 1991 [DIRS 102010]. The referenced source by Jury et al. on a the theory supporting analytical solutions supporting stead-state flow in porous media, information regarding vapor diffusion and enhanced vapor diffusion, heat capacity of geologic media, and the volumetric heat capacity of air is described in the fifth edition of this source which was initially published in 1972. The authors of this source have published extensively on these subjects as evidenced by their appearance in the bibliography of Hillel (1998 [DIRS 165404]). W.A Jury is cited seven times, W.R. Gardner is cited 18 times, and W.H. Gardner is cited three times. The qualifications of the personnel generating the source of information is considered adequate through extensive publication over 30 years (from 1972), and thus the information from the source by Jury et al. (1991 [DIRS 102010]) is consider reliable for the intended uses. The extent to which this source of information addresses the topics noted here is considered adequate because these topics are well known, as documented here.

Qualification of the reference by Kays, W.M. and Leung. E.Y. 1963 [DIRS 160763]. The referenced source by Kays and Leung is referenced in the handbook by Rohsenow et al. (1998 [DIRS 169241], reference 111 in Chapter 5: Forced Convection, Internal Flow in Ducts). The information from the source by Kays and Leung is reliable and qualified for the intended use because it is a topic-specific paper published in the *International Journal of Heat and Mass Transfer* and is cited in a handbook. The extent to which this source of information addresses forced convection in annular passages is considered adequate because this topic is well known, as documented here.

Qualification of the reference by Kays, W.M. and Perkins, H.C. [DIRS 160782]. The referenced source by Kays and Pekins is referenced in the handbook by Rohsenow et al. (1998 [DIRS 169241], reference number 263 in Chaper 5: Forced Convection, Internal Flow in Ducts). The information from the source by Kays and Perkins is reliable and qualified for the intended use because it is a topic-specific paper published in an earlier edition of the *Handbook of Heat Transfer* (see reference number 263 as noted) and is (still) cited in a handbook. The extent to which this source of information addresses forced convection, internal flow in ducts, is considered adequate because this topic is well known, as documented here.

Qualification of the reference by Kern, D.Q. 1950 [DIRS 130111]. The referenced source by Kern is referenced by Perry et al. (1984 [DIRS 125806], general references for Section 10: Heat Transmission). The information from the source by Kern is reliable and qualified for the intended use because it is cited in a handbook. The extent to which this source of information addresses the linearization of radiative heat transfer and definitions is considered adequate because these topics are well known, as documented here.

Qualification of the reference by Kuehn, T.H. and Goldstein, R.J. 1976 [DIRS 100675]. The referenced source by Kuehn and Goldstein is referenced in the handbook by Rohsenow et al. (1998 [DIRS 169241], reference number 163 in Chapter 4: Natural Convection). Also, it is referenced in the textbook by Incropera and Dewitt (1996 [DIRS 108184], Chapter 9, Free Convection, reference number 38). The information from the source by Kuehn and Goldstein is reliable and qualified for the intended use because it is based on experimental data, has been in the open literature for over three decades, is cited in a handbook and textbook on this topic, and thus is widely used in the standard work practices on the topic of natural convection. The extent to which this source of information addresses natural convection heat transfer correlations between concentric cylinders is considered adequate because the correlation is well known and based on experimental measurements, as documented here.

Qualification of the reference by Kuehn, T.H. and Goldstein, R.J. 1978 [DIRS 130084]. The referenced source by Kuehn and Goldstein is referenced in the handbook by Rohsenow et al. (1998 [DIRS 169241], reference number 164 in Chapter 4: Natural Convection). The information from the source by Kuehn and Goldstein is reliable and qualified for the intended use because it is based on experimental data, has been in the open literature for over three decades, is cited in a handbook on this topic, and thus is widely used in the standard work practices on the topic of natural convection. The extent to which this source of information addresses natural convection heat transfer correlations between concentric cylinders is considered adequate because the correlation is well known and based on experimental measurements, as documented here.

Qualification of the reference by Morgan, V.T. 1975 [DIRS 160791]. The referenced source by Morgan is referenced in the handbook by Rohsenow et al. (1998 [DIRS 169241], reference 198 in Chapter 4: Natural Convection). The information from the source by Morgan is reliable and qualified for the intended use because it is cited in a handbook on this topic, and widely used in the standard work practices on the topic of natural convection heat transfer. The extent to which this source addresses natural convection heat transfer is considered adequate because this topic is well known, as documented here.

Qualification of the reference by Moyne, C.; Batsale, J.C.; Degiovanni, A; and Maillet, D. 1990 [DIRS 153164]. The referenced source by Moyne et al. is the source of experimental results for vapor diffusion and enhanced vapor diffusion. This particular reference is a summary paper of two previous publications, one by Azizi et al. (1988 [DIRS 154108]), and the other by Moyne et al (1988 [DIRS 154107]). These two publications are detailed descriptions of the experimental and theoretical approach of the thermal conductivity of wet porous media: experiments and theory. The cited reference and the two that precede it more than adequately demonstrate the information of interest, and this is experimental results. The extent to which this source of information addresses the experimental results of vapor diffusion and enhanced vapor

diffusion in porous media is adequate because of the detailed documentation available, as noted here.

Qualification of the reference by Nagle, R.K. and Saff, E.B. 1994 [DIRS 100922]. The referenced source by Nagle and Saff is the source of mathematics describing the superposition principle. This source is corroborated by Weinberger (1965 [DIRS 163216], Chapter 2) and Zwillinger (1996 [DIRS 152179], Chapter 5). Both of these cited corroborating references discuss the superposition principle as indicated. The Nagle and Saff source is reliable and qualified for the intended use because the superposition principle is widely known and used in the standard work practice of solving differential equations. The extent to which this source of information addresses the superposition principle is considered adequate, as documented here.

Qualification of information on the physical properties of air from Reid et al. 1977 [DIRS 130310]. The information used from Reid et al. pertains to the physical properties of air. The physical properties of interest are the compressibility factor (to demonstrated that air behaves as an ideal gas), viscosity and thermal conductivity. The reference by Reid et al. is referenced by Perry et al. (1984 [DIRS 125806]), in Section 3: Physical and Chemical Data, in the general references (on p. 3-5) and as reference number 196 (on p. 3-290). Thus the information on the physical properties of air from Reid et al. is considered reliable and qualified for intended use because Reid et al. is referenced by a handbook on the topic of physical properties. The extent to which this information on the physical properties of air address the properties of interest, applicability of the ideal gas law, viscosity and thermal conductivity, is adequate because this information is well known, as documented here.

Qualification of the reference by Sutherland, W.A. and Kays, W.M. 1964 [DIRS 160789]. The referenced source by Sutherland and Kays is referenced in a handbook by Kays and Perkins (1973 [DIRS 160782], reference number 144 in Chapter 7: Internal Flow in Ducts). The information from the source by Sutherland and Kays is reliable and qualified for the intended use because it is a single-topic paper cited in a handbook and thus is widely used in the standard work practices on the topic of heat transfer for internal flow in ducts. The extent to which this source of information addresses this topic is considered adequate because the topic is well known, as documented here.

Qualification of the information on the standard atmosphere from White 1986 [DIRS 111015]. The information on the standard atmosphere is atmospheric pressure at two elevations. This information can also be found in Perry et al. (1984 [DIRS 125806], Table 3-214). The pressure given by White for an elevation of 1000 m is 89,889 Pa, and from Perry et al., the pressure is 0.89876 bar. The conversion from bar to Newtons per square meter is to multiply bar by 1×10^5 (Perry et al. 1984 [DIRS 125806], Table 1-6). The conversion factor for Newtons per square meter to Pa (Pascal) is unity (Rohsenow et al. 1998 [DIRS 169241], Table 2.4). Therefore the information from White is considered established fact because it is corroborated in a handbook. The extent to which these data address the topic of interest is adequate because the standard atmosphere is well known, as documented here.

INTENTIONALLY LEFT BLANK

APPENDIX XIX

CALCULATION OF TOTAL PRESSURE AT THE REPOSITORY ELEVATION

This appendix estimates the total pressure at the elevation of the repository.

The minimum and maximum elevations of the repository are 1,039 m and 1,107 m (BSC 2004 [DIRS 164519]). The median elevation is therefore 1,073 m. Atmospheric pressure at this elevation can be determined from the U.S. Standard Atmosphere (White 1986 [DIRS 111015], Figure 2.7 and Table A.6). The atmospheric pressure drops off nearly linearly up to a few thousand meters, as can be ascertained from examining Figure 2.7 in the cited reference.

In the cited Table A.6 at elevations of 1,000 and 1,500 m, the pressures are 89,889 and 84,565 Pa. By linear interpolation, the atmospheric pressure at 1,073 m is 89,112 Pa, which is 0.879 atmosphere, using the conversion factors on p. xix of this report. Round this to 0.88 atmosphere.

INTENTIONALLY LEFT BLANK